Silesian University of Technology

Institute of Thermal Technology
Faculty of Energy and Environmental Engineering
Silesian University of Technology, Poland

UNIVERSITÀ DEGLI STUDI FIRENZE

Department of Industrial Engineering
School of Engineering
University of Florence, Italy

Analysis of solar energy application into hybrid heat nodes

Doctoral Dissertation of

Karolina Petela

Supervisors:

Prof. Giampaolo Manfrida, University of Florence

Prof. Andrzej Szlęk, Silesian University of Technology

Gliwice 2019

Abstract

The European Energy Sector is now facing the challenge to reconcile the increase of energy demand and the desired decrease in energy consumption. With 50% of EU energy consumption assigned to the heating and cooling market, this branch deserves special attention. Particularly, the cooling energy needs are growing at a higher pace and the market must reasonably adjust. To be able to please the end-consumer and still respect the legal law commitments, technologies assuring primary energy savings should be developed and incorporated in the systems. There is no better method to minimize the consumption of non-renewable natural resources than to extract renewable energy from nature. Additionally, if one accepts that the highest cooling demand usually coincides with the highest solar radiation availability, it is reasonable to integrate the thermal comfort provision nodes with solar energy. On the other hand, solar heating and cooling systems always rely on an energy source with time-dependent availability and therefore are usually considered unreliable. Specific technology improvements are hybrid heating and cooling nodes fitting into the idea of *4th generation district heating* (4GDH) where existing district heating systems are combined with locally converted renewable energy sources. The integration of district heat with solar energy might bring double side profits: Compensate the effect of intermittent solar energy source and compensate the load of district heating network during the summer season, especially profitable for the energy suppliers.

It is important to elaborate methods for reasonable plant management, to prove those systems effective. However, one should be also made aware of how such systems work under moderate climate conditions and what are the economic consequences. This research need motivates goals of the thesis. Aim of this work is to investigate the energy, exergy consumption indicators and exergo-economic costs of solar assisted cooling installations operated in two different geo-economic environments: Italy and Poland.

In the thesis, two real-existing, reference installations representing solar energy integrated nodes are modelled and analysed. The first installation is a solar cooling plant operated in Florence in Italy. The second reference plant is an advanced hybrid heating and cooling system that integrates centralized district heat rate with locally produced useful heat gain from flat plate collectors operated in Wrocław in Poland. Analyses covered full design and off-design models of both systems. Basing on available experimental data and curves, models could have been partially validated.

Exergy is accepted as the only rational basis to recognize process inefficiencies and by the means of a cumulative exergo-economic analysis, their effect on costs distribution in both plants is investigated. The exergy analyses allow for the identification of the magnitude and source of all the exergy destructions within the system. The study is supplemented with proposals for two control algorithms enhancing the operational phase of the two installations. Its potential effect is computationally simulated.

Results obtained in the thesis represent numerical values for the anticipated conclusions. It is computationally proven that the productivity of solar assisted systems is higher in locations

with better solar radiation conditions. Although the operational costs in the solar thermal cooling systems are incomparably lower than in conventional vapour-compression units, the cumulative exergo-economic costs of cold from solar integrated systems is higher. Additionally, even if the price tariffs of electricity and heat are more expensive in Italy, the levelized cost of cold from solar sorption chillers operated under Polish radiation conditions is higher than under Italian conditions. However, if no incentive programme is assumed, the obtained results confirmed that this technology cannot be profitable so far. But yet, the integration of solar assisted plant with a district heating network is positively reflected in the exergo-economic impact analysis for Polish location in the face of solar radiation insufficiency and the fact that the district heating network is there already existing.

It was also proven that the application of control algorithms for both systems may bring measurable operational profits. The procedure applied for the control system of a solar cooling plant allows for the increase of solar fraction. The magnitude of this effect is however dependent on location and the type of solar collectors installed. The control procedure applied for a hybrid heating and cooling node may contribute to decreasing the operational economic cost- and environmental-impact indicators.

Streszczenie

Europejski sektor energetyczny stoi obecnie przed wyzwaniem pogodzenia wzrostu zapotrzebowania na energię z pożądanym spadkiem zużycia energii. 50% zużycia energii w Unii Europejskiej przypisane jest rynkowi ciepła i chłodu, dlatego branża ta zasługuje na szczególną uwagę. W szczególności, rynek musi dostosować się do coraz prężniejszego wzrostu zapotrzebowania na moc chłodniczą. Aby spełnić wymagania użytkownika końcowego oraz nadal przestrzegać zobowiązań prawnych, powinny zostać opracowane i wdrożone technologie zapewniające oszczędność energii pierwotnej. Wykorzystanie energii odnawialnej bywa określane najlepszą metodą zastąpienia i tym samym ograniczenia zużycia nieodnawialnych zasobów naturalnych. Dodatkowo, jeśli zaakceptuje się fakt, że najwyższe zapotrzebowanie na chłód pokrywa się zazwyczaj z najwyższą dostępnością promieniowania słonecznego, integracja węzłów ciepła i chłodu z urządzeniami konwersji energii słonecznej jest uzasadnionym wyborem. Z drugiej strony, samodzielne solarne systemy ogrzewania i chłodzenia uzależnione są od czasowo dostępnego źródła energii. Z tego względu są często uważane za niestabilne. Rozwiązaniem mogą być hybrydowe węzły ciepła i chłodu wpisujące się w ideę systemów ciepłowniczych czwartej generacji (4GDH), w których istniejące systemy ciepłownicze współpracują z lokalnymi systemami konwersji energii odnawialnej. Integracja zasilania ciepłem sieciowym z energią słoneczną może przynieść podwójne korzyści: kompensacji czasowej niedostępności energii słonecznej oraz kompensacji obciążenia sieci ciepłowniczej w sezonie letnim, co może być szczególnie korzystne dla dostawców ciepła.

Aby dowieść niezawodności takich systemów, ważne jest opracowanie metod racjonalnego zarządzania pracą instalacji. Należy również uświadomić sobie, jak takie systemy funkcjonują w warunkach klimatu umiarkowanego i jakie są tego konsekwencje ekonomiczne. Tak zdefiniowana potrzeba badań motywuje przyjęty cel pracy doktorskiej. Celem pracy jest określenie wskaźników zużycia energii, wskaźników zużycia egzergii i wskaźników kosztu egzergo-ekonomicznego instalacji chłodzenia wspomaganego energią słoneczną eksploatowanych w dwóch różnych środowiskach geo-ekonomicznych: we Włoszech i w Polsce.

W pracy dyplomowej opracowano modele symulacyjne oraz dokonano analizy dwóch rzeczywistych instalacji referencyjnych reprezentujących węzły ciepła i chłodu zintegrowane z energią słoneczną. Pierwszą instalacją jest solarny system chłodzenia działający we Florencji we Włoszech. Drugi system funkcjonuje we Wrocławiu w Polsce. Jest to hybrydowy system ogrzewania i chłodzenia, który integruje ciepło sieciowe ze scentralizowanego źródła z ciepłem użytkowym z płaskich kolektorów słonecznych. Analiza obejmowała opracowanie modeli w projektowym punkcie pracy oraz symulacje off-design obu systemów. W oparciu o dostępne dane doświadczalne i charakterystyki sprawnościowe, modele mogły zostać częściowo zweryfikowane.

Egzergia jest uznana jako jedyny racjonalny wyznacznik pozwalający na określenie nieodwracalności procesów w analizowanych układach oraz strat w nich występujących. Analiza egzergetyczna pozwoliła na identyfikację wielkości i źródła wszystkich wewnętrznych strat egzergii w analizowanych systemach. Za pomocą skumulowanej analizy egzergo-ekonomicznej określony został wpływ nieodwracalności procesów i strat na rozkład kosztów w obu układach.

W pracy zaproponowano także dwie procedury kontrolne służące optymalizacji fazy eksploatacyjnej dwóch instalacji. Potencjalny efekt działania procedur został zweryfikowany symulacyjnie.
W rozprawie udowodniono obliczeniowo, że wydajność systemów wspomaganych energią słoneczną jest wyższa w lokalizacjach o lepszych warunkach napromieniowania słonecznego. Chociaż koszty operacyjne systemów chłodzenia zasilanych odnawialną energią słoneczną są nieporównywalnie niższe niż w przypadku konwencjonalnych systemów sprężarkowych, łączne koszty egzergo-ekonomiczne obejmujące fazę inwestycyjną są wyższe dla układów solarnych. Ze względu na większy możliwy udział energii słonecznej w procesie dostarczania chłodu we włoskiej lokalizacji, średni wskaźnik egzergo-ekonomiczny dla chłodu jest tam niższy, mimo iż taryfy cenowe energii elektrycznej i ciepła są wyższe we Włoszech niż w Polsce. Jednakże w obydwu przypadkach, uzyskane wyniki potwierdziły, że technologia ta nie może być obecnie uznana za opłacalną, jeżeli nie założy się istnienia systemu wsparcia na etapie inwestycji. Niemniej jednak, idea zintegrowania węzła zasilanego ciepłem sieciowym z lokalnie uzyskanym ciepłem z energii słonecznej może być uzasadniona dla polskiej lokalizacji. Wynika to z możliwości kompensacji niedoborów promieniowania słonecznego w tym regionie oraz z tego, że sieć ciepłownicza w tej lokalizacji jest obecnie dostępna. W pracy sprawdzono tezę, że wdrożenie algorytmów sterowania dla obu systemów może przynieść wymierne korzyści dla fazy eksploatacyjnej. Dyskusja dowodzi, że wymiar i rodzaj korzyści zależy od lokalizacji i technologii zastosowanej w układzie.

Sommario

Il settore europeo dell'energia si trova attualmente ad affrontare la sfida di conciliare l'aumento della domanda di energia e l'auspicata riduzione del consumo energetico. Con il 50% del consumo energetico della UE attribuibile al settore del riscaldamento e del raffreddamento, questo aspetto merita specifica attenzione. In particolare, il fabbisogno energetico di
adeguarsi. Per poter soddisfare il consumatore finale e rispettare le normative, è necessario sviluppare ed integrare nei sistemi di conversione tecnologie che garantiscano il risparmio di energia primaria. Il metodo migliore per minimizzare il consumo di risorse non rinnovabili è estrarre energia rinnovabile da fonti naturali. Inoltre, poiché il picco di richiesta di raffreddamento coincide in genere con una maggiore disponibilità di radiazione solare, è ragionevole integrare i sistemi di fornitura di energia termica con l'energia solare. Di contro, i sistemi di riscaldamento e raffreddamento solare si basano su una sorgente energetica con disponibilità dipendente dal tempo e sono quindi solitamente considerati limitatamente affidabili. Miglioramenti tecnologici specifici sono rappresentati dai sistemi ibridi di riscaldamento e raffreddamento che nell'ambito del teleriscaldamento di quarta generazione (4GDH). Poiché i sistemi di teleriscaldamento esistenti sono combinati con fonti di energia rinnovabile convertite localmente, la loro integrazione con l'energia solare potrebbe portare a doppi profitti collaterali: compensare gli effetti della fonte di energia solare non costantemente disponibile e compensare il carico della rete di teleriscaldamento durante la stagione estiva, aspetto particolarmente vantaggioso per i fornitori di energia.
È importante elaborare metodi di gestione razionale dell'impianto, per dimostrare l'efficacia di tali sistemi. Tuttavia, bisogna anche essere consapevoli di come questi sistemi funzionino in condizioni climatiche moderate e di quali sono le conseguenze economiche. Lo scopo di questo lavoro è studiare l'energia, gli indicatori di consumo di exergetico ed i costi exergo-economici di esercizio degli impianti di raffreddamento solare assistito funzionanti in due diversi ambienti geo-economici: Italia e Polonia.
Nella tesi vengono modellati ed analizzati due impianti di riferimento realmente esistenti che rappresentano sistemi integrati di energia solare. Il primo è un impianto di raffreddamento solare situato a Firenze, in Italia. Il secondo impianto di riferimento è un sistema ibrido avanzato di riscaldamento e raffreddamento che integra il teleriscaldamento centralizzato con il calore prodotto localmente da collettori piani installati a Wrocław, in Polonia. Le analisi hanno riguardato la progettazione completa ed i modelli di off-design di entrambi i sistemi. Sulla base dei dati sperimentali e delle curve di funzionamento disponibili, i modelli sono stati parzialmente convalidati.
Le analisi exergetiche sono considerate l'unico strumento razionale per individuare le inefficienze di processo; attraverso un'analisi economica cumulativa dell'esercizio, viene analizzato il loro effetto sulla distribuzione dei costi in entrambi gli impianti. Questa tipologia di analisi consente di identificare l'entità e la fonte di tutte le perdite di exergia presenti all'interno del sistema. Lo studio è stato integrato con le proposte di due algoritmi di controllo che migliorano la fase operativa dei due impianti. Il loro effetto potenziale è stato simulato nei calcoli.
I risultati ottenuti nella tesi rappresentano valori numerici che confermano le conclusioni attese. È stato dimostrato dai calcoli che la produttività dei sistemi solari assistiti è maggiore in luoghi

con migliori condizioni di radiazione solare. Sebbene i costi operativi dei sistemi solari termici di raffreddamento siano incomparabilmente inferiori rispetto a quelli delle unità convenzionali a vapore compresso, i costi economici cumulativi di esercizio dei sistemi solari integrati sono più elevati. Inoltre, anche se le tariffe dell'elettricità e del calore sono più elevate in Italia, il costo livellato del freddo proveniente dai refrigeratori ad assorbimento solare azionati in condizioni di radiazione tipiche della Polonia è superiore a quello delle condizioni tipiche della Italia. In assenza di un programma di incentivazione, i risultati ottenuti hanno confermato che questa tecnologia non può essere redditizia allo stato attuale. Tuttavia, l'integrazione dell'impianto solare assistito con una rete di teleriscaldamento si riflette positivamente sull'analisi dell'impatto economico del caso polacco a causa dell'insufficienza di radiazione solare e del fatto che la rete di teleriscaldamento è già esistente.

È stato inoltre dimostrato che l'utilizzo di algoritmi di controllo per entrambi i sistemi può portare a profitti operativi quantificabili. La procedura applicata per il sistema di controllo di un impianto di raffreddamento solare consente di aumentare la frazione solare. L'entità di questo effetto dipende tuttavia dalla posizione e dal tipo di collettori solari installati. La procedura di controllo applicata per un sistema ibrido di riscaldamento e raffreddamento può contribuire a ridurre i costi operativi economici e gli indicatori di impatto ambientale.

Acknowledgements

Foremost, I would like to express my sincere gratitude to the supervisors of this thesis: To Prof. Andrzej Szlęk and to Prof. Giampaolo Manfrida.

I want to thank Professor Szlęk for motivating me to step into this specific field of research that indeed turned out to be fascinating, for practical advices while shaping the thesis, but also for the opportunity to take part in the industry-based scientific projects that contributed to my self-development.

I am especially grateful to Prof. Giampaolo Manfrida for his guidance and mentorship, his constant inspiration, and for intriguing me with exergy-based methods and solar-assisted cycles way before the PhD-thesis-adventure began. I would like to thank him for the hospitality at the University of Florence and for the possibility of being a part of interesting research projects.

My sincere thanks go to Professor Maurizio De Lucia for introducing the Misericordia solar cooling plant to me, for sharing the project and validation data. At this place I want to say thank you to Giacomo Pierucci for the sacrifice of time, answering my questions and providing me with valuable data.

I would like to extend my gratitude to Professor Daniele Fiaschi for sharing the knowledge on the sorption chillers modelling issues. I am indebted to Lorenzo Ciappi for his support while translating the Sommario.

I also thank Fortum Power and Heat Polska company for fruitful cooperation and the possibility of taking part in the AHCS research project. I thank the colleagues from Wrocław University of Science and Technology: Bartosz Zajączkowski and Tomasz Hałon who provided and shared experimental expertise that greatly assisted the research.

I am profoundly grateful to my parents for my upbringing and the constant support during all of the years of my education.

Last, but not least, my love goes to my husband – Bartłomiej, who never stopped understanding, encouraging and inspiring me.

Karolina Petela

List of Contents

List of figures

List of tables

List of chosen Nomenclature

a_1	linear heat loss coefficient [W/(m^{2}K)]
a_2	quadratic heat loss coefficient [W/(m^{2}K^2)]
A	surface area [m^2]
b	specific exergy [kJ/kg]
$\dot{B}$	exergy rate [kW]
C	total investment cost [€]
$\dot{C}$	cost rate [€/h]
c	specific cost of exergy stream [€/kWh]
c_p	specific heat [kJ/kgK]
$coll_{inseries}$	number of collectors in series
Cl	clearance
d	diameter [m]
E	energy [kJ] or [kWh]
$\dot{E}$	energy rate [kW]
f	exergoeconomic factor
$F_{abs-amb}$	absorber versus ambient view factor
F_R	heat removal factor
G	solar radiation [W/m^2]
$\dot{H}$	enthalpy rate [kW]
h	specific enthalpy [kJ/kg K]
h_i	internal heat transfer coefficient [kW/m^{2}K]
h_o	external heat transfer coefficient [kW/m^{2}K]
h_{conv}	convective heat transfer coefficient [kW/m^{2}K]
h_{cond}	conductive heat transfer coefficient [kW/m^{2}K]
L	length [m]
m	mass [kg]
$\dot{m}$	mass flow rate[kg/s]
n	lifetime
N	electric power [kW]

N_{coll}	number of collectors
N_t	number of tubes
Nu	Nusselt number
p	pressure [bar] or [kPa]
P_t	tube pitch
Pr	Prandtl number
q	solution quality – vapour mass fraction
$\dot{Q}$	heat rate [kW]
R	ideal gas constant [kJ/mol K]
R_{wall}	thermal resistance of the wall [K/kW]
r	relative cost difference
$\dot{S}$	entropy rate [kW/K]
s	specific entropy [kJ/kg K]
T	temperature [K] or [°C]
U	overall heat transfer coefficient [kW/ m^2K]
V	volume [m^3]
$\dot{V}$	volumetric flow rate [l/s]
w	velocity [m/s]
$\dot{W}$	work rate [kW]
x	concentration of refrigerant in the refrigerant-absorbent solution
y_D	exergy destruction ratio
Z	investment [€]
$\dot{Z}$	investment rate [€/h]
ΔT	temperature difference [K]

Subscripts

0	reference environment
abs	absorbed
amb	ambient
ap	aperture
app	approach point

aux	auxiliary
av	average
b	bundle
beam	beam/direct
c	collector
C	cold
ch	chemical
coll	collector
comp	compressor
cond	condenser
conv	convection
cw	cooling water
chw	chilled water
e	equivalent
E	energy
f	fluid
F	fuel
gen	generator
H	hot
HE	heat exchanger
hw	hot water
I	irradiation
i	i-th stream
incoll	incoming to collector
ir	interest rate
in	input
j	j-th stream
k	k-th component of a system
kin	kinetic
L	loss

Lg	log-mean
m	medium
n	normal
out	output
P	product
ph	physical
pot	potential
pump	pump
Q	heat
r	receiver
rad	radiation
ref	reference
S	Sun
sc	solar collector
sol-air	solar-ambient
sys	system
tot	total
tr	triple point
u	useful
w	water
W	work

Superscripts

an	annual
CH	chemical
CI	capital investment
gross	gross
net	net
OM	operation and maintenance

Greek letters

α	solar altitude angle, °

α_s	surface azimuth angle, °
α_{sc}	absorptance
Δ	increase
ε	emissivity
η	efficiency
η_o	optical efficiency
λ	conductivity [W/mK]
Φ	location latitude
ρ	density [kg/m^3]
ρ_{sc}	reflectance of the concentrator
ψ	psi factor
ψ_{sc}	intercept factor
τ_{sc}	transmittance
τ	time step, s
θ	incidence angle, °

List of acronyms

AHCS	Advanced Heating and Cooling Substation
CEPCI	Chemical Engineering Plant Cost Index
COP	Coefficient of Performance
CTES	Cold Thermal Energy Storage
DNI	Direct Normal Irradiation
ESEER	European Seasonal Energy Efficiency Ratio
HE	Heat exchanger
HTF	Heat transfer fluid
IAM	Incidence Angle Modifier
IEA	International Energy Agency
Ins	Insurance
LCA	Life Cycle Assessment
LCOC	Levelized Cost of Cooling energy
Maint	Maintenance

PEC	Purchased Equipment Cost]
RHE	Regenerative Heat Exchanger
SPECO	Specific Exergy Costing
TCI	Total Capital Investment
TEGDME	Tetraethylene glycol dimethyl ether
TES	Thermal Energy Storage
TFE	Trifluoroethanol

Constants

c	speed of light ($3 \cdot 10^8$ m/s)
σ	Stefan-Boltzmann constant ($5.67 \cdot 10^{-8}$ W/m^{2}K^4)

Chapter 1. INTRODUCTION

According to the European Union's Strategy on Heating and Cooling, consumers should be always seen at the centre of energy or environmental policy decisions and recommendations [1]. In the end, consumers are the only real existing subjects steering the complex interdependencies between energy demand, supply, resources depletion and finally: the climate change. At the same time, the European Commission directly admits that "People's well-being, industrial competitiveness and the overall functioning of society are dependent on safe, secure, sustainable and affordable energy" [2]. Together with the consumer-society evolution and its development, the living standards and expectations towards them are increasing. It can be also observed in higher requirements to thermal comfort provision. Access to domestic hot water and central heating is not sufficient for thermal comfort satisfaction. The need for cooling energy became the third pillar of thermal comfort. Formal documents report that heating and cooling in residential and industrial sector accounts for 50% of the European Union's (EU) energy consumption [3]. 79% of final energy usage in EU households is assigned to central heating and domestic hot water preparation. The use of energy for cooling is smaller, but a specific share is rather unknown in the face of a lack of detailed monitoring. Energy consumption for the purpose of cooling is embedded in the total electric energy consumption in a household because the majority of installed air conditioning units are vapour-compression chillers [4]. It is, however, estimated that the cooling market will continue to grow at a rate of 3.14% per year [5]. Higher affordability of the chiller units, higher thermal comfort standards, and increasing residential floor area might be motivating this trend. Other prognoses state that by 2030 the energy consumption for residential cooling purposes in the EU will increase by 72%, while the energy consumption for heating will decrease by 30% [6]. Estimate models prepared for the global level indicate that the energy demand for heating aims will increase till 2030 and then remain constant and that by 2060 the energy consumption for residential cooling will exceed the consumption for heating [7].

In 2012 in Europe, fossil fuels accounted for 75% of the primary energy use for the purpose of heating and cooling. The statistic shares are shown in Fig.1.1.

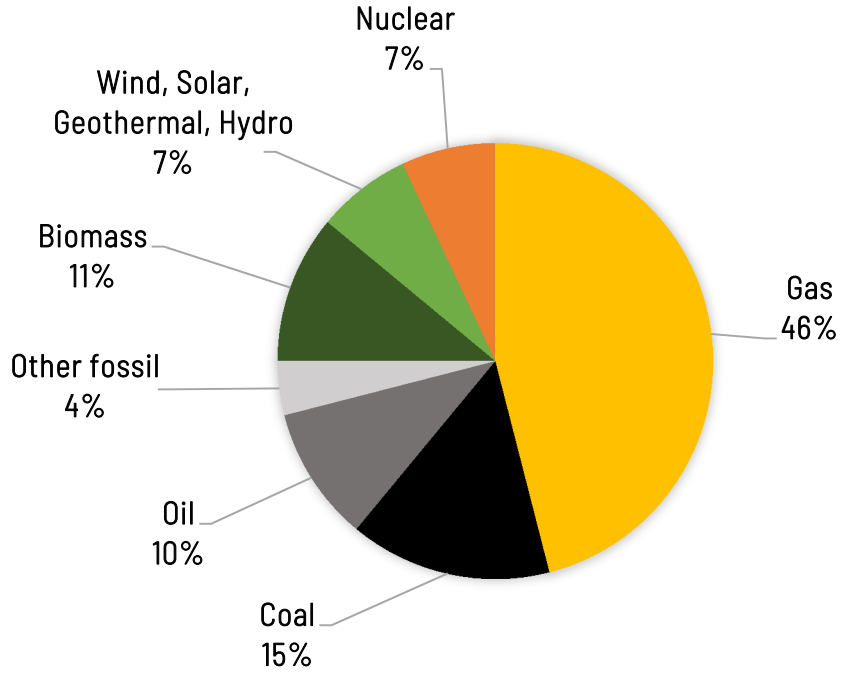

Fig.1.1 Primary energy consumption for heating and cooling in EU, 2012[1]

At this time the European Union has already begun its striving to a low-carbon society by accepting the 2020 Energy Strategy in 2007. Its aims were to reduce the greenhouse gases emissions by 20%, increase the share of renewable energy consumed to 20% and to improve the energy efficiency by 20% [8]. This vision was extended in October 2014, when the European Council introduced a new 2030 Framework for climate and energy. The updated objectives are: 40% reduction of greenhouse gas emissions compared to levels in 1990, 27% share of renewable energy, 27% improvement in energy efficiency [9]. The latest official document reporting the achievements on 2020 Energy Strategy goals was issued on 23 November 2017. According to this communication, between 1990 and 2016 the total emission decreased by 23%, in 2015 renewable energy share in gross final energy consumption equalled 16.7% and while EU consumed 2.5% less of primary energy compared to 1990, it should have been still reduced by further 3.1% to 2020 in order to reach the 20% improvement of energy efficiency target [10].

Although any updated report data for 2018 are not yet known, in the meantime, the ambitious targets for 2030 have become more rigorous in the frame of “Clean Energy for All Europeans package” that is currently being prepared and expects following developments: 45% emission reduction, 32% renewable energy share, 32.5% energy efficiency improvement. These goals would play a very important role in the next vision of the European Commission that was just

presented on 28 November 2018: *A Clean Planet for all - A European strategic long-term vision for a prosperous, modern, competitive and climate neutral economy* [11].

In the presence of increasing restrictions towards EU Energy Sector and of the fact that residential heating and cooling consume and will continue to consume a significant amount of primary energy, it can be concluded that, primarily, this branch should evolve and adapt to new conditions. It has been not overlooked by the European legislators and the Directive 2012/27/EU of the European Parliament and of the Council of 25 October 2012 on energy efficiency recognizes the need for the development of efficient heating and cooling systems. Additionally, it distinguishes between: *efficient heating and cooling* (a heating and cooling system that reduces primary energy need taking into account extraction, conversion, transport and distribution), *efficient district heating and cooling* (a district heating or cooling system with at least 50% renewable energy input, 50% waste heat, 75% cogeneration heat or 50% of a combination of such energy and heat) and *efficient individual heating and cooling* (being an individual heating and cooling system with reduced need for non-renewable primary energy or with the same need for non-renewable primary energy as the efficient district heating and cooling but obtained at lower cumulative cost) [12]. Moreover, the development of renewable energy integrated heating and cooling systems is recommended by the European Commission in its Energy Roadmap 2050 [2]. The Roadmap marks that combining district heating systems with locally converted renewable energy sources might be vital for the desired decarbonisation. Such an integration fits into the definition of the promoted *4th generation district heating* (4GDH). The idea of 4GDH is to provide sustainable energy systems that would deliver low-temperature district heating with low grid losses for space heating and domestic hot water, that would integrate renewable energy sources (solar, geothermal), that would regenerate waste heat from low-temperature sources, that would work within smart energy systems equipped with smart metering and load prognoses [13][14].

To sum up: existing legal acts are still focused on the development of new generation systems where renewable energy is integrated with conventionally derived district heat in order to satisfy the consumer's thermal comfort needs. Moreover, if one accepts that the highest cooling demand usually coincides with the highest solar radiation availability, solar energy should be considered as the best renewable energy candidate to be coupled to the production of cold. On the other hand, renewable energy integrated systems always rely on an energy source with time-dependent availability and therefore are usually considered unreliable. Hence, it is important to elaborate methods for reasonable plant management, to prove those systems effective.

In the face of current energy demands and of laws being in force, following thesis presents a detailed analysis of 2 solar integrated systems oriented on thermal comfort provision with a special focus on the economy and environment interaction. The choice of the research area is partially motivated by the above discussion. A preliminary comprehensive literature review confirmed the need for additional research. Chapter 3 reveals the research need and names the main challenges awaiting the heating and cooling sector.

Chapter 2. AIM AND SCOPE

The basic idea of the present study is to introduce, simulate and analyse two reference installations representing the solar integrated thermal comfort provision technology. The first real existing installation is a solar cooling plant operated in Florence, Italy designed and constructed by a research team from the University of Florence. It is an ammonia-water chiller driven by heat input from parabolic trough solar collectors with vapour compression chiller backup. The second reference plant was an advanced hybrid heating and cooling system that was designed during the preparation of this thesis. The system integrates centralized district heat rate with locally produced useful heat gain from flat plate collectors in order to provide the end user with cooling energy, central heating, and domestic hot water. It is already operated in Wrocław, Poland.

The goal of this thesis is multidimensional. The primary aim of the work is to investigate the energy and exergy consumption indicators that may be caused by exploiting solar assisted cooling installations of two different types working under two different meteorological conditions. The study over the meteorological impact on the sensitivity of technical solutions mirrored in two referential installations is included in the thesis. A further task is to confirm the usefulness of adapted cumulative impact assessment methodology in the assessment of renewable energy technologies. A further aim of this work is to show the potential advantages of implementing a proposed control algorithm into the management structure of the node and to indicate the influence of climate-dependant factors of implementation the estimated real-time performance.

The practical path to achieve the goal of this study is to perform energy, exergy and cumulative exergo-economic analyses of two reference solar integrated installations operated under different climate conditions. Once the structures of two referential installations were recognized, the simulation models of the systems were created. Simulation models were prepared adopting a modular structure of the system. It means that models were prepared for each component separately (solar collector fields, chillers, storage, intermediate heat exchangers) accepting the heat and mass transfer on its boundaries and then were connected following energy balancing rules. Work covered both design and off-design analyses recognizing variable load conditions depending on changing weather conditions. The thesis explains detailed path and theoretical background for the preparation of the models. Both solar integrated systems were assessed in terms of energy, exergy, and cumulative exergo-economic analyses. The Italian installation was analysed assuming both Italian weather conditions and its

potential operation under Polish climate conditions. Similarly, for comparative reasons, the Polish system performance was evaluated assuming Polish meteorological conditions and theoretical operation in the Italian climate. According to Köppen-Geiger classification, Poland belongs to oceanic climate type (Cfb), while Italy represents mainly hot-summer Mediterranean type (Csa) [15].

Finally, author proposes two control algorithms with possible potential for primary energy savings and improvement of environmental impact indicators. The first control procedure is prepared for the single stage absorption chiller and focuses on the optimal choice of the driving temperature. The second algorithm is proposed for the hybrid heating and cooling node. It supports the control and management system by adjusting the mass flow rates from the district network and solar field in order to minimize the operational economic impact or environmental impact indicators.

Results obtained in the study are analysed and discussed. The last section of the work collects the conclusions, indicates the recommendations for system management enhancement, but also pays the reader's attention to further challenges of the technology fitting into the 4th generation district heating and cooling systems definition.

It should be noted that the dissertation is partially based on the papers already registered in the SCOPUS research database. For this reason, some written parts presented in the dissertation are also to be found in [16,17]. What is more, the results discussed in Chapter 6.5 became part of the manuscript submitted to the Energy Conversion and Management journal. At the moment of the dissertation submission, the paper is under review.

Chapter 3. STATE OF THE ART

A comprehensive literature review was the first logical step for the preliminary part of the research. Solar heating technologies were confirmed as a mature and recognized technology, however, it was clear from the beginning that there should be no direct intention to analyse and optimise solo solar heating system; the review was thus devoted to the still-developing solar cooling, hybrid heating and cooling and energy storage technologies. The assessment of the state of the art included verifying what kind of systems exist on the market and which ones are still in the prototype condition. The review delivers a summary on existing performed research, provides cumulative impact analyses and reveals the challenges and the need for further research.

3.1 Solar cooling – History Background

It is historically affirmed that the first solar cooling system in the world was the one operated in Paris during the 1878 world exhibition. Augustin Mouchot was a French mathematician who invented the first concentrating solar collector. Thanks to the mirrors, solar energy was focused on a black copper container filled with water. Water was converted into steam and then was driving a thermal chiller to produce ice blocks. The solar concentrator is visible in the graphics from the 19th century presented in Fig. 3.1.

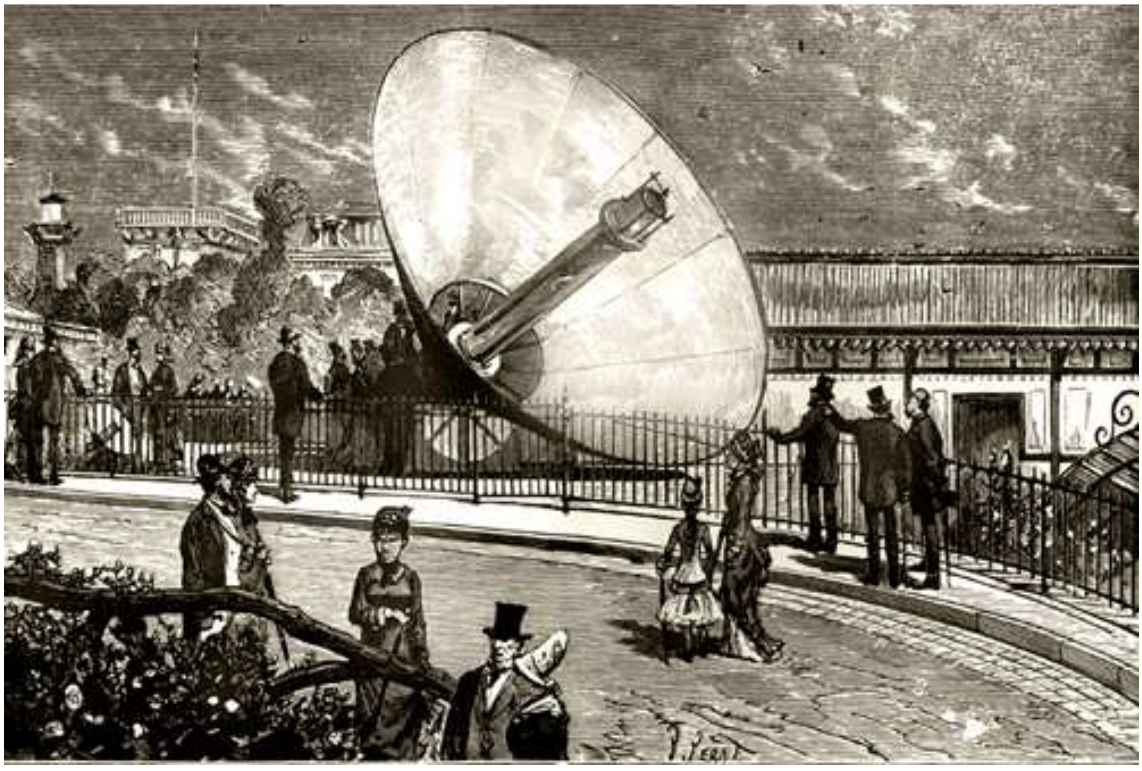

Fig. 3.1 Augustin Mouchot's Solar Concentrator at the World Exhibition in Paris, 1878 [18].

This invention won Mouchot a gold medal during the exhibition [19]. The idea was obviously revolutionary and had the potential to promote renewable energy sources already in the 19th century. However, since big resources of coal in France and of oil in the United States were discovered shortly after, the concept of solar-assisted cooling was abandoned for almost 100 years. The development of solar refrigeration technology began in the 1970s and it is worth mentioning that the initial impulse was not at all reasons of environmental protection. In 1973, OPEC members imposed an embargo on oil export to the countries supporting Israel in the Arab-Israeli conflict. It was the beginning of the oil crisis, especially severe for the United States, for the American industry mainly based on crude oil imported from Arabic countries. In order to motivate the American economy to implement the renewable energy based technologies, the International Energy Agency (IEA) started the Solar Heating and Cooling (SHC) Programme in 1977. Solar Heating and Cooling Programme is still performing as a technology and knowledge hub. Its greatest strength is the international collaboration leading to research exchange, market understanding and policy recommendation which can accelerate the deployment rate of solar heating and cooling systems. The SHC's constantly updated vision is oriented on lowering the CO_2 emission worldwide and today it is stated that "Solar energy technologies will provide more than 50% of low-temperature heating and cooling demand for buildings in 2050 and contribute a significant share to the heat supply for the agricultural and industrial sectors. Thus, solar heating and cooling will contribute significantly to lowering CO_2 emissions worldwide and reaching the Paris Agreement goal" [20]. SHC Programme's beginning in 1977 is recognized as the ringleader for solar refrigeration technologies development and their commercialization during the next three decades [21]. Some research programmes were also carried out at the European level. The SACE (Solar Air Conditioning in Europe) project started in 2002, lasted 2 years and was supported by the European Commission. Researchers from five countries gathered to assess the feasibility, cost savings potential of solar cooling development in Europe. After a detailed analysis of 53 projects, they found out that solar refrigeration might help saving up to 0.07 €/kWh [22]. Subsequent SOLAIR project was oriented on market analyses as a path for solar cooling technologies commercialization [21]. SOLAR COMBI+ (led 2007-2010) and HIGH COMBI (2007-2011) were EU projects oriented on the promotion of systems combining conventional residential heating and cooling systems with small-scale solar cooling.

Although the SHC research programme has already started in the 70s, the sinusoidal trend of oil price during the following decades affected negatively the expected market penetration pace. The solar cooling market seems to flourish just lately. According to available sources [23,24],

the number of installed solar cooling systems has increased from 60 in 2004 to 1175 in 2014. These data indicate that the market was growing in these years at a 40-70% increment rate. Together with the gradual dissemination of commercial solar cooling system, the specific cost of solar cooling kits kept decreasing. The price for medium capacity systems (up to 50kW cooling power) dropped from 6500 €/kW in 2007 to approximately 3500 €/kW in 2012 (averaged over absorption and adsorption units) [24]. However, it was higher than the cost of a conventional vapour-compression chiller, which ranged from 500 to 1000 €/kW in 2012. Relatively high investment cost and complexity are one of the main aspects restraining a faster spread of the technology [25].

3.2 Solar cooling – Theory Background

Fundamentally, cooling systems can take advantage of solar energy in one of the two ways: to generate electric energy or to convert it into useful heat. Schemes in Fig. 3.2 are a simplified visualisation of thermodynamic cycles both for solar-electric and solar-thermal refrigeration systems types. This sketch underlines the relation of heat sources towards ambient temperature (T_{amb}) and states the fundamentals of the definition of the Coefficient Of Performance (COP). The amount of heat rejected to the environment (Q_{loss}) could be recycled and used as a driving heat for low-temperature demanding processes.

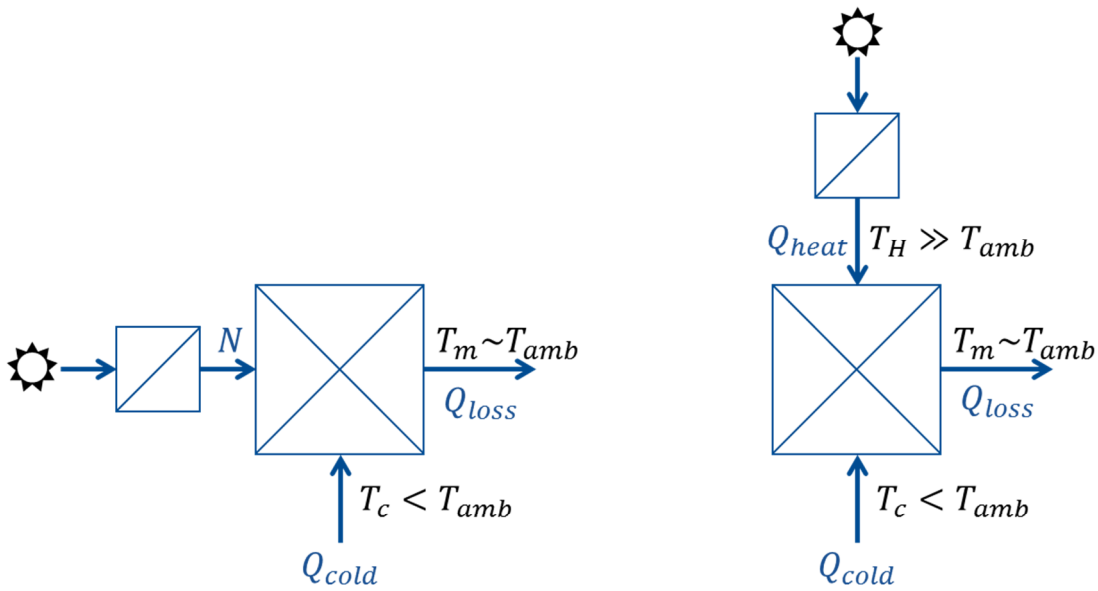

$$COP = \frac{Q_{cold}}{N} \qquad COP = \frac{Q_{cold}}{Q_{heat}}$$

Fig. 3.2 Basic thermodynamic schemes of electric driven and heat driven chillers.

In the solar-electric systems, solar energy can be utilized by photovoltaic panels so that the generated electric energy can drive a vapour-compression chiller or be used by a Peltier module. The driving electric energy can be also obtained from a system where the solar thermal collector is connected to a heat engine (e.g. Stirling engine).

Among solar-thermal cooling technologies, one can differentiate between thermo-mechanical systems, open or closed cycles. Thermo-mechanical solar refrigeration is based on the ejector refrigeration cycle principle. Open refrigeration cycles can be divided into liquid and solid desiccant systems. They belong to the sorption refrigeration systems group because desiccation is a sorption process in which a desiccant (sorbent) removes moisture from the air. Dehumidification is then combined with the evaporative process in order to achieve a cooling effect. [21,26]

While open cycles rely on direct treatment of air in a ventilation system, closed cycles deliver chilled water from a thermally driven sorption chiller. Closed solar refrigeration cycles are divided by analogy to open cycles: to liquid sorbent based (absorption systems) and solid sorbent-based (adsorption cycles). Sorption cycles take advantage of the physical effect of refrigerant sorption by a sorbent.

A schematic tree in Fig. 3.3 collects the processes known for the conversion of solar radiation into cooling energy.

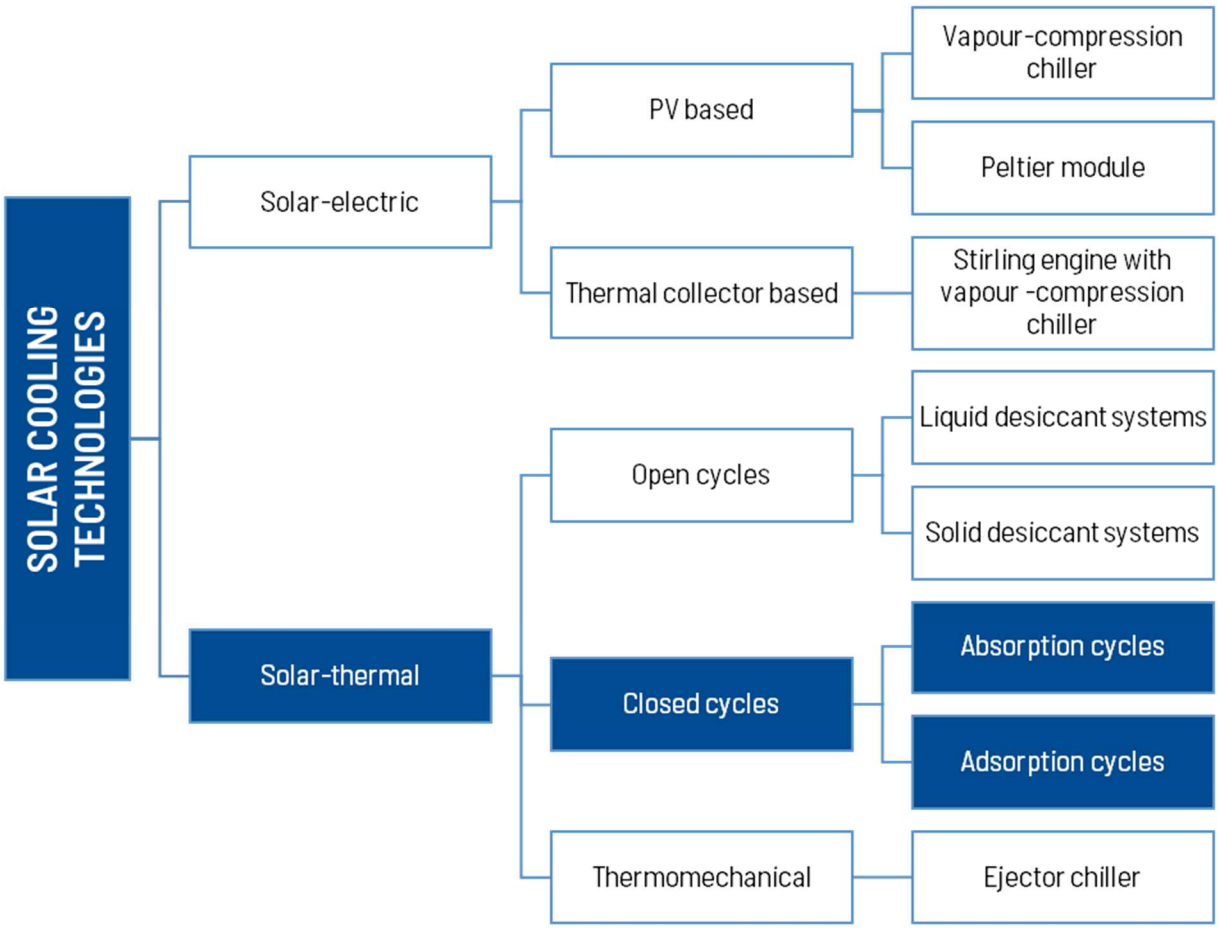

Fig. 3.3 Solar cooling technologies overview [26–29].

Taking into consideration the aim and scope of the thesis, the following review will focus on the state of the art of closed-cycle solar thermal absorption and adsorption chillers (blue background in Fig. 3.3) presenting both: available technologies and current state of research. Scope of the work motivates also to investigate the present technology of hybrid heating and cooling nodes and to share available conclusions from cumulative impact analyses of solar integrated hybrid systems.

3.3 Solar absorption chillers

Absorption cycles are considered as one of the oldest refrigeration technologies [26,30]. From the refrigerant perspective, the working principle of an absorption chiller is fundamentally similar to that of a vapour compression chiller. Each absorption cycle includes an evaporator and condenser, but the mechanical compressor is replaced by a so-called sorption compressor. The sorption compressor is typically a set of the absorber, generator (desorber) and regenerative

heat exchanger (RHE). Fig. 3.4 presents a basic scheme of a single-stage absorption chiller cycle.

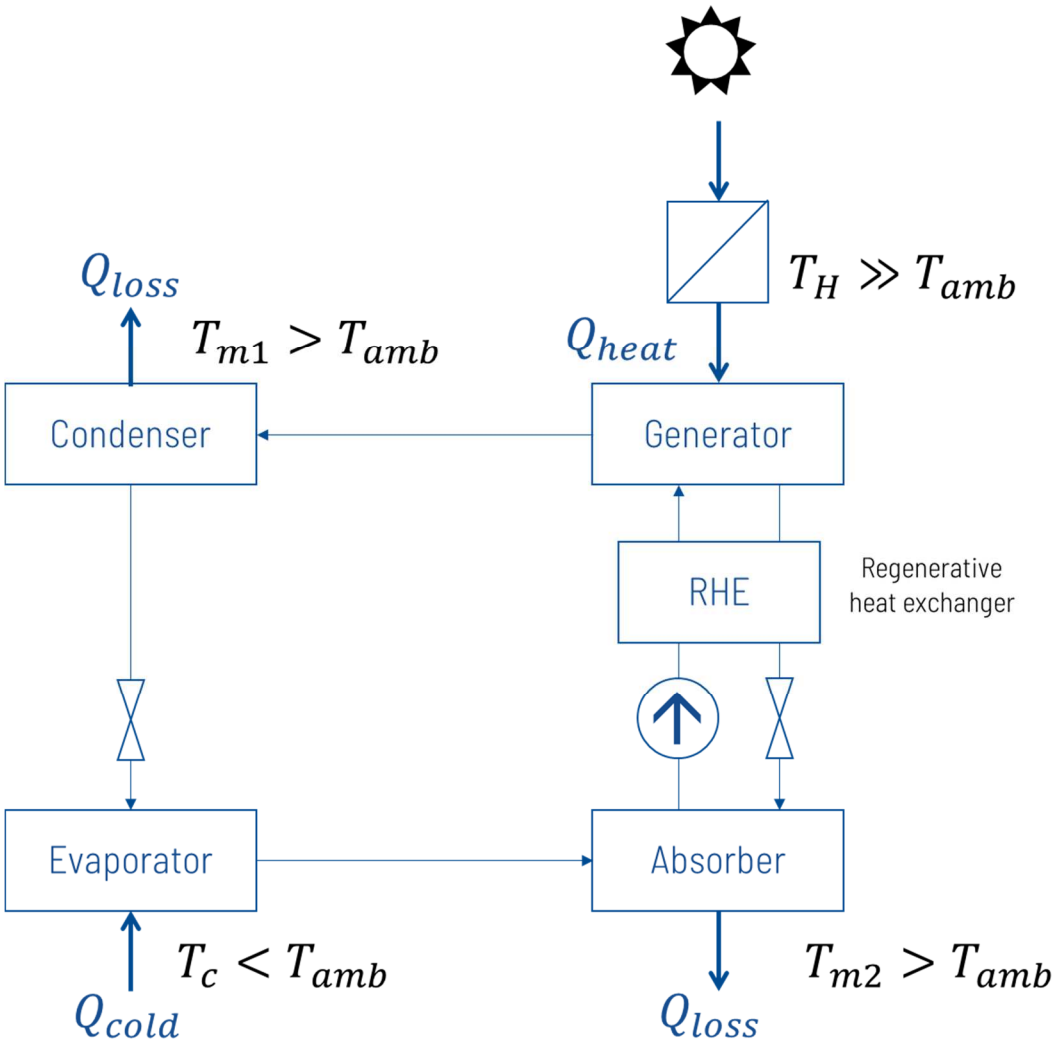

Fig. 3.4 Single-stage solar absorption chiller cycle scheme.

Just like in the conventional compression chiller, the cooling effect emerges during the low-temperature evaporation of a refrigerant mixture at a specified pressure in the evaporator section. The outflowing refrigerant vapour is then captured by sorbent in the absorber component operating at the same pressure. In the absorption chillers, two basic groups of solution streams can be differentiated: rich/strong and lean/weak solution. Rich solution means always a high concentration of refrigerant in the refrigerant-absorbent solution, while a lean solution is a solution of low concentration of refrigerant. The absorption process requires external cooling. The pressure of the mixture is then increased by a solution pump consuming positively less energy than a compressor in conventional cycles [26]. The rich solution flows then into the generator section. Since refrigerant is more volatile than sorbent, it separates from the solution as a consequence of heat input. The rich solution becomes lean and the refrigerant

vapour stream is generated. This stream is then condensed in the condenser with simultaneous waste heat generation. The subcooled condensate is throttled to evaporation pressure and again evaporated, guaranteeing constant cooling energy delivery.

Two working fluid pairs are predominant on the absorption chiller market: H_2O-LiBr and NH_3-H_2O. Chillers with water-lithium bromide mixture require a heat input at a temperature level of 70-90°C, while the ammonia-water cycles demand even 140-160°C. On the other hand, only ammonia-water chiller can deliver cooling energy at a temperature level below 0°C [28][25]. Absorption chillers can be single-, double- or multistage, Single-stage chillers base on a single set of absorber, generator, evaporator and condenser. A single stage H_2O-LiBr chiller requires a heat source at 70-90°C temperature level and therefore it is possible to apply the least expensive flat plate collectors. The average COP of single stage absorption chillers is of the order 0.7. According to the latest review papers [25], it is stated that in consequence of multiple and detailed analyses of single-stage lithium bromide chillers, this can be now considered a mature technology. It is expected to have a real perspective for further building market penetration [31]. Double-effect absorption chillers can rest on two generators and two regenerative heat exchangers. This design is approximately presented in Fig. 3.5.

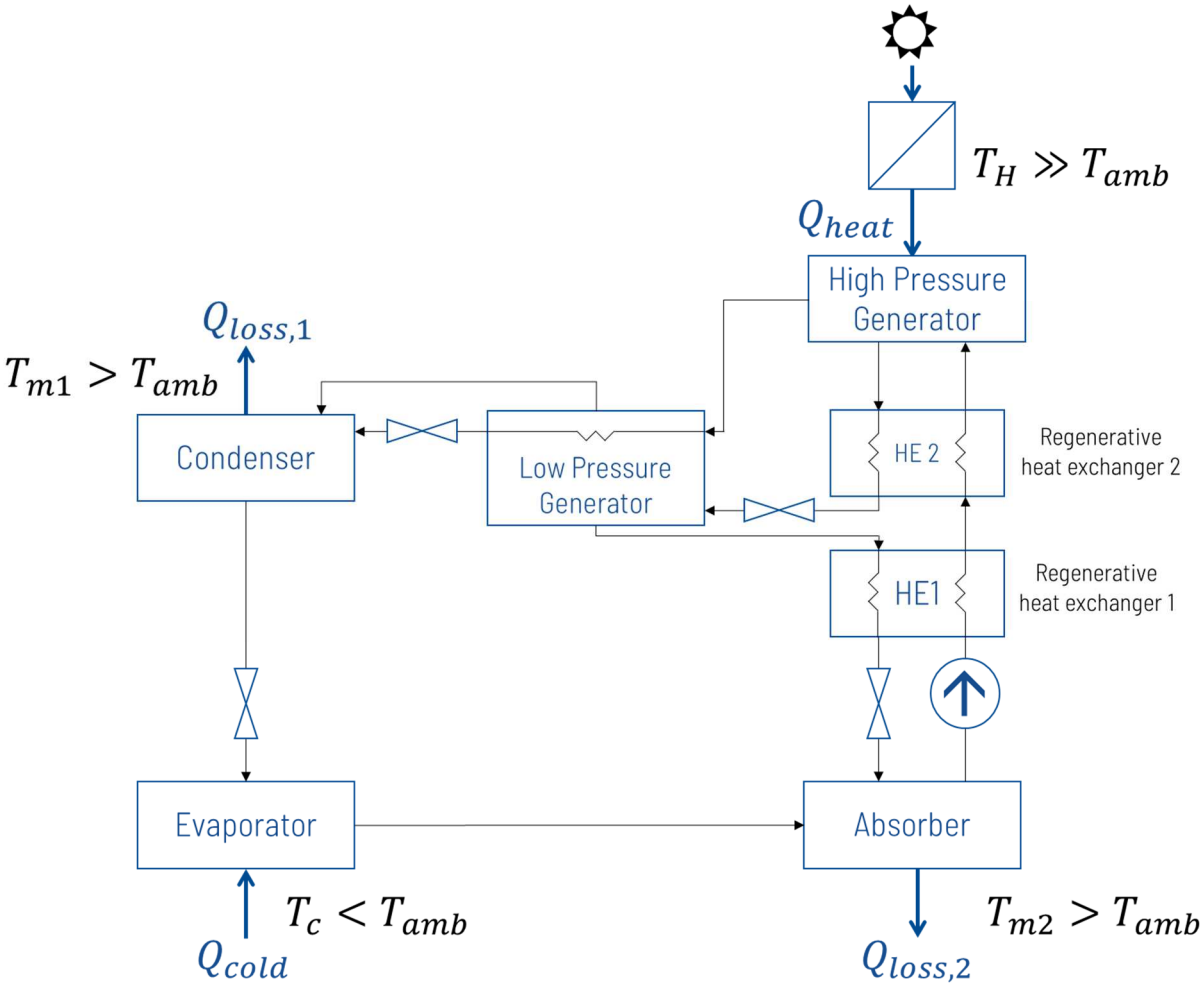

Fig. 3.5 Scheme of a double-effect absorption chiller.

The vapours from high pressure generator are acting as driving heat for the low pressure generator section. Another admissible design (discussed in [32]) of a double-effect absorption chiller includes two desorbers and two condensers working at variable temperature and pressure levels. Waste heat from the high-pressure condenser can be used as driving heat by the low-pressure desorber. The high pressure generator requires to be fed by a hot stream at a temperature level of 155-185°C (if lithium bromide chiller is considered). According to this requirement, the use of evacuated tube or concentrating collectors is inevitable. The typical COP for double-stage chiller equals 1.2. Triple-stage chillers would require a heat source above 200°C, which is possible only using concentrating collectors. According to estimates, the COP of a triple-stage absorption refrigeration cycle could equal 1.7. [26,33]

From the time-dependent point of view, solar absorption systems can work under continuous or intermittent operation modes [34]. The continuous cycle means the simultaneous generation of refrigerant vapours and of cooling energy. This type of cycle requires a complete set of chiller components. However, the cooling energy is delivered only during the day and energy storage

can be necessary. An absorption chiller that is working intermittently utilizes solar heat during the day to generate pressurized vapours, while cold is generated at night. The components of such system are bi-functional: the generator plays the role of the absorber in the night, while the condenser becomes an evaporator. Similarly, since cooling happens only during the night, storage od heat and/or cold becomes inevitable. Assuming a COP of a continuously working absorption chiller equal to 0.7 (single-stage unit), that of an intermittent unit is lower and is equal to about 0.45. On the other hand, its advantage might be observed in the fact that it requires fewer components to operate. Nonetheless, the continuous working absorption chillers are definitely more often analysed in current research [34].

In the literature, absorption chillers are more often analysed in simulation works rather than with an experimental approach [35,36]. Ammonia-water and water-lithium bromide are usually considered as possible working pairs. However, available research reviews report also following working fluid pairs: lithium nitrate-ammonia, methanol-TEGDME, TFE-TEGDME or sodium thiocyanate-ammonia [35]. The investigated chillers are driven by heat from flat plate collectors, evacuated tube, parabolic trough or Fresnel collectors [35,37]. The condenser and absorber are usually cooled by water using a cooling tower, however direct air-cooled condensers are also present [26].

The performance of absorption chillers is simulated over a wide range of thermodynamic working parameters. The lowest temperature of the working fluid driving the generator that was found in the literature equalled 50°C. The estimated COP for this conditions equalled 0.2 [38]. The lowest evaporation temperature was experimentally obtained in a 1 kW Sodium thiocyanate-ammonia chiller and equalled -20°C[39].

The scientific literature offers many examples of energy, exergy and thermo-economic analyses of solar absorption chillers of variable cooling power and working under various climate conditions. A vast number of parametric studies can already support designers and operators of solar absorption chillers. Taking into account a strong dependence on external conditions, dynamic analyses were also performed. Research on solar absorption chillers has been collected and summarized by many review articles, e.g. in [21,26,37,40]. Numerous investigations confirm the statement about maturity of the technology.

Intermittent availability of the solar energy source calls for the use of energy storage. Apart from that, the possibility of a back-up energy source is also often considered. However, it has not been concluded yet whether a back-up gas heater or a back-up compression chiller is more convenient [41].

Many authors present also results of the economic assessment of absorption cooling technology [42]. As marked in the 3.1 section, the cost of a chiller depends on cooling power installed but also on its complexity (single-stage, double-stage). Authors in [21] reported typical prices for solar assisted double-effect and single-effect absorption chillers as 1200 €/kW and 1000 €/kW, respectively. According to that source, the cost of solar collectors represents 60-75% of the purchase equipment cost.

Research collected in [26] informs that the typical average solar collector field required for a single-stage solar absorption chiller equals 4.67 m^2/kW of cold, with an average volume of installed heat storage of 0.21 m^3/kW. The typical COP indicator equals 0.68 and the mean temperature of the heat source reaches 88.5°C.

3.4 Solar adsorption chillers

Adsorption units might become an interesting alternative to absorption units because they enable heat regeneration at a very wide range of heat source temperatures: from 50°C to even 500°C [43]. Fundamentally, a cooling adsorption cycle is built up by 2 phases. One of them bases on vapour adsorption process in the (usually) water-cooled adsorber. It is connected with the refrigerant evaporation in the evaporator section, thus achieving the cooling effect. The base element of an adsorption system is a porous solid having a large surface area. When a vapour particle contacts the surface it is adsorbed, which results from Van der Waals and electrostatic forces. The process is exothermal and fully reversible. In the second phase, the generation of refrigerant vapours occurs. The adsorbent requires a heat input to regenerate and to release the adsorbed vapours [22, 23]. The solid adsorbent cannot be transported, and therefore a switchable batch arrangement is adopted (Fig. 3.6), where each of the two adsorbent beds plays interchangeably the role of generator or adsorber. Consequently, adsorption chiller always works in intermittent mode.

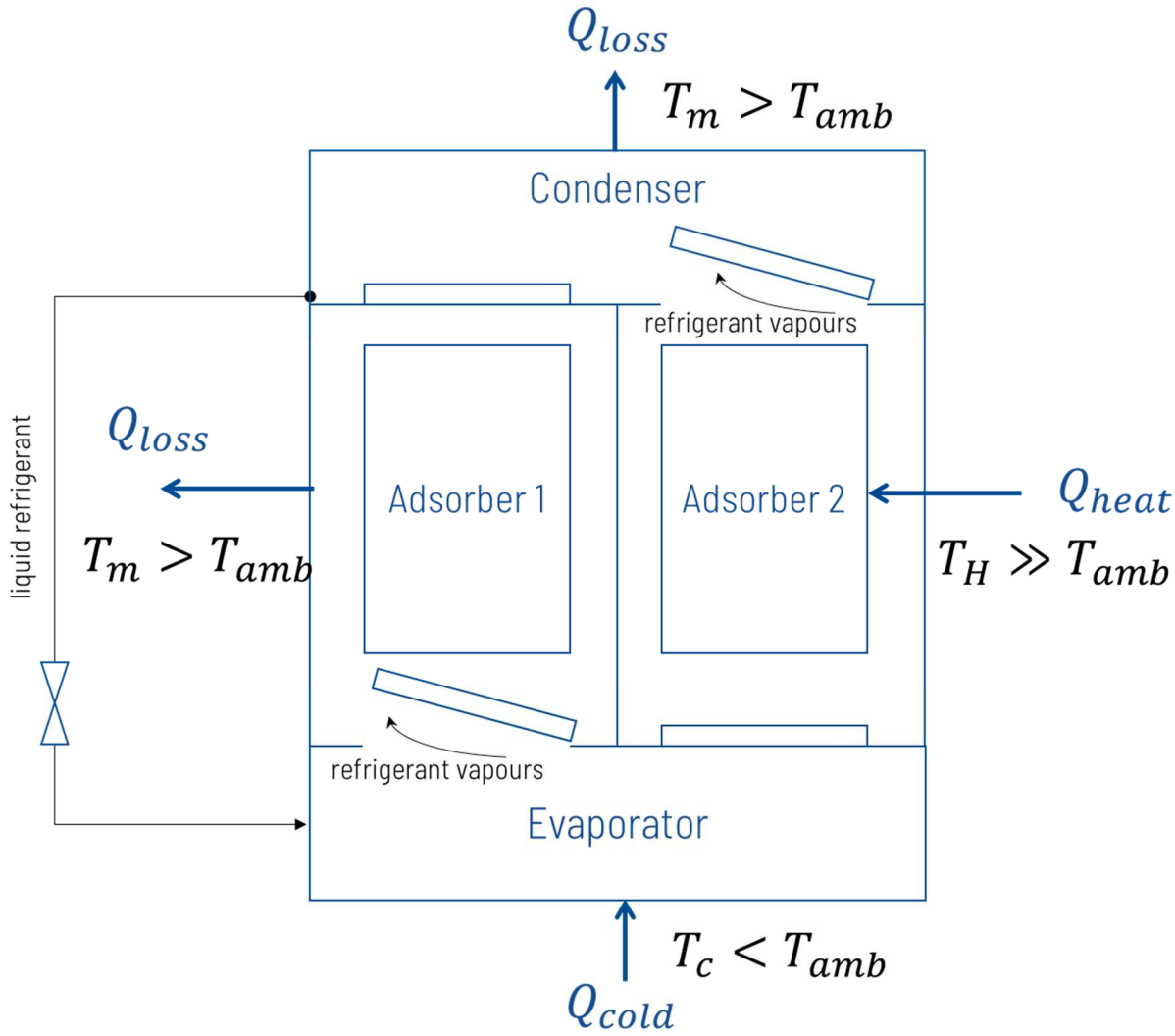

Fig. 3.6 Schematic of an adsorption chiller during one phase (Adsorber 1 at adsorption phase, Adsorber 2 at desorption phase).

The most common working pair in an adsorption chiller is silica gel – water, but there are also other pairs that meet the requirements of large adsorption ability, compatibility with the refrigerant, isothermal behaviour. The working pairs under consideration are: activated carbon-methanol, activated carbon – ammonia, zeolite – water, metal chloride – ammonia, metal oxides and oxygen [45].

The possibility of being driven by a low-temperature heat source is an evident advantage of the adsorption units and make it possible to integrate the device with a low-cost flat plate solar collector, but also make adsorption chillers potential candidates to become integrated with a district heat network. Apart from that, adsorption chillers are characterized by simple control, lack of vibrations, low operational costs, no corrosion problems, resistance to shakes and change of position. The last features make adsorption chillers attractive to be used in means of transport [45].

Negative aspects of adsorption chillers are their low coefficient of performance (even below 0.4) and low specific cooling power. However, it is said that these disadvantages could be eliminated if the heat and mass transport processes in the adsorber were intensified, if the adsorption properties of working pairs were enhanced and if the cycle heat management were improved. Striving to meet these challenges, the majority of available research in this area focuses on finding possible new working pairs adsorbent-refrigerant but also on simulation models investigating possible cooperation of these working pairs with adsorption chiller.[26,43]

Again, the research reviewed in [7] reports a typical average solar collector field installed for solar adsorption chiller as 11.17 m^2/kW, with an average heat storage volume of 0.36 m^3/kW and an average COP equal to 0.4.

3.5 Energy storage

If a solar energy integrated system is considered, one has to take into account that heating or cooling demand will not always follow the driving energy availability. For this reason, thermal energy storage becomes necessary.

If the basic theory is considered, the storage process requires three parts: charging, storing and discharging. If the energy is accumulated in a form of thermal energy (heat or cold), the storage process is called thermal energy storage (TES). TES is a widely recognized method allowing for effective thermal energy usage. It helps to mitigate the negative effects of mismatches occurring between energy supply and energy demand periods. Hence, storage is most profitable in systems basing on energy resources of intermittent availability (in the case of this research: solar energy) or on waste heat recovery. TES should be acknowledged both by energy suppliers and by the end-users. On one hand, it reduces the peak electricity and thermal energy demand which helps to compensate the peak-valley demands differences. On the other hand, end-consumers are allowed to buy off-peak energy at convenient cost-rate and utilize it (e.g. converted in an air-conditioning unit into cool energy) in the peak-demand time. The same, installing thermal energy storage means lower exploitation costs, but also a possibility to install smaller energy conversion units [46].

It is possible to think of thermal energy storage in both the hot and cold side of every system. Cold thermal energy storage (CTES) should be understood as storing the cool energy (e.g. from a chiller). Cool energy refers to the energy of a stream or of a volume of fluid that is below ambient temperature. To avoid an unfavourable discontinuous operation of a chiller when the cooling demand lowers, cold storage may be recommended which can allow long continuous

working periods of the machine with long term performance closer to nominal [47]. CTES is then very important for load-levelling issues. The implementation of a storage system would enable the decoupling between the cold energy generation and the user requirements, allowing to manage the energy consumption during the day and to optimize the chiller power output, by thus leading to an increase in the energy efficiency rating. What is more, CTES is also important for food preservation processes, where cool energy stored for a longer time is released rapidly in a short period.[48]

From the classification point of view, energy storage can be short-term (few-hours or few-days accumulation) or long-term (seasonal storage) [47]. TES can be realized in the form of the sensible heat (connected to thermal capacity and temperature rise or drop of a liquid or solid substance), the latent heat (phase change process at an almost constant temperature, connected to the latent heat of given substance called phase change material), or by a chemical reaction.

There are already several forms of energy storage investigated and accepted for solar cooling applications. Three basic forms result from the literature sources. The most common method is to store the useful heat from the solar collector in a tank placed as a buffer between the solar collector field and generator of the sorption chiller. As mentioned above, it is also possible to store cooling energy. The widespread solution is to install a chilled water tank between the evaporator section and cold distribution system. A very different type of storage is the refrigerant storage. Basing on the example of ammonia-water single stage absorption chiller liquid ammonia, lean or rich solutions can be stored. During the daily operation, the container for the ammonia-water rich solution is empty and it is filled during the night pause. When the night is going to an end, liquid ammonia and lean solution containers are emptied and the rich solution container is fully filled, ready for the daily operation [34].

The available literature does already provide a list of suggested features and properties that a good storage material should possess. It should be characterized by a high thermal heat capacity, high conductivity and low unit cost. Phase change material should be also chosen in such a way that the melting temperature fits in the temperature range of the chiller operation, the material is not corrosive and not harmful. If latent storage is considered, available research focuses usually on solar heat accumulation rather than cold storage (it might result from the fact that the heat source is of a more intermittent nature, and since PCM materials are more expensive, the payback time for storage at the hot side is shorter; hot water storage increases the operational time as well and the same, the chiller size could be reduced; another reason is that a wider choice of PCM materials with phase change temperature above 80°C and higher

availability might cause lower prices of the material). However, since the technology is still at the development phase, a lot of new reviews and research works are emerging [46,49–52].

Looking at all the types of energy storage foreseen for solar heating and cooling technologies, it is understandable that the majority of present investigations takes the thread of the selection of proper storage material, storage tank construction and its latter cooperation with the system. A separate, though the important topic is the temperature stratification of material inside tank and such research is very often presented by the scientists coping with computational fluid dynamics analyses. [36]

Moreover, the literature is also rich with optimization analyses performed for storage components. The objectives of optimization are usually: maximization of the installation solar fraction, of the storage efficiency, of primary energy savings, of life-cycle savings, and/or minimization of the capital investment costs and the payback time. The optimization parameters are variable: type of the tank and its configuration, type of the solar collector, solar collector area, solar collector slope, working fluid flow rates, temperature levels in the heat exchangers, chiller cooling power, tank volume or storage material [36].

Although many investigations have already been conducted, there is still no unequivocal statement on the general influence of storage units number increase on the country's energy system because simulation or experimental research is usually conducted at the level of single residential or office installations.

3.6 Hybrid heating and cooling

The hybrid heating and cooling nodes are said to be the core technology investigated in this thesis. It is, therefore, of great importance to introduce the main definitions present in the literature. This will enable to discuss and confront the technology analysed in this work with installations already proposed and presented in the literature sources. This review will also signal possible control approaches for such systems.

The first group of hybrid systems covers solar energy driven cycles that provide cooling energy and heat, while the utilization of district heat is not considered [53]. Studies over hybrid solar-driven systems have been emerging already since the 20th century, however, their effective commercialization has been inhibited by the lack of standardized test methods and effectiveness calculation. Scientists claim that because of this lack, hybrid solar systems cannot be fully objective and reliably presented to become competitive with conventional gas boilers or compression chillers [54]. Another family of hybrid nodes assumes that solar heat is used solely to drive a thermal chiller or to supplement the district heat to provide central heating or prepare

domestic hot water [55]. Hybrid nodes are also understood as systems where an absorption chiller is supported by compression chiller or where waste heat from a separate process becomes the driving energy for the sorption chiller [56]. Hybridization in the heating and cooling substation system can also concern the storage system. Authors in [57] performed an exergo-economic analysis over a hybrid storage absorption refrigeration cycle integrating three types of storage: cold storage, weak and rich solution storages.

In the majority of cases, control of the heat sub-station is aimed at providing the end consumer with an energy stream at the desired temperature level. This last is controlled and usually adapted to ambient temperature [58]. Apart from that, it is also possible to propose smart management solutions. For instance, authors in [59] suggest the implementation of a control algorithm taking care that the electric energy-driven devices in the substation are used during lower electricity price tariff periods.

What is important, in many articles authors underline that systems integrating energy sources of variable availability: e.g. stable district heat with an intermittent renewable energy source, are facing serious challenges connected with control and management system. By integrating renewable energy with conventional energy, one should deal with variable characteristics, operational costs, and technical limits. [60,61]

3.7 Exergy, exergo-economic and exergo-environmental analyses of solar assisted heating and/or cooling systems

According to the scope presented in Chapter 2, in this work exergy is used as a proper measure allowing for evaluation of the usefulness of natural resources; next to the energy analysis, an exergy-based evaluation will be proposed to assess the installations. Hence, it has been verified what achievements have already been made on that topic and are documented in the literature.

Sola- assisted heating and/or cooling installations have been widely analysed in terms of their techno-economic feasibility [35,62–66]. Moreover, exergy analyses and cumulative impact assessment analyses keep appearing more often as a research approach. They enable to differentiate between energy quality and useful effects but also to appreciate the cumulative effect of the system operation. It is important to realize and to remember that solar-driven systems rely on an exergy source with time-dependent availability. Moreover, these are cycles where the useful output (cryogenic exergy or exergy of cold) is an effect of processes with inevitable exergy destruction in preceding components. It is of high importance to properly define the exergy streams and the boundary conditions. Only in that way it is possible to obtain

correct operational indicators that could be taken into account in potential subsequent diagnostic cumulative impact assessment.

The definition of exergy assigned to incoming solar radiation has been a topic for several treatises with variable conclusions [67,68]. Despite the lack of standardized definition for driving exergy, scientists have already delivered numerous papers on exergy analysis and exergy-based cumulative assessment of solar integrated heating and/or cooling cycles. As an example, researchers in [69] performed an exergy and life cycle analysis of a solar system for space heating, cooling and domestic hot water production. Already in the assumption phase, they stated that since almost all of the environmental impacts of the renewable energies are associated with the manufacturing process, the environmental impacts were analysed only at the manufacturing stage. In [70] authors performed an energy and exergy analysis of a 10 kW ammonia-water chiller and found that the cycle is more thermodynamically effective if the cooling system is using low-temperature heat sources rather than high-temperature heat sources. The highest exergy destructions were discovered in the absorber and generator (around 76%). An exergoeconomic analysis of a solar driven hybrid storage absorption cooling cycle was done by researchers in [57]. The exergo-economic analysis was here performed to compare the components in terms of the initial capital investment costs and the costs of irreversibilities. Generator and evaporator are mostly responsible for exergy destructions. However, the highest exergo-economic cost is allocated to the evaporator and the solution heat exchanger. Authors noticed the improvement potential in optimizing the design variables of the system. Authors in [71] proposed a tool allowing for minimization of the total cost and the environmental impact of solar-assisted absorption cooling systems. According to the findings it is recommended to increase the number of solar collectors installed. Increase of the solar fraction ensures the reduction of environmental impact, although the cost allocation caused by the manufacturing process for these components is the highest.

According to these sources, the construction and decommissioning phases have a meaningful share while generally analysing the ecological impact and economic indicators when dealing with cold obtained from a solar chiller. Nevertheless, one should not forget about the significance of the operational phase.

3.8 Literature review – conclusions

The review on the current state of knowledge about solar thermal cooling and/or heating system confirms that this technology is becoming mature and is still the object of scientific investigations. Researchers are still today revealing emerging challenges and areas for further

research. The first obstacle negatively affecting the opinion on sorption technology is its high investment cost compared with compression units. Additionally, the renewable energy source of intermittent availability remains a constant challenge and motivates to establish rules for smart control and management of the system performance. Storage systems are also expensive, so the optimization aim should concern the proper selection of volume and storage material. Researchers indicate that the analysis of conventional compression cycles integrated with thermal chillers and storage systems is needed, so is the optimization under variable meteorological conditions. Although analyses of solar-driven systems performance under moderate and poor radiation conditions are already present in the literature (both for solar sorption cycles [72] and for tri-generation systems [73]), they are most certainly in minority and none is presenting an impact assessment similar to that presented, modelled and analysed in this thesis. Conclusions from this type of analysis could be essential to decide whether solar -energy based thermal comfort units can have an energetic and economic rationale; not only under Polish meteorological conditions but also in the Polish economic environment. It was extensively repeated and concluded in [25] that the process of adoption of solar heating and cooling technologies is constantly counterbalanced by their complexity and high investment costs. The majority of existing installations are still at demo phase (with no standardized incentives programme) or are connected to a research project.

What is more, from the perspective of current discussions and environmental limitations, the idea of promoting hybrid poli-generation heating and cooling substations appears to be fully motivated and the sooner it becomes recognized the better. Especially, if one is reminded that the early stage of every technology implementation can involve a high transaction, information, and risk costs [74] which can only be eliminated once the technology is widely accepted and implemented.

Chapter 4. METHODOLOGY OF ANALYSIS

This chapter presents the core analytical methods used in the research. The 1st law of thermodynamics is always the starting point while preparing a simulation model of a single component or of the whole system. Energy and mass conservation laws are important tools for thermal processes investigation and as such are commonly applied in the engineering practice. However, in order to be able to properly assess the excellence of the processes, it is essential to introduce tools allowing for the recognition of losses and for the introduction of quality indicators. Such an assessment helps to improve the effectiveness and the rationalization of resources management. Therefore, it seems vital to introduce the exergy-based analysis which explicitly addresses these issues. Following that, the exergo-economic analysis combines exergy and economics: it is a composition loop that enables assessing the economic performance of a system and allows the evaluation of the progressive buildup of the cost of products along the process.

The general concept of the methodology is given here, while details and assumptions adapted for modelling tasks will be described in the specific following Chapter 5 and Chapter 6.

4.1 Energy-based analysis

Energy and mass conservation laws are mutually dependant as it is indicated by Einstein theorem presented by Eq. (4-1):

$$\Delta E_{sys} = \Delta m_{sys} \cdot c^2 \tag{4-1}$$

This means that the increase of mass in the system Δm_{sys} depends on the energy increase ΔE_{sys} and vice versa. One should, however, distinguish between mass and the amount of substance. Mass is a property of matter deciding about inertia and gravity interaction between bodies. The unit of mass in the International System of Units (SI) is kilogram (kg). Amount of the substance can be described by mass or weight. The unit for the mass of a substance can be understood as such an amount of a substance for which the normal mass equals 1 kg. Since the increases of energy present in thermal engineering practice have an insignificant influence on the mass, there is only a conceptual difference between mass and amount of substance and they have the same numerical value. [75]

The results of investigations of thermodynamic processes are usually presented by means of a balance. According to previous considerations, a balance resulting from the conservation of the amount of substance law is called interchangeably a substance balance or a mass balance. Balancing requires a clear definition of the control volume or balance boundary. According to the substance conservation law, the substance balances can be separately defined for each substance in a physical process (specifically important for further investigation of H_2O-LiBr and NH_3-H_2O absorption chillers) or for each chemical element in a chemical process. If an exemplary system is closed by a balance boundary like in Fig. 4.1, the mass (substance) balance for the *i*-th substance integrated over a time step can be written like in Eq. (4-2).

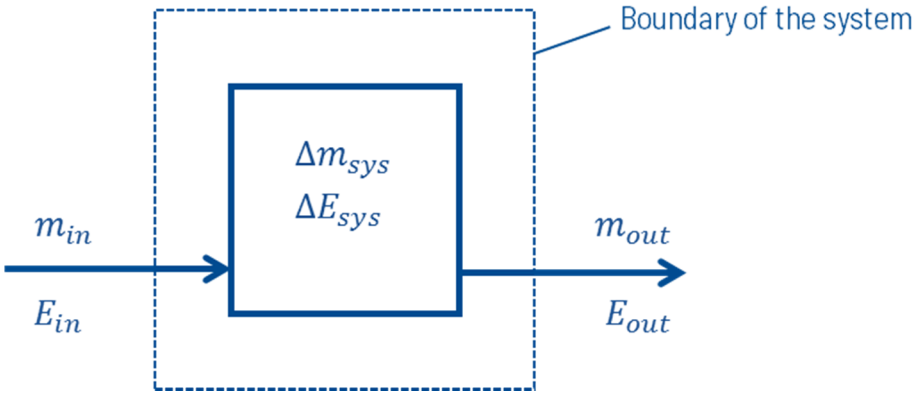

Fig. 4.1 System and its balance boundary

$$m_{in,i} = \Delta m_{sys,i} + m_{out,i} \tag{4-2}$$

In thermal engineering applications, steady-state processes play a significant role. The mass balance is written for the i-th substance in a system working under steady-state conditions where no internal increase of mass occurs ($\Delta m_{sys,i} = 0$) is presented by Eq. (4-3):

$$m_{in,i} = m_{out,i} \tag{4-3}$$

Similar considerations can be conducted for energy. Energy is the property of matter and is directly associated with matter or material flows. 1st Law of Thermodynamics is a special case of energy conservation rule. Joule, Kelvin and Clausius were the first to investigate the rules of energy conservation and their conclusions were then interpreted by Helmholtz in 1847. He stated that in an isolated system all forms of energy are equivalent and no amount of energy in one form can disappear without the simultaneous appearance of the same amount of energy in a different form. In other words: energy is conserved: it can neither be created nor destroyed, but it can be converted in a different form. The 1st Law of Thermodynamics states the equivalence of heat (*Q*) and work (*W*) and the conservation of energy of an isolated system.

Mathematically, the 1st Law of Thermodynamics can be expressed as a form of the energy balance like in Eq. (4-4):

$$Q = \Delta U + \mathrm{W} \tag{4-4}$$

The energy balance results from the energy conservation law. The energy balance for a system like in Fig. 4.1 is written in Eq. (4-5):

$$E_{in} = \Delta E_{sys} + E_{out} \tag{4-5}$$

The energy of the system E_{sys} includes, macroscopically, kinetic energy E_k, potential energy E_p and internal energy *U*. If a system is working under a steady state, the energy increase becomes zero ($\Delta E_{sys} = 0$).

$$E_{in} = E_{out} \tag{4-6}$$

It shows that a machine working in the steady state has to be constantly driven by energy E_{in} and, as a further conclusion, it implies that the creation of a perpetual motion machine of the first kind is not possible [75,76].

The general Eq. (4-6) can be rewritten for a system where a flow of matter occurs, heat is utilized and transferred and where the input energy is also converted into internal power. This is presented in Eq. (4-7):

$$\dot{m}_{in} h_{in} + \dot{Q}_{in} = \dot{m}_{out} h_{out} + \dot{Q}_{out} + N_i \tag{4-7}$$

Where $\dot{m}$ is mass flow rate (kg/s), h is enthalpy (kJ/kg), $\dot{Q}$ means heat rate (kW), while N_i stands for internal energy rate (internal power, kW). Subscripts *in* and *out* are again associated with inlet or outlet to/from analysed system. Enthalpy (h) is an energy transfer mode specific for a stream of matter. In practical calculations, energy balances for an open system operating at steady-state are prepared for the surplus of enthalpy above the reference state. It is symbolically represented by Eq. (4-8):

$$h = h(p, T) - h_0(p_0, T_0) \tag{4-8}$$

Where p and T are pressure and temperature and subscript *0* is connected with reference system properties. Enthalpy is built up by two elements: physical enthalpy and chemical enthalpy.

The approach to the reference state as well as to the physical and chemical part of the enthalpy while analysing absorption chillers is specifically important. The assumptions will be described in the devoted sections (5.6.2 and 6.3).

For the energy-based analysis, a typical effectiveness indicator is energy efficiency (η_E). It is defined as a ratio of useful product expressed in energy units (E_P) to the energy input (E_F) and is visualized in Eq. (4-9).

$$\eta_E = \frac{E_P}{E_F} \tag{4-9}$$

4.2 Exergy-based analysis

Although energy analysis is widely used for the purpose of modelling and assessment of energy conversion systems, it does not provide information on the specific location of thermodynamic inefficiencies in the system; moreover, it does not recognize differences in the quality of energy. The irreversibilities burdening a thermodynamic process can be investigated by the means of the 2nd Law of Thermodynamics. The overall irreversibility is proportional to the total entropy generation. Entropy generation is a direct measure of losing the potential to perform work [76]. This potential expresses the thermodynamic value of an energy carrier and it is represented by exergy.

4.2.1 2nd Law of Thermodynamics

The 2nd Law of Thermodynamics is one of the fundamental laws of nature indicating the direction of conversion processes. The definition of the 2nd law was addressed by many scientists. One of the first was Rudolf Clausius with his statement that "*Heat can never pass from a colder to a warmer body without some other change, connected therewith, occurring at the same time*"[77]. Further Kelvin-Planck's statement said that "*It is impossible to devise a cyclically operating device, the sole effect of which is to absorb energy in the form of heat from a single thermal reservoir and to deliver an equivalent amount of work*"[78]. Additionally, Schmidt stated that "*it is impossible to reverse a thermodynamic conversion process in which friction occurs*"[75].

The 2nd Law of Thermodynamics does not only present the only possible direction of thermodynamic conversion processes but also declares the need of two separate heat sources for the process to happen; moreover, it allows to determine the equilibrium conditions to which the system is striving to. It is especially important while considering the theoretical maximum effectiveness of processes. Thermodynamic optimization based on the 2nd Law of Thermodynamics is an important tool needed also for the management of natural resources.

4.2.2 Environment

Every system operates interacting with the surroundings. The surroundings are not a part of the system. The Environment is a specific part of surroundings, the properties of which remain constant despite the processes occurring in the system. The conditions of the environment must obligatorily be defined in order to know the reference state of equilibrium to which the system is striving, but also to know the reference state in relation to which the system still has the potential to perform work [79].

According to generalized models, the environment is free of irreversibilities and its exergy equals 0. It is modelled as a system, with uniform temperature (T_0) and pressure (p_0). Typically, the values are taken as ambient conditions. No chemical reactions (apart from equilibrium reactions) can happen between the chemical components of the environment. The environment is said to be composed by the common substances that exist in the atmosphere, in the oceans and in the crust of the Earth. If there is any difference of temperature, pressure, chemical composition, but also of velocity or elevation of the system in relation to the conditions present in the environment, it is said that the system is able to perform work. The smaller is the difference, the smaller is the potential to develop work and if the system finds itself in equilibrium with the environment, it lands in the so-called *dead state* (thermo-mechanical equilibrium). In a *restricted dead state* only mechanical and temperature equilibrium are satisfied (thermo-chemical equilibrium). [79]

Understanding the definition of the environment is very important in the present case because in this work one of the systems under consideration converts energy from a very-high-temperature heat source into a refrigeration useful effect with interaction with the surroundings. The amount of driving energy depends in our case on the ambient conditions which are dictated by the climate. Thus, the uniform temperature (T_0) and pressure (p_0) are always equal to the changing ambient temperature and ambient pressure.

4.2.3 Exergy

According to definition present in the literature, exergy is “the maximum theoretical useful work obtainable from a thermal system as it is brought into thermodynamic equilibrium with the environment while interacting with the environment only”[80]. It measures the quality of energy, and it accounts for the differences between work and heat. Unlike energy, exergy is not conserved, but it informs if there is a potential to improve the process, to minimize exergy destruction. Exergy destruction is defined by the Gouy-Stodola theorem ($\Delta B = T_0 \sum \Delta S$) [75].

The exergy of every system includes physical exergy (b_{ph}), chemical exergy (b_{ch}), potential exergy (b_{pot}) and kinetic exergy (b_{kin}). The same rule applies for the exergy of a material stream. It is shown in Eq. (4-10)

$$b_{tot} = b_{ph} + b_{ch} + b_{kin} + b_{pot} \tag{4-10}$$

Although in some components of the analysed in this thesis, like valves, a steady state conversion from enthalpy to kinetic energy happens, it is generally assumed that the systems are at rest. Hence the kinetic exergy is neglected ((b_{kin}=0). Following the assumption of non-elevated components the potential exergy contributions is also zero ($b_{pot} = 0$).

The physical exergy is the maximum theoretical work that is possible to perform by a system moving from the initial state (T, p) to a restricted dead state (T_0, p_0). Consequently, chemical exergy is the amount of maximum theoretical work obtainable while passing from the restricted dead state to complete dead state conditions. The specific physical exergy of a stream can be calculated from Eq. (4-11):

$$b_{ph} = (h - h_0) - T_0(s - s_0) \tag{4-11}$$

Where s means entropy (kJ/kgK). Calculation of the specific chemical exergy demands knowledge of the standard chemical exergies of substances present in the environment. However, the natural environment of the humankind is never in the equilibrium. Therefore, the definition of Exergy Reference Environment (ExRE) was needed and addressed by scientists. Standard chemical exergies of substances ($\bar{b}_{ch,k}$) were then estimated in relation to the ExRE [81–83]. The specific chemical exergy for gas mixtures and ideal liquid solutions can be found applying Eq. (4-12):

$$b_{ch} = \sum_{k=1}^{N} x_k \bar{b}_{ch,k} + \bar{R}T_0 \sum_{k=1}^{N} x_k \ln(x_k) \tag{4-12}$$

Where the additional symbols are: x_k meaning concentration of k-a th substance in the mixture and $\bar{R}$ is the average gas constant. The approach to the change of chemical exergy of streams within the balance boundary of the analysed systems will be discussed in following chapters.

The exergy rate of j-th flow rate ($\dot{B}_j$) can be then found from Eq.(4-13).

$$\dot{B}_j = \dot{m}_j\left(b_{ph,j} + b_{ch,j}\right) \tag{4-13}$$

Furthermore, a specific exergy definition must be here recalled as very important for solar energy driven systems. Namely: the exergy of solar radiation. The question of how to define

the ability to perform work by solar radiation reaching a given surface has already been raised in several research works. The approaches have been collected by the author in [17].

One should be reminded that exergy, like enthalpy or entropy, is a function of state and thus a property of matter. Hence, instead of solar radiation exergy, one should rather speak about exergy change of radiation source. Nevertheless, the "solar radiation exergy" term is more common in the literature as an accepted form of concept shortcut. It will be also used in this work.

Following the literature review, there is a trend to define solar radiation exergy relating to black-body radiation [67,84,85], taking into consideration spectral radiation distribution [86], and declaring separately exergy for direct and diffuse radiation [87,88].

Szargut [84] and Petela [67,84,85] were among the firsts to present a method to calculate exergy of undiluted thermal radiation. It can be recalled with an example of the ideally reversible thermodynamic cycle. It is assumed the cycle is driven by an energy E_s coming from a source (e.g. Sun) of equivalent black-body temperature T_s (5780 K can be assumed for the Sun). Being driven by E_s, the cycle can perform the maximum work W_{max}. This maximum work is equal to source exergy of (solar) radiation B_s. At the same time, the cycle is losing heat to the ambient Q_0 and is emitting radiation E_e. The exergy balance for this ideal cycle is given by Eq. (4-14).

$$\dot{E}_s = \dot{W}_{max} + \dot{Q}_0 + \dot{E}_e \tag{4-14}$$

Knowing that maximum work is equal to the source exergy, Eq. 11 is transformed into Eq. (4-15).

$$\dot{E}_s = \dot{B}_s + \dot{Q}_0 + \dot{E}_e \tag{4-15}$$

In [67,84,85] Petela delivered a complete procedure to define the entropy of thermal radiation. He introduced the ψ ratio for the maximum conversion efficiency indicating the maximum work obtainable from radiation energy. Its formula is given in Eq. (4-16). It is commonly used to evaluate the exergy value of solar radiation:

$$\psi = \frac{\dot{B}_s}{G} = \left(1 - \frac{4}{3}\frac{T_0}{T_s} + \frac{1}{3}\frac{T_0^4}{T_s^4}\right) \tag{4-16}$$

Where G can be treated as incoming solar radiation (G_s) or, for cases other than solar, as thermal radiation energy following Stefan-Boltzmann's law (σT_s^4).

This formula was confirmed by other researchers (Press [89]; Landsberg [90]).

In 1964 Spanner independently published a formula to calculate the exergy of direct radiation [91]. It was partially in line with Petela's considerations. However, it was assuming no emission

from the theoretical thermodynamic cycle (E_e=0). Spanner obtained the formula presented in Eq. (4-17).

$$\dot{B}_S = \sigma {T_s}^4 \left(1 - \frac{4}{3}\frac{T_0}{T_s}\right) \tag{4-17}$$

20 years later, with different assumptions, Jeter was proving that the Carnot cycle analysis can be utilized for the purpose of solar radiation exergy calculation [92]. Solar energy was then treated as heat. If solar radiation exergy was equal to work from a heat engine, the maximum fuel conversion efficiency would be 1-$\frac{T_0}{T_s}$. Consequently, the exergy of solar radiation can be calculated by Eq.(4-18):

$$\dot{B}_S = G\left(1 - \frac{T_0}{T_s}\right) \tag{4-18}$$

Petela himself thoroughly analysed the origin of differing formulas obtained [67]. These 3 approaches (Szargut and Petela's, Spanner's, Jeter's) were investigated independently by Bejan [68]. He stated that the 3 theories do not exclude each other and if they are all individually correct, they may complement each other. The differences result from various assumptions: how the energy stream of which we want to calculate the useful effect is defined: whether it is heat or radiation and how the useful effect is identified.

Researchers also point out that one should differentiate between direct solar radiation exergy and diffuse solar radiation exergy, since scattered radiation is the source of higher entropy than direct radiation. Scattering is an irreversible process generating entropy. This definition was developed by Pons [87] and by Chu and Liu [86] who were defining the solar radiation exergy using spectral distribution.

For the purpose of incoming solar radiation exergy evaluation, Petela's approach [67,84,85] will be utilized in this work.

4.2.4 Exergy balances and analysis

According to guidelines present in [76] and [93], every component in the system can be described by an exergy balance that distinguishes between the exergy rate of fuel and the exergy rate of a product related to the component. In order to maintain consistency, it is important to note how those two terms should be accounted for. A Product is treated as the expected result of the component's performance, while a Fuel is connected with the exergy that is consumed to provide the results. Specific directions say that [23, 24]:

- One should operate with exergy differences associated with each material stream between inlet and outlet. Exergy differences should be applied to all exergy streams

associated with a change of physical exergy and to exergy streams associated with the conversion of chemical exergy.

- Exergy streams that are associated with the energy streams (e.g. heat or work) can appear either at the component inlet becoming a part of the fuel, or at the outlet, becoming a part of the product of the component.
- The product equals the sum of all the exergy values to be considered at the outlet (including the exergy of energy streams generated in the component) and all the exergy increases between inlet and outlet.
- The fuel is defined as all the exergy values to be considered at the inlet (including the exergy of energy streams supplied to the component) plus all exergy decreases from inlet to outlet, minus all exergy increases that are a side-effect and not in accord with the component working purpose.

Taking into account these guidelines, the fuel and product parts can be defined for each type of component that will be considered in this study. The components can be collected in main groups: heat exchangers, pumps, mixers and separately solar collector. The specific components present in an ammonia-water chiller will be a subject of detailed discussion over fuel and product definition in a devoted chapter. Table 4.1 collects useful equations that can be a starting point for estimating the fuel ($\dot{B}_F$) and product exergy rates ($\dot{B}_P$).

Table 4.1 Exergy rates of product and fuel for exemplary components.

Component type		Exergy rate of product	Exergy rate of fuel
Heat exchanger (aim: heating)	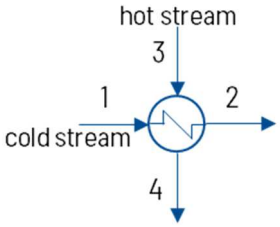	$\dot{B}_P = \dot{B}_2 - \dot{B}_1$	$\dot{B}_F = \dot{B}_3 - \dot{B}_4$
Heat exchanger (aim: cooling)	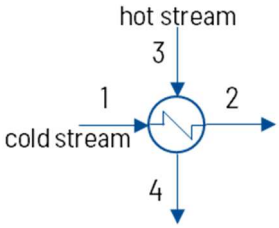	$\dot{B}_P = \dot{B}_4 - \dot{B}_3$	$\dot{B}_F = \dot{B}_1 - \dot{B}_2$
Solar collector	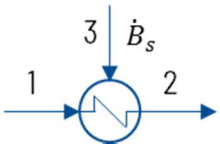	$\dot{B}_P = \dot{B}_2 - \dot{B}_1$	$\dot{B}_F = \dot{B}_S$
Pump	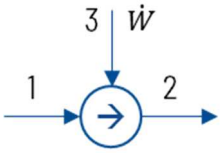	$\dot{B}_P = \dot{B}_2 - \dot{B}_1$	$\dot{B}_F = \dot{W}$
Mixer	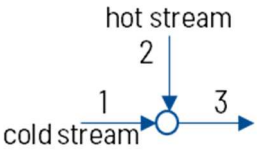	$\dot{B}_P = \dot{B}_3$	$\dot{B}_F = \dot{B}_1 + \dot{B}_2$

Once the fuel and products are recognized, each component (e.g. k-th) can be described by an exergy balance like in Eq. (4-19):

$$\dot{B}_{\mathrm{F,k}} = \dot{B}_{\mathrm{P,k}} + \sum \dot{B}_{\mathrm{D,k}} + \sum \dot{B}_{\mathrm{L,k}} \tag{4-19}$$

The equation also takes into account differentiating between exergy destructions ($\sum \dot{B}_{\mathrm{D,k}}$) and exergy losses ($\sum \dot{B}_{\mathrm{L,k}}$). Exergy destruction is caused by the irreversibilities (i.e. entropy generation) occurring within a system. These inefficiencies might be connected with friction, unrestrained expansion, mixing, heat transfer at finite temperature difference or chemical reaction [96]. Exergy destruction can be divided between avoidable and unavoidable part (first

can be considered in improvement phase, the latter cannot be reduced due to technological limitations) as well as between endogenous (connected only with the inefficiencies within the component) and exogenous parts (caused by the inefficiencies in the remaining components). This approach can be of help to understand the real potential for improving the components [97,98]. The exergy loss, on the other hand, is associated to exergy transfer (waste) to the surroundings. This exergy transfer is not further used in any component.

Exergy analysis rests on performing balances at the component and at the whole system level. It is then possible to calculate the exergy efficiency shown in Eq. (4-20) for k-th component (η_k) and in Eq. (4-21) for the whole system. (η_{tot})

$$\eta_k = \frac{\dot{B}_{P,k}}{\dot{B}_{F,k}} = 1 - \frac{\dot{B}_{D,k} + \dot{B}_{L,k}}{\dot{B}_{F,k}} \tag{4-20}$$

$$\eta_{tot} = \frac{\dot{B}_{P,tot}}{\dot{B}_{F,tot}} = 1 - \frac{\dot{B}_{D,tot} + \dot{B}_{L,tot}}{\dot{B}_{F,tot}} \tag{4-21}$$

If the exergy efficiency is properly defined, it is the only indicator that directly characterized the effectiveness of the system or a component from the strictly thermodynamic point of view, respecting the quality. It also allows for comparison of similar components operating under similar conditions.

A second indicator is the exergy destruction ratio ($y_{D,k}$) that helps visualizing the distribution of inefficiencies through the whole system. It is calculated with Eq.(4-22):

$$y_{D,k} = \frac{\dot{B}_{D,k}}{\dot{B}_{F,tot}} \tag{4-22}$$

The second type of exergy destruction ratio is in it allows for comparison of exergy destruction within the component to the total exergy destruction in the system. It is given in Eq. (4-23).

$$y^*_{D,k} = \frac{\dot{B}_{D,k}}{\dot{B}_{D,tot}} \tag{4-23}$$

These indicators help to recognize the components within a system that are burdened with the highest irreversibilities. The same, they could indicate the components whose improvement would give the highest performance benefits. The components with the highest exergy destruction ratio are the main source of inefficiencies in the system and should be improved first.

Similarly, the exergy loss ratio ($y_{L,tot}$) can be defined and it is given by Eq. (4-24).

$$y_{L,tot} = \frac{\dot{B}_{L,\mathrm{tot}}}{\dot{B}_{F,tot}} \tag{4-24}$$

This equation shows how to calculate the exergy loss ratio for the whole system because according to authors in [96], exergy loss is usually defined at the system level. However, it is also possible to perform this analysis at the component level. A specific approach to the dissipative components in the analysed systems will be described in the following chapters (5 and 6).

4.3 Exergoeconomic analysis

Exergy is a proper measure allowing for evaluation of the usefulness of natural resources. It is also a reasonable basis to assign the economic costs to the interactions with the surroundings and to the sources of thermodynamic irreversibilities. An exergoeconomic analysis connects exergy and economic analyses by the means of the cost per unit of exergy [98]. It allows for the estimation of costs of every process stream and also of the occurring inefficiencies. Its features should be used for the purpose of optimization and minimization of the product unitary cost.

The tool used to perform the exergoeconomic analysis is the Specific Exergy Costing (SPECO) method. Its first assumptions were already introduced in the 80's [93]. It requires the identification of all exergy streams within the system, then the definition of fuel and the definition of cost equations.

Cost equations are first written separately for each exergy rate (Eq. (4-25)), for exergy transfer associated with work (Eq. (4-26)) or heat transfer (Eq. (4-27)). It allows performing the exergy-based monetary costing.

$$\dot{C}_j = c_j \dot{B}_j = c_j b_j \dot{m}_j \tag{4-25}$$

$$\dot{C}_w = c_w \dot{W} \tag{4-26}$$

$$\dot{C}_Q = c_Q \dot{B}_Q \tag{4-27}$$

In the equations $\dot{C}$ stands for cost rate (e.g. €/s), c is the specific cost of exergy rate (e.g. €/kW), subscript *j* is connected with the *j* -th stream, *w* with work, *Q* with heat.

Subsequently, each component should be described by the means of a cost balance. This can be done on the inlet-outlet basis for each component, as is presented by Eq. (4-28).

$$\sum_{out} \left(c_{out} \dot{B}_{out}\right)_k + c_{w,k} \dot{W} = \sum_{in} \left(c_{in} \dot{B}_{in}\right)_k + c_{Q,k} \dot{B}_{Q,k} + \dot{Z}_k \tag{4-28}$$

This balance shows that the difference between the sum of costs of all exiting exergy streams and the sum of costs of all entering exergy streams is supplemented by the cost rate $\dot{Z}_k$ (e.g. €/kW), associated with capital investment and operation & maintenance costs of each

component. If a component has N exiting exergy streams, then the one cost balance includes N unknowns. Therefore it is obligatory to define N-1 auxiliary equations to perform the analysis [93].

Cost balance can be also written on the fuel-product basis. A typical formula applicable to each component is shown as Eq. (4-29).

$$c_{P,k}\dot{B}_{P,k} = c_{F,k}\dot{B}_{F,k} + \dot{Z}_k \quad (4\text{-}29)$$

$c_{P,k}$ and $c_{F,k}$ represent the costs per unit of exergy of product or fuel respectively (e.g. €/kW),. The cost of exergy loss equals zero. Table 4.2 collects cost equations for fuel and product rates for the same components as in Table 4.1.

Table 4.2 Thermoeconomic cost rates of product and fuel for exemplary components.

Component type		**Cost rate of product**	**Cost rate of fuel**	**Auxiliary thermoeconomic relations**
Heat exchanger (aim: heating)	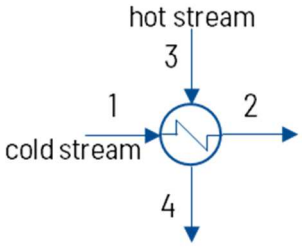	$\dot{C}_2 - \dot{C}_1$	$\dot{C}_3 - \dot{C}_4$	$c_3 = c_4$
Heat exchanger (aim: cooling)	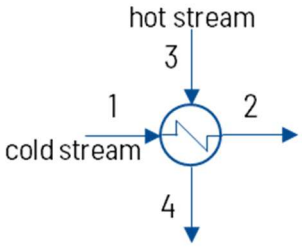	$\dot{C}_4 - \dot{C}_3$	$\dot{C}_1 - \dot{C}_2$	$c_1 = c_2$
Solar collector	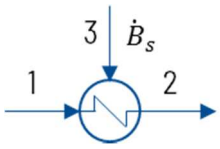	$\dot{C}_2 - \dot{C}_1$	0	$c_1 = c_2$
Pump	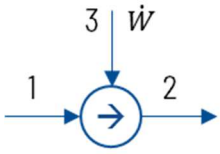	$\dot{C}_2 - \dot{C}_1$	$\dot{C_W}$	none
Mixer	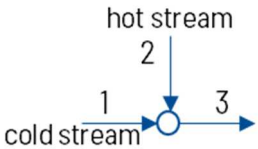	$\dot{C}_3$	$\dot{C}_1 + \dot{C}_2$	none

The expenditure cost rate $\dot{Z}_k$ (which, depending on the balance assumptions, can be defined as cost per second, per day or per year) is estimated, once the annual investment cost is calculated (Eq. (4-30)). The annual cost (Z_k^{an}) takes into account the interest rate (ir) and the expected

lifetime of the system (n). It bases on the value of purchase equipment cost which can be found directly in the literature, in the technical brochures or can be calculated from cost functions.

$$Z_k^{an} = \frac{ir \cdot (1+ir)^n}{(1+ir)^n - 1} Z_k \tag{4-30}$$

Subsequently, it is also possible to assign a cost rate to the exergy destruction within a component and it can be found, if Eq. (4-31)is applied.

$$\dot{C}_{D,k} = c_{F,k} \Sigma \dot{B}_{D,k} \tag{4-31}$$

The exergoeconomic analysis is concluded with the estimation of relative cost difference r_k and the exergoeconomic factor f_k. The relative cost difference describes the relative increase in the cost per exergy unit in the k-th component of the system. If the relative cost difference of a component is high, there is a great potential for the cost reduction. The exergoeconomic factor relates the investment cost of a component to the sum of the investment cost and the cost of exergy destruction. If its value is high, the investment is mainly creating the cost. If it is low, irreversibilities are the main source of the costs.

$$r_k = \frac{c_{P,k} - c_{F,k}}{c_{F,k}} \tag{4-32}$$

$$f_k = \frac{\dot{Z}_k}{\dot{Z}_k + \dot{C}_{D,k}} \tag{4-33}$$

The results of the exergoeconomic analysis can be used in design analysis and optimization, in operation optimization and in diagnostics while identifying malfunction of components. Exergoeconomic optimization could lead to the minimization of the cost per unit of a useful product. According to the recommendations present in the literature, the first indicator saying if there is a potential for cost reduction is always the exergy efficiency. Subsequently, the exergoeconomic indicators r_k and f_k provide guidelines to the discovery of major cost sources and to the understanding of the improvement potential.

PART I

Chapter 5. REFERENCE INSTALLATION IN FLORENCE, ITALY

The first part of the thesis focuses on a solar cooling system. Assumptions about the technology and main technical parameters rest on a real existing reference installation operated in Italy, in Badia a Ripoli in the province of Florence. The reference installation was designed and constructed within a Collaborative Project "Small scale solar cooling device" No. TREN/FP7/EN/218952 of European Seventh Framework Programme. The project was coordinated by prof. Maurizio De Lucia from University of Florence and performed by a consortium of researchers from the University of Florence (CREAR group), Eurac Research Centre, German Aerospace Centre (DLR), Solitem and Climatewell companies. The project started in October 2008 and lasted for 48 months. Its main aim was to provide a market-ready autonomous solar heating and cooling system for residential or small commercial applications. According to the primary concept, three absorption chiller technologies were to be applied: ammonia-water chiller and lithium-bromide double-stage chiller in Florence while a lithium chloride chiller was planned to be tested in Bronzolo, the province of Bolzano. The plant in Florence was designed to partially satisfy the thermal comfort needs of a Misericordia building (Italian Red Cross health care centre), assisting the already operating air-conditioning equipment. Geolocation of the Florentine plant is presented in Fig. 5.1.

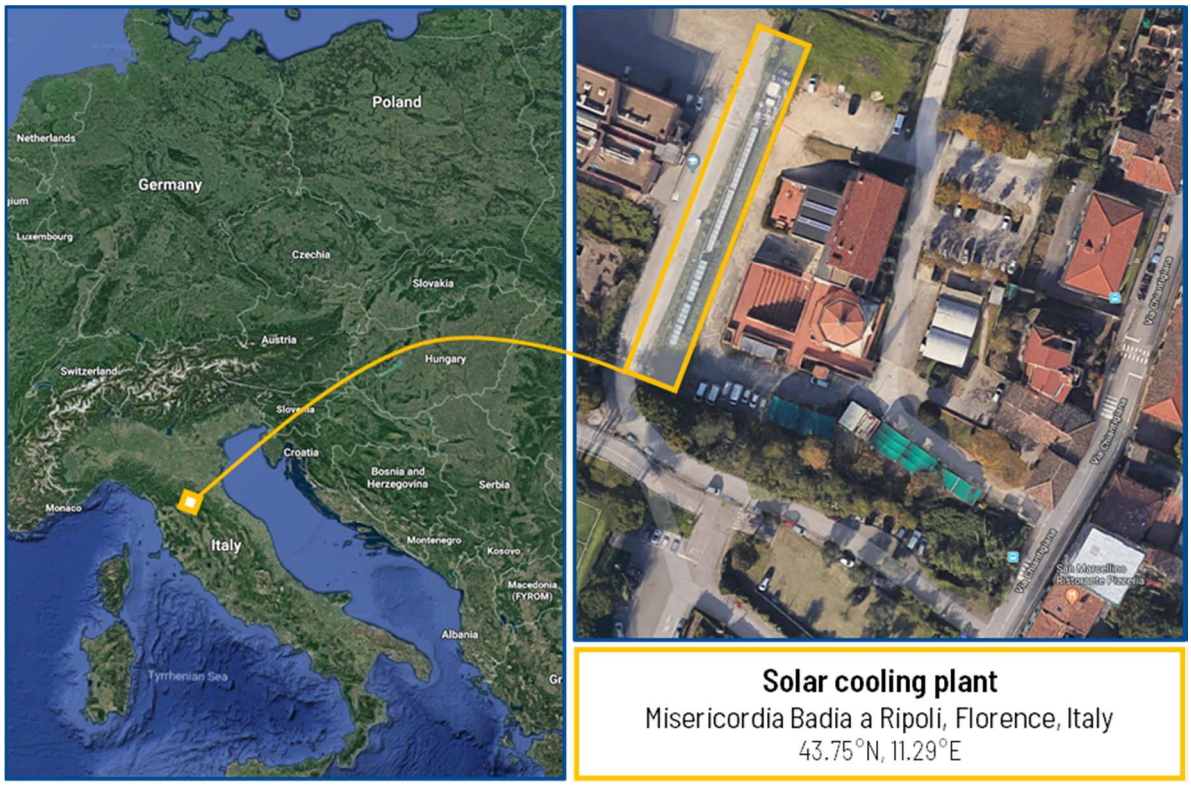

Fig. 5.1 Location of the solar cooling plant at the Misericordia of Badia a Ripoli.

The system was meant to comprise of a row of parabolic trough solar collectors that would deliver heat to a single-stage ammonia water chiller or, alternatively, to a double-stage lithium bromide chiller. According to reports, the main objective considering the plant and met by the Consortium during the FP7 project was to optimize the layout of the solar collectors field in order to maximize the cooling energy production; secondary objectives were to optimize a market available ammonia-water chiller in order to assure a possibility of direct steam driving, to optimize the parabolic trough collectors enhancing the solar field performance, and finally to develop the *Energy Box* – an assistance tool needed to control and manage the energy flows in the system. The design of the plant assumed combining commercially available components: 8 parabolic trough solar collectors SOLITEM PTC 1800, a single-effect ammonia-water absorption chiller ROBUR GAHP-W and a LiBr double-effect absorption chiller BROAD BCTZH23. The chosen ammonia-water chiller is originally manufactured as a gas-fired unit. Hence, one of the clue-goals of the researchers at the time of the project was to modify the design of chiller desorber to enable direct steam driving so that it can accept saturated heat from parabolic trough solar collectors. The construction was re-designed and modified by CREAR group in cooperation with Robur company. The new design was tested with the chiller driven by saturated steam (130-185°C) or – alternatively- by pressurized water (140-160°C, 12bar), or diathermic oil. Tests proved the chiller compatibility with this driving media and the highest coefficient of performance was obtained when the desorber was driven by saturated steam. According to data present in reports, the modification of generator design could be summed up by two main points: equipping the desorber vessel with vertical fins instead of helical and adding a condensate collector at the bottom of generator with a level controller for the condensate recirculation (it should be noted, that such a modification is not necessary for pressurized water driving, which was also proved to be possible). Re-designing of the generator improved the heat transfer and allowed for a 25% increase of cooling power output and 23% increase of a COP value, with the highest obtained COP at the level of 0.8 [99]. Although the Misericordia solar cooling plant has been also equipped with a double-stage lithium-bromide chiller, according to documentation, no specific research was devoted to that unit. It is possible to operate the chiller with pressurized water driving the generator as an alternative to the ammonia-water chiller. However, there is no technical possibility to run the two devices simultaneously. A special added value of the project was also the development of the *Energy Box* – a unit responsible for solar energy distribution in the system including hydraulic and control elements. Basing on measured input/output parameters the *Energy Box* allows for the control of system performance, managing the flow rates, valves settings but also defocus of the

collectors or shut-down conditions. The *Energy Box* was designed to be a universal system coping with different solar collector types and different absorption chillers available on the market. [99,100]

Since the project finished at the end of 2012, the solar cooling plant in Badia a Ripoli became an operative unit, managed by the University associates. It still assists the existing air-conditioning assembly in the Misericordia health care centre. At the same time, since it is not a laboratory installation anymore, there is no need for detailed measurement instrumentation. Additionally, after a few years, the commercial Solitem parabolic collectors were replaced with a new type of collectors: parabolic trough prototype designed by the CREAR group. They are placed in the same location, with the same solar azimuth and are equipped with a constant tracking system on a horizontal axis, however, their efficiency coefficients were not yet published at the time the work of the author was performed.

Technical reports, verbal information, and experiences shared by the CREAR group with the author became an inspiration while accomplishing the first part of the thesis, namely: preparing the simulation model of a solar cooling plant. The task was to mirror the operation of a solar heat driven chiller in a form of the simulation model with a further control procedure proposal. Basing on a part of the Misericordia plant structure, the primary simulation model would represent an ammonia-water chiller driven by heat from the parabolic trough solar collectors. A motivation of choosing an ammonia-water chiller for the analysis instead of the lithium-bromide chiller (still present in Misericordia plant) could be seen in a fact that since NH_3-H_2O chillers are characterized by 10-15% lower solar fraction than H_2O-LiBr chillers and they require higher driving temperature, they could be treated as a more demanding technology, less attractive to potential buyers [101]. Therefore, the optimization control for NH_3-H_2O chillers should be still developed in order to prove them also competitive.

Creation of the simulation model forced some modifications of the original design. One of the main goals of the thesis is to perform the impact assessment of meteorological conditions on the solar cooling plant, and next on the hybrid node's performance. It should be explained that by taking care of this goal, the solar cooling device should be conceptually adapted to work also under unfavourable climate conditions. In Florence, the working fluid in solar collectors is not endangered with freezing. If a twin installation were to be operated in Poland, it would be exposed to low ambient temperatures in winter, down to -15°C. Therefore, for the purpose of the simulation model, a commercially available thermal oil was adopted as a working fluid in the solar collectors loop.

A detailed methodology of modelling the ammonia-water chiller and solar field is outlined below. The simulation results are followed by exergy and exergoeconomic analyses of the system performance. A proposal of control procedure is closing this chapter. All analyses are performed in parallel: for a system operated in Italy and a potential system operated in Poland.

5.1 A simulation model of the absorption chiller

A simplified scheme of a single stage ammonia-water chiller under consideration is presented Fig. 5.2. The schematic diagram was elaborated on the base of technical data sheets of the manufacturer [102]. Following components are included in the model: a desorber (1) co-working with a rectifier (2), a common vessel for condenser and absorber (3), a subcooler (4), an evaporator (5) and a preabsorber (6). The working fluid is circulated by a pump (7). The system operates at three pressure levels and therefore three throttling valves are present.

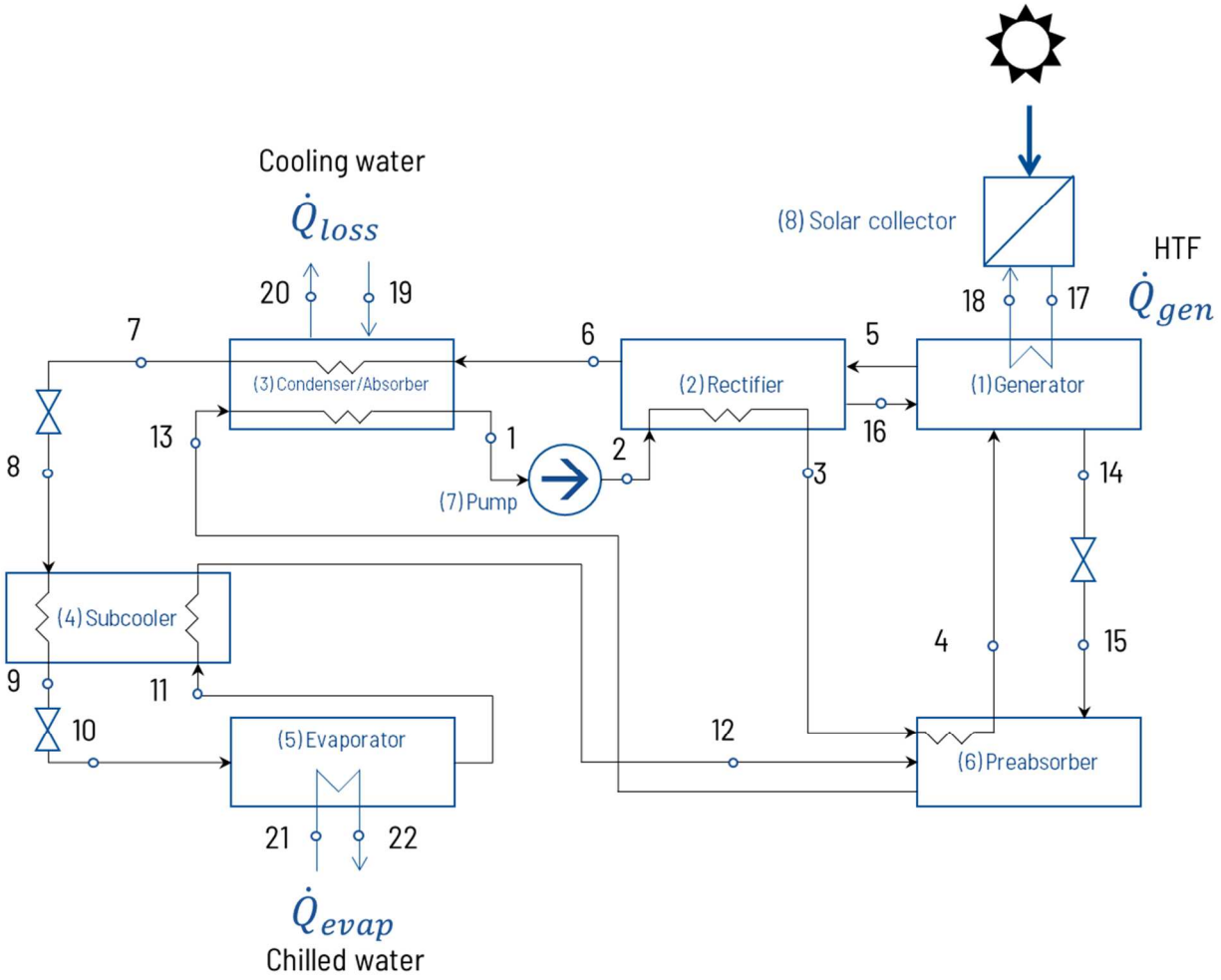

Fig. 5.2 Simplified scheme of the single stage ammonia-water absorption chiller.

The ammonia-water solution is heated in the generator by the hot heat transfer fluid (HTF) coming from the solar collector field (8). The simulation model of the solar field is presented in the following subchapters 5.2 and 5.3. According to technical deliverables of the Misericordia project, the generator (1) is a vertical cylinder consisting of bottom boiling (stripping) section and an upper adiabatic section. Vertical fins are attached to the bottom part, enhancing the heat transfer between the HTF and the mixture inside. The heat rate $\dot{Q}_{gen}$ coming from the solar field causes the separation of ammonia vapour from the mixture. Separated vapours still contain some fraction of water vapour. The hot lean solution (meaning the low concentration of NH3 in the NH_3-H_2O solution) collected in the bottom of the cylinder is directed upwards in a tube coil heating up the rich solution (stream 4). Rich solution means a high concentration of ammonia in the NH_3-H_2O solution. The lean solution can leave the desorber as a saturated or subcooled liquid (stream 14). The saturated vapour from the desorber (stream 5) reaches the rectifier (2). It is there cooled down by the passing rich solution (stream 2). Utilizing the two-phase properties of the mixture and their different phase change parameters, the solution with a high concentration of water is then condensed and flows back to the generator (stream 16). The almost pure ammonia saturated vapour flows to the condenser (stream 6). It is there cooled down by external cooling water (or air, depending on model assumptions) and latent heat is released. The pressure of the condensed ammonia is reduced by an intermediate throttling valve (streams 7-8). A subcooler (4) lowers the temperature of the liquid (streams 8-9). Pressure is finally reduced to the evaporation pressure in the next throttling valve (streams 9-10). The ammonia-rich liquid is evaporated by external chilled water (streams 21-22) and the low temperature evaporation process is responsible for the provision of cooling useful effect ($\dot{Q}_{evap}$). The refrigerant still contains a small amount of water and therefore it is not possible to evaporate the whole solution, but the mixture leaving the evaporator is characterized by high quality (q - understood as vapour mass fraction). Ammonia vapours are warmed up by liquid ammonia in the subcooler (4) improving their quality. The vapours (stream 12) flow into the preabsorber section (6) where they are mixed with the lean solution of NH_3-H_2O (stream 15). The rich solution which is passing through (streams 3-4) cools down the mixture, taking care of the beginning of the absorption process. The absorption is completed in the condenser/absorber vessel and the heat of absorption is released to the external cooling water (or air). The regenerated rich solution (stream 1) in saturated state flows into the solution pump (7) and its pressure is increased. The strong solution plays now the role of coolant in a rectifier (2) and a preabsorber (6). At the same time, the temperature of the rich solution is

gradually increased, reducing the temperature difference in the generator, where the solution finally arrives (stream 4).

The performance of the ammonia-water chiller is described by means of a mathematical simulation model adopting a lumped-parameter approach. Each component can be then represented by mass, species and energy conservation equation. The design model is created assuming that the system works under steady state conditions, the two-phase mixtures of liquid and vapour exist at thermodynamic equilibrium, and that the pressure losses and heat losses along the cycle are negligible.

The thermo-physical properties of NH_3-H_2O mixture are dictated by pressure, temperature and concentration of the solution. More than thirty correlations for thermodynamic properties of an ammonia-water mixture are available in the literature [103]. In this study, thermodynamic properties of ammonia-water solution were provided by an external routine available in EES which is based on the mixture equations of state described by Ibrahim O.M and Klein S.A. in [104].

5.1.1 Thermodynamic analysis of the ammonia-water chiller

In the following, a complete system of equations needed to solve the thermodynamic model of the chiller is given. In the formulas $\dot{m}_j$ stands for a mass flow rate of a j-th stream (kg/s), x_j means the ammonia concentration (kgNH_3/kgNH_3-H_2O) in the j-th stream, h_j is the specific enthalpy of the j-th solution stream (kJ/kg). Components that are in contact with external flows, additionally exchange a heat rate $\dot{Q}_i$ (kW).

Component 1 - Generator

- Mixture mass balance

$$\dot{m}_4 + \dot{m}_{16} = \dot{m}_5 + \dot{m}_{14} \tag{5-1}$$

- Ammonia mass balance

$$x_4\dot{m}_4 + x_{16}\dot{m}_{16} = x_5\dot{m}_5 + x_{14}\dot{m}_{14} \tag{5-2}$$

- Energy balance

$$\dot{m}_4 h_4 + \dot{m}_{16} h_{16} + \dot{Q}_{gen} = \dot{m}_5 h_5 + \dot{m}_{14} h_{14} \tag{5-3}$$

- External flow energy balance

$$\dot{Q}_{gen} = \dot{m}_{17}(h_{17} - h_{18}) = \dot{m}_{18}(h_{17} - h_{18}) \tag{5-4}$$

Discussion:

The generator is warmed by hot heat transfer fluid from the solar field, receiving the heat input $\dot{Q}_{gen}$. Incoming heat rate determines the desorption process and ammonia vapours are separated. It is assumed that the vapours are at saturation conditions. They are directed to the rectifier and the stream 16 coming back from the rectifier is a liquid containing almost all rests of separated water (or actually a solution with a very high water content).

Component 2 - Rectifier

- Mixture mass balance

$$\dot{m}_5 = \dot{m}_{16} + \dot{m}_6 \tag{5-5}$$

$$\dot{m}_3 = \dot{m}_2 \tag{5-6}$$

- Ammonia mass balance

$$x_5\dot{m}_5 = x_6\dot{m}_6 + x_{16}\dot{m}_{16} \tag{5-7}$$

$$x_3\dot{m}_3 = x_2\dot{m}_2 \tag{5-8}$$

- Energy balance

$$\dot{m}_5h_5 + \dot{m}_2h_2 = \dot{m}_6h_6 + \dot{m}_{16}h_{16} + \dot{m}_3h_3 \tag{5-9}$$

Discussion:

Ammonia vapours separated by warming up in the desorber section contains more of the more volatile ingredient (ammonia). In order to enable further separation and purify the ammonia vapours, stream 5 is cooled down by a rich solution coming from the absorber section (stream 2-3). Decrease of the temperature causes a partial condensation. Simultaneously, stream 6 is still saturated vapour but with higher ammonia concentration (almost 100%). The rules of rectification can be presented using an isobaric (p=constant) temperature-concentration phase equilibrium diagram presented in Fig. 5.3. Streams are numbered in correspondence with the scheme in Fig. 5.2. Point 14’ represents a potential state of the saturated weak solution before its mixing with stream 16 and before possible subcooling.

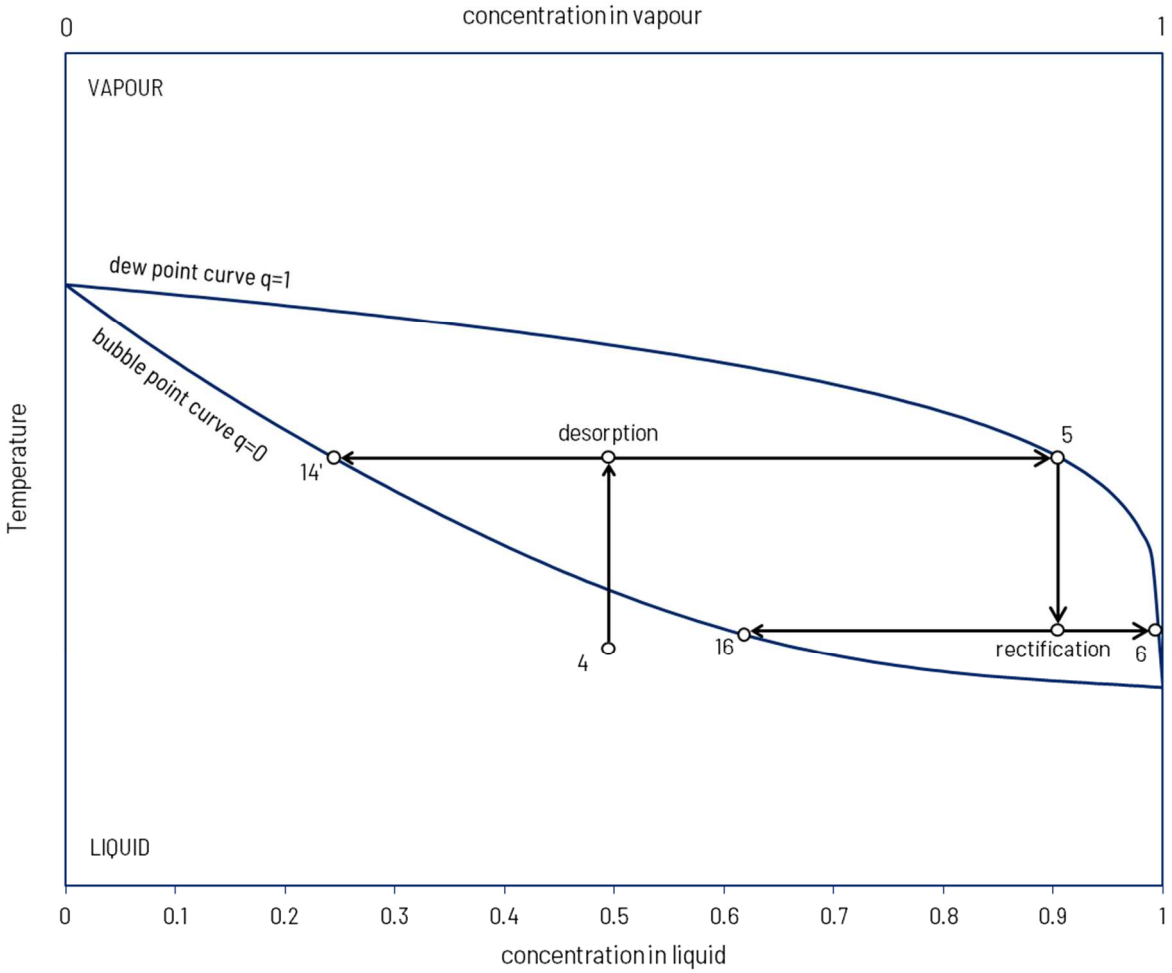

Fig. 5.3 Rules of rectification presented on a temperature-concentration diagram

Component 3 – Condenser/Absorber

- Mixture mass balance

$$\dot{m}_6 = \dot{m}_7 \tag{5-10}$$

$$\dot{m}_{13} = \dot{m}_1 \tag{5-11}$$

- Ammonia mass balance

$$x_6\dot{m}_6 = x_7\dot{m}_7 \tag{5-12}$$

$$x_{13}\dot{m}_{13} = x_1\dot{m}_1 \tag{5-13}$$

- Energy balance

$$\dot{m}_6 h_6 + \dot{m}_{13} h_{13} = \dot{m}_7 h_7 + \dot{m}_1 h_1 + \dot{Q}_{waste} \tag{5-14}$$

- External flow energy balance

$$\dot{Q}_{waste} = \dot{m}_{20}(h_{20} - h_{19}) = \dot{m}_{19}(h_{20} - h_{19}) \tag{5-15}$$

Discussion:

The condenser and absorber sections are contained in one common vessel that is cooled by the external cooling fluid. In the default conditions, it is a water-cooled component. External flow's mass flow rates and their temperature level are governing the conditions of the mixture in the cycle. Assuming the temperature surplus of the mixture at the outlet of condenser over cooling fluid temperature, and presuming saturation conditions for liquid at the outlet of condenser, the level of high of the cycle can be determined. A very specific feature of ammonia-water chillers is the behaviour of refrigerant during condensation or evaporation process. It can be recalled while this discussion over the condenser component. The refrigerant at the inlet to condenser section is almost 100% ammonia, nevertheless, the small amount of water makes it a two-components mixture in strict terms. The ammonia-water mixture is zeotropic: ammonia and water have different boiling point temperature at the same pressure. During a phase change, the mixture experiences a temperature glide. The condensation process of the ammonia-water refrigerant on the example of the analysed chiller is shown on the temperature-composition graph in Fig. 5.4.

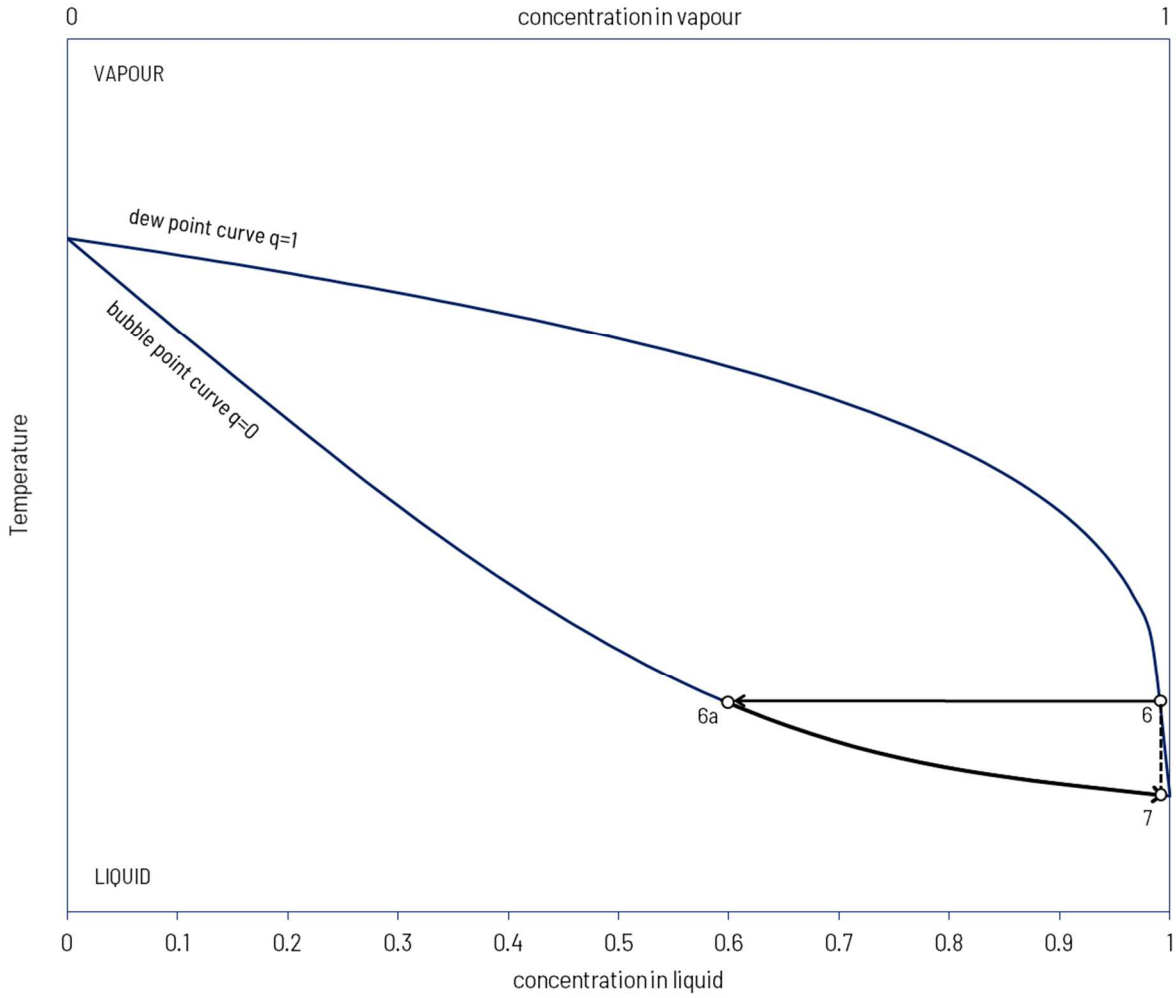

Fig. 5.4 Condensation path for a zeotropic mixture shown on the temperature-concentration diagram

During heat removal, the first to condensate is the less volatile water, therefore the concentration of ammonia in the liquid phase is smaller in the first step of the process (6a). As the process of condensation proceeds and more and more ammonia becomes liquid, the composition of the liquid phase changes (from point 6a to 7) and the temperature required to condense the whole mixture also changes. Therefore, it cannot be neglected that the enthalpy of the ammonia-water mixture varies along the heat exchanger, however for the purpose of design thermodynamic analysis only the inlet-outlet state is considered.

Component 4 - Subcooler

- Mixture mass balance

$$\dot{m}_8 = \dot{m}_9 \tag{5-16}$$

$$\dot{m}_{11} = \dot{m}_{12} \tag{5-17}$$

- Ammonia mass balance

$$x_8\dot{m}_8 = x_9\dot{m}_9 \tag{5-18}$$

$$x_{11}\dot{m}_{11} = x_{12}\dot{m}_{12} \tag{5-19}$$

- Energy balance

$$\dot{m}_8 h_8 + \dot{m}_{11} h_{11} = \dot{m}_9 h_9 + \dot{m}_{12} h_{12} \tag{5-20}$$

Discussion:

The refrigerant heat exchanger subcools the condensate from the condenser. For that component, the energy balance is supplemented with the heat exchanger effectiveness considerations. The effectiveness of heat exchanger is assumed to be known for design conditions and is defined as the ratio between the actual heat rate removed from the refrigerant condensate and the ideal, maximum heat rate that would be removed if the refrigerant would be subcooled to the temperature of the secondary fluid at inlet to the heat exchanger (assuming T_9=T_{11}). For general considerations, the refrigerant heat exchanger (RHE) energy effectiveness ($\varepsilon_{e,RHE}$) is described by Eq. (5-21).

$$\varepsilon_{e,RHE} = \frac{\dot{m}_8(h_8 - h_9)}{\dot{m}_8\big(h_8 - h(t_{11}, p_9, x_9)\big)} \tag{5-21}$$

Component 5 - Evaporator

- Mixture mass balance

$$\dot{m}_{10} = \dot{m}_{11} \tag{5-22}$$

- Ammonia mass balance

$$x_{10}\dot{m}_{10} = x_{11}\dot{m}_{11} \tag{5-23}$$

- Energy balance

$$\dot{m}_{10} h_{10} + \dot{Q}_{evap} = \dot{m}_{11} h_{11} \tag{5-24}$$

- External flow energy balance

$$\dot{Q}_{evap} = \dot{m}_{21}(h_{21} - h_{22}) = \dot{m}_{22}(h_{21} - h_{22}) \tag{5-25}$$

Discussion:

The subcooled refrigerant solution exiting from the subcooler is throttled in a valve and becomes a two-phase mixture (slightly above the bubble point curve). The chilled water is heating up the mixture, but still, because of the small water content, it is not possible to evaporate the whole solution at a given pressure. The hat rate removed from the chilled water is the cooling effect of the absorption chiller operation. The stream leaving the evaporator

section is a two-phase mixture of high quality level. It then flows as a secondary liquid to the subcooler section. By removing heat from the condensate, the quality of flow from the evaporator is improved.

Component 6 - Preabsorber

- Mixture mass balance

$$\dot{m}_{15} + \dot{m}_{12} = \dot{m}_{13} \tag{5-26}$$

$$\dot{m}_3 = \dot{m}_4 \tag{5-27}$$

- Ammonia mass balance

$$x_{15}\dot{m}_{15} + x_{12}\dot{m}_{12} = x_{13}\dot{m}_{13} \tag{5-28}$$

$$x_3\dot{m}_3 = x_4\dot{m}_4 \tag{5-29}$$

- Energy balance

$$\dot{m}_3 h_3 + \dot{m}_{12} h_{12} + \dot{m}_{15} h_{15} = \dot{m}_4 h_4 + \dot{m}_{13} h_{13} \tag{5-30}$$

Discussion:

The preabsorber component could also be called a solution-cooled absorber. The vapours generated in the evaporator and warmed in the subcooler (stream 12) are here mixed with the lean solution (stream 15). The mixture is cooled by the colder rich solution that is passing the preabsorber in a coil or a tube. Owing to the low-temperature heat source, the absorption process can begin here. The fluid leaving the preabsorber (stream 13) is a two-phase mixture that is further cooled in the absorber section and will be leaving it as a saturated liquid (stream 1).

Component 7 - Pump

- Mixture mass balance

$$\dot{m}_1 = \dot{m}_2 \tag{5-31}$$

- Ammonia mass balance

$$x_1\dot{m}_1 = x_2\dot{m}_2 \tag{5-32}$$

- Energy balance

$$\dot{m}_1 h_1 + N_{pump} = \dot{m}_2 h_2 \tag{5-33}$$

$$N_{pump} = \frac{\dot{m}_1 \cdot \Delta p}{\rho \cdot \eta_{pump}} \tag{5-34}$$

Discussion:

The solution pump is the only component inside the cycle that requires an electricity input. Knowing the value of the pump isentropic efficiency for nominal working conditions and the required pressure increase, the pump energy consumption can be defined. Single value of pump efficiency will become a function of variable mass flow rate in the off-design mode.

Trivial balances for all system

Table 5.1 collects all of the remaining simplified balances required to fully define the thermodynamic model of the chiller.

Table 5.1 Trivial balances considering concentration, pressure, enthalpy and mass flow rates values

concentration	**pressure**	**enthalpy**	**mass flow rates**
$x_1 = x_2$	$p_2 = p_3$	$h_{14} = h_{15}$	$\dot{m}_{14} = \dot{m}_{15}$
$x_2 = x_3$	$p_3 = p_4$	$h_7 = h_8$	$\dot{m}_7 = \dot{m}_8$
$x_3 = x_4$	$p_4 = p_5$	$h_9 = h_{10}$	$\dot{m}_9 = \dot{m}_{10}$
$x_6 = x_7$	$p_4 = p_{14}$		
$x_7 = x_8$	$p_5 = p_{16}$		
$x_8 = x_9$	$p_5 = p_6$		
$x_9 = x_{10}$	$p_6 = p_7$		
$x_{10} = x_{11}$	$p_8 = p_9$		
$x_{11} = x_{12}$	$p_{10} = p_{11}$		
$x_{13} = x_1$	$p_{11} = p_{12}$		
$x_{14} = x_{15}$	$p_{12} = p_{15}$		
	$p_{15} = p_{13}$		
	$p_{13} = p_1$		

The coefficient of performance for the chiller is calculated as in Eq. (5-35).

$$COP = \frac{\dot{m}_{21}(h_{21} - h_{22})}{\dot{Q}_F + N_{pump}} \tag{5-35}$$

Where N_{pump} is the electric power consumed by the solution pump and $\dot{Q}_F$ is the driving heat rate. Depending on the assumed boundary of the system, it can be understood as useful heat gain from the solar collector ($\dot{Q}_{gen}$), or if the boundary was widened: as the incoming solar radiation on the aperture area. Results for both approaches will be presented.

5.1.2 Approximate heat transfer analysis of ammonia-water chiller

The analysis of the chiller performance under design conditions is completed, if the heat exchangers are sized. A precise representation of heat and mass transfer for the two-phase flow conditions present in the analysed chiller is very challenging and out of scope of the study here presented. There are various flow-patterns for two-phase flows and as many correlation equations. It is evident that in that type of chiller the heat and mass transfer between phases and the phase change of the ammonia-water mixture takes place in every component. The two-phase flow and transport features of the mixture should be included in a detailed analysis. This precise approach is presented for example in [105]. However, it should be marked that the aim of this study is not to prepare a new design concept of the sorption refrigeration machine nor a fully detailed heat transfer model, but a system analysis. The surface area of each heat exchanger is found by accepting some simplification assumptions. They will be described and motivated in the following paragraphs. Additionally, the external routine calling the thermodynamic properties of ammonia-water solution while preparing the simulation model does not include the transport properties of a mixture. Transport properties are essential while preparing the heat transfer model and evaluating heat transfer coefficient. For that reason, a major simplification had to be accepted. Namely: heat transfer coefficients are concentration-weighted averages of coefficients found from separate flow models. Moreover, in the face of lack of specific details on the unique construction of chiller components (like generator, preabsorber), a simplified construction is also assumed. The goal is to identify a possible heat transfer mechanism and finalize thus a design in order to find the heat transfer surface of a component that would fit into the chiller housing.

In general, each component can be described by the means of the Peclet equation. Calculating the heat exchanger log-mean temperature difference ΔT_{lg}, the value of overall heat transfer coefficient multiplied by the heat exchanger size can be found (UA, W/K). The formula for component *k* is given in Eq. (5-36).

$$\dot{Q}_k = (UA)_k \cdot \Delta T_{lg,k} \tag{5-36}$$

A heat exchanger usually involves two fluids that are separated by a solid wall. The thermal resistance network between two fluids includes firstly the mechanism of convection between the hot fluid and wall, then conduction through the wall, and finally convection from the wall to the cold fluid. If this path is recognized, the UA value can be found if a typical equation for the example of double-pipe heat exchanger is considered (Eq. (5-37)).

$$\frac{1}{(UA)_k} = \frac{1}{U_i A_i} = \frac{1}{U_o A_o} = \frac{1}{h_i A_i} + R_{wall} + \frac{1}{h_o A_o} \quad (5\text{-}37)$$

In the formula, A_i is the internal surface area of the wall (tube) that separates two fluids, while A_o is the external surface area. While R_{wall} (the thermal conductive resistance of the wall) is not challenging to estimate, if only the material of the device is known, a more complex task is to evaluate the internal and external convective heat transfer coefficients, respectively: h_i and h_o. This requires that the heat transfer mechanism is properly assessed.

The available thermodynamic properties of flows and transport properties of pure substances (ammonia and water) allow for the heat transfer coefficients estimation, if only a possible correlation is applied. The approach is discussed in the following, while all of the log-mean temperature differences definition are shown in Appendix A.

Component 1 – Generator

According to available documentation, the generator could be generally described as a cylinder with vertical fins covering the bottom half of the external surface. The cylinder contains a tube coil through which the hot weak solution is flowing up and warming up the solution that is flowing down around the coil. The cylinder is placed in a vertical annulus tube where the heat transfer fluid from solar collectors is warming up the solution inside of the cylinder. Heat transfer in the generator is a complex multi-stage process. Variable approaches to modelling this component can be found in the literature. Authors in [105] separated model of the generator cylinder from the model of the coil inside the cylinder. Heat transfer in the cylinder is modelled analysing the heat transfer coefficient influenced by nucleate boiling and forced convective boiling, according to Chen correlation [106]. Heat transfer between solution in the cylinder and the solution inside the coil is analysed assuming internal single-phase heat transfer coefficient adopting correlation of Seban and McLaughlin [107]. A completely different approach is presented in [108] where the desorber is modelled as a plate heat exchanger adopting the correlations for the convective heat transfer coefficient for the evaporation process. In here presented study it was decided to reconcile the complexity of the process in the desorber and the scarcity of construction data by the means of a replacement model. Desorber is modelled as a shell and tube heat exchanger. Heat transfer fluid is flowing on the shell side, while ammonia-water mixture flows inside tubes. The tube side represents the thermal effects of all of the processes that take place inside the cylinder basing on the reference logarithmic temperature

difference. It is a reference temperature difference taking into account the boundary values of the temperature of the mixture.

Component 2 – Rectifier

The rectifier is constructed as a horizontal cylinder with a tube coil inside. It is modelled as a shell and tube heat exchanger. Single-phase rich solution is flowing through the tubes and the internal convective heat transfer coefficient is calculated as a concentration average of heat transfer coefficients obtained for water and ammonia fluids. Ammonia vapours are flowing through shell in which the separation takes place. Therefore, the convective heat transfer coefficient is calculated as a concentration average basing on the values for heat transfer coefficient for boiling water and the convective heat loss coefficient for ammonia.

Component 3 – Condenser/Absorber

While analysing this heat exchanger as a water-cooled, it is assumed that both condenser and absorber sections are cooled by external water flow, but are not exchanging heat between each other. Hence, the heat exchanger can be considered as having two separate heat transfer surfaces but with the same temperature parameters at the inlet and outlet of the external flow. Total heat transfer is the sum as indicated by Eq. (5-38).

$$\dot{Q}_3 = \dot{Q}_{cond} + \dot{Q}_{abs} = (UA)_{cond} \cdot \Delta T_{lg,cond} + (UA)_{abs} \cdot \Delta T_{lg,abs} \qquad (5\text{-}38)$$

Condenser part is modelled as a shell and tube heat exchanger. Cooling water is flowing on the shell side, while the internal convective heat transfer coefficient is calculated for condensing ammonia. The absorber part in the model is also shell and tube heat exchanger with water in the shell. A single-phase, liquid rich solution is flowing through tubes, therefore internal convective heat transfer coefficient is calculated as a concentration average of coefficients calculated separately for ammonia and water. Ammonia and water are transferring heat by forced convection.

Component 4 – Subcooler

Subcooler is modelled as a shell and tube heat exchanger. The mixture from evaporator flows inside the inner tubes, while the condensate flows in the annulus. Owing to the high concentration of ammonia, the internal and external convective heat transfer coefficients are calculated basing on thermodynamic and transport properties of ammonia.

Component 5 – Evaporator

The evaporator can be designed as a horizontal cylinder with a helical coil inside of which the chilled water is sprayed. However, for simplification reasons, it could be treated as a special case of shell and tube heat exchanger as a replacement model. The chilled water is flowing on

the shell side warming up solution inside the tubes. The internal convective heat transfer coefficient is estimated assuming the boiling process of pure ammonia.

Component 6 - Preabsorber

According to the manufacturer data and a promotional sketch of the chiller presented in the technical data sheet [102,109], the preabsorber is a vertical cylinder with a helical coil inside. The lean solution is sprinkled from the top on the coil and mixes with the ammonia vapours coming from the subcooler. Reach solution is flowing inside the coil cooling the external mixture. Modelling of absorbers is a complex issue raised by many researchers that attempted to develop calculation algorithms taking into account heat and mass transfer during the condensation process of a binary vapour [110–112]. In here presented study, it was decided that for the purpose of the system analysis, a simplified approach can be applied, accepting all of the possible deviations from the reality it could cause. Following the approach presented in [113], the preabsorber (a solution cooled absorber) is modelled as a shell and tube heat exchanger with rich solution flowing through tubes.

5.1.2.1 Shell and tube heat exchanger

Shell and tube heat exchangers are probably the most common type of heat exchangers in industrial applications [114], also in some air conditioning or refrigeration systems. They are said to be characterized by large ratios of heat transfer area to volume and weight. These heat exchangers contain tubes inside a shell with their axes parallel to the shell. Fluid flowing inside the tubes is transferring or withdrawing heat to or from the fluid flowing through the shell. Major components of the heat exchanger are tubes, shell, front-end head, rear-end head. A common part of the design is to place baffles in the shell. These elements cause a cross flow of fluid in the shell, enhancing the heat transfer between shell-side and tube-side. Estimation of the size of the heat exchanger rests on the heat rate value calculated in the thermodynamic model and assumptions towards the construction of the heat exchanger influencing the overall heat transfer coefficient. Modifying Eq. (5-36) the outside heat transfer surface (A_o) can be obtained from Eq.(5-39).

$$A_o = \frac{\dot{Q}_k}{U_0 \Delta T_{lg,k}} \tag{5-39}$$

The overall heat transfer coefficient (U_o) basing on the external diameters of the tubes in the shell can be found if the tube-side and shell-side heat transfer coefficients (h_i, h_o), as well as the wall thermal resistance (R_{wall}) are known. It is shown by Eq. (5-40).

$$\frac{1}{U_o} = \frac{A_o}{A_i}\left(\frac{1}{h_i}\right) + A_o R_{wall} + \frac{1}{h_o} \tag{5-40}$$

Outside heat transfer surface (A_o) is given by Eq. (5-41), while the internal heat transfer surface (A_i) can be estimated by Eq. (5-42).

$$A_o = \pi d_o N_t L \tag{5-41}$$

$$A_i = \pi d_i N_t L \tag{5-42}$$

The equations take into account the number of tubes in the shell (N_t), the length of one tube (L) and its external or internal diameter (d_o or d_i respectively). The system of equations 25-28 is a configuration of four equations with ten unknowns. It has to be supplemented with three correlation equations allowing for calculation of h_i, h_o and R_{wall}. Three lacking equations are the assumptions towards construction details, namely the values of internal and external tube diameter and the shell diameter (d_s). These assumptions and presumptions towards heat exchanger layout enable the calculation of number of tubes. The method for establishing an approximate construction design for the shell and tube heat exchangers has been here taken from [115]. The tube layout has been assumed to be triangular with a 30° angle between tubes of external diameter d_o. It is presented in Fig. 5.5.

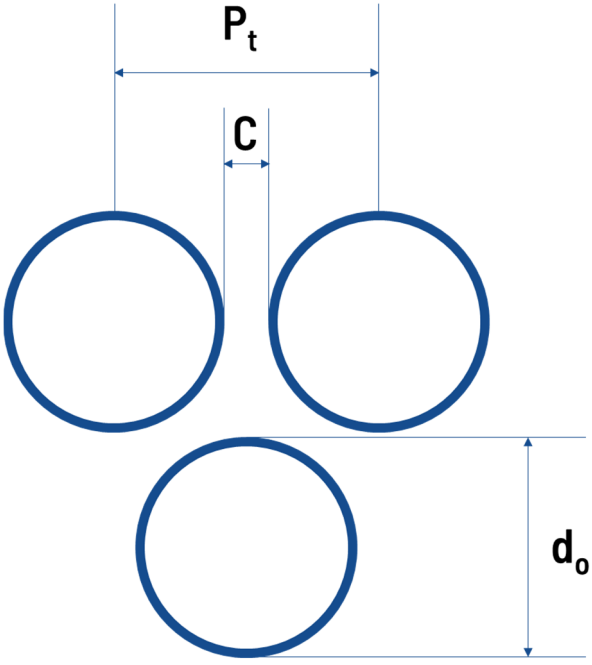

Fig. 5.5 Tube bundle layout with a triangular pitch.

Tube pitch (P_t) takes into account the distance between tubes called the clearance (C). These can be estimated from the dependence in Eq. (5-43) and (5-44).

$$P_t = d_o + C \tag{5-43}$$

$$P_t = 1.25 d_o \tag{5-44}$$

All tubes make together a tube bundle. Its diameter (d_b) can be estimated by Eq. (5-45).

$$d_b = d_o \left(\frac{N_t}{k_1}\right)^{\frac{1}{n_1}} \tag{5-45}$$

If it is assumed that tube bundle diameter equals the known shell diameter, Eq. 27 can serve to calculate the number of tubes fitting into the shell. For triangular layout and a two-passes heat exchanger, parameters k_1 and n_1 are 0.249 and 2.207, respectively.

The tube-side and shell-side heat transfer coefficients were evaluated by means of correlation functions allowing the estimate of the Nusselt number. This is defined as in Eq. (5-46) and (5-47) for tube-side and shell-side respectively (Nu_{tube} and Nu_{shell}):

$$Nu_{tube} = \frac{h_i d_i}{\lambda_{fluid,tube}} \tag{5-46}$$

$$Nu_{shell} = \frac{h_o D_e}{\lambda_{fluid,shell}} \tag{5-47}$$

where λ_{fluid} is the thermal conductivity of the fluid on tube-side or shell-side. The characteristic dimensions for the two flows are: inner tube diameter for the tube-side and an equivalent diameter for the shell side (D_e). The equivalent diameter is usually understood as a proportion between quadruple of the free-flow area and the wetted perimeter. For the assumed triangular pitch layout it can be calculated with Eq. (5-48).

$$D_e = \frac{4\left(\frac{P_t^2\sqrt{3}}{4} - \frac{\pi {d_o}^2}{8}\right)}{\pi \frac{d_o}{2}} \tag{5-48}$$

Depending on the recognition of the thermal process and flow type, a correlation from Table 5.2 was chosen. A procedure created in EES code allowed for automatic adjustment of desired correlation function to a flow regime.

Table 5.2 Correlation functions for calculating heat transfer coefficients in the ammonia-chiller components

Flow side	Thermal process	Flow regime	Correlation function	Reference
Tube side	Condensation in horizontal tube	Wavy or annular	*Dobson and Chato (1998)*	[116]
Tube side	Boiling	Flow boiling	*Shah (1976, 1982)*	[117,118]
Tube side	Flow	Laminar	*Shah and London (1978)*	[119,120]
Tube side	Flow	Turbulent Pr > 0.5	*Gnielinski (1976)*	[114,119]
Tube side	Flow	Turbulent Pr < 0.1	*Notter and Sleicher (1973)*	[119,121]
Shell side	Flow	Laminar Transient Turbulent	*Bell-Delaware (1981,1988)*	[122,123]

If forced convection on the tube-side is considered, the table presents only correlation function base for laminar and turbulent flow regime. The procedure prepared in EES code determines if the flow is laminar or turbulent. Transitional flow is assumed to occur for Reynold's numbers between 2300 and 3000 and interpolation is applied between the laminar and turbulent correlations. If the flow is turbulent with $0.1<Pr<0.5$, the convective heat transfer coefficient is interpolated between the two values obtained from the Gnielinski approach and Notter and Sleicher correlation function.[119]

It should be marked that the Bell-Delaware method was applied for the shell-side flows because it is accepted as a correlation function system that is the most reliable method that takes into account the whole complexity of the shell flow. Shell flow combines cross-flow, baffle window flow as well as baffle-shell and bundle-shell bypass streams. The bell-delaware method is supposed to apply a correction factor to all of the phenomena [115].

Thermal conductivity resistance of the tube wall depends on the material properties. Copper cannot be used in the ammonia refrigeration systems because of its corrosion interactions. Technical literature indicates that aluminum was proved to be a good construction material for the ammonia cycles with negligible corrosiveness tendency [124]. However, according to the project deliverables [99], the vessels and heat exchangers are made of stainless steel. Hence, the conductivity λ_{wall} of this material was used in the analysis. Eq. (5-40) can be simplified to the form of Eq. (5-49)

$$\frac{1}{U_o} = \frac{d_o}{d_i}\left(\frac{1}{h_i}\right) + d_o \frac{\ln \frac{d_o}{d_i}}{2\lambda_{wall}} + \frac{1}{h_o} \quad (5\text{-}49)$$

Having a complete equation system, the sizes of the heat exchangers and their respective overall heat transfer coefficients could have been defined.

5.2 Simulation model of the solar collector field

In a solar thermal collector, solar radiation energy is converted into useful heat gain. Preparation of solar collector model demands a detailed forecast of the collector's efficiency, acknowledging that the performance is limited both by the optical and thermal losses. Basic energy balance equations are similar for flat plate collectors as well as for the concentrating parabolic trough collectors, while the optical characteristics are unique to each design.

The solar energy absorbed by the receiver's tube ($\dot{Q}_{abs}$) is equal to the sum of the useful heat gain ($\dot{Q}_u$) and the thermal energy losses due to the processes of convection ($\dot{Q}_{conv}$) and radiation ($\dot{Q}_{rad}$). It is presented in Eq. (5-50).

$$\dot{Q}_{abs} = \dot{Q}_u + \dot{Q}_{conv} + \dot{Q}_{rad} \quad (5\text{-}50)$$

The heat absorbed by the receiver of a concentrating collector depends on the amount of the direct solar radiation beaming on the given aperture area (*G*). The mathematical formulation is shown in the Eq. (5-51). Referring to concentrating collectors, the diffuse part of total solar radiation cannot be taken into account, because the directional properties of light transmission are lost with scattering by the atmosphere. Scattered rays cannot be concentrated on the focal point of the collector. However, concentrators make better usage of the direct (beam) radiation than stationary collectors due to the sun tracking mechanism. According to documentation, the simulated solar field is equipped with a constant tracking on the horizontal axis. In this study, values of incoming direct solar radiation on the tracking surface are already given as instant values thanks to a solar radiation processor prepared in TRNSYS environment.

The amount of solar energy absorbed is equal to the difference between the incident solar radiation and the optical losses [125]. The relationship is relevant for all of concentrating collectors, thus the quantity of general collector area (A_c) appears. For the further analysis of parabolic trough concentrators, the aperture area (A_{ap}) will be introduced. It is the surface of mirror diminished by the receiver area, which is shadowing the concentrator. Hence, it will constitute the area from which radiation is collected.

$$\dot{Q}_{abs} = G \cdot A_c \cdot \rho_{sc} \cdot (\psi\tau\alpha)_{sc} \quad (5\text{-}51)$$

The optical losses are represented here by the optical efficiency of the collector that is given by Eq. (5-52)[125]. The optical efficiency depends on the optical properties of the collector's elements (ρ_{sc} reflectance of the concentrator, τ transmittance, α absorptance) as well as on the intercept factor, ψ (defined below). Beyond these, an impact on the real value of the optical efficiency have the following factors: cleanliness of reflector and of glass, incidence angle modifier (IAM), shading of the rows and end losses.

$$\eta_0 = \rho_{sc} \cdot (\psi\tau\alpha)_{sc} \quad (5\text{-}52)$$

It takes under consideration the value of the transmittance-absorbance effective product, which under operational conditions is time-variant, as it depends on the angle of incidence. The intercept factor is understood as the fraction of the incident radiation that is intercepted, captured by the receiver under conditions of normal incidence angle. Assuming the parabolic trough concentrator's design, if there were no mirror imperfections, considering the sun as a point source, with the receiver tube perfectly aligned along the focal, the intercept factor would only depend on the geometry of collector. However, this ideal case is impossible, so that ψ is also a function of optical deficiencies. The influence of the incidence angle on transmittance, absorptance and the intercept factor may be considered individually, or be represented by the incidence angle modifier. Because manufacturers usually provide the information of the transmittance-absorbance product for the normal angle, it could be evaluated from the formula in Eq. (5-53).

$$(\psi\tau\alpha)_{sc} = (\psi\tau\alpha)_{sc,n} \cdot IAM \quad (5\text{-}53)$$

The IAM is a correction factor that takes into account the fact that angle of incidence (θ, angle between the direct radiation beaming on the surface of interest and the normal to that surface [125]) changes consequently throughout the day and the same causes losses influenced by change of the glass envelope absorptance and mirror reflection. IAM is typically provided by manufacturers as a function dependent on the incidence angle value for the analysed surface.

The thermal losses decreasing the collector's efficiency may be detailed into the receiver thermal losses, the piping thermal losses and by the design of bellows and supports that also influence the thermal losses. Therefore, the heat losses in the right-hand part of the equation

(5-50) could be substituted by the following equations (5-54) and (5-55), where A_r is already the receiver area.

$$\dot{Q}_{conv} = h_{conv} \cdot A_r \cdot (T_{abs} - T_{amb}) \tag{5-54}$$

$$\dot{Q}_{rad} = \varepsilon_{abs} \cdot \sigma \cdot F_{abs-amb} \cdot A_r \cdot (T_{abs}^4 - T_{amb}^4) \tag{5-55}$$

h stands here for convective heat transfer coefficient, T_{abs} is the absorber temperature, ε_{abs} is the absorber's emissivity and $F_{abs-amb}$ is the absorber versus ambient view factor. The useful heat gain derives directly from the energy balance presented in Eq. (5-56)

$$\dot{Q}_u = \dot{m}_{HTF} \cdot \left(c_{pfout} t_{out} - c_{pfin} t_{in}\right) \tag{5-56}$$

Referring to measurements over a specified period of time dτ, the collector's overall efficiency can be written as in Eq. (5-57).

$$\eta = \frac{\int \dot{Q}_u \, d\tau}{A_c \cdot \int G \, d\tau} \tag{5-57}$$

As this quantity of converted energy, described as useful heat gain, is in particular important for the development of a model of the solar collector, a uniform collector energy balance has been introduced. The theoretical equation was developed by Hottel, Whillier and Bliss [125] and is presented in the Eq. (5-58).

$$\dot{Q}_u = F_R \cdot A_c \cdot [G \cdot \eta_0 - U_L \cdot (t_{in} - t_{amb})] \tag{5-58}$$

Thus, the former Eq. (5-57) leads to an updated version of efficiency formulation, presented in Eq. (5-59).

$$\eta = F_R \cdot \eta_0 - \frac{F_R \cdot U_L \cdot (t_{in} - t_{amb})}{G} \tag{5-59}$$

F_R is the heat removal factor describing the ratio of actual useful energy gain to the reference energy gain which would be produced, if the collector (absorber) surface were at the heat transfer fluid inlet temperature. Therefore it is equal to the effectiveness of a conventional heat exchanger, expressing this last as the ratio of the actual heat transfer to its maximum possible value. Heat removal factor can be calculated from the equation (5-60), which is a result of combination of equations (5-56) and (5-58).

$$F_R = \frac{\dot{m} \cdot C_p \cdot (t_{out} - t_{in})}{A_c \cdot [G \cdot \eta_0 - U_L \cdot (t_{in} - t_{amb})]} \quad (5\text{-}60)$$

U_L is the overall heat loss coefficient expressed by the equation (5-61). The coefficient is a sum taking into account radiation and convection from the surface and conduction through the support structure, which can be omitted as in equation (5-50)[126]. Consequently, $F_R(\tau\alpha)$ describes how the energy is absorbed, while $F_R U_L$ indicates how energy is lost.

$$U_L = h_{conv} + h_{rad} + h_{cond} \quad (5\text{-}61)$$

In order to estimate the overall heat loss coefficient, the knowledge about the glass cover properties and especially about the temperature of the glass cover is required. Therefore also empirical equations for the estimation of the overall heat loss coefficient, eliminating the need for iterative calculations, have been developed. Equation (5-62) presents the evaluation defined by Mullick and Nanda [126]. The main variables are the local receiver temperature T_r, cover temperature T_c and ambient temperature T_{amb}.

$$\frac{1}{U_L} = \frac{1}{C_3 \cdot (T_r - T_c)^{0,25} + \frac{[\sigma \cdot (T_r^2 + T_c^2) \cdot (T_r + T_c)]}{\left[\frac{1}{\varepsilon_r} + \frac{D_o}{D_i} \cdot \left(\frac{1}{\varepsilon_c} - 1\right)\right]}} + \frac{D_o}{D_c} \cdot \left(\frac{1}{h_{conv} + \sigma \cdot \varepsilon_c \cdot (T_c^2 + T_{amb}^2) \cdot (T_c + T_{amb})}\right) \quad (5\text{-}62)$$

The included constant C_3 can be obtained from a correlation of Raithby and Hollands [126] described by Eq. (5-63):

$$C_3 = \frac{17{,}74}{(T_r + T_c)^{0,4} D_o \left(D_o^{-0,75} + D_i^{-0,75}\right)} \quad (5\text{-}63)$$

As the mentioned formulas demand the knowledge of details considering the heat transfer quantities of the collector under operational conditions, this modelling approach is frequently applied, when detailed experimental (or certified test-) data are available. On the other hand, the TRNSYS manual [127] claims for type 536, that the $F_R U_L$ standard collector loss coefficient should be the value provided by the manufacturers. If this was the case, this would lead to a linear representation of the efficiency function depending on a parameter relating temperature to radiation, which is not adequate. While the efficiency of every solar collector should be

defined as the ratio of the useful heat gain and the incident solar irradiation on the aperture area, it is usually given as a function, where $\frac{\Delta T}{G}$ is the variable. It represents the value of the difference between the average heat transfer fluid temperature and the ambient temperature, divided by the aperture normal irradiance. So, the efficiency can be given by the second order polynomial Eq. (5-64).

$$\eta_{coll} = \eta_o - (a_1 + a_2 \Delta T) \frac{\Delta T}{G} \tag{5-64}$$

Depending on the physical process in the collector, the value of average heat transfer fluid temperature (needed for ΔT) can be defined differently. If there was a direct steam generation inside the collector, which leads to a two-phase condition, the best solution would be given by an entropy-mean temperature, as shown in equation (5-65). Such an approach takes under consideration the existence of sub-cooled and superheated parts as well as phase changes that result in constant zone temperature [128]. In the case of this analysis, a single phase solar collector, where the heat transfer oil is heated, is analysed. Therefore the T_{HTF} can be given by the arithmetic-mean, as in equation (5-66).

$$T_{HTF} = \frac{h_{out} - h_{in}}{s_{out} - s_{in}} \tag{5-65}$$

$$T_{HTF} = \frac{T_{out} + T_{in}}{2} \tag{5-66}$$

The parameter η_{0_n} is the optical efficiency without accounting for the influence of the incidence angle. Whereas a_1 and a_2 are the linear and quadratic heat loss coefficients due to the convection, conduction and radiation. The values of those parameters are obtained during original thermal performance tests.

Formula (5-64) is a fundamental equation for a steady-state model when the incidence angle is near to normal. For this reason, to conduct calculations in real conditions, it is necessary to apply the IAM to the optical efficiency is necessary. Then the efficiency would be given by equation (5-67). Details on IAM function used in this simulation model are given in section 5.4.

$$\eta_{coll} = \eta_{0_n} \cdot IAM - (a_1 + a_2 \Delta T) \frac{\Delta T}{G} \quad (5\text{-}67)$$

$$\eta_0 = \eta_{0_n} \cdot IAM \quad (5\text{-}68)$$

At this stage, the efficiency parameters for the specific unit collector are known, it is then possible to extract the useful energy gain for N_{coll} number of collectors. This is done using the following equations (5-69), (5-70).

$$\dot{Q}_u = \eta_{coll} \cdot \dot{Q}_{incoll} \quad (5\text{-}69)$$

$$\dot{Q}_{incoll} = A_{ap} \cdot N_{coll} \cdot G \quad (5\text{-}70)$$

As it can be observed, the gross amount of heat transferred to collector ($\dot{Q}_{incoll}$) is a function of the aperture collector area for the whole Solar Field available.

5.3 Off-design simulation of a solar energy driven ammonia-water chiller

The analysed ammonia-water chiller relies on driving energy of intermittent availability. Therefore there are only several hours during the whole cooling season when the cooling system operates under design conditions. The majority of operation time is done under the conditions when the load differs from the design point. Simulation of performance under these conditions and off-design analysis is of high importance. It is feasible, once the sizes and construction of the components were defined during the design analysis phase. Now, knowing the heat transfer area limitation and instant thermodynamic parameters of incoming external flows (cooling water, hot water, chilled water) and by the control of external mass flow rates, the heat transfer rate in each heat exchanger can be defined. It leads to finding the temperature, pressure, concentration and mass flow rates distribution in the ammonia-water cycle. Changing the mass flow rate in off-design should also affect the circulation pumps performance. The effect is investigated by finding a correlation function for the exemplary performance curves of a small pump [129]. The pump flow control is performed by adjusting the pump speed. Variable speed drive should allow for the pump speed adjustment over a continuous range. It should be emphasized that 6 components in the cooling cycle are heat exchangers which performances are defined by the Peclet equations (5-36), where the temperatures are entangled in logarithmic temperature difference, but also in the correlation functions needed to find the overall heat

transfer coefficient. Therefore, the off-design analysis task is brought to a complex iterative procedure with interdependent loops. The procedure finds the parameters distribution basing on presumed external flow conditions and constants from sizing phase.

The dynamic behaviour of the system is particularly caused by the driving energy rate – the useful heat gain from the solar collectors that is strictly depending on variable meteorological conditions. The off-design analysis is built upon a time-forward simulation, which requires a time discretization. The evolutionary variable time step (τ_{i}), given by Eq. (5-71), is physically determined as the time needed by the unit volume of heat transfer fluid (HTF) to flow through the whole solar field (represented by the calculated length L_{pipes}) and come back to the same point.

$$\tau_{\mathrm{i}} = \frac{L_{pipes}}{w_{\mathrm{av,i}}} \tag{5-71}$$

The velocity $w_{\mathrm{av,i}}$ is calculated step by step from the mass flow rate in the collectors considering an average density of the HTF and the absorber pipe diameter (d_{absorber}) , as in equation (5-72). Author is aware of the simplification: This estimate assumes that the heat transfer velocity calculated for the collector conditions is maintained in the whole solar field neglecting variations of hydraulics. However, this approach has already been used in published works [130–132].

$$w_{\mathrm{av,i}} = \frac{\dot{m}_{\mathrm{HTF,i}}}{\rho_{av,HTF} \cdot \pi \frac{d_{\mathrm{absorber}}{}^{2}}{4}} \tag{5-72}$$

The daily off-design simulation of the solar cooling system performance starts with the solo operation of the solar field. The solar field has to warm up before the heat rate is directed to the generator of the chiller. Alone project deliverables report that the minimum driving temperature for the ammonia-water chiller is 130°C. The simulation starts in the morning (at 7:00) and the procedure calculates the collectors outlet temperature for every time step assuming constant mass flow rate. Since the efficiency of the solar collector depends on the average heat transfer fluid temperature, it is again an iterative procedure. Till the outlet temperature does not exceed the desired driving temperature value, the heat transfer fluid is only circulating in the field and warming up. Once the outlet temperature reaches the desired value, a heat rate from the solar field is passed to the desorber section. For the base case, the temperature difference of the heat transfer fluid is constant and to maintain both the defined temperature difference and desired outlet temperature, the mass flow rate has to be controlled. (A procedure looking for an optimal temperature difference in solar collector aimed at maximizing the exergy efficiency of a solar

collector was proposed in [128]. However, in here presented study potential advantages of variable driving temperatures in solar ammonia-water chiller will be presented in section 5.8.) From this hour the simulation also includes a chiller section. Simulation of chiller performance lasts till solar collectors are able to deliver heat input.

5.3.1 Correction to efficiency due to flow rate other than under test conditions

It has been stated that in order to maintain a defined temperature difference in the solar field section, the mass flow rate is controlled. On the other hand, the simulation model of solar collectors performance rests on the second order Bliss equation as given in Eq. (5-67). The values for optical efficiency and heat loss coefficients a_1, a_2 are usually delivered by the manufacturer, basing on their certification measurements. The measurements are done under specific test conditions with a specified mass flow rate that is also included in the manufacturer technical data sheets as "test mass flow rate" in kg/s or "area specific mass flow rate" in kg/m^{2}s. If the mass flow rate is changing, it would also affect the final efficiency parameters. The influence can be taken into account following the computational path suggested in [125].

It is claimed that, if a collector operates at a flow rate other than that of the test conditions, some corrections to the values of $F_R(\tau\alpha)$ (or in the case of concentrating collectors: $F_R\rho(\gamma\tau\alpha)$) and F_RU_L should be introduced. That is a consequence of the fact the heat removal factor (F_R) is a function of the mass flow rate, which was presented in equation (5-60). Theoretically, the correction factor (r) accounting for the variable mass flow rate is represented by the ratio given by equation (5-73) [125].

$$r = \frac{F_R U_L|_{use}}{F_R U_L|_{test}} = \frac{F_R(\tau\alpha)|_{use}}{F_R(\tau\alpha)|_{test}} \tag{5-73}$$

As in this study the test-obtained efficiency definition is used, instead of design approach, some modifications to the formula have to be applied. According to the sources [125,127] two modifiers should be calculated. Obviously, the mass flow rate passing the absorber tubes can be evaluated at every hour point from the equation (5-74).

$$\dot{m} = \frac{\dot{Q}_u}{c_{fout} \cdot t_{out} - c_{fin} \cdot t_{in}} \tag{5-74}$$

The R_1 and R_2 modifiers are said to correct the useful heat gain equation for flow rates other than under test conditions. Consequently, the corrected value of heat produced by collectors can be determined by equations (5-75) and (5-76).

$$\dot{Q}_{u\_test} = R_1 \cdot R_2 \cdot \dot{Q}_u \quad (5\text{-}75)$$

$$\dot{Q}_{u\_test} = R_1 \cdot R_2 \cdot A_{ap} \cdot coll_{in\ series}[F_R \cdot \eta_0 \cdot G - F_R \cdot U_L \cdot (t_{in} - t_{amb})] \quad (5\text{-}76)$$

Where the mass flow rate correction factors may be calculated as shown in equations (5-77) and (5-78).

$$R_1 = \frac{\dot{m} \cdot C_p}{A_{ap}} \left(\frac{1 - e^{\left(\frac{-F' U_L \cdot A_{ap}}{coll_{in\ series} \cdot \dot{m} \cdot C_p} \right)}}{R_{test}} \right) \quad (5\text{-}77)$$

$$R_2 = \frac{1 - \left(1 - \frac{R_1 \cdot A_{ap} \cdot F_R U_L}{\dot{m} \cdot C_p \cdot coll_{in\ series}}\right)^{coll_{in\ series}}}{coll_{in\ series} \cdot \left(\frac{R_1 \cdot A_{ap} \cdot F_R U_L}{\dot{m} \cdot C_p \cdot coll_{in\ series}} \right)} \quad (5\text{-}78)$$

R_1 includes a term R_{test} which allows to enter the original test mass flow rate value into the modifiers. R_{test} can be evaluated from (5-79).

$$R_{test} = \dot{m}_{test} \cdot C_p \left(1 - e^{\left(\frac{-F' U_L}{\dot{m}_{test} \cdot C_p} \right)} \right) \quad (5\text{-}79)$$

The above-mentioned equations still contain an unknown modified loss coefficient called $F'U_L$. It is an internal variable, based on the standard collector loss coefficient F_RU_L, introduced to correct the mass flow rate. It is given by the conditional equation (5-80).

$$F' U_L = \begin{cases} F_R U_L & if\ \frac{F_R U_L}{\dot{m}_{test} \cdot C_p} \geq 1 \\ m_{test} \cdot C_p \left(1 - e^{\left(\frac{F_R U_L}{\dot{m}_{test} \cdot C_p} \right)} \right) & if\ \frac{F_R U_L}{\dot{m}_{test} \cdot C_p} < 1 \end{cases} \quad (5\text{-}80)$$

As only the test performance data as the second-order polynomial efficiency fit are available, the standard collector loss coefficient F_RU_L can be determined from the already known energy balance equations and basing on the calculated useful heat gain value. The calculated mass flow rate modifiers can be subsequently implemented to the equation (5-75), in order to determine a more realistic value of the heat gain from the Solar Field.

5.4 Assumptions

5.4.1 Design conditions

As it was already mentioned, the design analysis is aimed at an estimate of the heat transfer surfaces. It is known that the heat rate derives from eight parabolic troughs collector. They are presented in Fig. 5.6.

Fig. 5.6 Row of parabolic trough collectors in Misericordia Solar cooling plant[1].

Their efficiency parameters are given in Table 5.3. Because of the lack of certified efficiency data for the new CREAR-manufactured solar collectors, the data of previously installed SOLITEM collectors is used. It is also motivated by the fact, that the deliverables of the project and some measurements results are available for the chiller cooperating with that kind of concentrators [133]. Table 5.3. reports also the size of the solar field and the design meteorological data. The value of incoming beam radiation ($G=500W/m^2$) does not correspond to the hour with the best solar radiation conditions. It was assumed that it is of higher importance to size the device for average summer conditions taking into account, that the lower irradiation level occurs more frequently and therefore, the chiller works more often close to design conditions. It has to be also noted that in order to eliminate the risk of frosts and maintain the wide temperature range of operation, thermal oil is assumed to be the heat transfer fluid in the

[1] Photography taken by the author

solar field loop. Thermodynamic properties of Therminol® 55 are provided for the analysis, taking advantage of EES properties library [134].

Table 5.3 Design input parameters for the solar field simulation.

Parameter	**Symbol**	**Unit**	**Value**
Optical efficiency	η_{0_n}	-	0.75
Linear heat loss coefficient	a_1	W/(m^{2}K)	0.1123
Quadratic heat loss coefficient	a_2	W/(m^{2}K^2)	0.00128
Number of solar collectors	N_{coll}	-	8
Aperture of N_{coll} solar collectors	A_{ap}	m^2	73.3
Beam radiation	G	W/m^2	500
Ambient temperature	T_{amb}	°C	25
Heat transfer fluid temperature increase	$T_{17} - T_{18}$	K	10

Group of assumptions needed for the design simulation of the ammonia-water chiller is presented in Table 5.4.

Table 5.4 Assumptions for the design analysis of the ammonia-water chiller.

Parameter	**Symbol**	**Unit**	**Value**
Cooling water inlet temperature	T_{19}	$°C$	30
Cooling water temperature increase	$T_{20} - T_{19}$	K	10
Pinch point temperature difference in condenser	$T_7 - T_{19}$	K	5
Chilled water inlet temperature	T_{21}	$°C$	15
Chilled water temperature decrease	$T_{21} - T_{22}$	K	5
Pinch point temperature difference in evaporator	$T_{22} - T_{11}$	K	5
temperature difference in generator	$T_{18} - T_5$	K	10
Subcooling of lean solution from generator	$T_{sat,14} - T_{14}$	K	5
Concentration of ammonia-water solution	x_6 x_1-x_{14}	- -	0.995 0.13
Quality of ammonia-water solution	q_{11} q_7		0.93 0

q_1		0
q_{16}		0
q_5		1
q_6		1

Simulation is performed assuming that for the moment of analysis system is in steady state. Condenser and evaporator pressures are the equilibrium pressures found for the temperatures and concentration at the outlet of these components. The pressure losses in pipes and components are negligible. The strong solution leaving absorber is at saturated state conditions (hence: $q_1=0$)

5.4.2 Off-design conditions simulation

The off-design analysis is stimulated by variable meteorological conditions. The meteorological data are obtained by means of a simulation in TRNSYS. The simulation prepared in TRNSYS allows for converting the normal irradiance data retrieved from Meteonorm databases into the beam and diffuse radiation reaching a tracking surface. It is assumed that the collectors are constantly tracking the Sun on a horizontal axis and that the solar azimuth angle equals 21°.

The simulations are performed for the reference days of cooling season months respectively in Italy and Poland. Reference days of the months are represented by hourly values of incoming solar radiation (both beam and diffused, however remembering that parabolic trough collectors are able to only absorb the beam radiation) and ambient temperature. The hourly values are obtained as averages for given hours of the day over one month. The representative days of the months were evaluated basing on annual hourly meteorological data from Meteonorm library available in TRNSYS software [135]. Since the data recovered from the Meteonorm library are hourly, a cubic interpolation was applied to simulate the operation according to the smaller time step.

In the face of no exact meteorological databases for Florence and Wrocław, the corresponding data from Pisa and Poznań are here used. The meteorological processed data for representative days of the months for Florence and Wrocław indicating on average beam radiation and ambient temperature are presented in Appendix B and Appendix C, respectively. The appendices include a discussion over the *cosine effect* burdening the tracking surface and affecting the daily profile of incoming solar radiation.

The monthly integrals of solar radiation for the two locations are presented in Fig. 5.7. The bars take into account the difference in months duration.

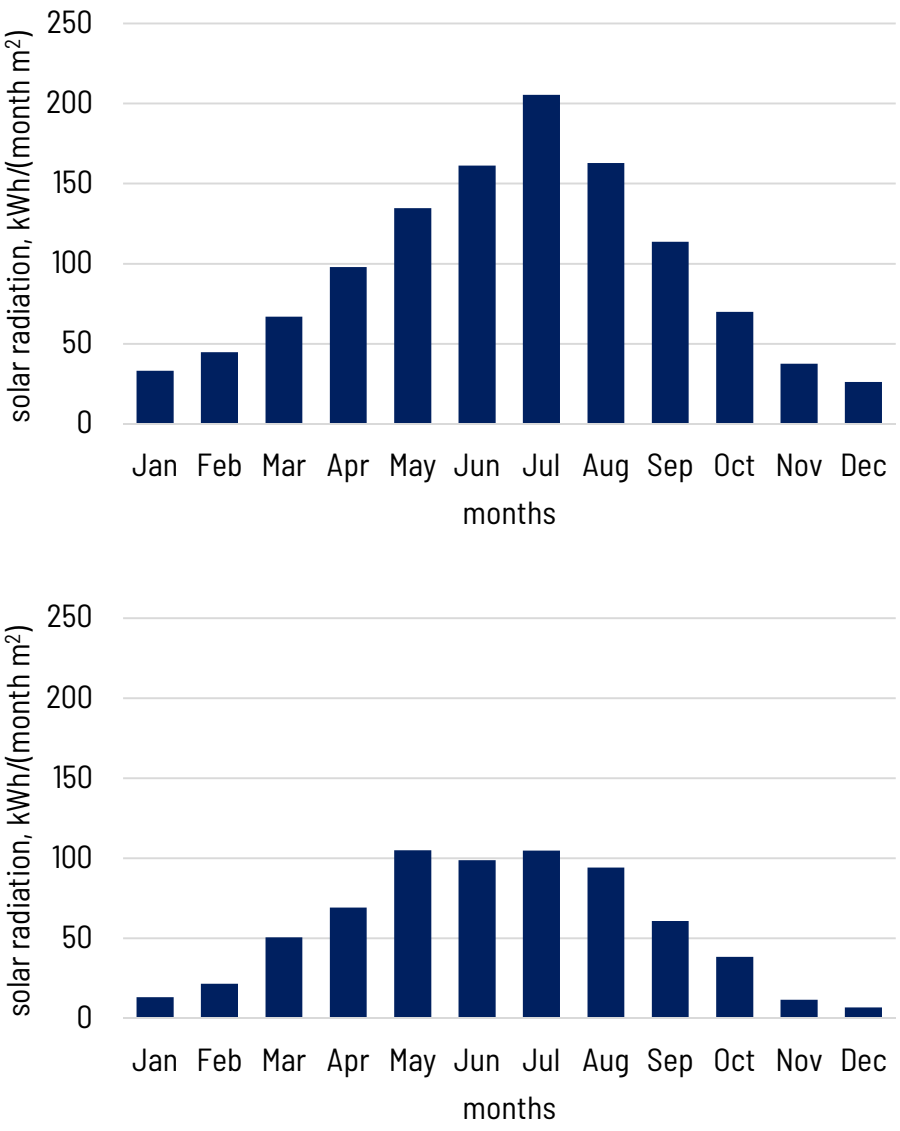

Fig. 5.7 Monthly integrals of incoming beam radiation on tracking surface in Florence (upper chart) and in Wrocław (bottom chart)

It is said, that the cooling season lasts when the temperatures during the day exceed 24°C [136,137]. Observing whole year meteorological data, it occurred that cooling season in Florence lasts from April till October and in Wrocław from May till September.

To achieve a useful heat gain for every time step during the day, the IAM value has to be applied. As it was stated in section 5.2, the optical efficiency should be also corrected by the means of incidence angle modifier (IAM). It has already been evaluated experimentally for that type of solar concentrating collector and a correlation function is applied. The function of variable incidence angle (θ, °) is given by Eq. (5-81) [138]. Value of incidence angle can be estimated analysing solar angles, but here it is also given for each hour of the day by the TRNSYS' solar radiation processer.

$$IAM = 1 - 5.782 \cdot 10^{-3}\theta + 1.485 \cdot 10^{-4}\theta^2 - 2.955 \cdot 10^{-6}\theta^3 \qquad (5\text{-}81)$$

According to Eq. (5-71), the variable time step is found assuming that the solar loop is 89 meters long.

For the base case, it is assumed that once the outlet temperature from the solar collector exceeds 160°C, the whole heat gain from the solar collector is directed to the ammonia water chiller. The solar cooling plant delivers cooling power to the building where it is supplemented by cold from vapour compression chillers that are already out of the scope of here presented analysis. For the base case off-design analysis temperatures of external inlet/outlet flows are assumed according to data given in Table 5.5.

Table 5.5 Off-design assumptions for the simulation of ammonia-water chiller – temperatures of the external flows

Parameter	**Symbol**	**Unit**	**Value**
Cooling water inlet temperature	T_{19}	$°C$	35
Cooling water temperature increase	$T_{20} - T_{19}$	K	10
Chilled water inlet temperature	T_{21}	$°C$	12
Chilled water temperature decrease	$T_{21} - T_{22}$	K	5

5.5 Results and verification

5.5.1 Design results

Table 5.6 contains the thermodynamic parameters obtained for the design conditions.

Table 5.6 Design analysis results for simulation of solar energy driven ammonia-water chiller.

i-th flow	$\dot{m}_i$	**T**$_i$	**p**$_i$	**q**$_i$	**x**$_i$	**h**$_i$	**s**$_i$
	kg/s	*°C*	*bar*	-	-	*kJ/kg*	*kJ/kgK*
1	0.05466	40	4.835	0	0.4914	-60.65	0.4385
2	0.05466	40.17	15.48	-0.001	0.4914	-59.02	0.4395
3	0.05466	58.44	15.48	-0.001	0.4914	23.33	0.695
4	0.05466	73.83	15.48	-0.001	0.4914	93.91	0.903
5	0.01296	109.2	15.48	1	0.9409	1555	4.91
6	0.01121	67.26	15.48	1	0.995	1383	4.445
7	0.01121	40	15.48	0	0.995	187.3	0.6622
8	0.01121	38.82	14.98	0.005284	0.995	187.3	0.6626
9	0.01121	8.61	14.98	-0.001	0.995	36.77	0.1562
10	0.01121	3.349	4.835	0.01982	0.995	36.77	0.1624
11	0.01121	5	4.835	0.93	0.995	1185	4.293
12	0.01121	31.4	4.835	0.9937	0.995	1336	4.816
13	0.05466	66.01	4.835	0.2327	0.4914	399.8	1.847
14	0.04344	104.2	15.48	-0.001	0.3614	247	1.306
15	0.04344	74.33	4.835	0.08591	0.3614	247	1.33
16	0.001749	67.26	15.48	0	0.5938	79.56	0.8318
17	0.6014	134.2	8			564.5	1.678
18	0.6014	124.2	8			521.9	1.572
19	0.923	35	1.013			146.7	0.5051
20	0.923	45	1.013			188.5	0.6386
21	0.6144	15	1.013			63.08	0.2244
22	0.6144	10	1.013			42.12	0.1511

If quality (vapour mass fraction) of the solution is described here as -0.001, it means it is subcooled. Under design conditions chiller utilizes 25.6 kW of heat from solar collectors ($\dot{Q}_{gen}$), 0.089 kW of electric energy is consumed by the pump (N_{pump}). 12.9 kW of cooling power are produced and 38.6 kW of heat are dissipated in the condenser/absorber section. The COP for these conditions is equal to 0.501. According to technical data of Robur, the design thermal coefficient of performance should equal 0.67 and the cooling power output of the chiller is 17 kW [102]. However, these data are given for the original gas-fired chiller before

modifications. According to experimental data obtained by the CREAR group, the COP for a solar driven chiller with diathermic oil remains within range of 0.42-0.52 [139].

Table 5.7 collects results associated with heat transfer rates, overall heat transfer coefficients and heat transfer areas of the components of the chiller.

Table 5.7 Sizing results for the solar chiller.

k-th component	**Name**	**UA**	**A**
		kW/K	m^2
1	Generator	0.6518	0.8918
2	Rectifier	0.1194	8.568
3	Condenser/absorber	3.397	7.731
4	Subcooler	0.3192	2.355
5	Evaporator	1.568	7.668
6	Preabsorber	1.482	9.569

The effect of varying the design assumptions was also tested for several cases. The influence of different cooling water inlet temperature on the value of COP is presented in Fig. 5.8.

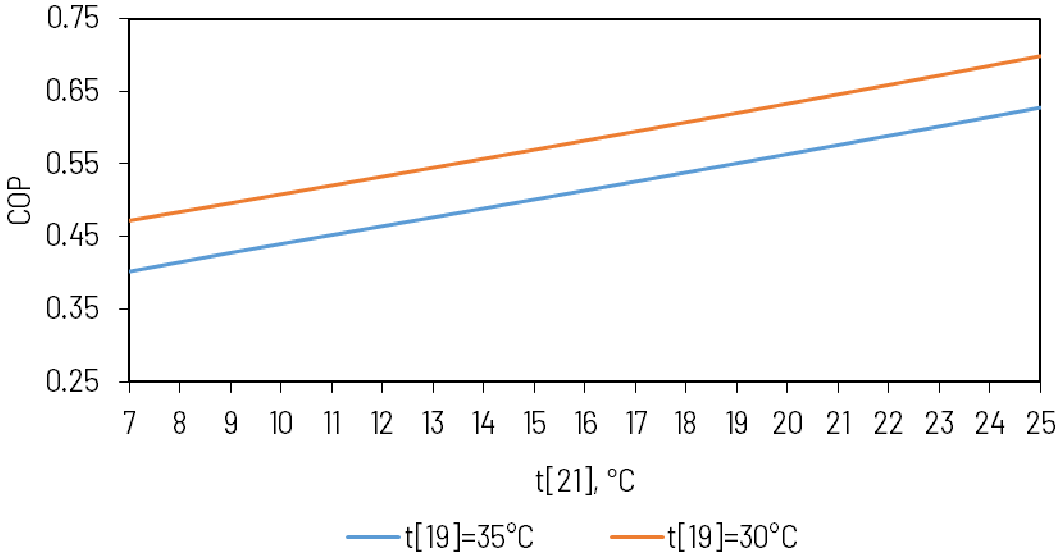

Fig. 5.8 COP value for differently assumed chilled water inlet temperatures for two variants: cooling water inlet temperature at 35°C or 30°C.

The higher the chilled water temperature, the higher becomes the COP. Nevertheless, the chilled water temperature level is resulting from the heat transfer from the chilled space and the cooling demand, it would be unreasonable to increase the chilled water temperature on purpose, when the direct useful effect of chiller operation is to obtain a cooling energy rate at the temperature

level lower than ambient temperature. Therefore, the manufacturer provided chilled water inlet temperature was applied for the final design analysis.

Similarly, the effect of changing the cooling water inlet temperature was checked and the results are shown in Fig. 5.9.

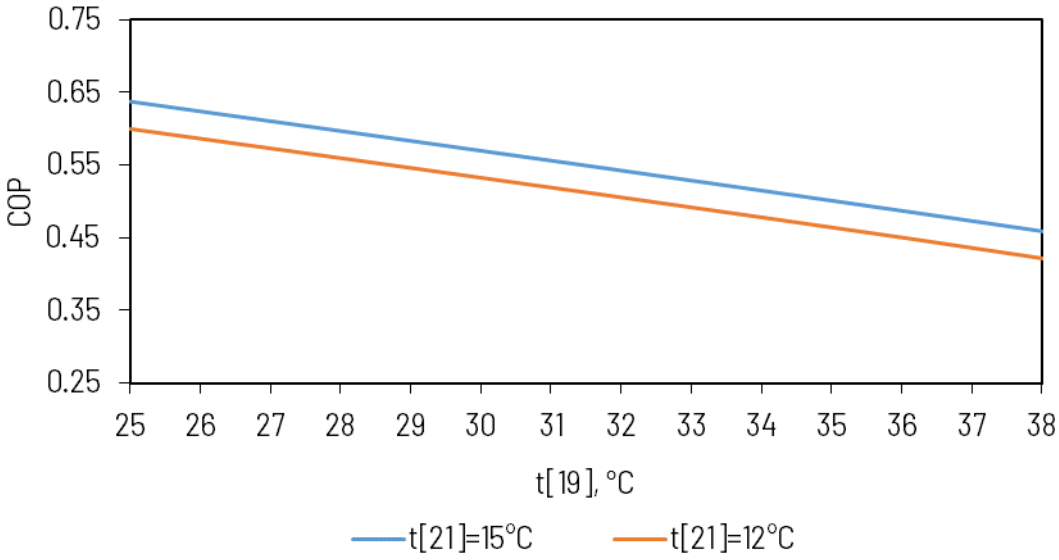

Fig. 5.9 COP value for changing cooling water inlet temperature for two variants: chilled water inlet temperature at 15°C or 12°C.

When the final size of chiller is not defined yet, the highest COP could be obtained by lowering the cooling water inlet temperature. Again: as it is not possible to cool the absorber and condenser by a mid-temperature heat rate at the temperature level below ambient conditions, a typical value of 31°C was chosen for design analysis. It also occurred that increasing the assumed difference in concentrations between weak and strong solution can lead to an increase in the coefficient of performance, but also to some point. The function has its maximum at x_1-x_{14}=0.13 and COP decreases at higher concentration differences. This behaviour is shown in Fig. 5.10 COP of the chiller in function of concentration difference between rich and lean solution. This value of concentration difference was applied to the model.

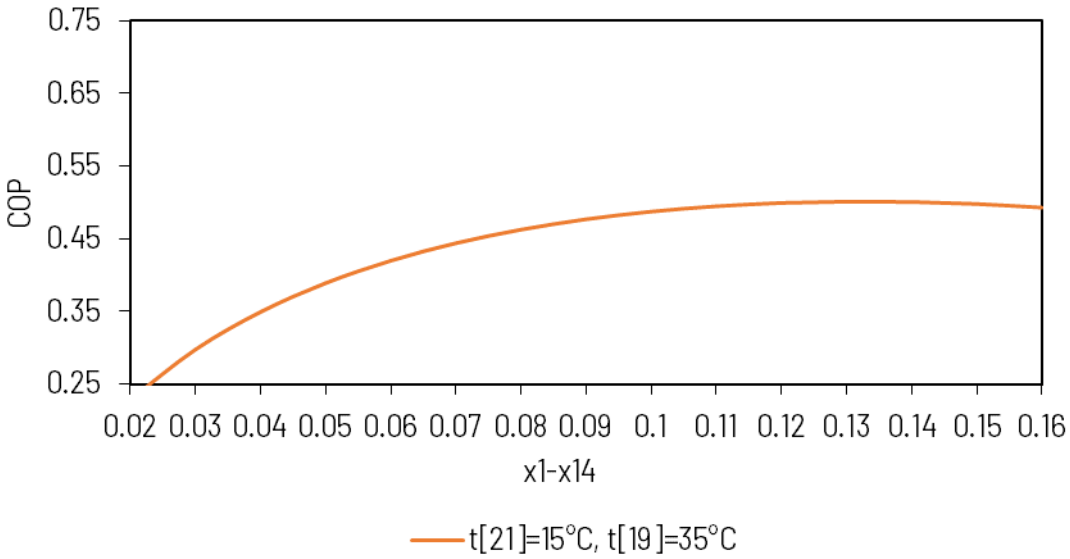

Fig. 5.10 COP of the chiller in function of concentration difference between rich and lean solution.

5.5.2 Off-design simulation results

Before the off-design simulation for cooling seasons in the two locations was performed, the preliminary off-design analysis was done. Fig. 5.11 shows the COP in the function of generator driving temperature (here: t[17] – outlet temperature from the solar field).

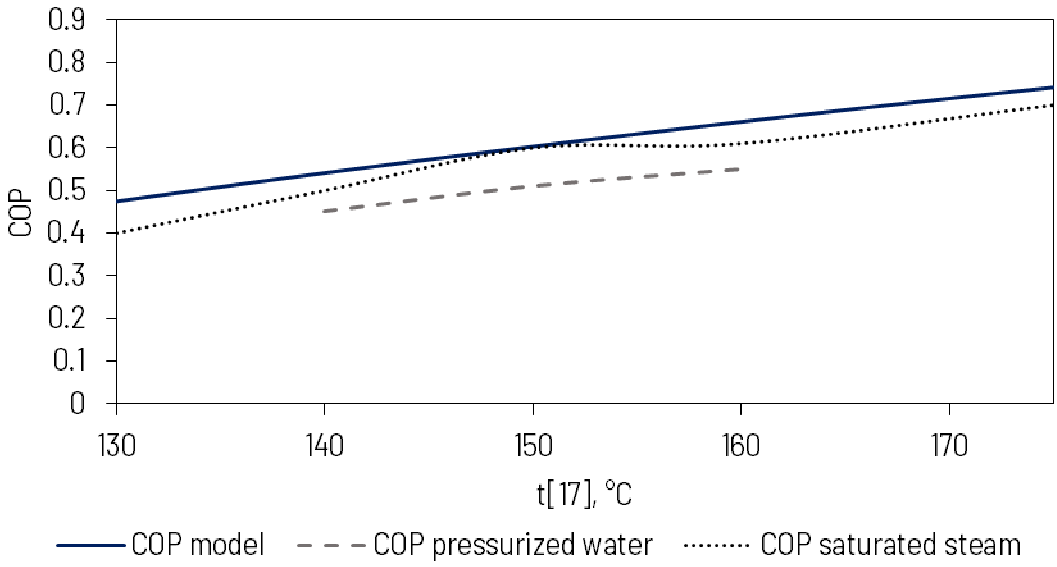

Fig. 5.11 COP of the ammonia-water chiller in the function of generator driving temperature (t[17]) – simulation results compared with experimentally obtained COP;, t[21]=12°C, t[22]=7°C, t[19]=35°C, t[20]=45°C, t[17]-t[18]=10K

This analysis was performed assuming chilled water temperature changing from T_{21}=12°C to T_{22}=7°C and that cooling water is warmed from T_{19}=35°C to T_{20}=45°C. The decrease of the driving temperature is 10K. These assumptions should be in accordance with the conditions used for testing by CREAR group [139]. In the figure estimations of COP resulting from the

experiments is also shown. COP obtained in the simulation model by the author is close to that obtained for experiments with saturated steam as heat transfer fluid from the solar collector.

According to written procedure solar field is warming up till the desired temperature of 160°C is obtained. Afterward it is operated at constant temperature difference, maintaining the output temperature. For the representative day of July, Fig. 5.12. shows the simulation effect of the procedure for the solar field operated in Florence, while Fig. 5.13 shows parallel results but for solar field operated in Wrocław.

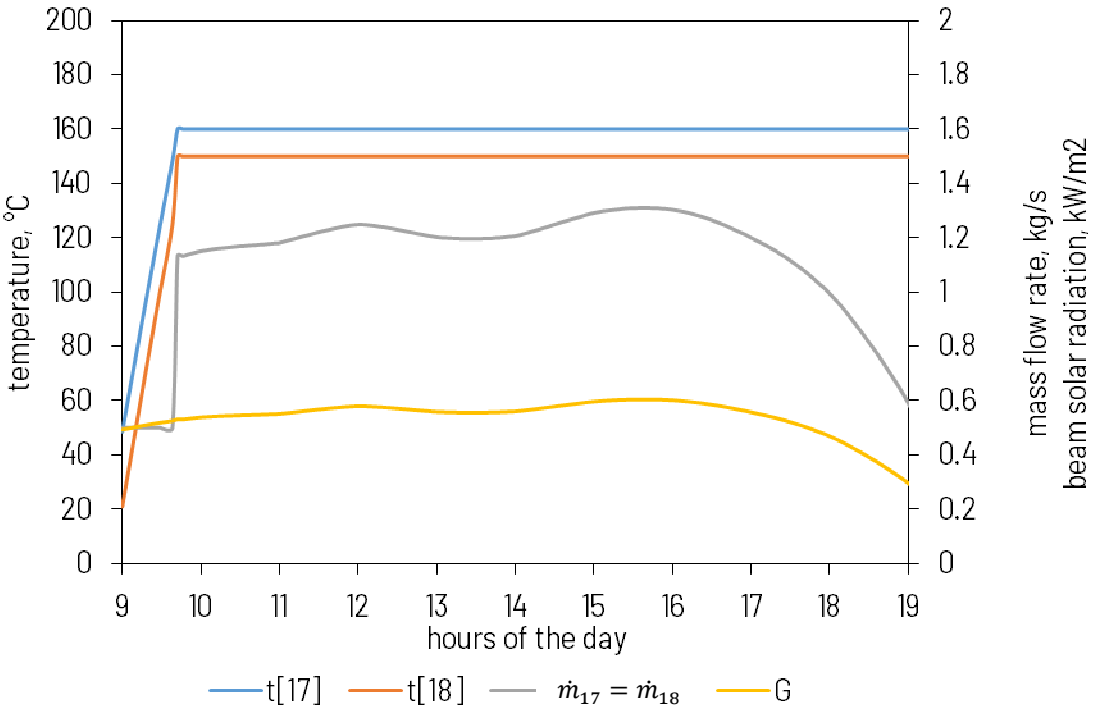

Fig. 5.12. Daily distribution of heat transfer fluid's temperature and HTF mass flow rate during the representative day of July in Florence set with incoming beam solar radiation, G

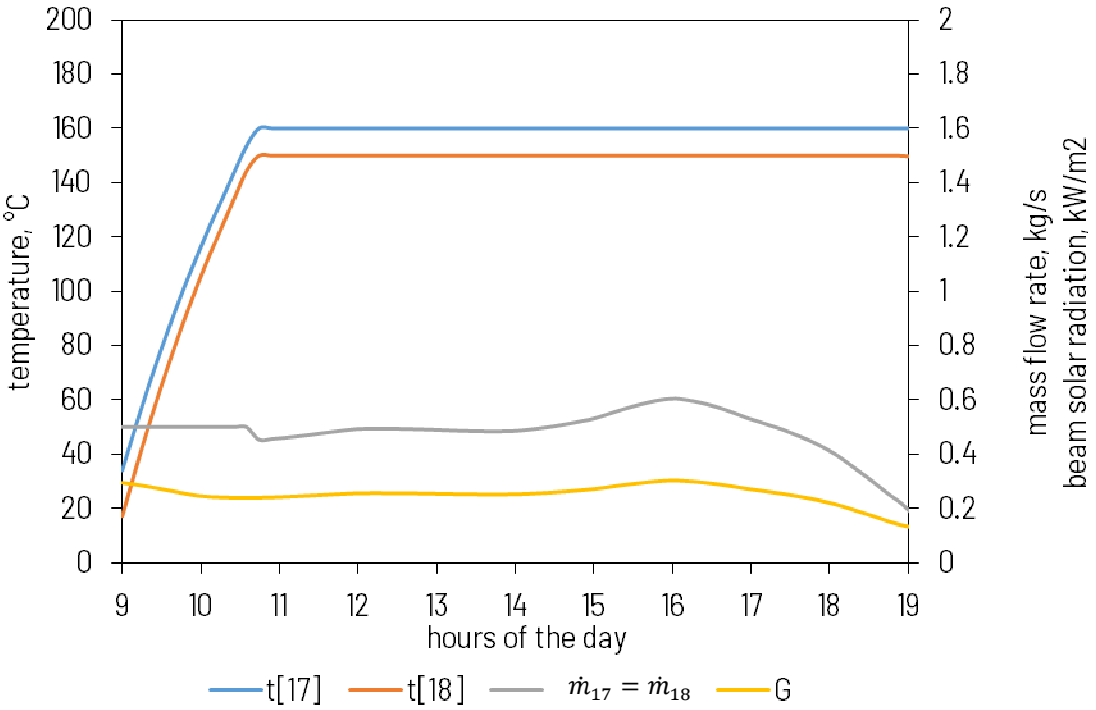

Fig. 5.13. Daily distribution of heat transfer fluid's temperature and HTF mass flow rate during the representative day of July in Wroclaw set with incoming beam solar radiation, G.

It is clearly visible that due to lower irradiation, the warming-up phase in Poland would last twice than for the solar field operated in Italy. The differences in beam solar radiation in those two locations have a relevant effect on the performance of the plant during the whole cooling season. This phenomenon is visualized by Fig. 5.14 and Fig. 5.15.

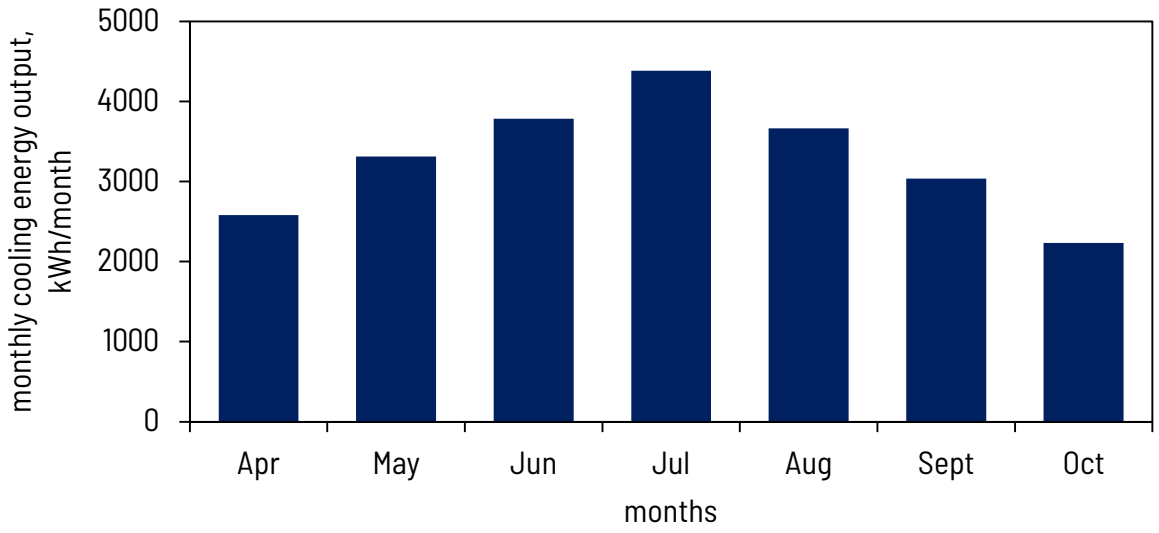

Fig. 5.14 Monthly cooling energy outputs distribution for the system operated in Italy

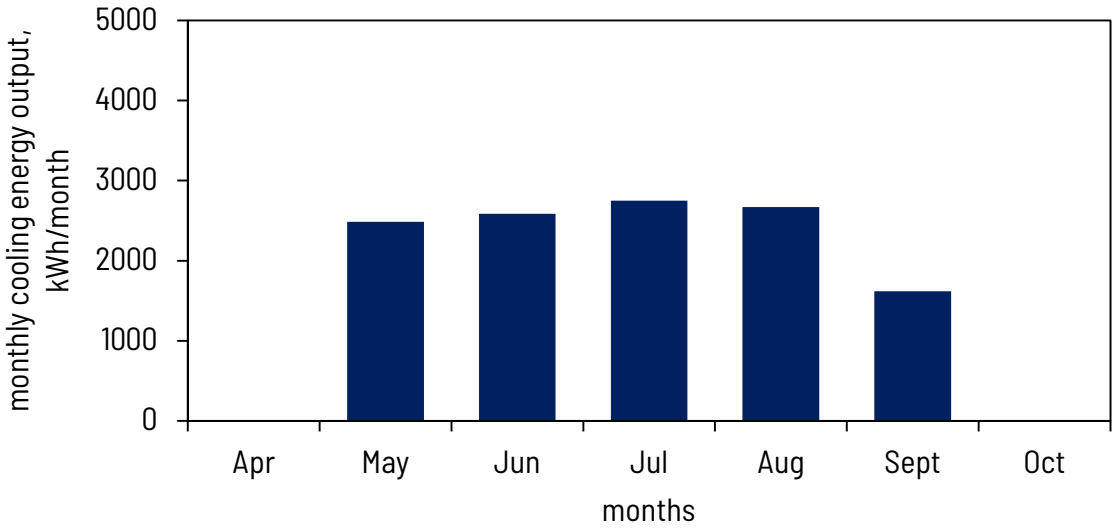

Fig. 5.15 monthly cooling energy outputs distribution for the system theoretically operated in Poland

Since the cooling season in Wrocław, Poland is limited to May-September range, no cooling energy is delivered during April and October. During the rest of cooling season months, the monthly cooling energy output is lower than in Italy. One should be reminded that the only difference is here the meteorological data. The monthly amount of cooling energy delivered does not experience any peak value during the summer months. On the contrary, the cooling energy output in July in Florence is evidently the highest (2.6 times higher than the output in October). The reason for lower productivity of the Polish solar cooling plant is not only the generally lower solar irradiance, but also the fact that the diffuse radiation predominates in the total radiation value. It cannot be however utilized for the sake of concentrating technology used.

5.6 Exergy analysis of the solar integrated absorption chiller

Author performed an exergy analysis of a solar heat driven ammonia-water chiller and evaluated the effect of variable balance boundary. The results of these analyses were published in [17].

5.6.1 Methodology

Following the discussion available in [76], one can define the exergy balances of the components in such a way that only the increases of enthalpy, entropy and exergy will be calculated (incremental approach). Therefore, to calculate the specific reference enthalpy and entropy, any freely chosen reference conditions can be adapted. Moreover, while performing the analysis with an incremental approach, chemical exergy balances are not obligatory. For

this reason, the most comfortable way is to choose such reference conditions for which no negative values of enthalpy, entropy or exergy will be obtained. Authors decided to use similar approach and assumed that the reference parameters are that of water under triple point state conditions.

Exergy of a j-th flow, of fuel and product are defined in accordance with Chapter 4 and literature sources, e.g. [76,140].

- *Exergy efficiency of an absorption chiller*

Following the discussion in [84], one could be reminded that the temperatures of the bottom heat sources present in refrigeration cycles are lower than ambient temperature. In those cases, exergy is irreplaceable to reasonably judge the quality of withdrawn heat. The lower than ambient temperature is the chilled water temperature, the higher is its exergy, although its enthalpy decreases. It may happen that the change of exergy of the bottom heat source is much higher than amount of heat transferred from this source.

Exergy analysis can help assess the reversibility of chiller processes. For its purposes, several system boundary conditions can be adopted. Szargut [84] suggested three sizes of the cycle boundary. The first boundary separates the chiller itself without the evaporator component. Exergy efficiency of such a system provides a measure of how close the thermodynamic transformations in the chiller approach ideality. Exergy efficiency could be then treated as a gross efficiency (η_b^{gross}), for cycle shown in Fig. 1 following the Eq. (5-82) 4.

$$\eta_b^{gross} = \frac{\dot{m}_{10}(b_{10} - b_{11})}{\dot{B}_F} \tag{5-82}$$

In general, for thermal absorption chillers $\dot{B}_F$ is the exergy of driving heat stream and the driving electric power of circulation pump inside the boundary.

The second balance boundary also includes auxiliary components (chilled and cooling water pumping power N_{aux}) and the change of chilled water exergy. Exergy efficiency can be then treated as net efficiency (η_b^{net}) and be calculated from Eq. (5-83).

$$\eta_b^{net} = \frac{\dot{m}_{21}(b_{22} - b_{21})}{\dot{B}_F + N_{aux}} \tag{5-83}$$

Szargut also singled out the third boundary which covers the whole package of thermal processes in the chiller. Exergy efficiency of the whole system may be called ‘general exergy efficiency’ and is given by Eq. (5-84). It takes into account the final useful effect of chiller operation, namely e.g. exergy increase of the chilled space or chilled matter ($\Delta B_{chilled\ space}$).

$$\eta_b^{gen} = \frac{\Delta B_{chilled\ space}}{\dot{B}_F + N_{aux}} \tag{5-84}$$

In the present work, authors analyse the solar ammonia-water chiller covered by a boundary of the second type. It is, however, modified: the boundary is widened by the exergy analysis of the solar collector. Consequently, the driving exergy becomes that of incoming solar radiation ($\dot{B}_s$).

Table 5.8 collects formulas for fuel and product rates evaluation following a narrow and wide balance boundary approach.

Table 5.8 Fuel-product definition for the overall system of solar ammonia-water chiller for two analyzed balance boundary conditions

Component	Fuel exergy rate	Product exergy rate
Overall system – narrow boundary	$\dot{B}_F = \dot{B}_{17} - \dot{B}_{18}$	$\dot{B}_P = \dot{B}_{22} - \dot{B}_{21}$
Overall system – wide boundary	$\dot{B}_F = \dot{B}_S$	$\dot{B}_P = \dot{B}_{22} - \dot{B}_{21}$

- *Exergy efficiency of solar collectors*

Similarly, solar collector exergy efficiency is the ratio between useful effect and driving exergy. The useful effect is understood as an increase in physical exergy stream of the heat transfer fluid ($\dot{B}_{sc}$). It is presented in Eq. (5-85).

$$\dot{B}_{sc} = \dot{m}_{17} \cdot \left(h_{17} - h_{18} - T_0 \cdot (s_{17} - s_{18})\right) \tag{5-85}$$

Where T_0 is the ambient temperature ($T_0 = T_{amb}$)

Driving exergy stream is the solar radiation exergy stream $\dot{B}_s$ discussed in Chapter 4. Collector exergy efficiency is obtained with Eq. (5-86).

$$\eta_{b\ sc} = \frac{\dot{B}_{sc}}{\dot{B}_s} \tag{5-86}$$

- *Exergy loss in solar ammonia-water chiller*

Exergy destruction caused by the process irreversibility is present in every component of the chiller and calculated following Eq. (4-19). However, there are only two components to which exergy losses are assigned. These are: condenser-absorber component and solar collector. Exergy loss in the condenser-absorber vessel is connected with waste heat removal, as given in Eq. (5-87).

$$\dot{B}_{\mathrm{L},3} = \dot{B}_{20} - \dot{B}_{19} \tag{5-87}$$

On the other hand, approach to the definition of exergy loss in the solar collector component can be variable. In here presented study, analysis presented in [141] is accepted. Exergy loss is associated with heat transfer loss taking place in the collector. Energy from a very high temperature source (temperature of the sun) is degraded to the level of absorber temperature T_{coll}. It is difficult to evaluate this temperature, but according to [142], T_{coll} could be estimated as heat transfer fluid logarithmic average temperature, accepting error this approach can introduce.

5.6.2 Assumptions

Exergy analysis was performed in parallel with the energy analysis. Thence, design point working parameters were the same as indicated in Table 5.4. Off-design exergy analysis was performed for the cooling season following variable ambient conditions that influence the system load.

For the purpose of exergy analysis, it was assumed that reference enthalpy and entropy are that of water under triple point conditions (T_{tr} *= 0.01 °C,* p_{tr} *= 0.6117 kPa).* Exergy analysis for the design conditions rests on following ambient parameters: T_0 *= 25 °C,* p_0*=101.325 kPa.* Exergy analysis performed for the whole cooling season operation bases on variable meteorological conditions retrieved from the Meteonorm library.

5.6.3 Results

Net exergy efficiency calculated after Eq. 5 equals 2.62%. If the boundaries were narrowed and the driving exergy was understood as the exergy product rate from solar collector, the exergy efficiency of considered absorption chiller would equal 11.82%. Results of exergy balance under design conditions are presented in Table 5.9 and graphically in Fig. 5.16. This band chart shows how the driving exergy is step-by-step destroyed or lost to finally achieve the useful cooling effect.

Table 5.9 Exergy balance results for the analysis of solar ammonia-water chiller.

k-th component	**Name**	$\dot{B}_{F,k}$	$\dot{B}_{P,k}$	$\dot{B}_{D,k}$	$\dot{B}_{L,k}$	$y_{D,k} = \frac{\dot{B}_{D,k}}{\dot{B}_{F,tot}}$	$y^*_{D,k} = \frac{\dot{B}_{D,k}}{\dot{B}_{D,tot}}$	η_k
		kW	kW	kW	kW	-	-	-
1	Generator	10.6	8.5	2.088	0.0	0.0436	0.071	0.803
2	Rectifier	0.4	0.1	0.246	0.0	0.0051	0.008	0.378
3	Condenser-absorber	11.5	6.8	1.869	2.8	0.0390	0.063	0.592
4	Subcooler	6.4	6.3	0.118	0.0	0.0025	0.004	0.982
5	Evaporator	2.1	1.2	0.863	0.0	0.0180	0.029	0.591
6	Preabsorber	3.2	2.4	0.869	0.0	0.0181	0.03	0.731
7	Pump	0.1	0.1	0.022	0.0	0.0005	0.0008	0.809
8	Solar collector	47.8	10.6	22.8	14.4	0.4757	0.774	0.222
9	Valve 9-10	4.3	4.2	0.044	0.0	0.0009	0.002	0.990
10	Valve 14-15	7.6	7.1	0.523	0.0	0.0109	0.018	0.931
11	Valve 7-8	4.3	4.3	0.004	0.0	0.0001	0.0001	0.999

According to previously presented methodology in Chapter 4, the exergy loss ratio is usually defined for the whole system and here $y_{L,tot} = \frac{\dot{B}_{L,\mathrm{tot}}}{\dot{B}_{F,tot}}$ =0.36. It should be, however, distinctly marked that exergy loss assigned to solar collector constitutes 84% of all exergy losses in the system.

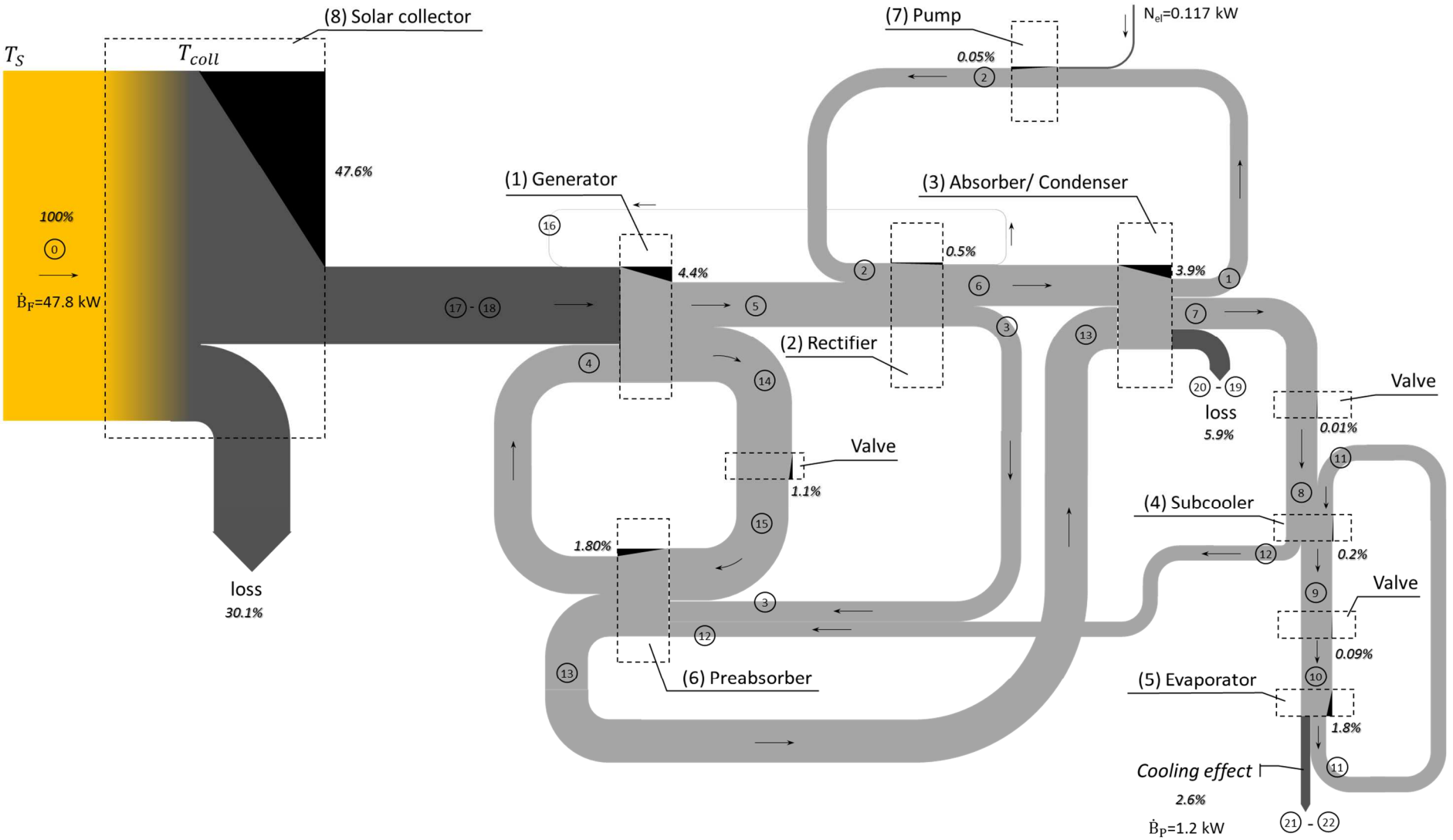

Fig. 5.16 Exergy balance- Sankey diagram of the solar driven ammonia-water chiller.

As expected, it is shown that solar collector and its efficiency parameters play the predominant role in the exergy destruction/losses allocation. Results distribution is consistent with those discussed in [84] or more recently in [70]. Apart from solar collector, highest exergy destruction and losses rates are assigned to generator and condenser/absorber components. Subsequently, the distribution of exergy destructions in the component related to the total destructions ($y^*_{D,k}$) within the system is presented in a pie chart in Fig. 5.17.

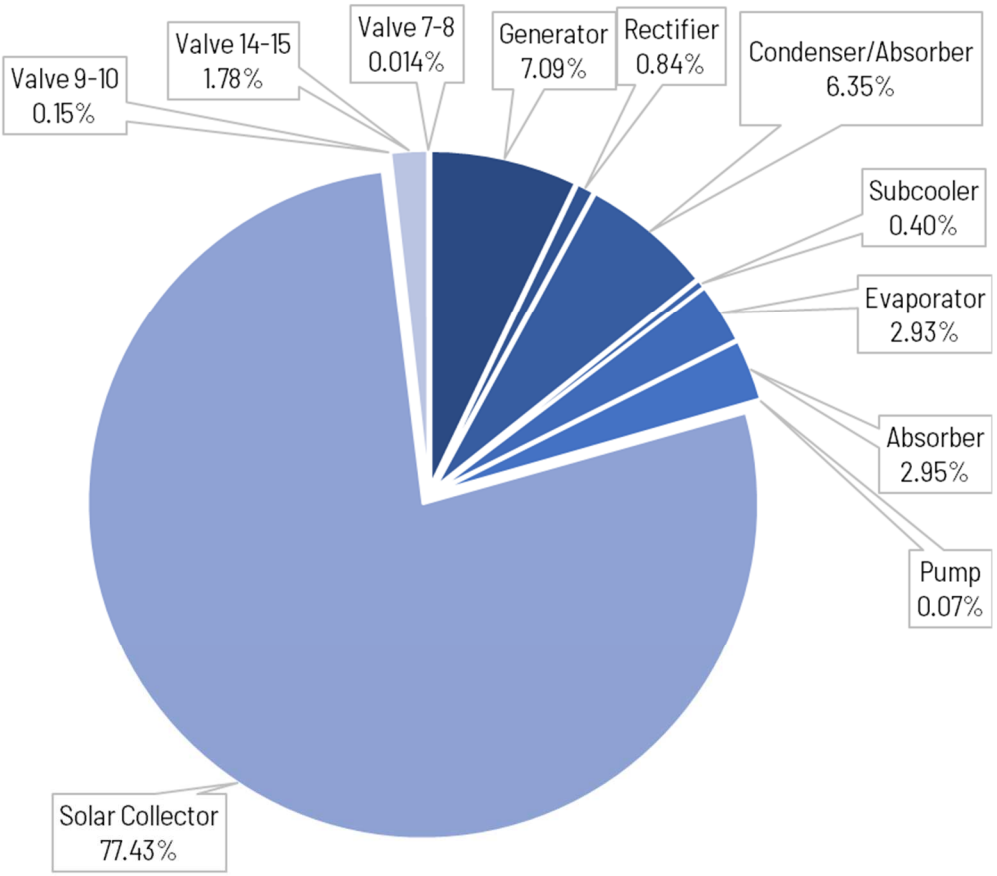

Fig. 5.17 Relative exergy destructions in the solar ammonia-water chiller system under design conditions.

Results of off-design whole season exergy analysis are included in the following considerations over exergoeconomic analysis in section 5.7.

5.7 Exergo-economic analysis of the solar integrated ammonia-water absorption chiller

5.7.1 Methodology and assumptions

- **Total cost of the plant assessment**

Mandatory rules needed to perform an exergoeconomic analysis of any system have already been brought about in Chapter 4. The first step prior to cost balance analysis is always the estimation of the total investment cost depending on the cost of components and operation and maintenance costs. In the analysis of solar ammonia-water chiller, the investment cost is evaluated basing on the estimates of the costs of every component in the chiller. A different approach is presented in the second analysis in this thesis in section 6.4.

Purchase equipment cost (PEC) of each component in the chiller could be obtained from manufacturer, market data. In this study, in the face of lack of such details, the only component which price is based on the data available in the literature is the solar collector component. Purchase cost of each other device derives from cost functions present in the literature. Cost functions origin from an interpolation among values of available costs, depending on one or more project parameters [95]. Exemplary cost functions were set in [143]. A function, presented in Eq. (5-88) was prepared for devices made of carbon steel and operated at ambient pressure:

$$\log_{10} C_p^0 = K_1 + K_2 \log_{10} A + K_3 [\log_{10} A]^2 \tag{5-88}$$

where C_p^0 is the searched equipment cost for base conditions, A is a capacity or specific size parameter for discussed equipment, while K_1, K_2, K_3 are the correlation coefficients typical for the equipment and adopted from tables available in [143]. If the range of size for which the correlation function was prepared does not correspond to the analysed case, a scale factor has to be introduced. It can be found by Eq. (5-89):

$$\frac{C_a}{C_b} = \left(\frac{A_a}{A_b}\right)^X \tag{5-89}$$

Where subscript a is connected with the component we are analysing, while subscript b refers to equipment with the base attribute. Cost exponent x can be typical for each device, but according to discussion presented in [143], it is usually 0.6. This relationship is called a 'six-tenths rule' and is in line with the economy of scale indicating on the statement that the larger the equipment, the lower is the cost of equipment per unit of capacity. Moreover, if the process is conducted at a pressure other than ambient, a pressure factor (F_P) correcting the evaluated cost has to be introduced. A relation used to estimate this factor is given in Eq. (5-90):

$$\log_{10} F_P = C_1 + C_2 \log_{10} P + C_3 [\log_{10} P]^2 \tag{5-90}$$

where P is the operating pressure of given component, and constants C_1, C_2, C_3 are again typical values for given equipment, specified in a table in [143]. Further corrections should also be made, if the material of analysed equipment is different than carbon steel (in this study case: stainless steel). Material factor (F_M) is read from a chart in [143] that differentiate between

types of construction material used for specific equipment. Taking the correction factors into account, the purchase equipment cost C_{BM} can be found by Eq. (5-91).

$$C_{BM} = C_p^0 F_{BM} = C_p^0 (B_1 + B_2 F_M F_P) \quad (5\text{-}91)$$

According to approach presented before, components of the chiller were modelled as a shell and tube heat exchangers. The constants needed for the cost functions were found in the table in [143] for shell and tube heat exchangers (differentiating if a phase change occurs in a component like condenser, evaporator, generator) and separately for the circulation pump.

The cost functions and constants available in the literature source were normalized for the conditions in 2001. In order to convert this cost into an accurate for present time it is obligatory to recalculate it using defined cost indexes. It is done with Eq. (5-92):

$$C_{BM,2017} = C_{BM,2001} \left(\frac{I_{2017}}{I_{2001}} \right) \quad (5\text{-}92)$$

where $C_{BM,2017}$ is the purchase equipment cost updated to 2017, $C_{BM,2001}$ is the cost normalized for 2001, resulting from the equations, while I_{2017} and I_{2001} are the cost indexes for 2017 and 2001, respectively. For the purpose of this study a Chemical Engineering Plan Cost Index (CEPCI) was applied. It is a nonnumeric value following the changes of the money value according to inflation and deflation processes in Europe. In 2001 CEPCI equaled 397, while in 2017 it raised to 567.5 [144].

The purchase costs of the components sum up to the total purchased equipment cost (PEC_{tot}). Referring to this value, operation and maintenance costs could be evaluated and finally the total investment cost can be calculated. Total investment cost is built by fixed capital cost of the investment (FCI) and additional costs (AC). FCI cost covers direct (DC) and indirect costs (IC). Direct costs are divided between on-site costs (ONSC: purchased equipment costs, installation, piping. instrumentation costs) and off-site costs (OFSC: terrain, civil operations, service facilities). Indirect costs are those related to project, construction. Additional costs are connected with transportation, working capital, licenses etc. According to findings presented in [98], assumed shares of these costs in relation to PEC_{tot} are given in Table 5.10.

Table 5.10 Percentage shares of the capital investment costs

Fixed Capital Investment		**Additional Costs**
Direct Costs	**Indirect Costs**	
On-site costs: • PEC • Piping (7% PEC) • Instrumentation, controls and electrical equipment (5% PEC) Off-site costs: • Land (10% PEC) • Civil work (7% PEC)	• Engineering and supervision (6% PEC) • Construction (3% PEC) • Contingency (8% PEC)	• Startup costs (1% PEC) • Working capital (3% PEC)

Next to the capital investment costs the operation and maintenance costs have to be defined. They are incurred continuously during the lifetime of the cooling plant. According to the observations, only one person is needed to operate the system in the cooling season, maintenance costs (*Maint*) are assumed as 1.5% of PEC (it should include mirror washing, technical service of the chiller device and ground keeping). Insurance rate (*Ins*) is evaluated as 1.5% PEC.

Following the methodology outlined in Chapter 4, performing the exergoeconomic analysis requires the definition of a cost balance for each system. The balance is repeated in Eq. (5-93):

$$c_{P,k}\dot{B}_{P,k} = c_{F,k}\dot{B}_{F,k} + \dot{Z}_k \quad (5\text{-}93)$$

Where $c_{P,k}$ and $c_{F,k}$ represent the costs per unit of exergy of product or fuel respectively. $\dot{Z}_k$ is the cost rate including capital investment and operating and maintenance costs. A path to calculate it for each component is given in Eq. (5-94):

$$\dot{Z}_k = \frac{cost_{tot,plant} \cdot PEC_k}{\tau_{annual} PEC_{tot}} \quad (5\text{-}94)$$

Where $cost_{tot,plant}$ expresses the total cost of the plant including total capital investment cost, maintenance and insurance. The total capital investment cost is the sum of FCI and AC from Table 5.10. This value is also corrected by a capital recovery factor mentioned in Eq. 4-30 and applied in Eq.

$$TCI_{ir} = \frac{ir \cdot (1+ir)^n}{(1+ir)^n - 1} TCI \quad (5\text{-}95)$$

$$cost_{tot,plant} = TCI_{ir} + Maint + Ins \quad (5\text{-}96)$$

Subsequently, PEC_k in Eq. (5-93) stands for the purchase equipment cost of the *k*-th component and τ_{annual} is the annual operation time of the plant. If τ_{annual} is given in seconds, the cost rate $\dot{Z}_k$ is expressed in €/s, if it is given in hours it would be €/h. The final assumptions for calculating the equipment cost rates are the operation lifetime of 20 years and interest rate at the level of 5%.

- **Cost balances for the components**

According to SPECO method explained in Chapter 4, each component can be described by a cost balance. Exemplary balances were outlined in Table 4.2. In order to solve the balance, the stream cost rates of flows crossing the balance boundary are required. Cost of electricity needed to drive the circulation pumps is based on the Eurostat values. For the system operated in Italy, the price of electricity equals 0.2€/kWh, while for the system potentially operated in Poland: 0.14€/kWh [145]. A hypothesis towards the exergy fuel rate driving the solar ammonia-water chiller is that the Solar source of energy is renewable and its cost is 0 €/kWh. Additionally, a common practice in exergo-economics is to assign zero costs to exergy loss (occurring in solar collector and condenser/absorber component) [93].

5.7.2 Results

The chart in Fig. 5.18 shows the percentage shares of costs building the total capital investment cost. PEC constitutes 66% of the total cost, however, it is worth notice that it is presumed, that installation cost is already a built-in cost of purchase equipment cost. In the analyses of industrial plants, the installation costs could be additionally 20-90% of PEC.

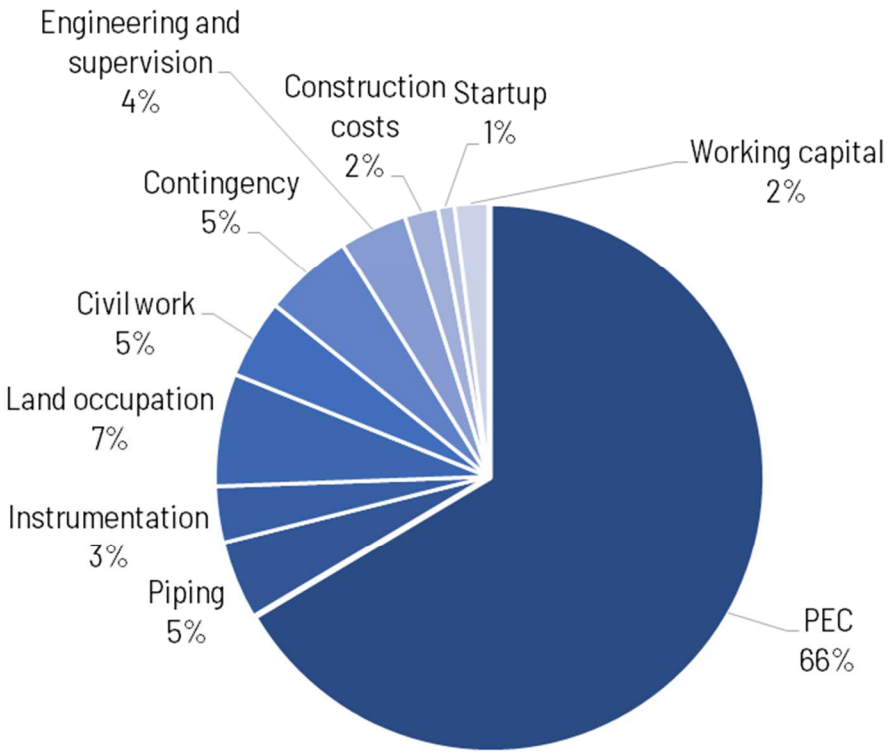

Fig. 5.18 Total capital investment shares for the solar energy driven ammonia-water chiller.

Overall specific investment cost of the whole system equals 1342 €/kW of cold. It is a higher value than that reported e.g. in [21] (1000-1200 €/kW of cold), but one should realize it cannot be directly compared, as authors did not specify type of absorption chiller for which this specific cost is given. If only purchase equipment cost was considered, the specific purchase cost would equal 893 €/kW of cooling power.

Since the cooling energy output from the cycle is strictly dependent on the daily meteorological conditions, the cost of cold from the solar cooling plant is also subject to seasonal change.

Table 5.11 presents the results obtained from the exergo-economic analysis of the solar heat driven ammonia-water chiller potentially operated in Italy, during the representative day of July at 2 pm. Table 5.12 presents analogous results for the system placed in Poland.

Table 5.11 Values of selected exergo-economic variables for system operating on reference day of July, at 2pm in Florence, Italy

k	Component	PEC [€]	$\dot{Z}_k$ [€/h]	$\dot{C}_{D,k}$ [€/h]	$\dot{Z}_k+\dot{C}_{D,k}$ [€/h]	$c_{F,k}$ [€/kWh]	$c_{P,k}$ [€/kWh]	f_k [-]	r_k [-]
1	Generator	1085	0.15	0.52	0.67	0.29	0.38	0.22	0.34
2	Rectifier	1502	0.21	0.08	0.29	0.38	2.73	0.71	6.11
3	Condenser-absorber	5560	0.76	6.11	6.87	3.28	6.93	0.11	1.11
4	Subcooler	2092	0.29	0.01	0.29	0.09	0.17	0.97	0.93
5	Evaporator	1176	0.16	1.73	1.89	2.54	**4.26**	0.09	0.68
6	Preabsorber	3616	0.49	3.13	3.62	4.27	7.26	0.14	0.70
7	Pump	136	0.02	0.00	0.02	0.20	0.49	0.84	1.44
8	Solar collector	18324	2.50	0.00	2.50	0.00	0.29	1.00	
9	Valve 9-10	200	0.03	0.09	0.12	2.50	2.54	0.24	0.02
10	Valve 14-15	200	0.03	1.93	1.96	4.17	4.59	0.01	0.10
11	Valve 7-8	200	0.03	0.00	0.03	2.31	2.32	1.00	0.00

Table 5.12 Values of selected exergo-economic variables for system operating on reference day of July, at 2pm in Wrocław, Poland.

k	Component	PEC [€]	$\dot{Z}_k$ [€/h]	$\dot{C}_{D,k}$ [€/h]	$\dot{Z}_k+\dot{C}_{D,k}$ [€/h]	$c_{F,k}$ [€/kWh]	$c_{P,k}$ [€/kWh]	f_k [-]	r_k [-]
1	Generator	1085	0.15	0.49	0.64	0.28	0.36	0.23	0.32
2	Rectifier	1502	0.21	0.08	0.28	0.36	2.17	0.73	4.95
3	Condenser-absorber	5560	0.76	7.52	8.28	4.14	9.98	0.09	1.41
4	Subcooler	2092	0.29	0.01	0.29	0.06	0.14	0.98	1.16
5	Evaporator	1176	0.16	2.07	2.23	3.12	**5.98**	0.07	0.92
6	Preabsorber	3616	0.49	3.90	4.40	5.44	8.69	0.11	0.60
7	Pump	136	0.02	0.00	0.02	0.14	0.41	0.88	1.95
8	Solar collector	18324	2.50	0.00	2.50	0.00	0.28	1.00	
9	Valve 9-10	200	0.03	0.11	0.13	3.07	3.12	0.20	0.02
10	Valve 14-15	200	0.03	2.47	2.50	5.48	6.01	0.01	0.10
11	Valve 7-8	200	0.03	0.00	0.03	2.85	2.86	1.00	0.00

In terms of economic analysis, the solar collectors and are here the most expensive components. From the exergo-economic point of view, if $\dot{Z}_k + \dot{C}_{D,k}$ are summed, the same components are of the highest importance. This sum is the highest for condenser/absorber vessel with exergy destruction mostly responsible for that. This component is followed by preabsorber. The same 2 components, where complete absorption process occurs, are inducing highest costs of exergy destruction in the system. If it was not for the assumption of assigning zero cost to incoming solar radiation, the solar collector component would have the highest $\dot{Z}_k + \dot{C}_{D,k}$ value.

If relative cost difference (r_k) and exergoeconomic factor (f_k) are considered, their trends in both locations are the same. Components with highest f_k are: solar collector, pump, rectifier and the intermediate valve. It means that the investment cost is mainly creating the overall cost of product in these components. In the rest of components the responsibility is carried by the destructions. Components with highest r_k are rectifier and pump. It means that in these devices the highest potential for cost reduction occurs. The same should be also mostly valid for solar collector. As the specific cost of exergy fuel is here 0, the r_k strives to infinity.

The specific cost of the exergy product c_{p5} associated with the evaporator represents the plant output product, i.e. the levelized cost of cold. It is the fundamental result of the exergo-economic analysis applied to each component. The cost presented for the analysis for the reference day of July at 14:00 for two locations is lower in Florence than in Wrocław. Higher solar radiation input is responsible for that. Nevertheless the direct specific cost value is evidently high: 4-6 €/kWh. It should be however clearly stated that this cost takes into account not only the instant operational spending but also whole capital investment phase. Moreover it is distributed only over the cooling season (1712 h in Florence, 1133 h in Wrocław). Presenting levelized cost calculated only on base of 1 hour simulation is not reliable. The specific cost is calculated for each reference day of the cooling season months, and it is thus subject to variation over this period is as presented in Table 5.13.

Table 5.13 Variation of daily cooling energy output and cost over the cooling season in Italy and Poland.

Location	month for reference day →	4	5	6	7	8	9	10
Florence, Italy	daily operation time, h	7	8	8	10	10	8	6
	daily cooling energy output, kWh	86.0	106.8	126.1	141.4	118.2	101.2	72.0
	Average cost of cold, €/kWh	18.8	9.6	6.9	4.9	5.1	7.3	13.0
Wrocław, Poland	daily operation time, h	-	7	8	8	8	6	-
	daily cooling energy output, kWh	-	80.2	86.2	88.8	86.2	53.9	-
	Average cost of cold, €/kWh	-	14.5	11.5	9.6	10.4	21.2	-

As expected, the lowest cooling energy cost corresponds to the highest daily cooling energy output in the summer months. Because of different climate conditions the off-design simulations not only the cooling season lasts longer in Italy. Also the time of available solar radiation during the day affected the length of the season during which chiller was active. Annual results are shortly presented in Table 5.14.

Table 5.14 Annual operational details for solar cooling plant operated in Italy or Poland.

No.	Location	Florence (Italy)	Wrocław (Poland)
1.	Coordinates	43.75°N 11.29°E	51.1°N 17.03°E
2.	Annual solar radiation on tracking surface, kWh/m^2	1155	676
3.	Total operation time, h/year	1712	1133
4.	Annual productivity, MWh/a	22.993	12.112
5.	Annual average cost of cold, €/kWh	8.98	12.96

5.8 Place for improvement – a control procedure

The concept presented in this section has already been proposed by the author and published in [146], it is however adopted specifically to the conditions of analysed solar cooling plant.

Solar absorption chillers are usually driven at a fixed temperature level in order to achieve a high COP. One should, however, take into consideration, that together with the change of external meteorological conditions (ambient temperature and incoming solar radiation), the efficiency of solar collector may suffer from trying to obtain the highest temperature possible. It is evident while looking again at the chart presented in Fig. 5.19. The collector efficiency curve has been prepared using equation (5-64) with the assumption of ambient temperature 25°C and incoming solar radiation of 900W/m^2. Efficiency curves for two types of solar collector are here plotted: for the SOLITEM parabolic troughs operated in Misericordia and for a vacuum tube solar collector. It is possible to warm up the heat transfer fluid to required level of temperature in that kind of collector. Nevertheless, the vacuum tube solar collector is characterized by worse efficiency parameters: optical efficiency η_0 =0.82, linear heat loss coefficient a_1 =1.62 W/(m^{2}K) and quadratic heat loss coefficient a_2 =0.0068 W/(m^{2}K^2) [147]. Although the optical efficiency is higher, the influence of heat loss coefficients is bigger if compared to concentrating collectors.

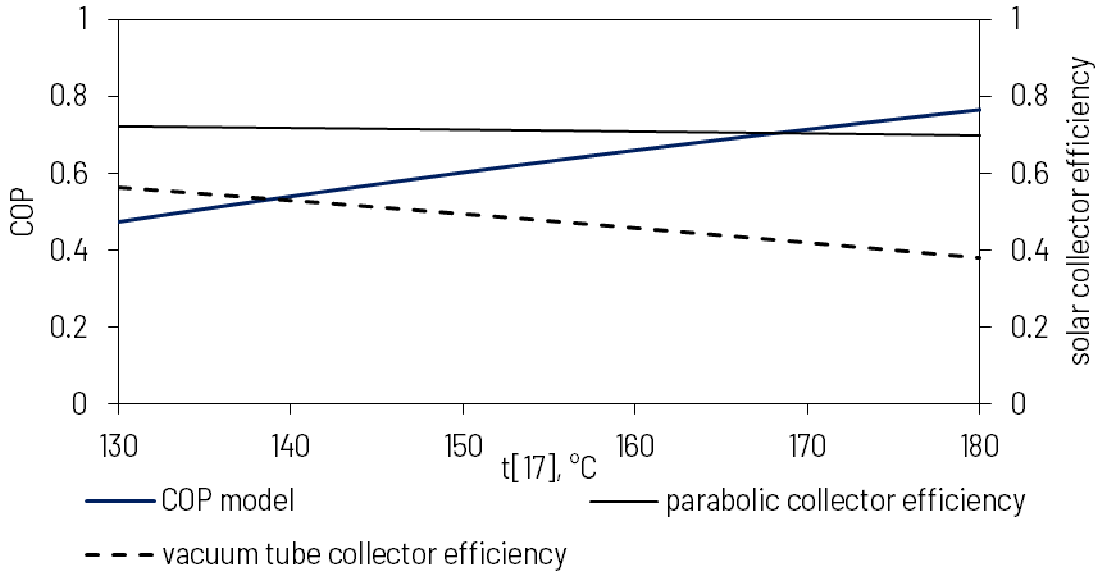

Fig. 5.19 COP curve of analysed chiller and solar collector efficiency curves (for parabolic trough collector and vacuum tube collector).

It is shown that, although the COP of the chiller increases with the growth of driving temperature, if the temperature difference between the outlet stream from the solar collector and the ambient is higher, the efficiency of the collector will be falling down. It is, however,

visible that parabolic collector is less dependent on the temperature than vacuum tube collector. This phenomenon of inverse dependence between those two performance coefficients speaks for operating the chiller at a variable driving temperature, adapting to outer conditions.

5.8.1 Concept

To investigate the potential of the phenomenon, a control strategy procedure is proposed. Authors state that it is not always a priority to maintain the generator temperature achieving the highest coefficient of performance (COP) under given conditions. If the solar radiation conditions are poor, it may occur that it is difficult to produce enough heat at the desired higher temperature level. Under these conditions, it may be profitable to produce more low-temperature heat, and accept a lower COP estimated from the curve, leading on the whole to a higher cooling power production from the solar collector.

Some simplifications were introduced to manage the control routine. The chiller is cooled down constantly by the inflowing cooling water temperature of 35°C, and the evaporator delivers chilled water at the level of 12/7°C, to maintain consistency with the exemplary COP recovered from off-design simulation. Following Fig. 5.19, COP depends on the generator temperature. Since the pump mechanical energy consumption constitutes only 0.4% of the heat input, its contribution is not taken under consideration in the following.

The heat transfer temperature differences are kept constant according to relations presented in Eq. (5-97) and Eq. (5-98). Authors in [148] mention that those ΔT usually ranges from 5 to 15 K.

$$\Delta T_{HTF} = T_{17} - T_{18} = 10\ K \tag{5-97}$$

$$\Delta T_{gen} = T_{18} - T_{gen} = 10\ K \tag{5-98}$$

ΔT_{HTF}, K is the temperature increase of the heat transfer fluid inside the solar collector, while the ΔT_{gen}, K is the temperature difference between the fluid stream coming back to the collector (T_{18}, °C) and the generator temperature ($T_{gen} = T_5$, °C). An example control routine for finding optimal working parameters of solar collector has also been described in [128], where the solar collector outlet temperature has been adapted to ensure maximum exergy efficiency of collector. It is ideally assumed that the useful heat gain from the collector equals the heat rate to generator assigned to solar contribution $\dot{Q}_u = \dot{Q}_{gen}$. In an iterative way, the procedure searches for the generator temperature at which the cooling power ($\dot{Q}_{evap}$) produced by the solar chiller is the highest, which at the same time means the highest possible solar fraction. The objective function of this routine is presented in Eq. (5-99).

$$T_{gen} = f\left(max{:}\ \dot{Q}_{evap} = COP \cdot \dot{Q}_u\right) \quad (5\text{-}99)$$

To maintain consistency with the before-mentioned considerations, the routine looks for the desired temperature in the range between 130°C and 160°C.The value of driving temperature is searched for raising values of the cooling power output; once the cooling power output begins to decrease, the optimal solution is refined by chord interpolation. The collector mass flow rate enabling heating the heat transfer fluid to the desired temperature is defined on the base of Eq. (5-56) and, consequently, it should be processed and transferred as a setup control signal to remote-controlled variable speed pump.

5.8.2 Results

Simulation of the control procedure potential was performed for ammonia water chiller driven by heat from already analysed parabolic trough collectors and for a theoretical ammonia water chiller that could be driven by heat from vacuum-tube solar collectors. Answer of both systems to the control strategy was computationally tested for Italian and Polish meteorological conditions.

The effect of the routine was tested in simulations performed with a 5-minutes time step for 3 representative days of the cooling season. The overall solar radiation and ambient temperature data were processed to generate 3 average days statistically representative of specific months of the year. The analysis covers May, June and July, as months belonging to cooling seasons in both locations. For comparative reasons meteorological data for Pisa and Poznan were used. Since the data recovered from Meteonorm library are hourly, a cubic interpolation was applied to simulate the operation according to the smaller time step.

The variable driving temperature study case is compared with the reference case operation.

The reference case follows an assumed standard operation routine. In this routine, the solar chiller is driven by the heat output of the solar collector. During every time step of operation, a constant value of the solar collector outlet temperature is maintained (160°C). This value was chosen for the simulation purpose, as the driving temperature assuring a high COP value. The analysed study case, on the other hand, assumes that the solar collector outlet temperature is optimized during every time step, according to the discussed objective function (Eq. (5-99))|. The chilled water and cooling water temperature remain the same for the reference and study case, so that the results ae comparable. The cooling power produced in both cases is referred to the unit surface area of the solar collector.

If the parabolic trough collectors integrated chiller is considered, it occurs that it is more profitable to operate the parabolic trough collectors on a reduced collector temperature (140°C)

only in the late afternoon hours (after 6 p.m.) in May, June or July. During the rest of the days the control procedure gives the same practical results as a fixed-temperature control. The lack of apparent profit is visible in Fig. 5.20 for Italian meteorological conditions and in Fig. 5.21 for Polish meteorological conditions on a reference day of August.

The upper chart (A) shows the amount of cooling power that could be produced from 1 m^2 of solar collector at a fixed driving temperature and the increment of cooling power production that constant adjusting of collector outlet temperature may bring is marked with black colour. Chart B presents the daily profiles of the outlet temperature and collector energy efficiency for both cases: with optimal adjustment of the outlet temperature (*temp. var*.) and for fixed value of it (*temp. fixed*). The bottom plot C is a zoomed chart of unit cooling power output during the evening hours, when the procedure indicates a lower driving temperature as an optimal one.

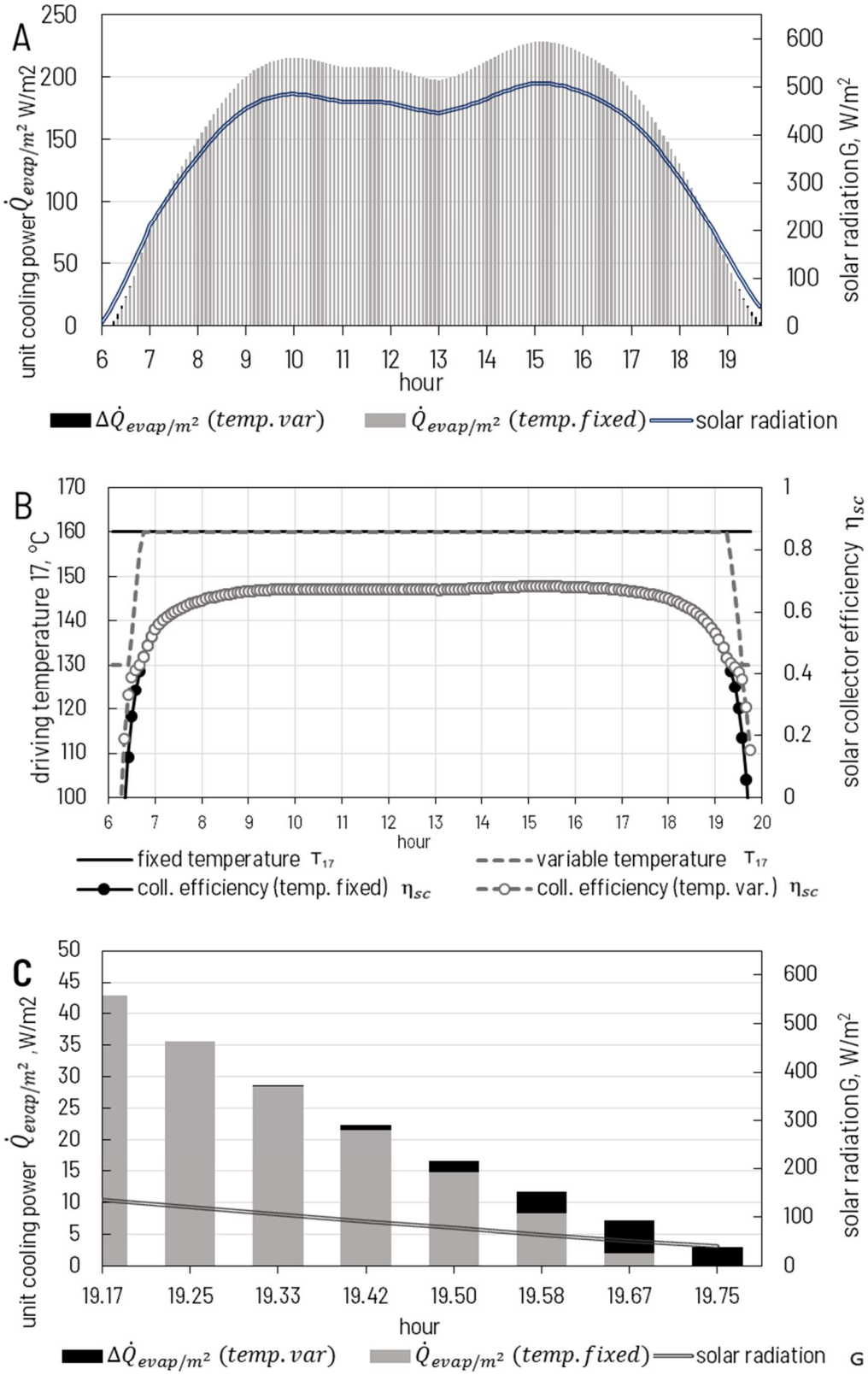

Fig. 5.20 Result of the simulation for a representative day of August in Florence, Italy; A:distribution of unit cooling power production and its increase at variable driving temperature, solar radiation distribution; B: distribution of driving temperature and collector efficiency for both study cases, C: zoom of unit cooling power increase in the evening hours

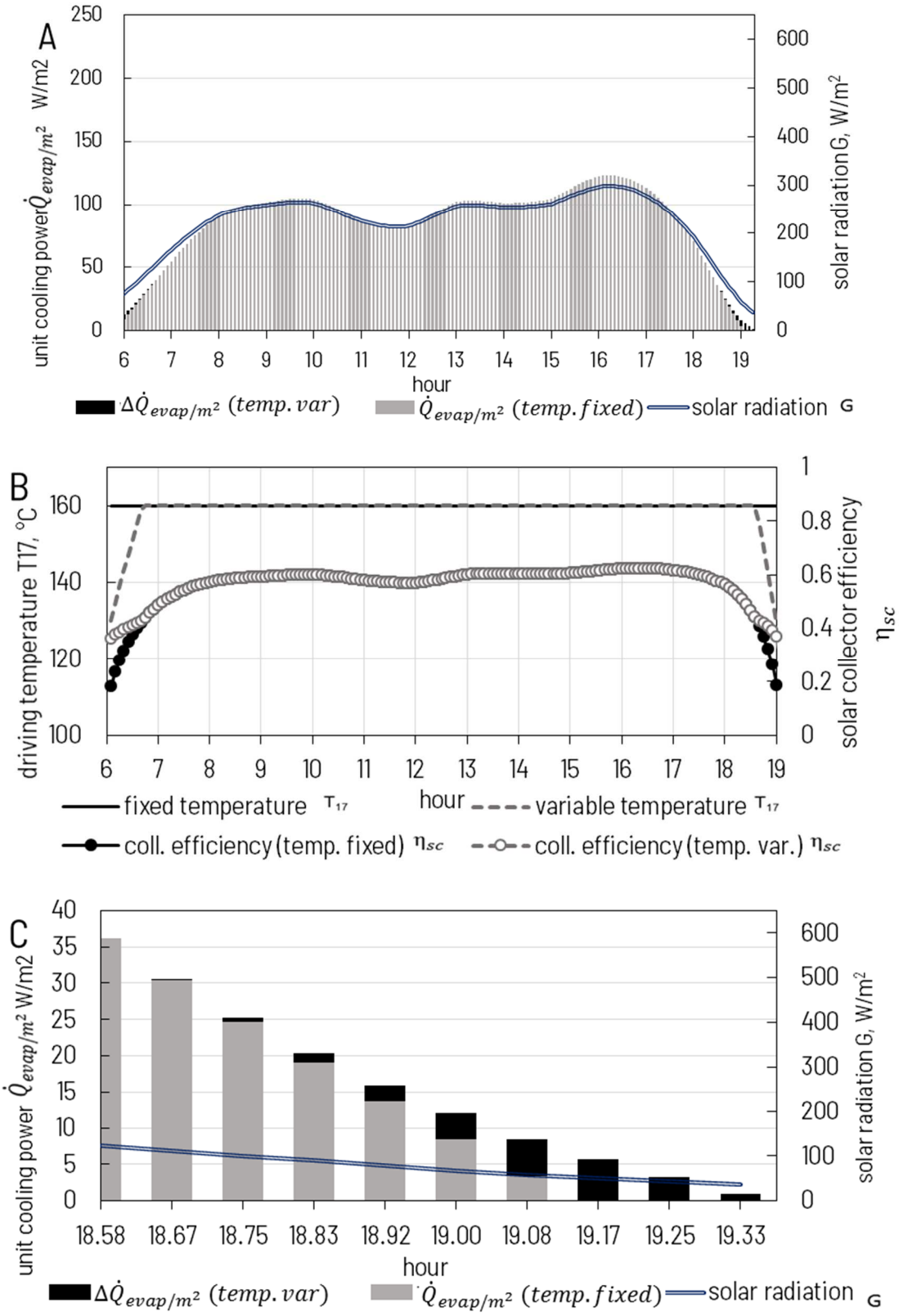

Fig. 5.21 Result of the simulation for a representative day of August in Wrocław, Poland; A:distribution of unit cooling power production and its increase at variable driving temperature, solar radiation distribution; B: distribution of driving temperature and collector efficiency for both study cases, C: zoom of unit cooling power increase in the evening hours

It is here again visible that the ammonia water chiller provides a double unit cooling power effect due to better solar radiation conditions. However, if the device of the parabolic collector is considered, it operates with very similar efficiency in both locations. It is less dependent on higher temperature difference between ambient and heat transfer fluid. The same, there is no apparent need to lower the temperature during the whole day of operation. The potential effect is visible here only in the evening hours (Poland 19-19:30, Italy 19-20) when it is very close to sunset.

Different conclusions can be drawn if the heat input from vacuum tube solar collectors is considered. Results for a representative day of August are pictured in: Fig. 5.22 for a system operated theoretically in Italy and in Fig. 5.23 for a system potentially operated in Poland.

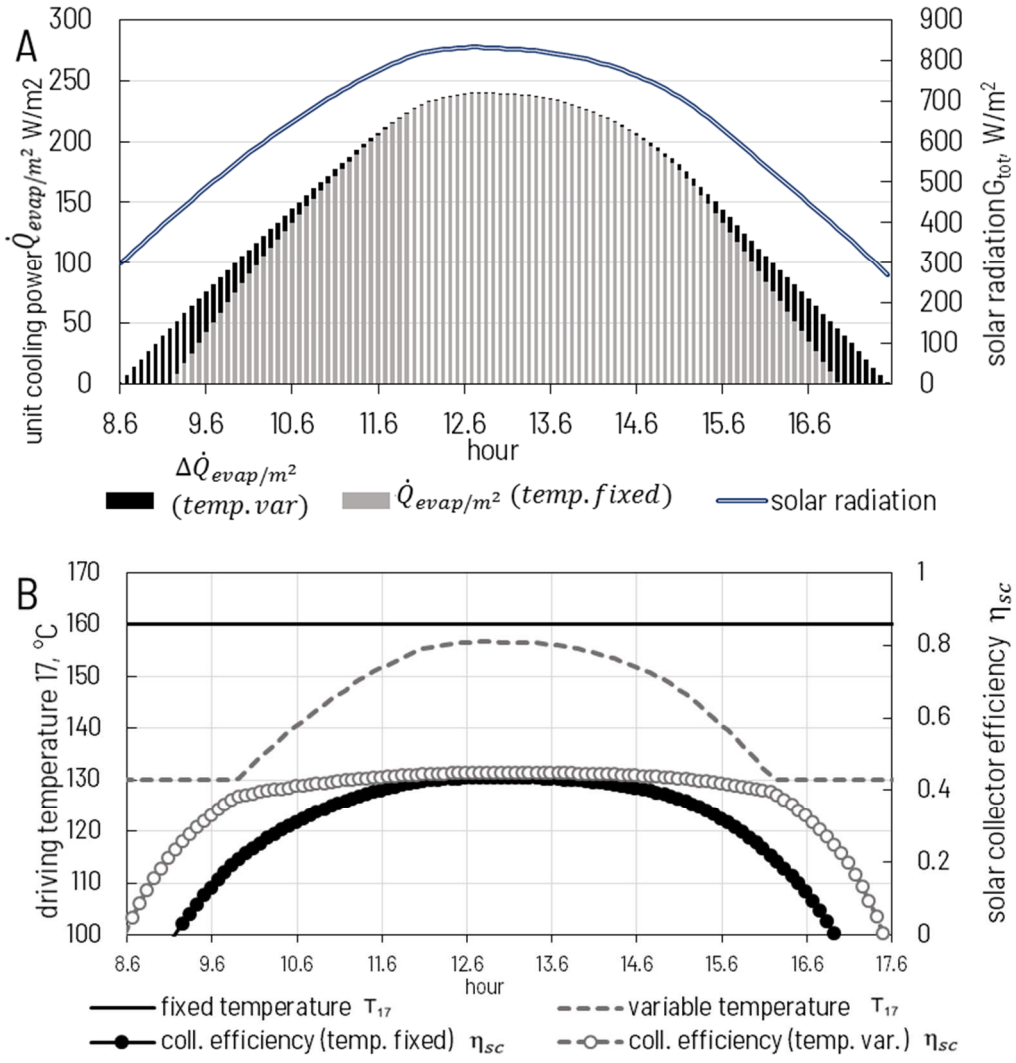

Fig. 5.22 Result of the simulation with vacuum tube collectors for a representative day of August in Florence, Italy; A:distribution of unit cooling power production and its increase at variable driving temperature, solar radiation distribution; B: distribution of driving temperature and collector efficiency for both study cases

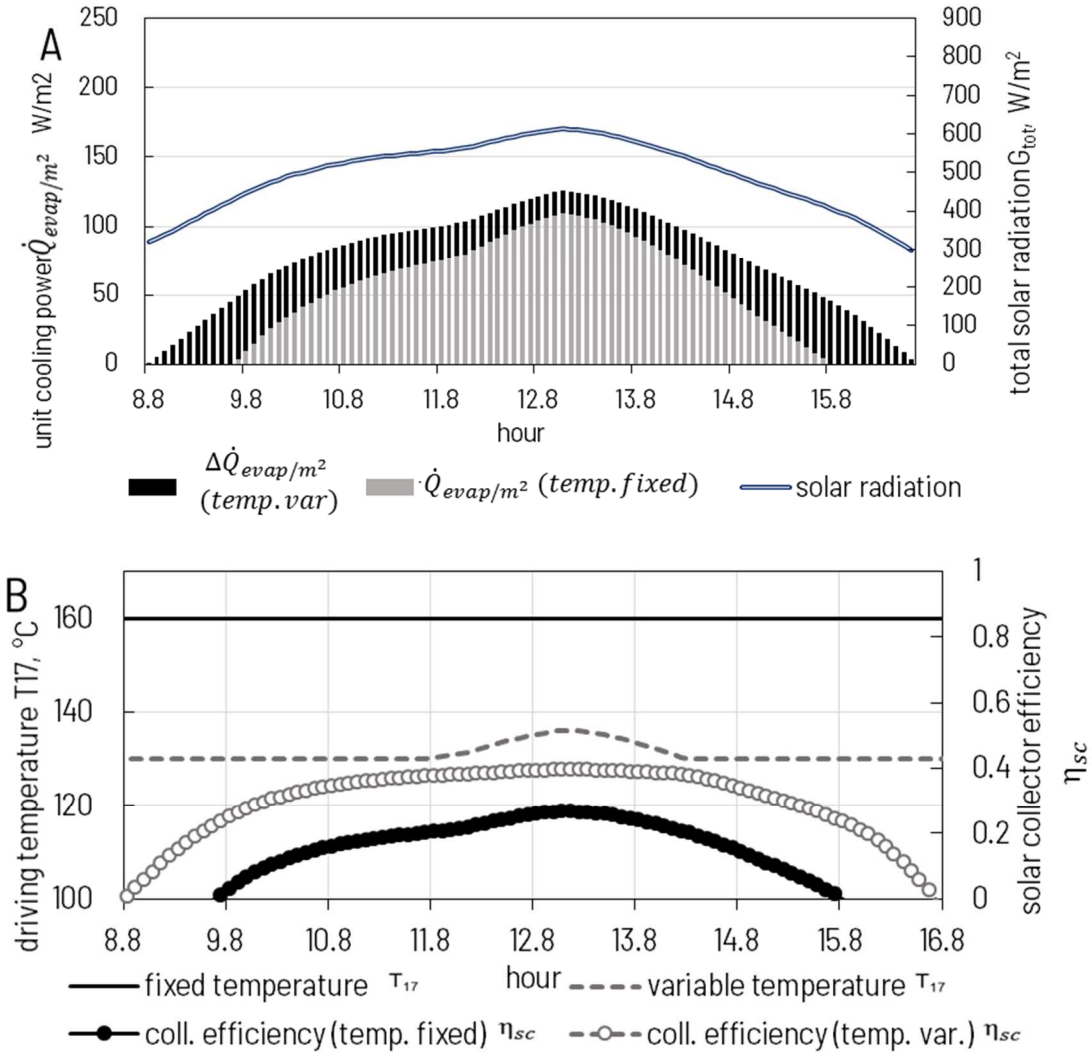

Fig. 5.23 Result of the simulation with vacuum tube collectors for a representative day of August in Wrocław, Poland; A:distribution of unit cooling power production and its increase at variable driving temperature, solar radiation distribution; B: distribution of driving temperature and collector efficiency for both study cases

Vacuum tube solar collectors are also able to utilize scattered solar radiation. Therefore, the value of total incoming solar radiation (on a surface directed to the south, with a 45° slope) is much higher than in the case of parabolic collectors where only the beam radiation could have been considered. However, as expected, high outlet temperature from solar collector acts very negatively on the collector's efficiency. According to the simulation results, in both systems: in Italy and in Poland it would be more convenient to operate at lower driving temperature than 160°C. The effect is double: it increases the collector's efficiency, but above all the cooling power output is higher. Incorporating the given control strategy may result in an increase of the cooling power production related to solar collector utilization by up to 45 W per 1 m^2 of collector. The simulation shows that under poor radiation conditions it is profitable to operate close to the minimal driving temperature allowing for ammonia vapour generation (here:

130°C). Optimal adaptation of driving temperature enables to obtain a positive value of cooling power around 8 a.m. and 5 p.m. in all of the analysed months. According to the charts, only for the Italian study case it is convenient to operate solar collectors at the highest outlet temperature level only when high radiation conditions are possible (during noon hours). During this time, the chosen temperature is close to the reference fixed of 160°C. As expected, a lower collector outlet temperature always leads to higher solar collector efficiency, as is visible in the bottom charts of Fig. 5.20 - Fig. 5.23.

PART II

Chapter 6. REFERENCE INSTALLATION IN WROCŁAW, POLAND

This second part of the thesis is devoted to an installation matching the concept of hybrid heating and cooling node. The reference plant was built by Fortum Power and Heat company in the Head Quarters of the company in Wrocław. The concept and primary design of the system is a result of cooperation between Fortum, Silesian University of Technology and Wrocław University of Science and Technology. The subsequent author's proposal of control procedure is a corollary of a common project application in 2015.

The first idea was to create an advanced heating and cooling substation (AHCS) is expected to integrate district heat supplied by a cogeneration source (CHP) with a renewable source of solar energy in order to generate central heating, domestic hot water (DHW), cooling power and waste heat for special purposes. This general concept is pictured in Fig. 6.1.

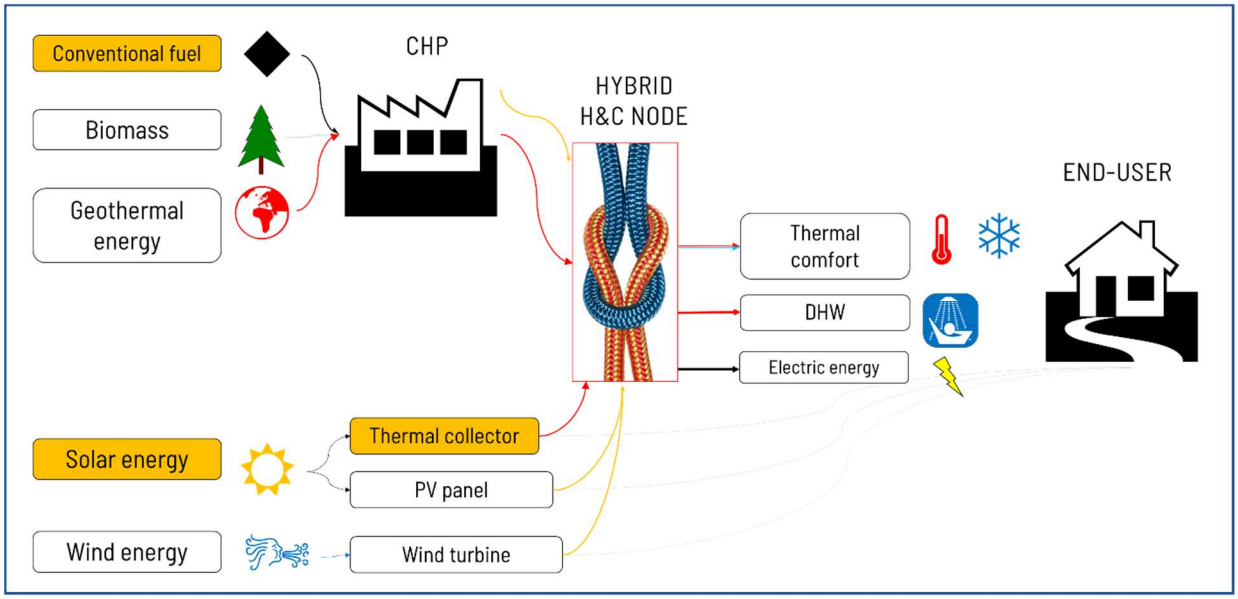

Fig. 6.1 Concept scheme of an advanced hybrid heating and cooling substation.

Since the node was meant to be located in Wrocław, the district heat rate is available from a coal-fired cogeneration unit. Space and budget limited renewable energy conversion devices to one type of solar thermal collectors. Although the idea was to design and build a demonstration installation, the hybrid node should also be operational and provide thermal comfort to workers and visitors of a canteen inside the office building.

Geolocation of the Wrocław plant is presented in Fig. 6.2.

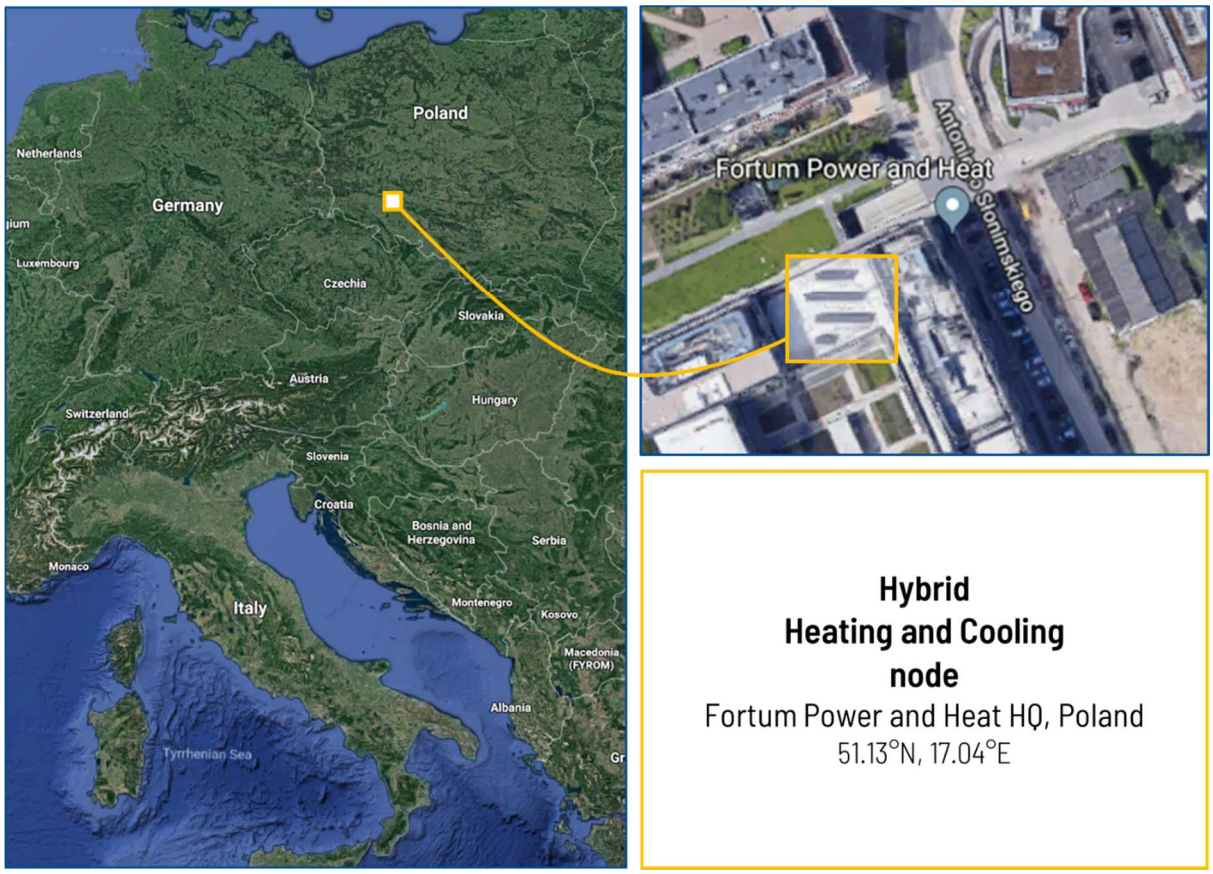

Fig. 6.2 Location of the reference installation in Wrocław.

It should be here marked that the scientific cooperation with the company was realized on the terms of the duly signed contract. According to provisions of the agreement some site-specific data, raw experimental results, direct simulation results, details on the algorithms cannot be shared publicly.

6.1 The primary design of the node

As was mentioned above, the installation in Wrocław is not fully operational, but rather a demonstration plant (on the occasion satisfying thermal comfort needs of the canteen). In order to make the installation size independent on the building construction and specific needs that could be furtherly defined, it was decided by the funders that the design cooling load is 60 kW. During primary discussions, it was suggested that half of the design cooling load (30 kW) will be delivered by thermal sorption chillers, while the rest should be covered by a conventional vapour-compression chiller. After the market insight research, it was proposed that the following sorption chillers could be installed: a 17.6 kW absorption chiller [149] and a 16 kW adsorption chiller [150]. For the purpose of rough estimations and initial budget planning, the number of solar collectors satisfying the chillers' heat demand was defined. Solar

collectors should be placed on a roof with limited space. The available area was a 17x15 m rectangle. Additionally, due to possible shading, collectors rows cannot be placed side by side. The minimum distance between rows is presented in Fig. 6.3.

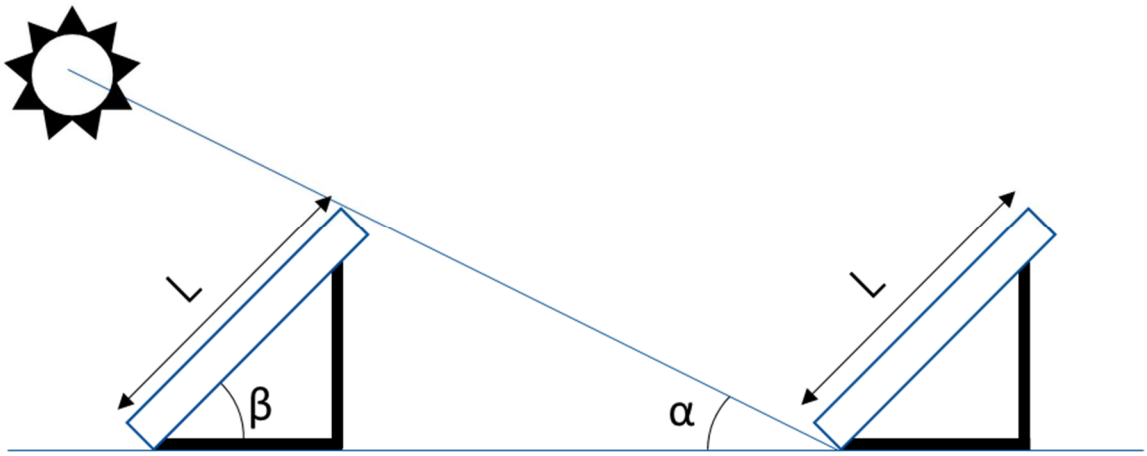

Fig. 6.3 A scheme showing the minimum distance between solar collector rows

According to engineering practices, the minimal distance between rows (*Dist*) is usually estimated from Eq. (6-1):

$$\frac{Dist}{L_{ap}} = \frac{\sin\left(180° - (\beta - \alpha)\right)}{\sin \alpha} \tag{6-1}$$

where L_{ap} is the height of the solar collector (m), β is the slope of the collector (°) and α is the solar altitude angle (°). The solar altitude angle for northern latitudes can be simplified to 66.5°-Φ, where Φ is the location latitude.

The solar collectors were planned to be placed on a roof neighbouring with a building under construction. It occurred that the building protruding above the roof causes a constant shading of the roof section. This shading factor had to be also taken into account while sizing the field. In the end, 36 flat plate solar thermal collectors with a constant slope of 45°, directed to the South were chosen to be placed on the roof. The project was evolving during the consultation meetings and the final structure of the node installed in the Headquarters includes:

- Solar thermal collectors field,
- Single stage LiBr-H_2O absorption chiller (cooling capacity 17.6 kW),
- Hybrid chiller – adsorption and vapour-compression chiller (cooling capacity 49.6 kW),
- High-temperature storage (latent and sensible heat type),
- Chilled water storage,
- Mid-temperature water storage,

- Auxiliary devices system (controlled valves, intermediate heat exchangers, splitters, mixers),

A simplified scheme of the node structure is given in Fig. 6.4. A specific characteristic of the designed node is the bypass connections between components, thanks to which the thermal energy conversion units can be independently or commonly driven by energy from cogeneration unit and/or from the renewable energy source. The details of the connections' arrangement remain, however, confidential.

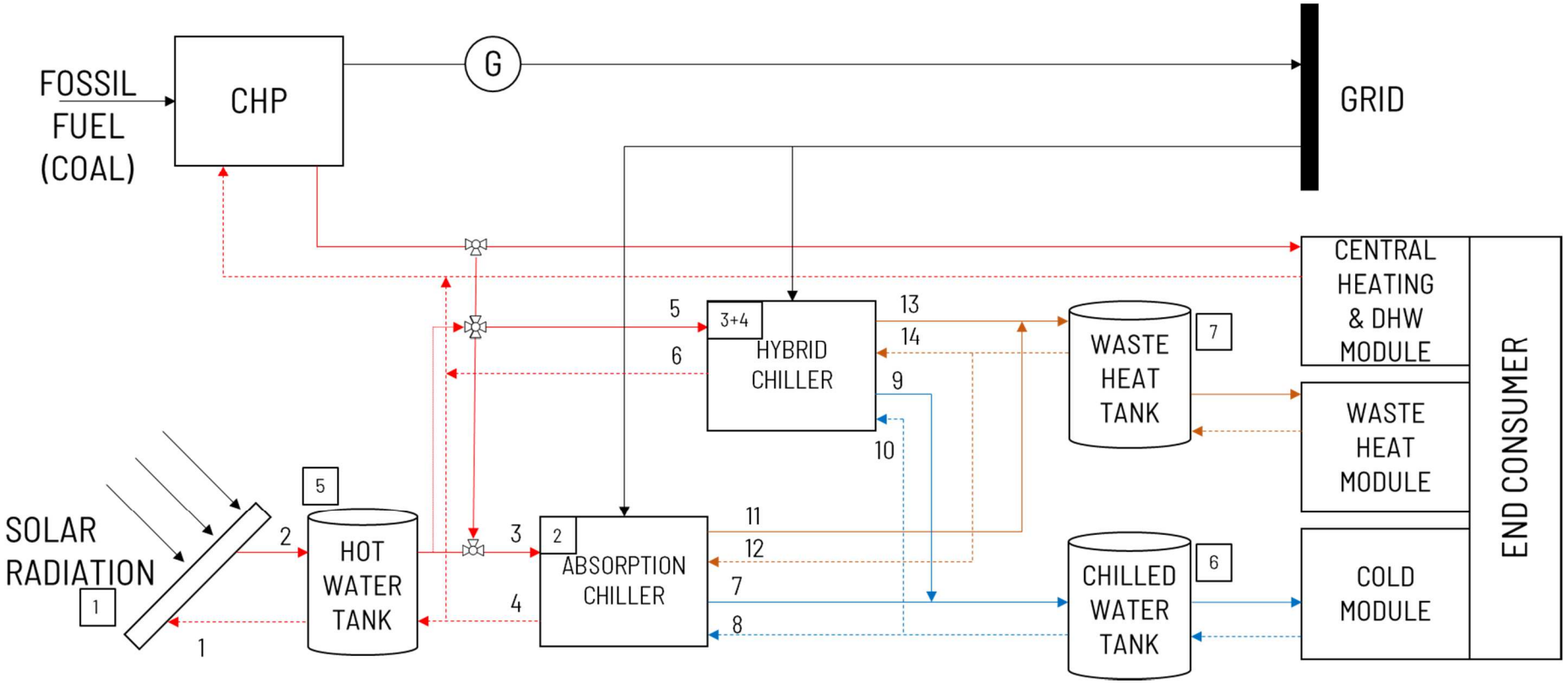

Fig. 6.4 Hybrid heating and cooling node in Wrocław – the idea of components connections

6.2 A simulation model of the node in Wrocław

The node is characterized by a modular structure and by thus its operation can be simulated using separate mathematical models of every component. At first, the mathematical description of devices operating within the node has been prepared to enable further simulation of the whole structure.

6.2.1 A simulation model of the LiBr-H_2O thermal absorption chiller: methodology and assumptions

According to technical data available in [149], the LiBr-H_2O absorption chiller present in the node is a single stage, water-cooled unit. Its modular scheme is presented in Fig. 6.5.

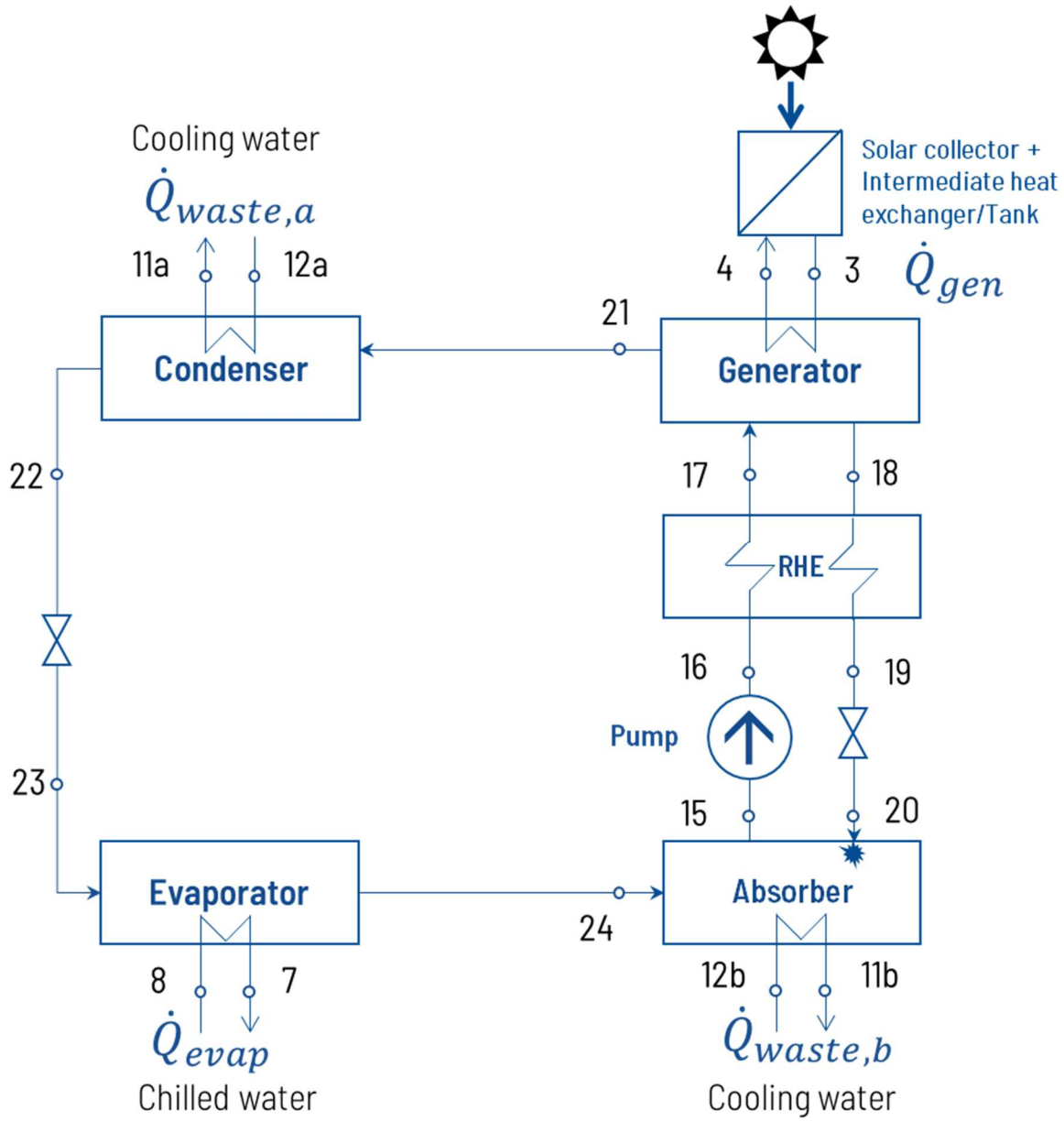

Fig. 6.5 A simplified scheme of the LiBr-H_2O chiller.

As already described in Chapter 2, unlike the ammonia-water chiller, in lithium bromide chiller water is the refrigerant and LiBr is the absorbent. Heat input from solar collectors causes the separation of water vapours. There is no need for the rectifier and the driving temperature in the generator section can be lower than in ammonia-water chiller (typically 70-90°C [149],) Pure water vapours are condensed and after throttling evaporated in the evaporator section providing the cooling effect. Waste heat derives from cooling the condenser and absorber components.

The mathematical model of the chiller was based on the 1st law of thermodynamic analysis including the definition of mass and energy conservation equations. Every component (*k*) can be universally described using the following balances (6-2) and (6-3).

$$\sum_{i=1}^{n} \dot{m}_{i_{in,k}} = \sum_{i=1}^{n} \dot{m}_{i_{out,k}} \tag{6-2}$$

$$\sum_{i=1}^{n} (\dot{m}_i h_i)_{in,k} = \sum_{i=1}^{n} (\dot{m}_i h_i)_{out,k} + \dot{Q}_k \tag{6-3}$$

where $\dot{m}_i$ is the mass flow rate of an i-th stream (kg/s), h_i is the specific enthalpy of the i-th stream (kJ/kg), subscript in means inlet to the component, subscript out means outlet from the component and finally $\dot{Q}_k$ is the heat transfer rate (kW) within every chiller component (for the balance of the pump it should be replaced with the electric energy consumption: N_{pump}). Design simulation recognizes the following idea: the two-phase mixture of liquid and vapour remains always in the thermodynamic equilibrium. The rich solution leaving the absorber is a saturated liquid at the absorber temperature. The weak solution is leaving the generator at saturated conditions, at the generator temperature. Water leaving the condenser is a saturated liquid at the condenser temperature, while the water flowing out of the evaporator is saturated vapour at the evaporator temperature. Effectiveness of a chiller is defined by the coefficient of performance (COP). Off-design simulation was enabled after the definition of heat exchangers size. Again, the primary sizing of the components is done on the base of the Peclet equation. Knowing the heat exchanger logarithmic temperature difference ΔT_{lg_k}, the value of overall heat loss coefficient multiplied by the heat exchanger size may be defined ($(UA)_k$, kW/K).

$$\dot{Q}_k = (UA)_k \cdot \Delta T_{lg_k} \tag{6-4}$$

Proper sizing of the heat exchangers was then verified and validated thanks to the experimental campaign.

The design model of lithium bromide absorption chiller was created so that its design performance parameters are in accordance with the nominal parameters indicated by the manufacturer. Technical data are presented in Table 6.1.

Table 6.1 Design parameters of an absorption chiller in [149].

Parameter		Symbol	Value
Chilled water	Cooling capacity	$\dot{Q}_{evap}$	17.6 kW
	Chilled water temperature	T_8/ T_7	12.5/7°C
	Inlet flow rate	$\dot{V}_7$	0.77 l/s
Hot water	Heat input	$\dot{Q}_{gen}$	25.1 kW
	Hot water temperature	T_3/ T_4	88/83°C
	Flow rate	$\dot{V}_3$	1.2 l/s
Cooling water	Heat rejection	$\dot{Q}_{waste}$	42.7 kW
	Cooling water temperature	T_{12}/T_{11}	31/35°C
	Flow rate	$\dot{V}_{12}$	2.55 l/s
Electrical	Pump power consumption	N_{pump}	48 W

The assumptions on the saturation state of flows as in the above discussion are reflected in the design simulation model. Additionally, assumptions towards relations between temperatures of external flows and flows in the cycle are made. They are written in Table 6.2.

Table 6.2 Assumptions for the design analysis of the LiBr-H_2O chiller.

Parameter	Symbol	Unit	Value
Cooling water inlet temperature	$T_{13} = T_{15}$	°C	31
Cooling water temperature increase	$T_{16} - T_{15} = T_{14} - T_{13}$	K	4
Chilled water inlet temperature	T_{17}	°C	12.5
Chilled water temperature decrease	$T_{17} - T_{18}$	K	5.5
Pinch point temperature difference in evaporator	$T_{18} - T_{10}$	K	3
Hot water inlet temperature	T_{11}	°C	88
Hot water temperature decrease	$T_{11} - T_{12}$	K	5
Temperature difference in generator	$T_{11} - T_4$	K	5

Nominal cooling energy output is maintained as the design simulation assumption ($\dot{Q}_{evap}$=17.6 kW), while the efficiency of the regenerative heat exchanger (RHE) is η_{RHE}=0.7. Subsequently, once the size of heat exchangers in the chiller are fixed, the off-design model of the chiller

allows for calculating the thermodynamic parameters inside the cycle knowing only the parameters of external flows and applying Eq. (6-4).

The mathematical model of the module was prepared in EES software taking advantage of built-in thermodynamic properties libraries of water, LiBr and LiBr-H_2O solution [134].

6.2.2 Model of the hybrid adsorption chiller: methodology and assumptions

The hybrid chiller chosen to be installed and operated in the structure of the node is a new construction type in the chiller design. One housing encompasses two chillers: an adsorption chiller and a vapour compression chiller. The idea standing behind this design is that the thermal adsorption chiller operates in the base load, while the peak demands are covered by the additional compression unit. Additionally, the manufacturer states that the fluctuations in the ambient temperature and driving temperature can be compensated by the compression chiller which allows for maintaining a precise temperature of chilled water [151].

In the face of scarce technical data about the chosen hybrid chiller, the model of this chiller is made of two separate simplified models: one describing the performance of the adsorption section and the second represents vapour-compression chiller.

Moreover, technical brochures do not provide any details on the adsorption unit, its configuration or working pair. It was agreed that the performance curve will be first reconstructed basing on training materials [151] and scientific papers [72,152] and then adjusted to the results coming from experiments. Table 6.1 presents general data retrieved from the technical brochure of the chiller[151].

Table 6.3 Design parameters of hybrid chiller [151].

Parameter		Symbol	Value
Max. cooling power		$\dot{Q}_{hybrid}$	49.6 kW
Compression chiller	Refrigeration power	$\dot{Q}_{evap\_el}$	32 kW
	Max. power consumption	N_{comp}	15.76 kW
	refrigerant	*type*	R 407 C
adsorption part Hot water	Max. heat input	$\dot{Q}_{gen}$	32.3 kW
	Hot water temperature range	T_5	50-95°*C*
	Flow rate	$\dot{V}_{hot}$	0.694 l/s
Chilled water circuit	Temperature range	T_9	8-22°*C*
	Flow rate	$\dot{V}_9$	2.06 l/s
Cooling water	Temperature range	T_{14}	20-40°*C*
	Flow rate	$\dot{V}_{14}$	1.42 l/s

As mentioned before, the approach to the creation of the model is simplified, and an off-design performance curve from the literature is adopted [72,152]. In the first iteration (before experimental data are available) coefficient of performance of adsorption chiller is given as a function (Eq. (6-5)) of generator inlet temperature (hot water inlet temperature), assuming stable cooling water temperature increase 31/35°*C*.

$$COP_{ads} = 0.04024 + 0.001331T_5 - 0.0000124{T_5}^2 + 3.82725588 \cdot 10^{-8} \cdot {T_5}^3 \quad (6\text{-}5)$$

The model of the vapour-compression chiller placed in the same housing is made following the assumptions of: single stage compression, isothermal evaporation and condensation, isenthalpic and isothermal throttling, the same temperature level for cooling water as for adsorption part (31/35°*C*), the same temperature level for chilled water as for adsorption part (12.5/7°*C)*.

6.2.3 Model of the Solar Field: methodology and assumptions

The approach to modelling the performance of the solar field remains in agreement with the methodology duly presented in section 5.2. The performance of collector was simulated taking advantage of a steady-state solar collector Bliss equation (Eq. (5-64)) and using manufacturer performance data presented in the following Table 6.4.

The optical efficiency of the solar collector is corrected by the IAM function provided by the manufacturer. It should be, however, noted that flat plate solar collector is able to absorb both beam and scattered radiation. The value of total solar radiation reaching a sloped surface

$G_{tot,sloped}$ is obtained basing on the value of total solar radiation falling on the horizontal surface available in the Meteonorm data library. It is then converted into $G_{tot,sloped}$ taking advantage of an earlier prepared, external simulation processer for solar radiation and weather data processor in TRNSYS software. The converter relies on the calculation of the cosine ratio between zenith angle and angle of incidence. Angle of incidence and zenith angle are a function of declination, local hour angle, latitude and solar azimuth angle also obtained from the solar radiation and weather data processor.

Table 6.4 Technical data of the Solar field in Wrocław

Parameter	**Symbol**	**Value**	**Comment**
Number of collectors	N_{coll}	36	
Aperture area of a single collector	A_{ap},	1.98 m^2	
Surface azimuth	α_s	0°	facing South
Slope of surface	β	45°	fixed
Heat Transfer Fluid concentration	x	36%	*Propylene Glycol-Water*
Optical efficiency	η_0	0.701	[153]
Linear heat loss coefficient	a_1	3.362 W/(m^2K)	[153]
Quadratic heat loss coefficient	a_2	0.011 W/(m^2K^2)	[153]

Additionally, the incidence angle modifier (IAM) is given by the manufacturer as a set of IAM factors associated with given incidence angles. Value of IAM for the simulation purpose can be interpolated basing on Table 6.5.

Table 6.5 Prediction of incidence angle modifier value according to manufacturer data [153].

Incidence angle θ	0	20	30	40	50	60	70	90
IAM	1	0.99	0.98	0.97	0.95	0.9	0.81	0

A primary separate model for the solar field was already prepared having in mind its further coupling with chillers and the assumption towards temperature levels results from this. Initial

relation between the outlet temperature from the collector and the design temperature of hot water flow driving the absorption chiller is given by Eq. (6-6).

$$T_1 = T_3 + \Delta T_{app} = T_3 + 5K \tag{6-6}$$

Collectors are connected in the Tichelmann's layout (in parallel [142]), therefore it is assumed that the mass flow rate is equally distributed between all of the collectors and that the same temperature increase is obtained in each collector, namely: $\Delta T_{HTF} = T_2 - T_1 = 10K$.

Anticipating the facts: final off-design simulation of the whole node structure is performed with a 1 hour time step. However, the primary off-design simulation of the separate model of the solar field was done with the evolutionary time step approach as discussed for the Italian system in section 5.3. This approach allowed for checking the period after which the flat plate collectors reach the design outlet temperature that allows for driving the chiller or charging the storage tank. The simulation is performed accepting following approach: heat transfer fluid is circulating in the field during the morning hours till the outlet temperature from the field exceeds the assumed 95°C, at that moment useful heat gain is started being directed to the tank or intermediate heat exchanger from which the absorption chiller could be driven. From that moment a constant ΔT_{HTF} is maintained in the solar collector by varying the mass flow rate in the field.

Just like in the previous analysis, the source meteorological data are imported from an external model prepared in TRNSYS software. The simulations are performed for the representative days of cooling season months respectively in Italy and Poland. The representative days of the months are defined by total solar radiation on a sloped surface and ambient temperature. They were evaluated basing on annual hourly meteorological data from Meteonorm library available in TRNSYS software [154,155]. A cubic interpolation was applied to simulate the operation according to a smaller time step.

Fig. 6.6 Solar collector row (one of three) on the roof in Wrocław[2]

6.2.4 Model of heat storage tanks: methodology and assumptions

The system is equipped with storage tanks at three temperature levels. These reservoirs allow for the accumulation of heat from solar collectors, accumulation of the waste heat and of chilled water from the chillers. Storage tanks are the carriers of the dynamic effect while performing a simulation. Neglecting thermal losses from the tank, energy storage simulation model always follows the energy conservation Eq. (6-7):

$$\dot{Q}_{supply} = \dot{Q}_{load} + \frac{dQ}{d\tau} \qquad (6\text{-}7)$$

where $\dot{Q}_{supply}$ is the energy rate supplied to the tank during the time step $d\tau$ (or charging time) and $\dot{Q}_{load}$is the heating load on the discharging side (depending on the control strategy a tank can be discharged already during the charging process or the discharge process can start once the charging process is finished). The change of accumulated heat amount in the storage fluid is represented by dQ and can be calculated from Eq. (6-8):

[2] Photography taken by the author

$$dQ = V\rho c_p dT \quad (6\text{-}8)$$

where V stands for the volume of material in the tank (volume of the tank, m^3), ρ is the density of storage material (kg/m^3), c_p is the temperature-averaged specific heat of the material (kJ/(kgK)) and dT is the temperature difference of the material (K) dependant on the length of the time step ($d\tau$, s).

Storage at each of the three temperature levels is secured by sensible water storage tanks. Their volume is given in Table 6.6.

Table 6.6 Basic technical data of storage tanks present in the node

Heat storage type	Storage material	Upper-temperature limit	Volume
Hot water	Water	90°*C*	4 m^3
Cooling water	Water	90°*C*	1.1 m^3
Chilled water	Water	90°*C*	3 m^3

An important assumption made while creating the simulation model of the node is that the storage tanks can be bypassed during the operation of the system. Hence, obtained heat rate from the solar collectors, or cooling energy rate from the evaporators of the chillers can be instantly utilized.

According to the design of the installation, one additional accumulator is foreseen for the high-temperature heat storage. It is a reservoir filled with phase change material (PCM). However, since the material placed there originally is characterized by a phase change temperature of 58°C, and maximum operational temperature of 70°C it is not suitable for the solar heat storage purposes. Therefore, the simulation model does not take this accumulator into account. The idea standing behind including this type of storage in the structure of the node was a plan to exchange the material inside the tank with a PCM of higher phase transition temperature (e.g. 82°C [156]).

6.2.5 Auxiliary devices

The energy rates are passed on with the help of intermediate heat exchangers. If operated under limited temperature range and mass flow rates, constant efficiency of heat transfer and approach point temperature is assumed. Intermediate heat exchanger efficiency η_{HE}=0.95 takes into account the heat transfer heat loss. It is assumed that the intermediate heat exchangers have a counter-flow layout. Approach point temperature $\Delta t_{app} = 5K$ is the temperature difference between the hot-side fluid inlet and the cold-side fluid outlet.

6.2.6 Simulation results for single devices and partial experimental validation

- **LiBr-H_2O thermal absorption chiller**

Once the design of the chiller is defined, a practical result from the off-design analysis is the dependence of COP coefficient on the external flows temperature. Fig. 6.7 presents the COP in function of generator driving temperature resulting from the model if the cooling water temperature is assumed as 31/35°C and the chilled water temperature is 12.5/7°C.

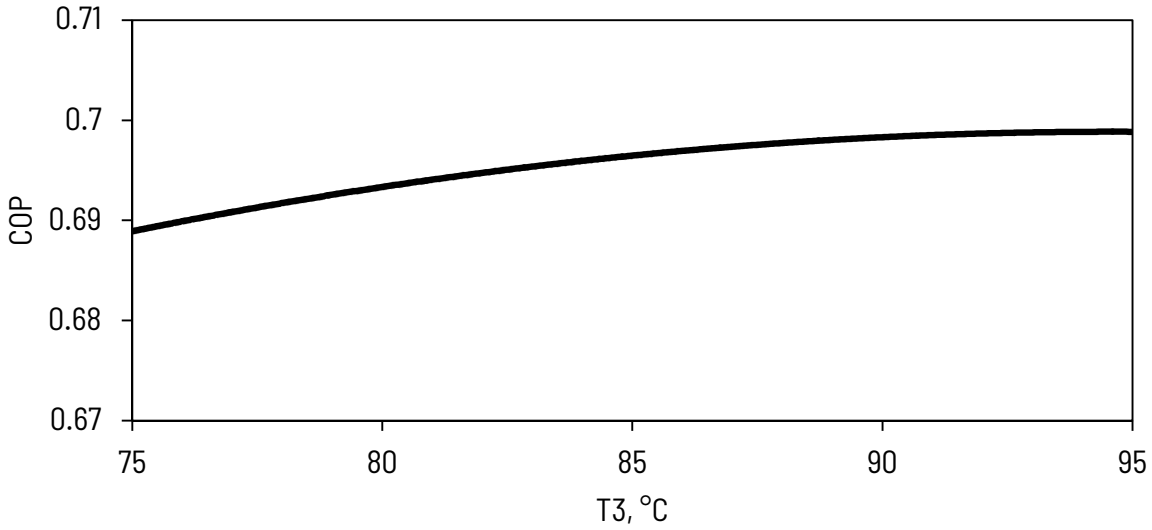

Fig. 6.7 COP curve of the lithium bromide absorption chiller (cooling water temperature 31/35°C, chilled water temperature 12.5/7°C).

The theoretical model of the chiller should be subsequently verified and validated. The absorption chiller performance was tested during a series of test campaigns under variable temperature parameters of external flows (T_8=10-19°C, T_{12}=27°C, T_3=70-80°C). The experimental works were performed by the researchers from Wrocław University of Science and Technology. Thanks to their courtesy, author was provided with the experimental results. These results allowed for modifications in the adapted design of the heat exchangers and therefore the final heat transfer coefficients have been modified. An exemplary effect of the model validation is shown in Fig. 6.8. The chart presents the coefficient of performance (COP) of the chiller obtained during a test campaign when the chilled water inlet temperature was maintained at T_8=13°C, the cooling water inlet temperature was T_{12}=27°C and hot water inlet temperature was T_3=70°C. 28 measurement points were obtained during this campaign as is shown in Fig. 6.8. At the same time, COP was defined computationally using the created model assuming the same input temperatures and flow rate parameters as in the experiment. After applying changes to the design modelling phase, the correlation coefficient (R^2) between

experimentally and theoretically obtained COP was increased from 0.8 to 0.87. For the sake of confidentiality agreement, direct values of the results are not presented.

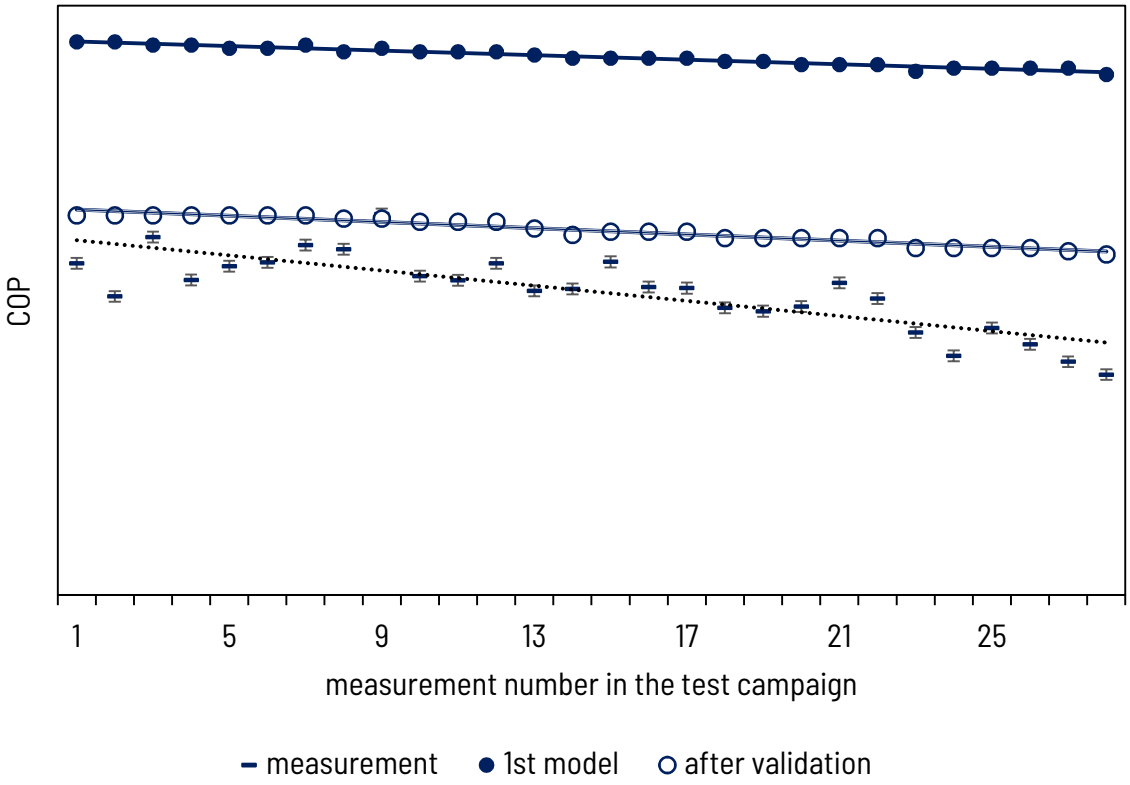

Fig. 6.8 COP profile for subsequent measurements with external flows temperatures close to T_8=13°C, T_{12}=27°C, T_3=70°C

The effect of validation and subsequent corrections of the chiller model is presented in Table 6.7. For each test campaign an average value of $\overline{COP}$ was calculated and uncertainty of the measurements was found ($u(\overline{COP})$). Simulation calculations were performed for the same external flow conditions like during the experiment. Average COP calculated in the simulation model before and after model modifications is also given.

Table 6.7 Average COP obtained from test campaigns, first theoretical simulation model and from the validated model together with correlation coefficients between model and experiment.

Measurements							**1st model**		**Validated model**	
Test campaign				measurements number	$\overline{COP}$	$u(\overline{COP})$	$\overline{COP}$	R^2	$\overline{COP}$	R^2
No.	$T_{8,}$ °C	$T_{12,}$ °C	$T_{3,}$ °C							
1	13	27	70	28	0.633	0.091	0.709	0.814	0.651	0.873
2	13	27	80	14	0.543	0.056	0.703	0.898	0.652	0.963
3	16	27	70	23	0.668	0.121	0.727	0.744	0.675	0.761
4	16	27	75	9	0.670	0.077	0.717	0.779	0.697	0.859
5	16	27	80	20	0.661	0.066	0.718	0.882	0.681	0.943

- **Hybrid chiller**

Performance of the adsorption part of the chiller was also tested during experimental works. In the face of lack of details on the construction and lack of a detailed mathematical model of the cooling unit, once the experimental results were available, a new performance function was elaborated. The function is dependent on the hot water inlet temperature, cooling water inlet temperature and chilled water inlet temperature. The correlation coefficient between experimental results and the function is R^2=0.86. However, for the sake of confidentiality agreement, it cannot be directly presented.

- **Solar field**

The solar field in Wrocław is not equipped with a data acquisition system. Therefore, the validation of the solar collector simulation model could have not been performed. However, as the model rests on the efficiency coefficients delivered by the manufacturer (η_0, a_1, a_2), takes into account the IAM function and the correction factor for mass flow rates other than under test conditions (like discussed in section 5.2.), it was considered reliable. Exemplary results for the solar field working during a representative day of July in Wrocław are presented in Fig. 6.9.

and the results for a representative day of July in Florence are shown in Fig. 6.10.

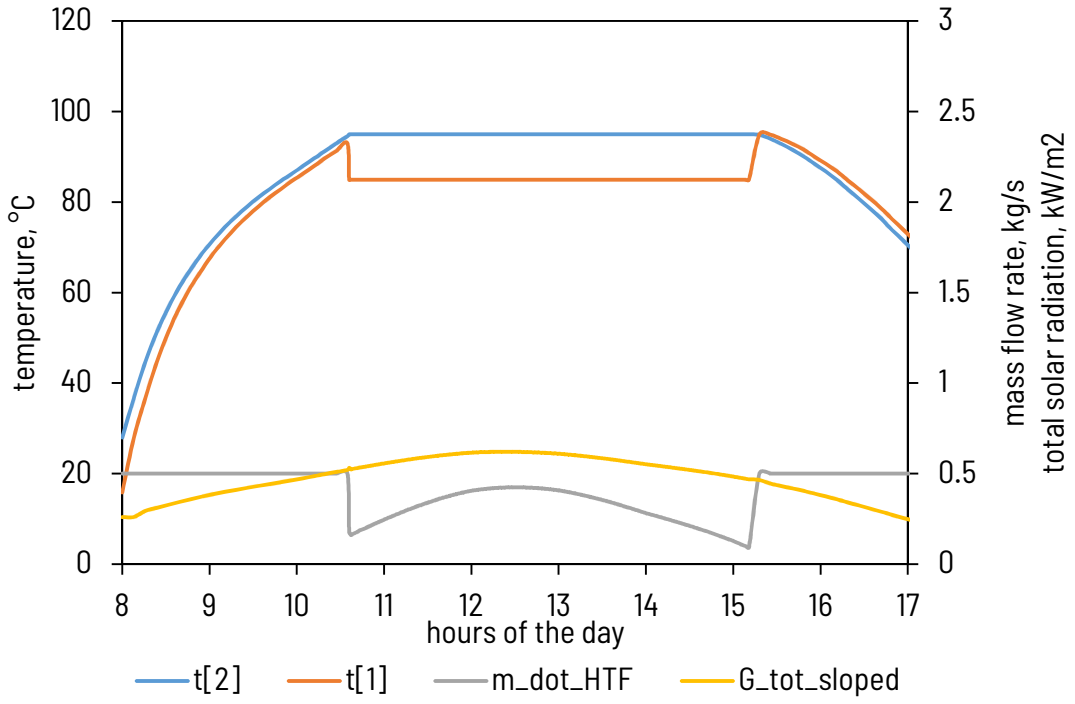

Fig. 6.9 Daily distribution of the heat transfer fluid's temperature and mass flow rate during the representative day of July in Wrocław set with incoming total solar radiation.

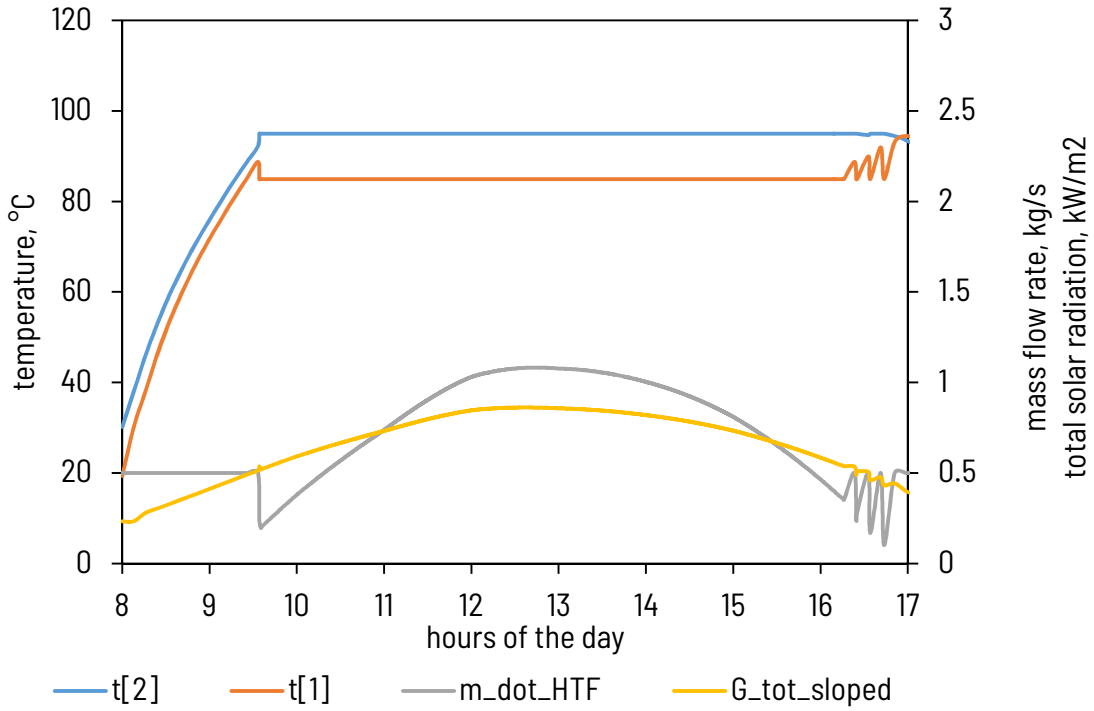

Fig. 6.10 Daily distribution of the heat transfer fluid's temperature and mass flow rate during the representative day of July in Florence set with incoming total solar radiation.

For this specific case, it is possible to obtain the temperature at the outlet of the solar collector at the level of 95°C after 2.5 hours of circulation inside the field in Wrocław. If the analogous field was placed in Florence, it would have happened already after 1.5 hours. This period could be shortened, if a lower value of mass flow rate during the warming up phase was set. It is also evident that the assumed ΔT_{HTF} of 10K can be maintained in Wrocław for only 5 hours, while in Florence it could be possible for 7 hours. To prolong the period of the useful heat output from the field, the value of ΔT_{HTF} should be chosen according to an optimization procedure. It was already proposed in [128,157].

6.2.7 Approach to the off-design simulation of the whole node

In order to simulate the performance of the whole hybrid node, its modular structure is considered. Singular models of the components are connected by the means of energy balances. A local balance boundary is put on each separate device (solar field, chillers, intermediate heat exchangers) and the components are only connected by external energy flows. The processes and parameters distributions inside the components are not investigated anymore while the whole node's performance is simulated. The off-design simulation of the node structure should visualize the system's potential to satisfy the thermal comfort needs during whole days of operation and how the energy streams are divided between components. It is important to mark that it was assumed that the heat for DHW preparation is delivered securely by the heating network and the simulation loops focused on stable cooling energy demand satisfaction. The surplus production of heat from the solar collector might be potentially used in the DHW module (although it should be clearly reminded that the solar field limited by the roof surface is too small and as it was checked during the simulations: if the solar heat is utilized by the chillers, a potential surplus never appears).

The simulation relies on input meteorological data which should influence the thermal comfort needs which are here represented solely by the cooling load. According to the primary approach, the energy flows distribution follows a subjective control procedure. An advanced control algorithm for the node is presented in the last section of this chapter (6.5).

Maintaining consistency with the approach presented in Chapter 5, the simulations were performed after processing the annual meteorological data to create average days statistically representative of cooling season months, basing on the meteorological data for Poznan – representing Wrocław, and Pisa – representing Florence. The set of meteorological data includes total radiation on a sloped surface and ambient temperature, as shown in Appendix B and Appendix C. The cooling season lasts from May to September in Wrocław and from April

to October in Florence. It is, additionally, preliminarily assumed that the node is operated during office working hours from 9 to 18.

The monthly integrals of total solar radiation for the two locations are presented in Fig. 6.11.

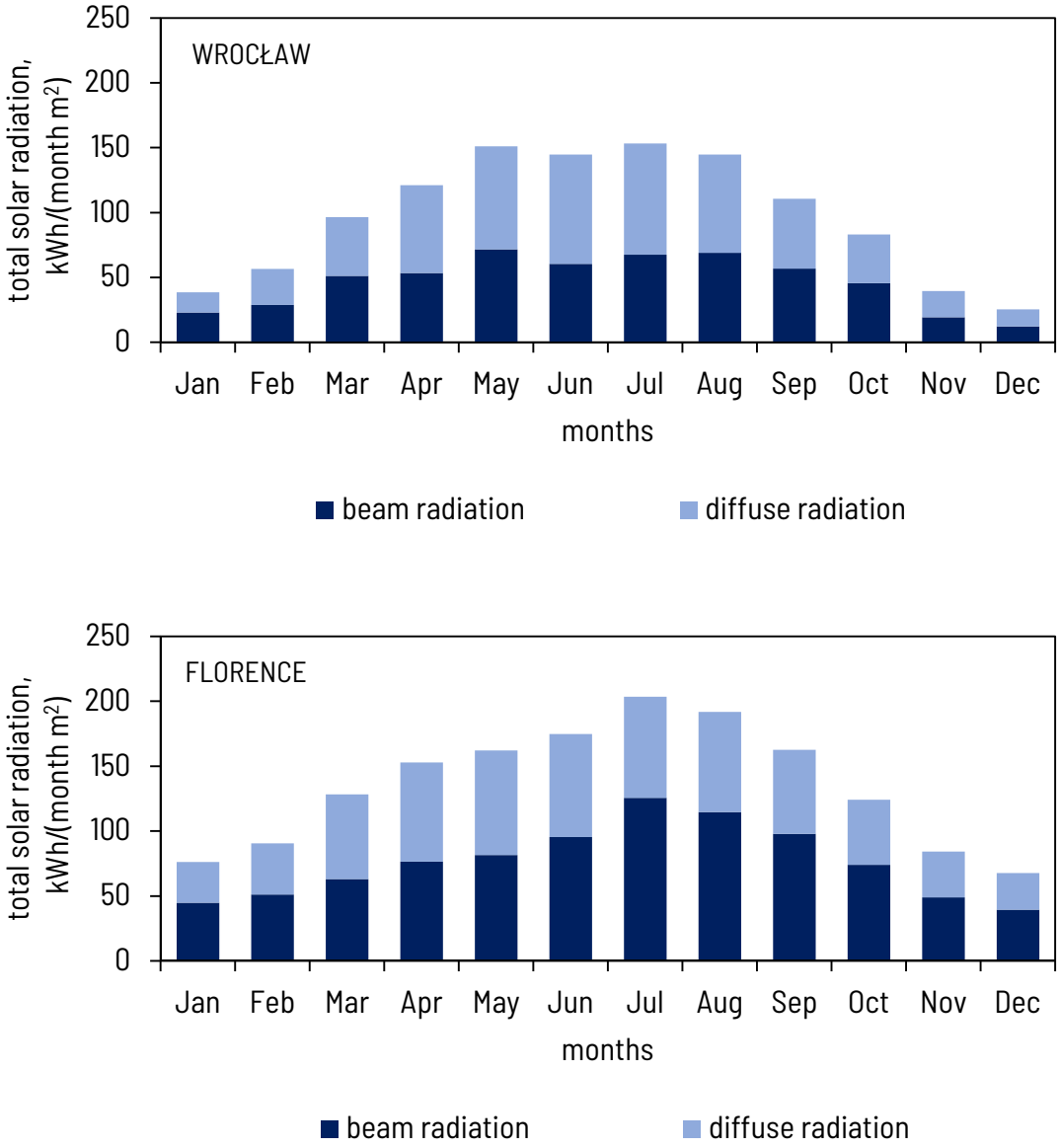

Fig. 6.11 Monthly integrals of incoming total radiation on a sloped surface in Wrocław (upper chart) and in Florence (bottom chart).

The nominal total cooling load was assumed at the level of 60 kW in both locations. One should note that the size of substation was designed for Polish radiation conditions and expect that the same installation under Italian weather conditions would be in reality oversized. This amount should be provided by the node under nominal conditions. It does not reflect the real needs of the office building where the substation is placed since it was designed as a demonstration installation to test variable configurations of cold and heat delivery. Therefore, in order to

perform seasonal simulations, making the thermal comfort needs dependant on the variable meteorological conditions, the cooling load had to be assumed. For that purpose, a simplified approach was adopted. It was estimated taking advantage of the definition of European Seasonal Energy Efficiency Ratio (ESEER) and of solar ambient temperature (so-called *sol-air* temperature - $T_{sol-air}$). ESEER indicator is a standardized method to declare the effectiveness of water chillers. According to its definition, it is assumed that 100% cooling load occurs during 3% of cooling season time, 75% of the cooling load is foreseen for 33% of time, 50% of the cooling load happens during 41% of the cooling season and 25% cooling load is defined for the rest of cooling season time (23%). Solar ambient temperature specifies the relation between incoming solar radiation and ambient temperature and was proposed by Mackey and Wright [158]. Sol-air temperature is a hypothetical value of ambient temperature at which heat rate absorbed by a shadowed external surface equals the heat rate absorbed by a solar-irradiated surface at ambient temperature. It can be assessed according to Eq. (6-9):

$$T_{sol-air} = T_{amb} + \frac{1}{h_{wall}} \cdot \alpha \cdot G_{tot} \quad (6\text{-}9)$$

Where T_{amb} is the ambient temperature, h_{wall} is the heat transfer coefficient for the external surface of a wall (22.7 W/m^{2}K [158]), α is the surface absorptivity (0.7 for grey plaster) and G_{tot} is the total incoming solar radiation (W/m^2). Sol-air temperatures were estimated for hourly meteorological data of the cooling season for a specific location. They were sorted from maximum to minimum value and divided into groups which sizes follow ESEER approach: 3%, 33%, 41%, and 23%. Cooling loads (100%, 75%, 50%, and 25%) were then assigned to these groups and a second-order polynomial function was found to describe the interdependence between assumed cooling load and the sol-air temperature. Coefficient of determination for this function equalled R^2=0.99. As a result, the distribution of cooling load for the representative days of the cooling season months is presented in Table 6.8

Table 6.8 Representative days of the cooling season months – cooling load distribution in Wrocław and Florence

hour	Cooling load in Wrocław				
	May	Jun.	Jul.	Aug.	Sep.
0	0.45	0.56	0.61	0.60	0.50
1	0.43	0.53	0.58	0.57	0.48
2	0.40	0.51	0.56	0.55	0.46
3	0.37	0.49	0.54	0.52	0.44
4	0.35	0.46	0.51	0.50	0.42
5	0.35	0.48	0.52	0.47	0.40
6	0.41	0.54	0.57	0.50	0.38
7	0.48	0.60	0.63	0.57	0.45
8	0.60	0.68	0.71	0.69	0.59
9	0.72	0.78	0.82	0.80	0.72
10	0.83	0.86	0.90	0.90	0.82
11	0.89	0.91	0.96	0.96	0.89
12	0.94	0.95	1.00	0.99	0.94
13	0.96	0.97	1.01	1.02	0.93
14	0.94	0.97	1.00	1.01	0.91
15	0.89	0.94	0.98	0.99	0.88
16	0.84	0.89	0.93	0.95	0.80
17	0.76	0.83	0.87	0.87	0.70
18	0.70	0.79	0.83	0.80	0.62
19	0.65	0.75	0.79	0.75	0.58
20	0.60	0.70	0.74	0.71	0.56
21	0.56	0.66	0.71	0.68	0.55
22	0.53	0.63	0.68	0.66	0.53
23	0.50	0.60	0.65	0.63	0.51

	Cooling load in Florence						
	Apr.	May	Jun.	Jul.	Aug.	Sep.	Oct.
0	0.46	0.57	0.67	0.75	0.77	0.70	0.60
1	0.43	0.55	0.64	0.73	0.75	0.68	0.58
2	0.41	0.52	0.62	0.71	0.74	0.67	0.56
3	0.39	0.50	0.60	0.69	0.72	0.65	0.54
4	0.37	0.48	0.58	0.67	0.70	0.63	0.53
5	0.35	0.45	0.55	0.64	0.68	0.61	0.51
6	0.33	0.46	0.58	0.65	0.66	0.59	0.49
7	0.37	0.53	0.65	0.71	0.71	0.61	0.47
8	0.48	0.61	0.72	0.78	0.79	0.73	0.59
9	0.63	0.72	0.80	0.87	0.90	0.88	0.77
10	0.76	0.83	0.90	0.97	1.00	0.99	0.88
11	0.86	0.92	0.97	1.04	1.07	1.06	0.96
12	0.92	0.96	1.01	1.09	1.11	1.10	1.00
13	0.95	0.99	1.03	1.10	1.12	1.10	1.02
14	0.94	0.98	1.03	1.10	1.12	1.09	1.03
15	0.90	0.95	1.02	1.09	1.11	1.08	1.00
16	0.85	0.91	0.98	1.05	1.07	1.03	0.93
17	0.76	0.84	0.91	0.99	1.01	0.95	0.81
18	0.65	0.78	0.88	0.95	0.94	0.86	0.70
19	0.58	0.73	0.84	0.91	0.90	0.80	0.67
20	0.54	0.68	0.79	0.87	0.86	0.77	0.66
21	0.52	0.65	0.75	0.83	0.84	0.76	0.64
22	0.50	0.63	0.72	0.81	0.82	0.74	0.62
23	0.48	0.60	0.70	0.78	0.80	0.72	0.61

6.2.8 Node performance simulation – chosen results

A demonstrative simulation was performed for a representative day of July. Fig. 3 shows from which devices would the cooling power originate. Without any optimization procedure, simulation regime prompts the solar driven absorption chiller to work in the base load, the demand is then covered by adsorption chiller, then by a vapour compression chiller being a part of the hybrid chiller and if that is not enough: by an additional vapour compression chiller that could work as a backup. Currently, the node is operated semi-manually and if it is not forced differently by the operator, in case of insufficient solar heat, the base load of absorption chiller will be satisfied by the support of district heat (if the minimum driving temperature level of 70°C is assured).

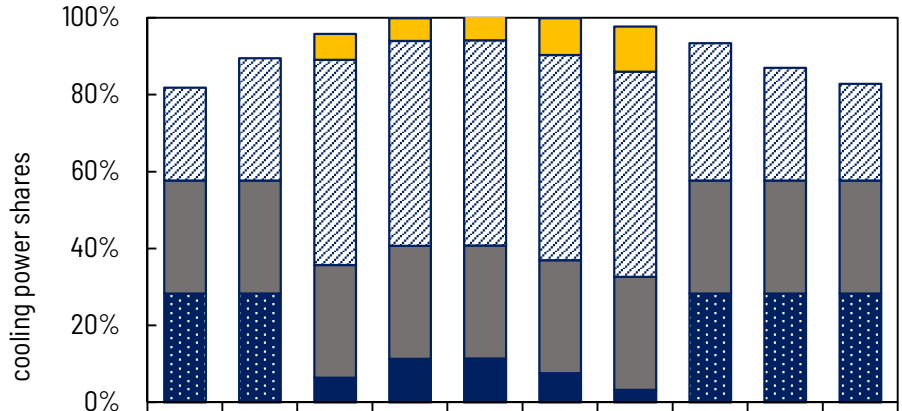

hour of the day →	9	10	11	12	13	14	15	16	17	18
additional vapour-compression chiller	0%	0%	7%	6%	7%	10%	12%	0%	0%	0%
hybrid chiller - compression part	24%	32%	53%	53%	53%	53%	53%	36%	29%	25%
district heat driven hybrid chiller - adsorption part	29%	29%	29%	29%	29%	29%	29%	29%	29%	29%
district heat driven absorption chiller	28%	28%	0%	0%	0%	0%	0%	28%	28%	28%
solar heat driven absorption chiller	0%	0%	6%	11%	11%	8%	3%	0%	0%	0%

Fig. 6.12 Division of cooling energy streams coming from solar driven absorption chiller , from district heat driven absorption chiller, district heat driven adsorption chiller, from built-in compression chiller and from a backup compression chiller during the representative day of July in Wroclaw.

It is visible, that during the morning and late afternoon the solar thermal collector heat yield is not sufficient to independently drive the absorption chiller. It is clear that the solar field is

undersized, but the number of collectors installed was limited by the roof available space. In these hours of poor radiation conditions, the absorption chiller has to be assisted by district heat (if only the temperature level of district hot water is over 70°C). Driving absorption chiller with district means achieving lower COP indicator (because of lower driving temperature level) and thus higher consumption of driving energy. Progressively, cooling energy demands are then supplemented by the adsorption and compression parts of the hybrid chiller. Absorption chiller can be driven directly by solar heat between 11 am and 3 pm. Noon hours on the reference day of July is also the time with highest cooling load and the lacking cold would have to be coproduced from a backup vapour compression chiller. This simulation is taking into account neither economical nor environmental impact of providing the end-user with cooling power coming from different devices driven by heat streams of variable origin.

6.3 Exergy analysis

6.3.1 Methodology

Exergy analysis of the node was done following specific exergy costing method (SPECO). The balance boundary covered: solar field, hot water tank (acting for the instant analysis like an intermediate heat exchanger), absorption chiller, hybrid chiller and an additional vapour-compression chiller supplementing the deficiencies of cooling energy production (not included in a scheme in Fig. 6.4). Definition of fuel and product exergy rates are found in Table 6.9

Table 6.9 Definition of fuel and product exergy rates of the components in the node

k-th component	**Name**	$\dot{B}_{F,k}$	$\dot{B}_{P,k}$	$\dot{B}_{L,k}$
1	Solar field	$\dot{B}_S$	$\dot{B}_2 - \dot{B}_1$	$\dot{B}_S - \dot{B}_{Q,coll}$
2	Absorption chiller	$\dot{B}_3 - \dot{B}_4$	$\dot{B}_7 - \dot{B}_8$	$\dot{B}_{11} - \dot{B}_{12}$
3+4	Hybrid chiller	$\dot{B}_5 - \dot{B}_6 + \dot{W}_4$	$\dot{B}_9 - \dot{B}_{10}$	$\dot{B}_{13} - \dot{B}_{14}$
5	Tank – intermediate heat exchanger	$\dot{B}_2 - \dot{B}_1$	$\dot{B}_3 - \dot{B}_4$	0
x	Additional vapour-compression chiller	$\dot{W}_x$	$\dot{B}_{x1} - \dot{B}_{x2}$	$\dot{B}_{x3} - \dot{B}_{x4}$

Exergy rate assigned to the incoming solar radiation is denoted as $\dot{B}_S$ and calculated following methodology presented in Chapter 4 (Eq. (4-13)). Approach to the calculation of exergy loss in the solar collector is similar as presented in section 5.6.1. Exergy loss results from energy degradation from infinite (very high) Sun temperature (Ts=5780K) to the average temperature of the solar collector. Hence, $\dot{B}_{Q,coll}$ is calculated with Eq. (6-10):

$$\dot{B}_{L,1} = \dot{B}_S - \dot{B}_{Q,coll} = \dot{B}_S - \dot{Q}_u \left(1 - \frac{T_{coll}}{T_s}\right) \quad (6\text{-}10)$$

Where $\dot{Q}_u$ is the useful heat gain from the solar field (kW), T_{coll} is the average collector surface temperature (approximated by the average temperature of the heat transfer fluid).
Exergy destruction in each device is calculated following Eq. (6-11).

$$\dot{B}_{D,k} = \dot{B}_{F,k} - \dot{B}_{P,k} - \dot{B}_{L,k} \quad (6\text{-}11)$$

Performing the exergy analysis at the level of whole devices requires calculation of exergy rates of external flows. $\dot{B}_1$ and $\dot{B}_2$ are the exergy rates of the propylene glycol, while $\dot{B}_3$-$\dot{B}_{14}$ and $\dot{B}_{x1}$-$\dot{B}_{x4}$ are the exergy rates of water. Reference state conditions are calculated for ambient temperature and pressure for glycol and water, respectively.
For the purpose of global analysis of the system, the total fuel exergy rate is calculated like in Eq. (6-12).

$$\dot{B}_{F,tot} = \dot{B}_S + \dot{B}_5 - \dot{B}_6 + \dot{W}_4 + \dot{W}_x \quad (6\text{-}12)$$

While the total product exergy could be presented by Eq. (6-13).

$$\dot{B}_{P,tot} = \dot{B}_7 - \dot{B}_8 + \dot{B}_9 - \dot{B}_{10} + \dot{B}_{x1} - \dot{B}_{x2} \quad (6\text{-}13)$$

6.3.2 Results

Exergy analysis was performed for every time step of the simulation. Exemplary results for the simulation performed for the system operated in Wrocław, at 14:00 during the representative day of July are given in *Table 6.10*. The nomenclature is in accordance with the presented methodology in 4.2.4.

Table 6.10 Exergy analysis results for the hybrid heating and cooling node in Wrocław (representative day of July, 14:00)

k	**Name**	$\dot{B}_{F,k}$	$\dot{B}_{P,k}$	$\dot{B}_{D,k}$	$\dot{B}_{L,k}$	$y_{D,k} = \frac{\dot{B}_{D,k}}{\dot{B}_{F,tot}}$	$y^*_{D,k} = \frac{\dot{B}_{D,k}}{\dot{B}_{D,tot}}$	η_k
		kW	kW	kW	kW	-	-	-
1	Solar field	36.6	1.6	7.284	27.7	0.14	0.39	4.5%
2	Absorption chiller	1.6	0.3	1.085	0.3	0.02	0.06	17.7%
3+4	Hybrid chiller	13.9	3.1	9.171	1.6	0.18	0.49	22.3%
5	Tank – intermediate heat exchanger	1.629	1.626	0.003	0.0	$43 \cdot 10^{-5}$	$12 \cdot 10^{-4}$	99%
x	Additional vapour-compression chiller	1.61	0.4	1.11	0.1	0.028	0.06	22.6%

One of the first issues that attract attention is the very low exergy efficiency of the solar collector component (4.5%). One should, however, realize that for that hour of simulation in Wrocław, total solar radiation reaching the sloped surface equals 551 W/m^2 and the temperature difference between heat transfer fluid and ambient is 67K. If the manufacturer-provided efficiency coefficients are treated as reliable, for those conditions, solely the energy efficiency equals only 24%. Apart from that, the low exergy rate of the useful cooling effect cannot be left unnoticed. Although the chilled water temperature is lower than ambient temperature, it is still too close to this temperature to be able to notice the clear increase of quality of the cryogenic effect.
Exergy flow and its degradation are shown in the simplified Sankey diagram (Fig. 6.13) for this simulation step.

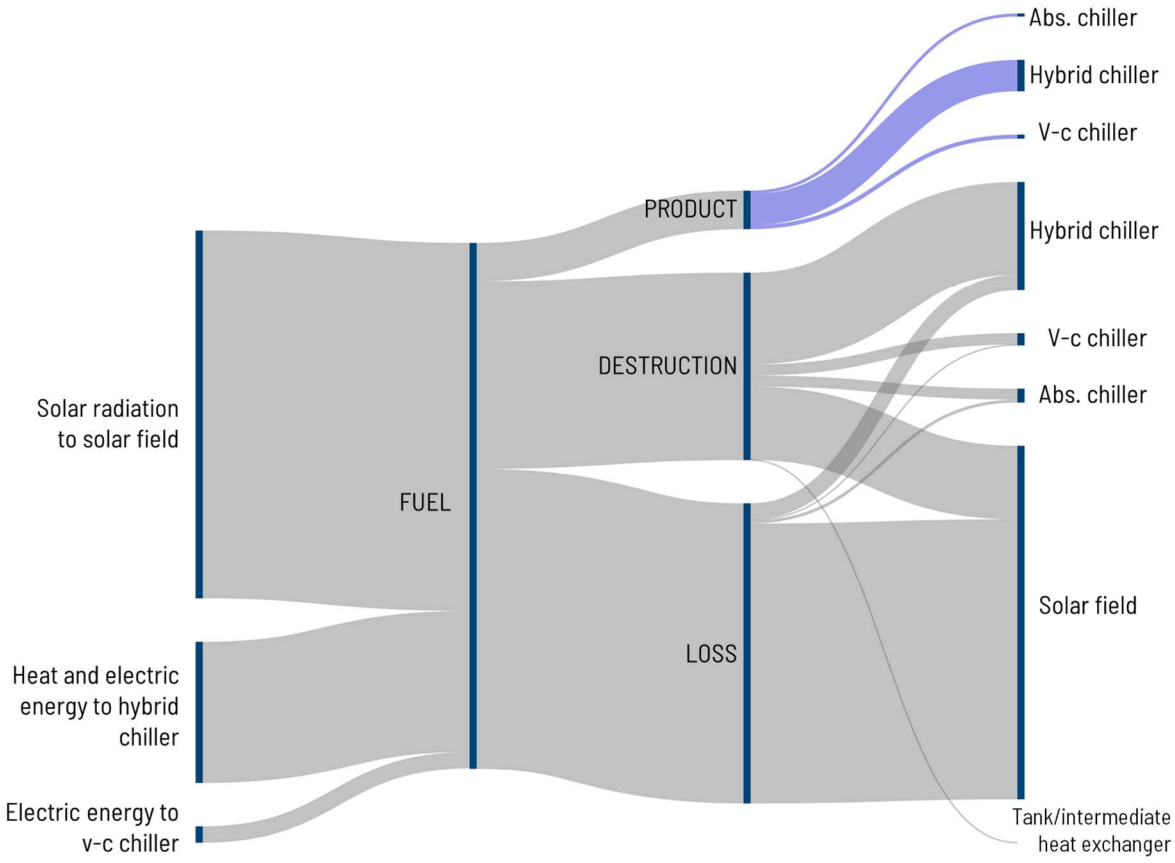

Fig. 6.13 Exergy balance of the hybrid node in Wrocław – shares of exergy product, destruction and loss deriving from fuel.

6.4 Exergoeconomic analysis

6.4.1 Methodology

Exergoeconomic analysis of the hybrid node was started with the assessment of the total cost of the plant. The methodology stands in a complete agreement specified in section 6.7.1 where the total cost of the solar ammonia-water cooling plant is evaluated. The estimated percentage of shares of fixed capital investment costs and additional costs remain unchanged. However, the approach to the estimation of the purchase equipment costs is here different. Instead of basing on specific cost functions for the equipment, the cost of the complete components are based on the cost rates of devices present in the literature [21,159]. Costs of the equipment were evaluated following the dependencies in Table 6.11. Usually, the cost of equipment should be corrected with the help of a scale factor (like in Chapter 5, Eq. (5-89)). However, the costs were borrowed from a literature source that analysed refrigeration cycles for residential applications of similar order of magnitude. Therefore, it was accepted that the cost functions correspond to the analysed case.

For the sake of simplification, it is assumed that the storage tanks price is already a built-in cost of the chillers equipment hidden in the cost rate.

Table 6.11 Cost functions of the complete pieces of equipment in the node structure

k-th component	Name	Cost, €	Parameter X
1	Solar field	$250 \cdot X$	A_{tot} – total area of solar collectors, m^2
2	Absorption chiller	$400 \cdot X$	Maximum cooling power output, kW
3	Hybrid chiller – adsorption part	$500 \cdot X$	Maximum cooling power output, kW
4	Hybrid chiller – compression part	$200 \cdot X$	Maximum cooling power output, kW
x	Additional vapour-compression chiller	$200 \cdot X$	Maximum cooling power output, kW

Following assumptions from section 5.7.1, the cost of electricity is based on Eurostat data (For the system operated in Poland, the price of electricity equals 0.14 €/kWh, while for the system potentially operated in Italy: 0.2 €/kWh [145]). Hybrid node consumes also district heat. The average operational cost rate of district heat in Wrocław equals 50 PLN/GJ, that is 0.042 €/kWh. Such value is almost impossible to evaluate for Florentine conditions since there is no district heating network. The simulation is performed assuming a potential presence of the cogeneration unit in Florence and that the price is equivalently higher like the electricity. Theoretical cost rate for district heat in Italy is therefore assumed as 0.06 €/kWh. The off-design analysis showed that the node in Poland can be operated during 1530 hours of the cooling season and the node potentially placed in Italy would be operated during 2140 hours.

6.4.2 Results

In order to maintain the same plane of comparison, exemplary results from the exergoeconomic analysis performed for the case of the representative day of July at 14:00 are shown in *Table 6.12* and *Table 6.13*.

Table 6.12 Values of selected exergo-economic variables for a hybrid system operating on reference day of July, at 2 pm in Wrocław, Poland

k	Component	PEC [€]	$\dot{Z}_k$ [€/h]	$\dot{C}_{D,k}$ [€/h]	$\dot{Z}_k + \dot{C}_{D,k}$ [€/h]	$c_{F,k}$ [€/kWh]	$c_{P,k}$ [€/kWh]	f_k [%]	r_k [%]
1	Solar field	17820	2.694	0	2.69	0	1.654	1	n/a
2	Absorption chiller	7040	1.064	1.717	2.78	1.654	13.05	0.383	13.11
3+4	Hybrid chiller	15200	2.298	1.152	3.45	0.1643	1.475	0.666	13.61
x	Additional vapour-compression chiller	1000	0.1512	0.158	0.31	0.14	1.126	0.489	9.258

Table 6.13 Values of selected exergo-economic variables for a hybrid system operating on reference day of July, at 2 pm in Florence, Italy.

k	Component	PEC [€]	$\dot{Z}_k$ [€/h]	$\dot{C}_{D,k}$ [€/h]	$\dot{Z}_k + \dot{C}_{D,k}$ [€/h]	$c_{F,k}$ [€/kWh]	$c_{P,k}$ [€/kWh]	f_k [%]	r_k [%]
1	Solar field	17820	1.926	0	1.93	0	0.4909	1	n/a
2	Absorption chiller	7040	0.761	1.109	1.87	0.4909	2.77	0.4071	4.643
3+4	Hybrid chiller	15200	1.643	1.199	2.84	0.2129	1.483	0.5781	7.522
x	Additional vapour-compression chiller	1000	0.1081	0.02201	0.13	0.2	2.635	0.8309	18.47

One should promptly notice the very high product cost rate in the absorption chiller for Polish location ($c_{P,2}$). It results from the combination of factors. The relatively low value of incoming solar radiation is a reason for low solar collector efficiency. Consequently, a low value of exergy rate from solar collectors is available to drive the absorption chiller. If the absorption chiller is driven only by the heat from solar collectors (like in this case), only a small amount of absorption chiller cooling potential is in reality used. At the same time, the hourly costs resulting from the investment phase remain unchangeable. This all causes a spectacular increase in the product cost rate. If the results for Polish and Italian conditions are compared, a difference in hourly investment cost rate is visible. It results directly from the difference of annual time of operation influencing the yearly cost distribution. Moreover, for the same hour in Italy, the total solar radiation is much higher (820 vs 550 W/m^2) which positively affects the collector efficiency (energy efficiency equals 39%, while the exergy efficiency is 7.5%). The cost rate

of cold from the absorption chiller is consequently much lower in the Italian case. However, since less cooling power has to be produced by the additional vapour-compression chiller, the cost rate connected with product from this device is increased. On the other hand, cost of cold from hybrid chiller at 14:00 on a representative day of July is almost the same in both locations. Hybrid chiller is here driven by district heat and electric energy. Therefore, cost of cold produced by this device relies on the price tariffs. A partial sensitivity analysis for this hour of simulation is presented in Fig. 6.14. It shows what would be the cost of cold from hybrid chiller exploited in Italy, if the electricity price was modified +/- 60% and what would it be like, if the price of district heat was modified in that manner. Price of electric energy is higher and the compression section of the hybrid chiller has a higher cooling output, therefore the cost of cold is more dependent on that value. It is directly visible, as the dark blue line on the chart (related to electric energy cost) is steeper. For comparison purpose, the value of cost of cold from hybrid chiller in Poland is also presented on the graph as a black X. The price tariffs of both electricity and heat in Poland are 70% of the Italian nominal tariffs for this study case. The graph shows what would be the cost of cold from a hybrid chiller operated in Italy, if the cost of electricity or heat was as low as in Poland. If the cost of heat was decreased to Polish tariffs, the cost of cold would be lowered by 5%. If the cost of electricity would be reduced to Polish price, the cost of cold from hybrid chiller would be decreased by 13.5%.

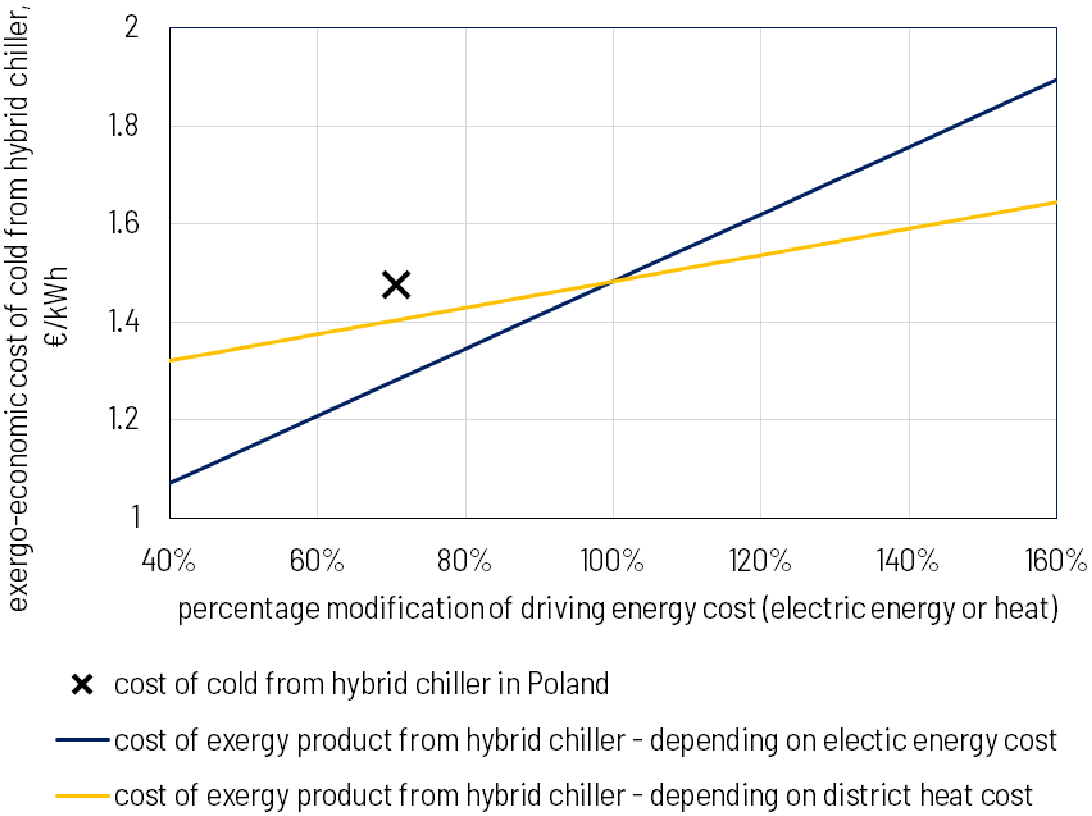

Fig. 6.14 Sensitivity analysis of cost of cold from hybrid chiller in the function of variable electricity cost and district heat cost in Italian geo-economic environment.

The tool of exergoeconomic analysis could be a support while striving to three goals: design optimization, operation optimization, and system diagnostics. The first aim means the minimization of the total costs of the system products by changing the design parameters. It cannot be met in the case of the here presented study, as the system has already been designed and constructed. However, exergoeconomic indicators can assist in operation optimization. It would use the average cost per unit of exergy to indicate the modification in the system operational parameters that could improve the cost effectiveness of the whole system.

Exergoeconomic analysis is usually performed with the thought of minimization the cost per unit of the system product. The economic importance of the analysed component (device) can be determined by the analysis of sum of the investment cost rate Żk and of the cost rate of exergy destruction. In the case of the study over a hybrid node, the component of highest importance is the hybrid chiller followed by the solar field and by the absorption chiller. The last two seem to have similar economic importance. The hybrid chiller is also characterized by a high relative cost difference. The exergo-economic factor f_k is close to 0.6 for both study cases. The same, capital investment cost constitutes 60% of the sum of capital investment cost and of the cost of exergy destruction.

Annual results are set in Table 6.14.

Table 6.14 Annual operational details for solar integrated hybrid cooling node.

No.	Location	Florence (Italy)	Wrocław (Poland)
1.	**Coordinates**	43.75°N 11.29°E	51.1°N 17.03°E
2.	**Annual solar radiation on fixed surface, kWh/m^2**	1619	1118
3.	**Total operation time, h/year**	2140	1133
4.	**Annual productivity, MWh/a**	1200	797
5.	**Annual average cost of cold from absorption chiller, €/kWh**	6.81	9.70
6.	**Annual average cost of cold from hybrid chiller, €/kWh**	2.14	1.94
5.	**Annual average cost of cold from back-up compression chiller, €/kWh**	3.31	2.34

Higher availability of solar radiation implicates longer cooling season and the same longer total operational time during the year. It also means higher annual production of cooling energy from the node following bigger thermal comfort demands towards cooling energy. As the meteorological conditions are more favourable under Italian climate conditions, solar energy is more utilizable while driving the sorption chillers. As a result, the solar fraction is higher in Italian installation than in Polish. The annual shares of cooling energy deriving from three types of energy sources (solar energy, district heat, electric energy) is presented in Fig. 6.15 for the plant operated in Wrocław and in Fig. 6.16 for the plan theoretically moved to and operated in Florence.

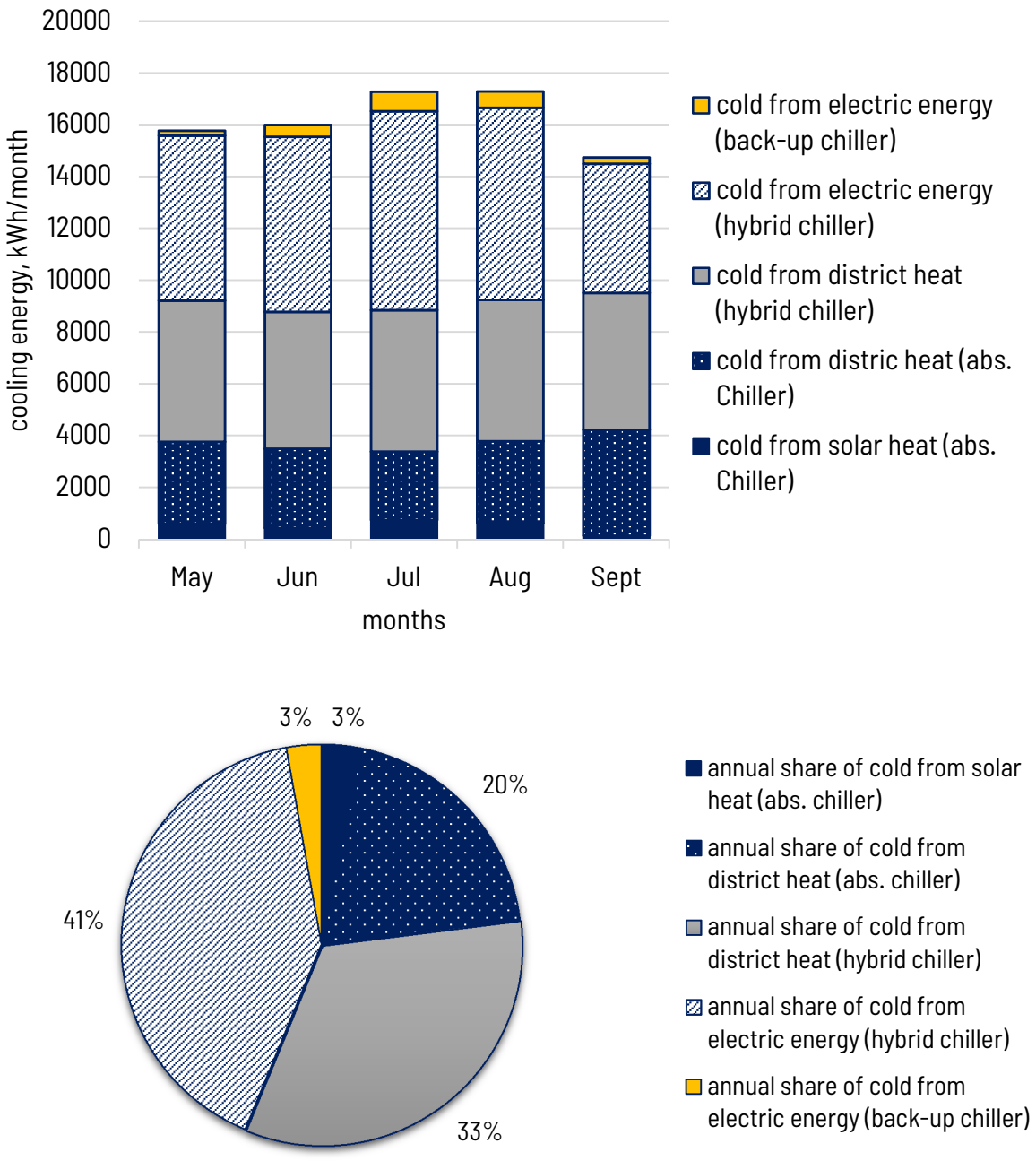

Fig. 6.15 Distribution of cooling energy produced over the year in Wrocław, Poland with the division between different energy source (upper chart) and annual shares of origin of driving energy delivered to the node (bottom chart)

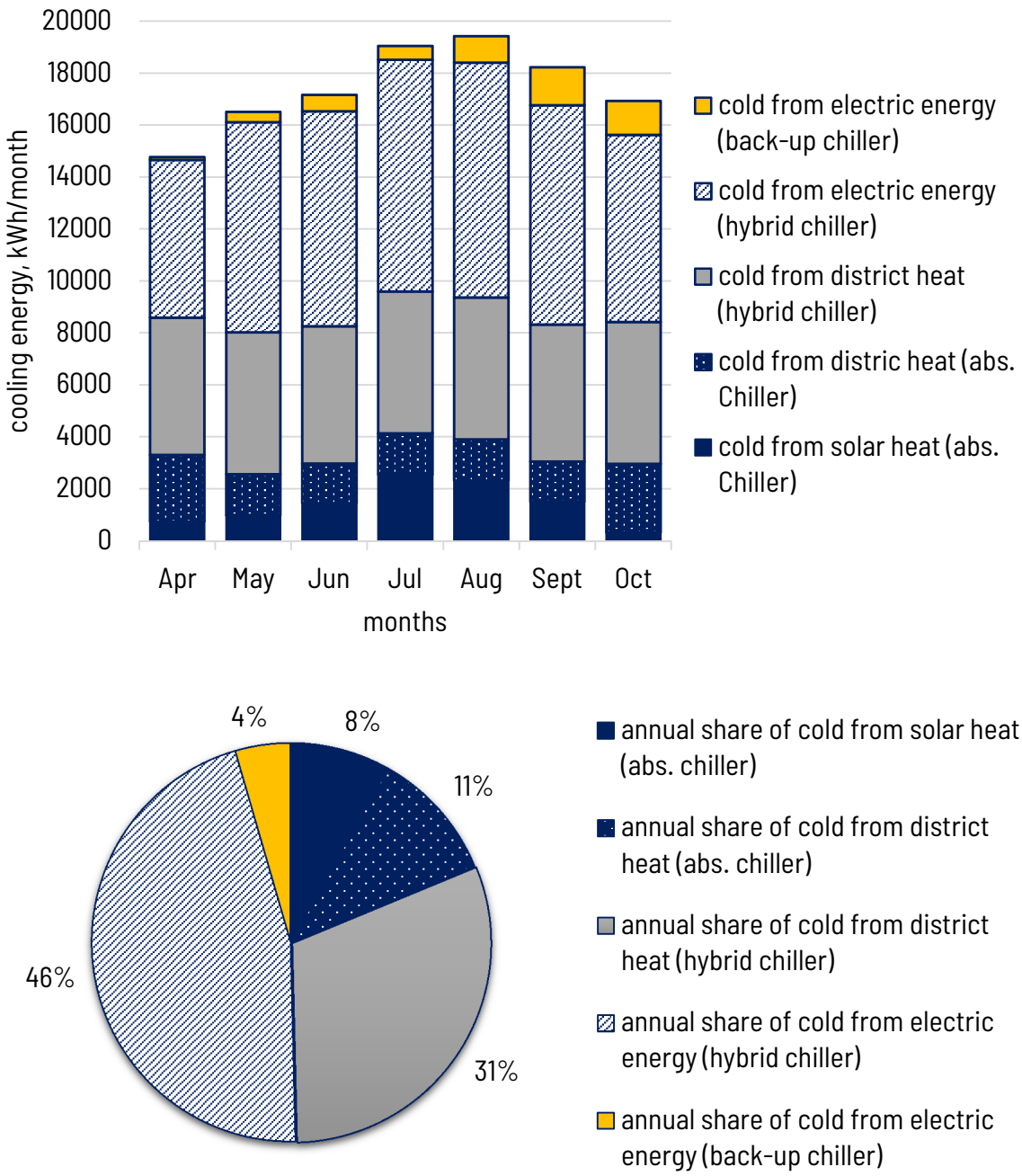

Fig. 6.16 Distribution of cooling energy produced over the year in Florence, Italy with the division between different energy source (upper chart) and annual shares of origin of driving energy delivered to the node (bottom chart)

It is clearly visible here, that only 3% of cooling energy produced over the season in Wrocław is deriving from solar energy, while for the same plant operated in Italy the share equals 8%. It should be also marked, that the annual average cost of cold from hybrid chiller in Polish location is close to the average cost in Florence. It can be justified by several factors: the cost rates of driving energy (district heat and electric energy) is higher in Italy. But meaningful is also the fact that while the solar radiation is available, mainly the solar absorption chiller is

delivering cooling energy and hybrid chiller is working under part load conditions and its whole potential is not used. At the same time, the investment cost rates remain constant.

Next, to that observation, annual results show also that the annual average cost of cold from the back-up compression chiller might be higher in Italy than in Poland. The reason for that can be again higher cost rate of the driving electric energy, but also the fact, that the same compression chiller is less used in Italy than in Poland. This is proven by the column chart above. It is however obvious, that the system size should be redesigned for the real operation in the Italian location.

6.5 Place for improvement – a control procedure

6.5.1 Concept

The aim of this part of the study is to create a control algorithm that, relying on current external conditions and defined optimization criterion, should provide indications on optimized flow settings: flow rates values and valves opening configuration. Depending on meteorological conditions and online updated measurements, the procedure should determine the way the chiller operates and how the streams of district hot water and hot water from the solar storage should be mixed and/or split. Optimum parameters can be chosen according to one adapted criterion: economic or environmental.

The economic criterion searches for parameters assuring the minimum value of the objective function, that is of the cost of district heat and electricity consumed to drive chillers, pumps and auxiliary devices. On the other hand, the goal of environmental optimization is to find the operation configuration minimizing the emission of harmful substances (e.g. SO_2, NO_x, CO_2) induced by the cumulative fossil fuel consumption.

For the sake of this research, control of the mass flow rates, and the same of the pump flow is done by adjusting the pump speed. Variable speed drive should allow for the pump speed adjustment over a continuous range. Mass flow rate required at a given time span is translated into a required speed signal. It should be clearly stated, that for that kind of applications, study over inertia effects should be subsequently taken into account.

The control algorithm has been written in the form of a logic procedure taking advantage of a mathematical bisection method, coupled to an iterative incremental loop method. Its effect has been tested on chosen operational cases.

According to a confidentiality agreement, details on the procedure cannot be shared, but the features are listed in the following section.

6.5.2 Limit and boundary conditions

The optimization procedure is meant to work as an automatic decision support tool for node self-management. It works as an Input-Output type. The procedure uses inputs which can be divided into subgroups: constants (geometry of the system, geo-location, emission indicators, performance coefficients), limitation conditions (minimal and maximal: cooling power, temperatures, mass flow rates, valve opening level, minimal driving energy requirements of the devices), external variables (date, hour, meteorological conditions, DHW demand, cold demand, heat unit price, electricity unit price), measured state of the system (temperatures, pressures, mass flow rates, position of the valves).

The procedure reads and converts the inputs. The inputs are a set of current information about the node collected from the measurements acquisition system (temperatures, mass flow rates, valves settings, meteorological conditions), data available from online databases (cost tariffs), and constants (chosen optimization criterion, system boundary conditions – technical limitations). On the base of the current thermal comfort demand (valid for one time step), availability of driving energy streams and their quality, applicable price paths, chosen optimization criterion, the algorithm should prompt the decision on how to set the valves arrangement, what should be the mass flow rates of district hot water and of water from hot storage warmed by solar energy, what amount of electric energy is needed.

The results are returned as a report which should be translated by the automatic control system to set the desired parameters.

6.5.3 Exemplary results and discussion

Fig. 6.17 is presenting a graph where the optimal mass flow rates minimizing the economic cost are indicated. Because of data confidentiality, all results are normalized. The mass flow rate of district hot water and of ‘solar hot water’(water that was warmed by the heat transfer fluid coming from solar collectors) from the storage is given as a percentage value of the design flow rate given by the pump manufacturer (Design flow rate values for district hot water and solar hot water were the same). The chart shows what mass flow rate coming from the solar hot water storage should be set and what should be the district hot water mass flow rate. The optimal pair of mass flow rates (affecting the position of the valve) is defined separately for different cooling loads (defined as a part of the nominal cooling power of the whole system). For the purpose of this simulation, it was assumed that the solar hot water storage tank is fully loaded: thus the outlet temperature from the solar hot water storage is 85°C, while the temperature of the incoming district hot water: 65°C.

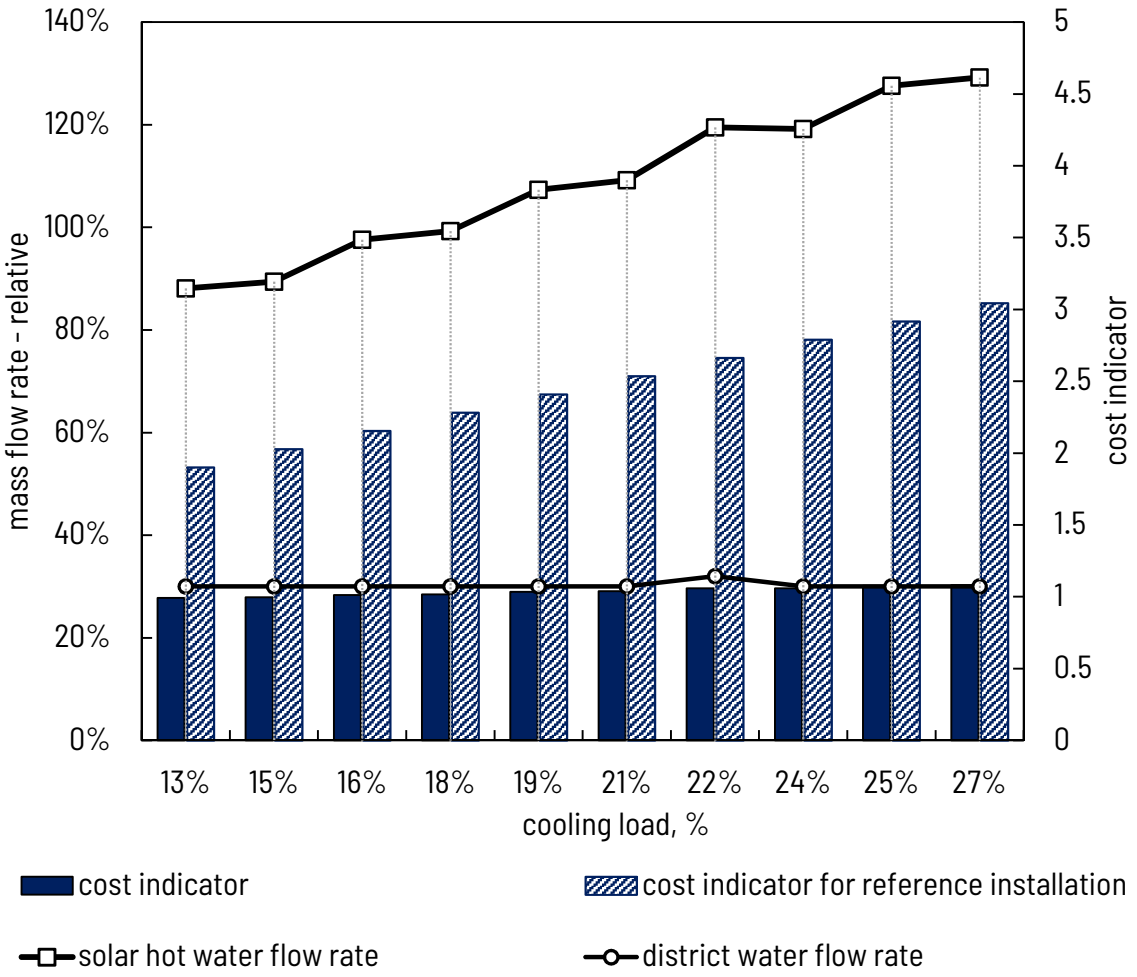

Fig. 6.17 Selection of optimal mass flow rates (district hot water and water from hot water storage) to drive the chillers system depending on the cooling load and the comparison of cost indicator if the economic optimization procedure is not used

Following the Industrial partner's suggestion, for the sake of this simulation, a minimum value of district hot water driving the hybrid node is always assumed (it is 50% of the nominal mass flow rate in the cycle). If the solar hot water storage is constantly delivering heat at the temperature level of 85°C, the absorption chiller could be constantly driven only by this heat rate. However, the assumption of non-zero district hot water mass flow rate, forces the mass flow rates from district network and from hot water tank (heated by solar heat) to mix. The chart presents such a selection of mass flow rates pair that assures the minimization of operational economic cost– In the case of solar collectors, the only energy paid for is the electric energy consumed by the pump. If no optimization procedure was applied, the cost could have been even three times higher for the highest cooling load here considered (27% of the rated load). On the other hand, it is worth noticing that the chosen optimal mass flow rate of water warmed by the heat transfer fluid (glycol-water) from solar collectors is never the highest possible. It is not reaching the maximum allowable mass flow rate conditions. It is limited by

the expense on pumping energy (the higher the mass flow rate, the higher the cost for the energy spent). This phenomenon is presented on the profile in Fig. 6.18.

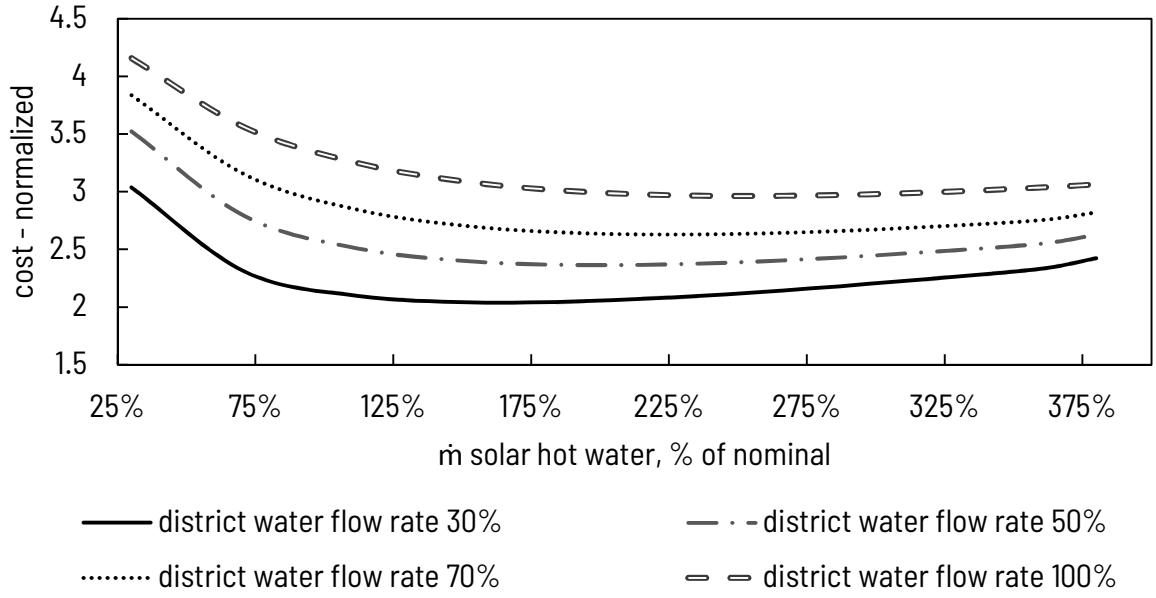

Fig. 6.18 Chart proving a minimum of cost indicator in the function of hot water flow rate

It is here visible that although utilizing more solar heat for energy conversion could induce economical savings, the higher the mass flow rate of water warmed by HTF from solar collectors, the higher the temporary pumping cost. At one point (the extreme of the function) it is no longer economical to increase the 'solar hot water' mass flow rate.

According to obtained results, of which only a fragment is here shown, if the control algorithm had been applied to the node management system, the cost and environmental influence indicators would have been lower than in a reference case without the procedure. At the same time, it occurred that it is not always of the highest benefit to demand the highest mass flow rate of water which was heated in the solar collector. Although it was warmed by a zero-cost source, the energy consumption of pump also contributes to the total cost indicators (not to mention the LCA which was out of the scope of this analysis).

Chapter 7. CONCLUSIONS

The dissertation focused on two real-existing installations representing two different types and levels of complexity of solar assisted hybrid heating and cooling nodes. The analysis covered a solar energy driven ammonia water chiller plant located in Florence and a substation in Wrocław that converts solar heat and district heat into the central heating and cooling energy using sorption technology. The Italian plant has been a practically operated unit since 2012, while the hybrid node in Wrocław was designed and built during realization of this thesis and has remained a demonstration plant. Both installations were analysed in the terms of energy efficiency and then, accepting exergy as the only rational basis to assess the cumulative economic performance, the exergy and subsequent exergo-economic analyses were performed. As simulations of two reference plants were performed for both Italian and Polish meteorological conditions, the meteorological impact on the exergy and exergo-economic indicators can be discussed. The study over Florentine installation required a separate analysis of each component of the chiller, while the analysis of node in Wrocław was already modular device-based. The two systems have a common type of energy source, that is of solar energy. Apart from that, however, they cannot be related directly to each other, but rather be treated as two examples representing solar sorption cooling technologies that serve us to widen the knowledge.

The aim of the thesis was to study and present the energy and exergy efficiency indicators of the two installations, to investigate the meteorological conditions' impact on the indicators, to verify the usefulness of exergo-economic methodology for the analysis, as well as to check the potential advantages of exemplary control procedures. The goal was achieved step by step during the completion of this work. Detailed summaries are presented in the following.

7.1 Summary of Part I - Solar cooling plant

Design analysis of the solar ammonia-water chiller in Florence revealed that the nominal Coefficient of Performance equals 0.501. If the balance boundary is widened and incoming solar radiation and electric energy driving the pump are treated as the fuel energy streams, the COP drops to 0.35. Similarly, if exergy is considered, the exergy efficiency of the wide system equals 2.6%. If the driving exergy was defined as the exergy product rate from solar collector, the exergy efficiency of the solar chiller would be 11.8%. These apparent differences reveal, that not only the quality of energy matters but also the definition of system boundaries. These results should be interpreted wisely to avoid manipulation: the exergy efficiency of an

absorption chiller will be always lower (if ideal machines are not considered) than the exergy efficiency of a typical compression chiller (around 25% [76]), but one should remember that the advantage of an absorption chiller is that it can be driven by a waste heat stream or, as in the present case, by renewable energy. It was shown that the solar collector and its efficiency parameters play a predominant role in the exergy destruction and losses allocation. It should be marked that it can never be the aspiration of the designer to actually improve the exergy balance of the solar collector by decreasing the irreversibilities occurring during reactions in the Sun at conditions equal to black-body temperature. Therefore, only the improvement of the design of the solar collector or introduction of control procedures (e.g. finding the optimal temperature difference of heat transfer fluid maximizing the exergy efficiency, like in [128]) can matter. However, the change of exergy destruction and losses in the whole device induced by changes in one component should be analysed. One should observe that minimizing irreversibilities in one component could lead to deterioration of performance in another one. These aspects could be thoroughly addressed by an advanced exergy analysis on endo- and exogenous parts of irreversibilities. Fig. 7.1 presents how the potential increase of solar collector efficiency affects the distribution of destruction ($\Delta\dot{B}_{D,i}$) and losses ($\Delta\dot{B}_{L,i}$) in the whole cycle. The distribution of exergy destruction and losses is related to total exergy input: fuel exergy of solar radiation.

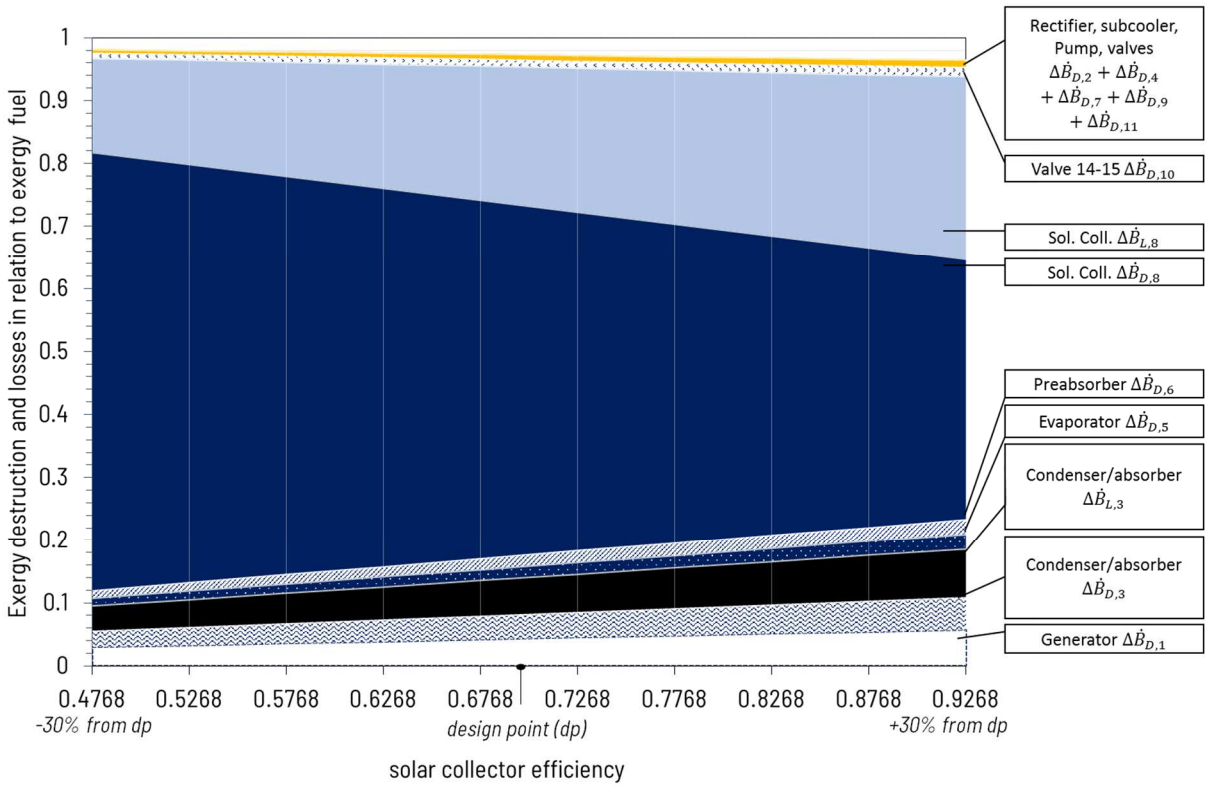

Fig. 7.1 Distribution of relative exergy destructions and losses in the components of the cycle in the function of modified solar collector efficiency.

Exergy destructions in the rectifier, subcooler, pump and valve (9) are so negligible that they were shown as a sum in the chart. The chart helps to realize that if solar collector efficiency parameters were potentially increased by 30%, the exergy destruction in the solar collector component would have also dropped by 30%. However, this modification of the design leads also to increase of exergy losses in the solar collector component. Although much smaller than destructions in the solar collector, the exergy destruction in generator and absorber/condenser are doubled. Hence, the processes are becoming more irreversible. If a similar sensitivity analysis was performed for the cooling water inlet temperature, it would turn out that lowering this temperature decreases the exergy loss and destruction in almost every component. However, it induces higher exergy destructions in two components: the exergy destruction increases in the evaporator (higher mass flow rate) and by 11% also in the solar collector (which is already afflicted by a considerable loss and destruction). This confirms that exergy analysis should be used at all levels, from design to off-design and diagnostic purposes, considering the whole system as a set of connected components.

When the off-design analysis is considered, the differences between operating the same installation in Italy and in Poland emerge. The fact that the annual incoming beam radiation

obtained by a tracking surface in Florence equals 1155 kWh/m^2 and is 676 kWh/m^2 in Poland directly determines a higher performance of the system operated under Italian weather conditions. Additionally, the more attractive solar radiation in Italy implies that the cooling season lasts longer. The same, the productivity of the analysed cooling plant is higher in Italy (23 vs. 12 MWh of cooling energy per year).

The longer cooling season and, the same, longer operational time has also a positive impact on the costs distribution. In the exergo-economic analysis, the purchased equipment costs constitute 66% of the total capital investment cost. The overall specific investment cost of the whole system equals 1342 €/kW of cold, which is marginally higher than the value of 1000-1200€/kW of cold reported in the literature [17]. According to the analysis, having in mind that the price of electricity is higher in Italy than in Poland, the cumulative levelized cost of cold from ammonia-water chiller operated in Italy is about 9 €/kWh, while in Poland it is 13 €/kWh. It can be concluded that more favourable meteorological conditions have a positive impact on the cumulative exergo-economic cost of the product. If the same cost was analysed for the peak of the cooling season (reference day of July, 14:00), the cost of cold in Italy equals 4.3€/kWh, while in Poland: 6 €/kWh. This directly confirms the importance of off-design analysis, also of the exergo-economic indicators. For both locations, the components with the highest exergo-economic factor f_k are (in order): solar collector, pump, rectifier and the intermediate valve. The investment cost is mainly creating the overall cost of products in these components. In the rest of the components, the product cost is associated with the exergy destructions. At the same time, the solar collector is always the most expensive equipment in the plant. Therefore, even a small reduction of its cost would bring a significant saving on the cooling plant total cost rate. Correct operation of a plant – especially of expensive solutions based on renewable, requiring high capital investments - is of primary importance. As an added value to the study, a simplified but effective method of controlling the solar collector outlet temperature (which represents the chillers driving temperature) was proposed. The final purpose is to increase the cooling power production and thereby to increase the solar fraction of the cycle. The idea relies on the observation of the inverse trend with the solar collector outlet temperature - referring to the collector efficiency and to the COP of the absorption cycle. The results presented in the thesis show that incorporating a control strategy adapting solar collector outlet temperature could bring a high profit to a system operated under moderate climate conditions (such as in Poland) and using vacuum tube solar collectors. The highest increase in cooling power production takes place during the morning and late afternoon hours when solar radiation is low. During these times of the day, the cooling effect can be more than double with the proposed control

procedure. On the other hand, less significant results were obtained when the same strategy was applied for the system operated in Italy and using high-efficiency parabolic trough solar collectors. This is mainly due to the fact that these collectors are less sensitive to the temperature difference between heat transfer fluid and ambient than the vacuum tube type.

7.2 Summary of Part II – Advanced Hybrid Heating and Cooling node

The substation in Wrocław fits into the definition of a hybrid heating and cooling node: it rests on solar heat, district heating and grid-derived electric energy. The incoming driving energy streams are delivered to satisfy thermal comfort needs. Useful cooling energy is obtained converting the driving energy in a series of different chillers: absorption, adsorption and conventional vapour-compression refrigeration units. In terms of exergy, the node operated under design conditions in Wrocław delivers the required cooling energy with aid of absorption, hybrid and vapour-compression chillers with 7% exergy efficiency under wide boundary conditions. If the boundary is narrowed, the incoming solar radiation is excluded and the fuel exergy rate is only built by the exergy of heat from the solar collectors, from district heat network and electric energy. For the narrow boundary conditions, the exergy efficiency equals 22%. This value is already close to the exergy efficiency of a standard vapour-compression chiller and it is understandable, since 65% of the cooling effect is here produced by the compression section of the hybrid chiller (53% of total cooling energy) and by the additional vapour-compression chiller (12% of cold).

The whole-season off-design simulation indicates that the node located in Poland is operated for 1224 hours; if it was moved to Italy, it would work for 1712 hours. The operational availability is a direct consequence of the 2-months-longer cooling season. The higher total incoming solar radiation (1620 kWh/m^2 in Italy vs 1160 kWh/m^2 in Poland) did not have any impact on the daily operational time, since the cooling demand was always to be covered by a backup chiller. Nevertheless, more convenient solar radiation conditions in Italy determine a different share of the sorption chillers output during the season. Thus, the exergoeconomic balance is affected by that. If the results for Polish and Italian conditions are compared, a difference in the hourly investment cost rate is visible. It results directly from the difference of annual time of operation influencing the yearly cost distribution. Hence, the investment cost rates of devices in Italy are lower.

Solar collectors are again causing the highest investment cost, but since the analysis is device-based this cost is closely followed by the cost of the hybrid chiller (17820 € vs 15200 €).

The profitability of a cooling system does not only depend on capital costs. Several factors such as electricity cost, discount rate and operational time deeply affect it. A controversial aspect of the analysis is to assume a fossil-fuel derived district heat to drive a hybrid node in Florence. In fact, such an energy stream is not available in this location and it would be attractive to consider a list of possible driving heat streams including e.g. geothermal heat. This is likely to be a possible option, basing e.g on the current geothermal district heating projects data [160]. According to them, the sale cost of a geothermal derived district heat equals 0.5-0.6 €/kWh which is ten times higher than the driving heat price assumed in this study.

7.3 Conclusions and future work ideas

After the discussion, one can conclude that, as expected, the meteorological conditions have an undeniable influence on the solar integrated system performance. For example, if only the direct solar radiation can be utilized, like in the Misericordia plant, the system located in Italy receives annually 1.7 more direct solar irradiation than a system located in Poland. It directly affects the annual cold productivity – it is 1.8 higher for the system operated in Italy. However, it is important to note that the same interdependences cannot be observed while analysing the cost indicators. Levelized costs of cold for a system operated in Poland are higher but the ratio between costs in Poland and in Italy is lower than the ratio between solar energy inputs. It can be explained by the fact that the cooling season lasts longer in more sunnier regions, and the investments costs are distributed over a different period of time and that the operational costs are also affected by longer exploitation. These two sides of meteorological impact should always be noticed.

Recalling the further aim of the thesis, it can be indeed concluded that the tool of a cumulative exergo-economic analysis is especially well suited for the systems taking advantage of renewable energy sources. Disregarding the location, the analyses of solar integrated systems have always two faces. Apart from considerable maintenance expense, there are actually no operational costs. If the ammonia-water chiller case is considered, delivery of 13 kW of cold is connected with consumption of, approximately, 0.1 kW of electric energy. If it was delivered steadily during the hour, the cost would equal 0.02 €. The same cooling energy obtained from a vapour-compression chiller with COP equal to 3.5 implies 0.74 € - a nearly 40 times higher unit cost. However, if the operational economic analysis is supplemented by a cumulative capital investment path and assessed by the exergo-economic analysis tool the cost indicators are reversed. The high capital investment cost of solar collectors and thermal sorption chillers makes the system unprofitable and economically uncompetitive, if compared with conventional

vapour-compression chillers. The cost of exergy product of cold evaluated basing on the exergo-economic analysis of a solar-assisted plant in Italy in July equalled 3 €/kWh; the same would be 1.5 €/kWh for the conventional compression chiller (one could consider also the option of PV-driven compression chiller and its effect on the cost distribution). In order to reduce the costs, the absorption chillers could be designed to cooperate with a smaller number of solar collectors or with less expensive collectors or switch to a less expensive heat source (e.g. geothermal if only it is available). This means that one should strive to increase the COP of the chiller, or decrease the driving temperature of the chiller. This is recognized at present as a challenge of modern sorption cooling technology, as it would have to lead to the development of new thermodynamic cycles or new working pairs of refrigerant/absorbent [21]. Exergo-economic analyses revealed also that in both locations the, as burdened with highest irreversibilities and costs, the component of the solar collector should be mainly addressed while striving to reduce the exergy destructions during the optimization process. A Proper HTF temperature increase management could improve the exergy efficiency of the collector improving the performance of the whole system.

At this point, it should be stressed that the author was deliberately referring to the levelized cost of cold (LCOC) as the reference result, keeping in mind its strong connotation with the term 'levelized cost of electricity' so much present in nowadays literature. This highlights the importance of cold on the market and promotes cold as a price holder. Additionally, the study included in this thesis helped developing a support tool allowing for elaborating scenarios of conditions at which solar integrated refrigeration systems can become competitive. The system to be analysed is always embedded under defined geo-economic conditions stimulated by weather and price-tariff factors.

However, the pessimistic conclusions resulting from exergo-economic analyses of both systems in both locations should not discourage from making efforts to increase the share of renewable energy sources in the final energy consumption. In the end, there is no better method to minimize the consumption of non-renewable natural resources of exergy than to extract renewable energy from nature.

This statement leads to a further conclusion, that the next step of the wide-picture analysis should be the exergo-environmental analysis and even a thermo-ecological cost analysis. The thermo-ecological cost, introduced in [161,162], provides the value of cumulative consumption of non-renewable exergy in all chains needed to obtain the final product. The same, it treats exergy as a proper measure allowing for evaluation of the usefulness of natural resources and reaches to the cradle phase.

Apart from the cumulative impact analyses, one should also realize that the thermal comfort market is currently, and will most likely be, undergoing relevant transformations. The challenges defined in Chapter 1 will for sure affect the behaviour of energy suppliers but also of the legislators. The costs distribution would strongly depend on incentive programmes that should for sure appear to attract the investors' attention. While striving to meet the Energy Roadmap requirements, the nodes integrating conventional and renewable driving energy are and will be becoming more common. Thence, the cost paths will gradually change requiring an update of the analysis. Therefore, having access to a structured procedure for performance and cost assessment, like that presented in this thesis, could serve as a convenient tool to support market development.

References

[1] European Commission. An EU strategy on heating and cooling 2016. J Chem Inf Model 2016;53:1689–99. doi:10.1017/CBO9781107415324.004.

[2] European Comission. COMMUNICATION FROM THE COMMISSION TO THE EUROPEAN PARLIAMENT, THE COUNCIL, THE EUROPEAN ECONOMIC AND SOCIAL COMMITTEE AND THE COMMITTEE OF THE REGIONS Energy Roadmap 2050. 2011.

[3] Pardo N, Vatopoulos K, Krook-Riekkola A, Moya JA, Perez A. Heat and cooling demand and market perspective. 2012. doi:10.2790/56532.

[4] Ecoheatcool and Euroheat & Power. The European Cold Market - Final Report. 2005.

[5] P. Capros, Mantzos L, Tasios N, Vita A De, Kouvaritakis N. EU energy trends to 2030. 2009.

[6] Analysis and market assessments to grow the share of renewables in heating and cooling. IRENA Int Renew Energy Agency 2017. https://www.irena.org/heatingcooling (accessed March 1, 2019).

[7] Isaac M, van Vuuren DP. Modeling global residential sector energy demand for heating and air conditioning in the context of climate change. Energy Policy 2009;37:507–21. doi:10.1016/j.enpol.2008.09.051.

[8] European Commission. Energy 2020 — a strategy for competitive, sustainable and secure energy. 2010. doi:10.2833/78930.

[9] 2030 Climate and Energy policy framework. Brussel: 2014. doi:10.1007/s13398-014-0173-7.2.

[10] European Commission. COMMUNICATION FROM THE COMMISSION TO THE EUROPEAN PARLIAMENT, THE COUNCIL, THE EUROPEAN ECONOMIC AND SOCIAL COMMITTEE, THE COMMITTEE OF THE REGIONS AND THE EUROPEAN INVESTMENT BANK Third Report on the State of the Energy Union. 2017.

[11] European Commission. A Clean Planet for all A European strategic long-term vision for a prosperous, modern, competitive and climate neutral economy. 2018.

[12] European Parliament. Directive 2012/27/EU of the European Parliament and of the

Council of 25 October 2012 on energy efficiency, amending Directives 2009/125/EC and 2010/30/EU and repealing Directives 2004/8/EC and 2006/32/EC. Off J Eur Union 2012;14/11/2012:1–56. doi:10.3000/19770677.L_2012.315.eng.

[13] Lund H, Werner S, Wiltshire R, Svendsen S, Thorsen JE, Hvelplund F, et al. 4th Generation District Heating (4GDH). Integrating smart thermal grids into future sustainable energy systems. Energy 2014;68:1–11. doi:10.1016/j.energy.2014.02.089.

[14] Lund H, Duic N, Østergaard PA, Mathiesen BV. Future district heating systems and technologies: On the role of smart energy systems and 4th generation district heating. Energy 2018;165:614–9. doi:10.1016/j.energy.2018.09.115.

[15] Weatheronline. Climate types n.d. https://www.weatheronline.co.uk/reports/climate (accessed March 1, 2019).

[16] Petela K, Manfrida G, Szlek A. Advantages of variable driving temperature in solar absorption chiller. Renew Energy 2017;114:716–24. doi:10.1016/j.renene.2017.07.060.

[17] Petela K, Szlek A. Energy and exergy analysis of solar heat driven chiller under wide system boundary conditions. Energy 2019;168:440–9. doi:10.1016/j.energy.2018.11.067.

[18] Alternative Energy. Augustin Mouchot's Solar Concentrator at the Universal Exhibition in Paris, 1878. n.d. https://alternativeenergy.procon.org/view.timeline.php?timelineID=000015 (accessed March 1, 2019).

[19] Gerhard Stryi-Hipp, editor. Renewable Heating and Cooling: Technologies and Applications. Woodhead Publishing; 2016. doi:https://doi.org/10.1016/C2013-0-16484-7.

[20] IEA. Internal Energy Agency, Solar and Heating Cooling Programme n.d. https://www.iea-shc.org/programme-description (accessed March 1, 2019).

[21] Kim DS, Infante Ferreira C a. Solar refrigeration options - a state-of-the-art review. Int J Refrig 2008;31:3–15. doi:10.1016/j.ijrefrig.2007.07.011.

[22] Balaras CA, Grossman G, Henning HM, Infante Ferreira CA, Podesser E, Wang L, et al. Solar air conditioning in Europe-an overview. Renew Sustain Energy Rev 2007;11:299–314. doi:10.1016/j.rser.2005.02.003.

[23] Mauthner F, Weiss W, Spörk-dür M. Solar Heat Worldwide. Sol Heat Cool Program

2016:29. doi:10.18777/ieashc-shw-2015-0001.

[24] Mugnier D, Jakob U. Status of solar cooling in the World: Markets and available products. Wiley Interdiscip Rev Energy Environ 2015;4:229–34. doi:10.1002/wene.132.

[25] Montagnino FM. Solar cooling technologies. Design, application and performance of existing projects. Sol Energy 2017;154:144–57. doi:10.1016/j.solener.2017.01.033.

[26] Al-Alili A, Hwang Y, Radermacher R. Review of solar thermal air conditioning technologies. Int J Refrig 2014;39:4–22. doi:10.1016/j.ijrefrig.2013.11.028.

[27] Henning HM. Solar assisted air conditioning of buildings - an overview. Appl Therm Eng 2007;27:1734–49. doi:10.1016/j.applthermaleng.2006.07.021.

[28] Lazzarin RM, Noro M. Past, present, future of solar cooling: Technical and economical considerations. Sol Energy 2018;172:2–13. doi:10.1016/j.solener.2017.12.055.

[29] Chwieduk DA, Grzebielec A, Rusowicz A. Solar cooling in buildings. Tech Trans Civ Eng 2014;R.111:65–73.

[30] Herold K, Radermacher R, Klein S. Absorption chillers and heat pumps. CRC Press; 1996.

[31] Safarik M. Solar cooling projects with water-LiBr absorption chillers. Fünftes Symp. Solares Kühlen der Praxis, 89, 2008, p. 81–90.

[32] Ezzine N Ben, Bellagi A. Thermodynamic Simulation of Ammonia-Water Double Effect Absorption Chiller 2004:1–8.

[33] Grossman G. Solar-powered systems for cooling, dehumidification and air-conditioning. Sol Energy 2002;72:53–62.

[34] Said S a M, El-Shaarawi M a I, Siddiqui MU. Alternative designs for a 24-h operating solar-powered absorption refrigeration technology. Int J Refrig 2012;35:1967–77. doi:10.1016/j.ijrefrig.2012.06.008.

[35] Siddiqui MU, Said S a. M. A review of solar powered absorption systems. Renew Sustain Energy Rev 2015;42:93–115. doi:10.1016/j.rser.2014.10.014.

[36] Pintaldi S, Perfumo C, Sethuvenkatraman S, White S, Rosengarten G. A review of thermal energy storage technologies and control approaches for solar cooling. Renew Sustain Energy Rev 2015;41:975–95. doi:10.1016/j.rser.2014.08.062.

[37] Best R, Ortega N. Solar refrigeration and cooling. Renew Energy 1999;16:685–90. doi:10.1016/S0960-1481(98)00252-3.

[38] Raghuvanshi S, Maheshwari G. Analysis of Ammonia – Water (NH3-H2O) Vapor Absorption Refrigeration System based on First Law of Thermodynamics. Int J Sci Eng Res 2011;2:1–7.

[39] Zhu L, Wang S, Gu J. Performance investigation of a thermal-driven refrigeration system. Int J Energy Res 2008;32:939–49. doi:10.1002/er.1408.

[40] Wang RZ, Ge TS, Chen CJ, Ma Q, Xiong ZQ. Solar sorption cooling systems for residential applications: Options and guidelines. Int J Refrig 2009;32:638–60. doi:10.1016/j.ijrefrig.2009.02.005.

[41] Molero-Villar N, Cejudo-López JM, Domínguez-Muñoz F, Carrillo-Andrés a. A comparison of solar absorption system configurations. Sol Energy 2012;86:242–52. doi:10.1016/j.solener.2011.09.027.

[42] Chidambaram L a., Ramana a. S, Kamaraj G, Velraj R. Review of solar cooling methods and thermal storage options. Renew Sustain Energy Rev 2011;15:3220–8. doi:10.1016/j.rser.2011.04.018.

[43] Wang RZ, Oliveira RG. ADSORPTION REFRIGERATION - AN EFFICIENT WAY TO MAKE GOOD USE OF WASTE HEAT AND SOLAR ENERGY. Int. Sorption Heat Pump Conf., 2005.

[44] Ullah KR, Saidur R, Ping HW, Akikur RK, Shuvo NH. A review of solar thermal refrigeration and cooling methods. Renew Sustain Energy Rev 2013;24:499–513. doi:10.1016/j.rser.2013.03.024.

[45] Xia YZ, Zhang JP, Li D, Wang DC, Li YH. A review on adsorption refrigeration technology and adsorption deterioration in physical adsorption systems. Renew Sustain Energy Rev 2009;14:344–53. doi:10.1016/j.rser.2009.08.001.

[46] Osterman E, Tyagi V V., Butala V, Rahim NA, Stritih U. Review of PCM based cooling technologies for buildings. Energy Build 2012;49:37–49. doi:10.1016/j.enbuild.2012.03.022.

[47] Noro M, Lazzarin RM, Busato F. Solar cooling and heating plants: An energy and economic analysis of liquid sensible vs phase change material (PCM) heat storage. Int J Refrig 2014;39:104–16. doi:10.1016/j.ijrefrig.2013.07.022.

[48] Tay NHS, Liu M, Belusko M, Bruno F. Review on transportable phase change material in thermal energy storage systems. Renew Sustain Energy Rev 2017;75:264–77. doi:10.1016/j.rser.2016.10.069.

[49] Oró E, Miró L, Farid MM, Martin V, Cabeza LF. Energy management and CO2mitigation using phase change materials (PCM) for thermal energy storage (TES) in cold storage and transport. Int J Refrig 2014;42:26–35. doi:10.1016/j.ijrefrig.2014.03.002.

[50] Oró E, de Gracia A, Castell A, Farid MM, Cabeza LF. Review on phase change materials (PCMs) for cold thermal energy storage applications. Appl Energy 2012;99:513–33. doi:10.1016/j.apenergy.2012.03.058.

[51] Veerakumar C, Sreekumar A. Phase change material based cold thermal energy storage: Materials, techniques and applications - A review. Int J Refrig 2016;67:271–89. doi:10.1016/j.ijrefrig.2015.12.005.

[52] Cabeza LF, Mehling H, Hiebler S, Ziegler F. Heat transfer enhancement in water when used as PCM in thermal energy storage. Appl Therm Eng 2002;22:1141–51. doi:10.1016/S1359-4311(02)00035-2.

[53] Frank E, Haller M. Systematic Classification of Combined Solar Thermal and Heat Pump Systems 2016:1–8. doi:10.18086/eurosun.2010.14.04.

[54] Fedrizzi R, Malenkovic I, Melograno P, Haller M, Schicktanz M, Herkel S, et al. Uniform representation of system performance for solar hybrid systems. Energy Procedia 2012;30:73–83. doi:10.1016/j.egypro.2012.11.010.

[55] Ben Hassine I, Eicker U. Impact of load structure variation and solar thermal energy integration on an existing district heating network. Appl Therm Eng 2013;50:1437–46. doi:10.1016/j.applthermaleng.2011.12.037.

[56] Han W, Sun L, Zheng D, Jin H, Ma S, Jing X. New hybrid absorption-compression refrigeration system based on cascade use of mid-temperature waste heat. Appl Energy 2013;106:383–90. doi:10.1016/j.apenergy.2013.01.067.

[57] Siddiqui FR, El-Shaarawi M a I, Said S a M. Exergo-economic analysis of a solar driven hybrid storage absorption refrigeration cycle. Energy Convers Manag 2014;80:165–72. doi:10.1016/j.enconman.2014.01.029.

[58] Skagestad B, Mildenstein P. District Heating and Cooling Connection Handbook. IEA

D ISTR. n.d.

[59] Andersen E, Chen Z, Fan J, Furbo S, Perers B. Investigations of intelligent solar heating systems for single family house. Energy Procedia 2014;48:1–8. doi:10.1016/j.egypro.2014.02.002.

[60] Carpaneto E, Lazzeroni P, Repetto M. Optimal integration of solar energy in a district heating network. Renew Energy 2015;75:714–21. doi:10.1016/j.renene.2014.10.055.

[61] Kantola M, Saari A. Renewable vs. traditional energy management solutions - A Finnish hospital facility case. Renew Energy 2013;57:539–45. doi:10.1016/j.renene.2013.02.023.

[62] Lamnatou C, Chemisana D, Mateus R, Almeida MG, Silva SM. Review and perspectives on Life Cycle Analysis of solar technologies with emphasis on building-integrated solar thermal systems. Renew Energy 2015;75:833–46. doi:10.1016/j.renene.2014.09.057.

[63] Desideri U, Proietti S, Sdringola P. Solar-powered cooling systems: Technical and economic analysis on industrial refrigeration and air-conditioning applications. Appl Energy 2009;86:1376–86. doi:10.1016/j.apenergy.2009.01.011.

[64] Poppi S, Sommerfeldt N, Bales C, Madani H, Lundqvist P. Techno-economic review of solar heat pump systems for residential heating applications. Renew Sustain Energy Rev 2018;81:22–32. doi:10.1016/j.rser.2017.07.041.

[65] Herrando M, Ramos A, Freeman J, Zabalza I, Markides CN. Technoeconomic modelling and optimisation of solar combined heat and power systems based on flat-box PVT collectors for domestic applications. Energy Convers Manag 2018;175:67–85. doi:10.1016/j.enconman.2018.07.045.

[66] Blackman C, Bales C, Thorin E. Techno-economic Evaluation of Solar-assisted Heating and Cooling Systems with Sorption Module Integrated Solar Collectors. Energy Procedia 2015;70:409–17. doi:10.1016/j.egypro.2015.02.142.

[67] Petela R. Exergy of undiluted thermal radiation. Sol Energy 2003;74:469–88. doi:10.1016/S0038-092X(03)00226-3.

[68] Bejan A. Unification of Three Different Theories Concerning the Ideal Conversion of Enclosed Radiation. J Sol Energy Eng 1987;109:46–51. doi:10.1115/1.3268177.

[69] Koroneos C, Tsarouhis M. Exergy analysis and life cycle assessment of solar heating

and cooling systems in the building environment. J Clean Prod 2012;32:52–60. doi:10.1016/j.jclepro.2012.03.012.

[70] Aman J, Ting DS, Henshaw P. Residential solar air conditioning : Energy and Exergy analyses of an ammonia-water absorption cooling system. Appl Therm Eng 2014;62:424–32. doi:https://doi.org/10.1016/j.applthermaleng.2013.10.006.

[71] Gebreslassie BH, Guillén-Gosálbez G, Jiménez L, Boer D. Solar assisted absorption cooling cycles for reduction of global warming: A multi-objective optimization approach. Sol Energy 2012;86:2083–94. doi:10.1016/j.solener.2012.04.010.

[72] Stanek W, Gazda W. Exergo-ecological evaluation of adsorption chiller system. Energy 2014;76:42–8. doi:10.1016/j.energy.2014.02.053.

[73] Eicker U, Pietruschka D, Haag M, Schmitt A. Systematic design and analysis of solar thermal cooling systems in different climates. Renew Energy 2015;80:827–36. doi:10.1016/j.renene.2015.02.019.

[74] Rowe D, White S. Review of International Solar Cooling Incentive Schemes. Energy Procedia 2015;57:3160–70. doi:10.1016/j.egypro.2015.06.065.

[75] Szargut JT. Termodynamika Techniczna. PWN. Warszawa: 1991.

[76] Stanek W. Analiza egzergetyczna w teorii i praktyce. Wydawnictw. Gliwiec: 2016.

[77] Clausius R. Ueber Die Bewegende Kraft Der Wärme Und Die Gesetze, Welche Sich Daraus Für Die Wärmelehre Selbst Ableiten Lassen. Ann Phys 1850;79:368-397,500-524. doi:10.1002/andp.18501550403.

[78] Rao YVC. Chemical Engineering Thermodynamics. Univ Press 1997:158.

[79] Valero Capilla A, Cuadra CT. Thermoeconomics - PhD Course. Circe. Center of Research for Energy Resources and Consumption University of Zaragoza. Spain; 2005.

[80] Szargut J, Morris DR, Steward FR. Exergy Analysis of THermal, Chemical, and Metallurgical Processes. New York: Hemisphere Publishing Corporation; 1988.

[81] Ahrendts J. The exergy pf chemically reacting systems. VDI Forschungsh. 579, Dusseldorf: 1977.

[82] Kameyama H, Yoshida YS. Evaluation of reference exergy for the elements. Appl Energy 1982;11:69–83.

[83] Szargut J. Chemical exergies of the elements. Appl Energy 1989;32:269–85.

[84] Szargut J, Petela R. Egzergia. Warszawa: WNT; 1965.

[85] Petela R. Exergy of Heat Radiation. ASME J Heat Transf 1964;86:187–92.

[86] Chu SX, Liu LH. Analysis of terrestrial solar radiation exergy. Sol Energy 2009;83:1390–404. doi:10.1016/j.solener.2009.03.011.

[87] Pons M. Exergy analysis of solar collectors, from incident radiation to dissipation. Renew Energy 2012;47:194–202. doi:10.1016/j.renene.2012.03.040.

[88] Neri M, Luscietti D, Pilotelli M. Computing the Exergy of Solar Radiation From Real Radiation Data on the Italian Area 2013:452–7.

[89] Press WH. Theoretical maximum for energy from direct and diffuse sunlight. Nature 1976;264:734–5.

[90] Landsberg PT, Tonge G. Thermodynamics of the conversion of diluted radiation. J Phys A Math Gen 1979;12:551–62.

[91] Spanner DC. Introduction to Thermodynamics. London: Academic Press; 1964.

[92] Jeter SM. Maximum Conversion Efficiency for the Utilization of Direct Solar Radiation. Sol Energy 1981;26:231–6.

[93] Lazzaretto A, Tsatsaronis G. SPECO : A systematic and general methodology for calculating efficiencies and costs in thermal systems 2006;31:1257–89. doi:10.1016/j.energy.2005.03.011.

[94] Lazzaretto A, Tsatsaronis G. On the Quest for Objective Equations in Exergy Costing. Proc ASME Adv Energy Syst Div 1997;37:197–210.

[95] Bonforte G. Exergoeconomic and Exergoenvironmental Analysis of an ISCCGT Plant and Comparison of Its Performance with That of a Conven- tional CCGT Plant R. 2015.

[96] Tsatsaronis G, Cziesla F. Exergy and thermodynamic analysis, 2014.

[97] Morosuk T, Tsatsaronis G, Zhang C. Conventional thermodynamic and advanced exergetic analysis of a refrigeration machine using a Voorhees ’ compression process. Energy Convers Manag 2012;60:143–51. doi:10.1016/j.enconman.2012.02.021.

[98] Bejan A, Tsatsaronis G (George), Moran MJ. Thermal design and optimization. Wiley; 1996.

[99] Krüger D, Schenk H, Marcucci T. “smAll scaLe sOlar cooliNg dEvice” Collaborative

Project Small or Medium-scale Focused Research Project DELIVERABLE – D5.1 – Evaluation of the systems and comparisons. 2008.

[100] Schenk H, Lichtenthäler N, Krüger D. smAll scaLe sOlar cooliNg dEvice ALONE - Deliverable 2.1 PTC First Evaluation, Recommendations and System Pre-Test. 2010.

[101] Li ZF, Sumathy K. Technology development in the solar absorption air-conditioning systems 2000;4:267–93.

[102] Robur GAHP-W technical data n.d. https://www.robur.com/heat_pumps/water_to_water_gas_absorption_heat_pump_gahp_ws (accessed January 22, 2019).

[103] Thorin E, Dejfors C, Svedberg G. Thermodynamic Properties of Ammonia-Water Mixtures for Power Cycles 1. Int J Thermophys 1998;19:501–10. doi:10.1023/A:1022525813769.

[104] Ibrahim O, Klein SA. Thermodynamic properties of ammonia-water mixtures. ASHRAE Trans. 99, 1993, p. 1495–502.

[105] Kim B, Park J. Dynamic simulation of a single-effect ammonia-water absorption chiller. Int J Refrig 2007;30:535–45. doi:10.1016/j.ijrefrig.2006.07.004.

[106] Chen JC. A correlation for boiling heat transfer to saturated fluids in convective flow. ASME 1963.

[107] Seban RA, McLaughlin EF. Heat transfer in tube coils with laminar and turbulent flow. Int J Heat Mass Transf 1963;6:387–95.

[108] Le Lostec B, Galanis N, Millette J. Simulation of an ammonia-water absorption chiller. Renew Energy 2013;60:269–83. doi:10.1016/j.renene.2013.05.027.

[109] Company R. Robur GAHP-W technical data sheet n.d. https://www.robur.com (accessed September 1, 2017).

[110] Colburn AP, Drew TB. The condensation of mixed vapors. Transcations Am Inst Chem Eng 1937;33:197–215. doi:10.1002/aic.690110511.

[111] Price BC, Bell KJ. Design of binary vapor condensers using the colburn-drew equations. AIChE Symp Ser Transf Des n.d.;70:163–71.

[112] Kang YT, Christensen NR. Development of a counter-current model for a vertical fluted tube GAX absorber. Proc. Int. Absorpt. Heat Pump Conf. Publ by ASME, 1994.

[113] Le Lostec B, Galanis N, Millette J. Simulation of an ammonia-water absorption chiller. Renew Energy 2013;60:269–83. doi:10.1016/j.renene.2013.05.027.

[114] Cengel Y. Heat transfer: A pracitcal Approach. McGraw-Hill; 2003.

[115] Kakac S, Liu H. Heat exchangers: selection, rating and thermal design. Boca Raton: CRC Press LLC; 2002.

[116] Dobson MK, Chato JC. Condensation in Smooth Horizontal Tubes. ASME J Heat Transf 1998:193–213.

[117] Shah MM. A new correlation for heat transfer during boiling flow through pipes. ASHRAE Trans 1976;82:66–86.

[118] Shah MM. Chart correlation for saturated boiling heat transfer: equations and further study. ASHRAE Trans 1982;88:185–96.

[119] Nellis G, Klein S. Heat Transfer. New York: Cambridge University Press; 2009.

[120] Shah RK, London AL. Laminar Flow Forced Convection in Ducts. Academic Press; 1978.

[121] Notter RH, C.A. Sleicher. A solution to the turbulent Graetz problem III. Fully developed and entry region heat transfer rates. Chem Eng Sci 1972;27:2073–93.

[122] Bell KJ. Delaware method for shell side design. Heat Exch. Therm. Hydraul. Fundam. Des., Washington, D.C.: Taylor and Francis; 1981.

[123] Bell KJ. Delaware method of shell-design. Heat Transf. Equip. Des., Washington, D.C.: Taylor and Francis; 1988.

[124] Aluminium as a construction material in ammonia refrigeration cycles n.d. http://www.eurammon.com/node/326 (accessed January 22, 2019).

[125] Beckman WA, Duffie JA. Solar Engineering of Thermal Processes. John Wiley and Sons; 1980.

[126] Kumar A, Chand S. UOP. DESIGN AND ANALYSIS FOR 1MWe PARABOLIC TROUGH SOLAR COLLECTOR PLANT BASED ON DSG METHOD. Int J Eng Res Technol n.d.;2.

[127] TRNSYS-software. TRNSYS 16 a TRaNsient SYstem Simulation program - Mathematical Reference. vol. 5. n.d.

[128] Manfrida G, Gerard V. Maximum exergy control of a solar thermal plant equipped

with direct steam collectors. Int J Thermodyn 2008;11:143–9. doi:10.5541/IJOT.1034000222.

[129] Lobanoff VS, Ross RR. Centrifugal pumps - Design & Application. Second Edi. Housron, Texas: Gulf Publishing Company; 1992.

[130] Manfrida G, Petela K, Rossi F. Natural circulation solar thermal system for water disinfection. Energy 2017;141. doi:10.1016/j.energy.2017.09.132.

[131] Dainelli N, Manfrida G, Petela K, Rossi F. Exergo-Economic Evaluation of the Cost for Solar Thermal Depuration of Water. Energies 2017:1–19. doi:10.3390/en10091395.

[132] Fiaschi D, Manfrida G, Petela K, Talluri L. Thermo-Electric Energy Storage with Solar Heat Integration: Exergy and Exergo-Economic Analysis. Energies 2019;12:648. doi:10.3390/en12040648.

[133] De Lucia M, Fissi D, Mengoni CP. DESIGN OF THE LAY-OUT OF A PTC SOLAR FIELD FOR A SHC PLANT AT THE MISERICORDIA OF BADIA A RIPOLI: A METHOD FOR THE OPTIMIZATION OF THE ENERGY COLLECTION. vol. 6. 2011.

[134] F-chart. Engineering Equation Solver – Help. F-Chart Software n.d. http://www.fchart.com/ees/.

[135] TRNSYS-software. Meteonorm Library Available within the Software Package. 2016.

[136] Wojewódka D, Wilk B. Sloneczna temperatura przegrody pionowej w warunkach klimatu lokalnego. Fiz Budowli w Teor i Prakt 2007;2:313–8.

[137] Wang Y, Wang L, Liu Y, Ding P, Deng S, Long E. Defining air-conditioning and heating seasons based on human thermal perception and building energy efficiency. Urban Clim 2015;14:544–53. doi:10.1016/j.uclim.2015.09.008.

[138] Janotte N, Meiser S, Pitz-paal R, Fischer S. Quasi-dynamic analysis of thermal performance of parabolic trough collectors. SolarPaces Conf 2009.

[139] Marcucci T. SMART ENERGY MANAGEMENT:SVILUPPO E TEST DI SISTEMI E COMPONENTI PER APPLICAZIONI SOLAR COOLING. University of Florence, Italy, n.d.

[140] Misra RD, Sahoo PK, Gupta A. Thermoeconomic evaluation and optimization of an aqua-ammonia vapour-absorption refrigeration system. Int J Refrig 2006;29:47–59. doi:10.1016/j.ijrefrig.2005.05.015.

[141] Manfrida G, Kawambwa SJM. Exergy control of a Flat-Plate collector/Rankine Cycle Solar Power System. J Sol Energy Eng 1991;113:89–93.

[142] Kalogirou S a. Solar Energy Engineering Processes and Systems. Academic Press; 2009. doi:https://doi.org/10.1016/B978-0-12-374501-9.X0001-5.

[143] Turton R, Bailie RC, Whiting WB, Shaeiwitz JA. Analysis, Synthesis, and Design of Chemical Processes. Upper Saddle River, United States: Pearson Education (US); 2012.

[144] Chemengonline. Chemical Engineering Plan Cost Index (CEPCI) in 2018 n.d. https://www.chemengonline.com/cepci-updates-january-2018-prelim-and-december-2017-final/?printmode=1%22 (accessed December 1, 2018).

[145] Eurostat. Statistics on electricity prices in Europe n.d. https://ec.europa.eu/eurostat/statistics-explained/index.php/Electricity_price_statistics (accessed March 1, 2019).

[146] Petela K, Manfrida G, Szlek A. Advantages of variable driving temperature in solar absorption chiller. Renew Energy 2017;114. doi:10.1016/j.renene.2017.07.060.

[147] IEA. Solar collectors database n.d.:2016. http://www.iea-shc.org (accessed June 1, 2018).

[148] Lecuona a., Ventas R, Venegas M, Zacarías a., Salgado R. Optimum hot water temperature for absorption solar cooling. Sol Energy 2009;83:1806–14. doi:10.1016/j.solener.2009.06.016.

[149] YAZAKI. absorption chiller technical data sheet. n.d.

[150] SORTECH. Ecoo adsorption chiller technical data sheet. n.d.

[151] SORTECH. hybrid chiller technical data sheet n.d.

[152] Gazda W, Stanek W. Influence of power source type on energy effectiveness and environmental impact of cooling system with adsorption refrigerator 2014;87:1107–15. doi:10.1016/j.enconman.2014.05.015.

[153] JARUS. solar collector technical data sheet (test report No. 10COL937). n.d.

[154] TRNSYS-software. Meteonorm Library Available within the Software Package. 2016.

[155] Meteonorm information. n.d. http://www.meteonorm.com/ (accessed December 13, 2018).

[156] Products P. A82 PCM material data sheet n.d. http://www.pcmproducts.net/files/PCM Summary 2013-A.pdf (accessed December 31, 2018).

[157] Bonforte G, Buchgeister J, Manfrida G, Petela K. Exergoeconomic and Exergoenvironmental Analysis of an Integrated Solar Gas Turbine/Combined Cycle Power Plant. Energy 2017;156:352–9. doi:10.1016/j.energy.2018.05.080.

[158] Mackey CO, Wright LTJ. Periodic heat flow. Composite walls or roofs. ASHVE Trans 1946;52:283–96.

[159] Henchoz S, Buchter F, Favrat D, Morandin M, Mercangöz M. Thermoeconomic analysis of a solar enhanced energy storage concept based on thermodynamic cycles. Energy 2012;45:358–65. doi:10.1016/j.energy.2012.02.010.

[160] Italy, Geothermal District Heating systems of the Municipality of Pomarance n.d. http://geodh.eu/wp-content/uploads/2015/01/IT_Pomarance_GeoDH.pdf (accessed April 1, 2019).

[161] Szargut JT. Application of exergy for the calculation of ecological cost. Polish Acad Sci Tech Sci 1986;34:475–80.

[162] Szargut JÃ, Stanek W. Thermo-ecological optimization of a solar collector 2007;32:584–90. doi:10.1016/j.energy.2006.06.010.

[163] Power from the Sun, Chapter 4. Collecting Solar Energy n.d. http://www.powerfromthesun.net/Book/chapter04/chapter04.html#4.1.2 Single-Axis Tracking Apertures (accessed March 1, 2019).

APPENDIX A

LOG-MEAN TEMPERATURE DIFFERENCES DEFINITIONS FOR AMMONIA-WATER CHILLER COMPONENTS

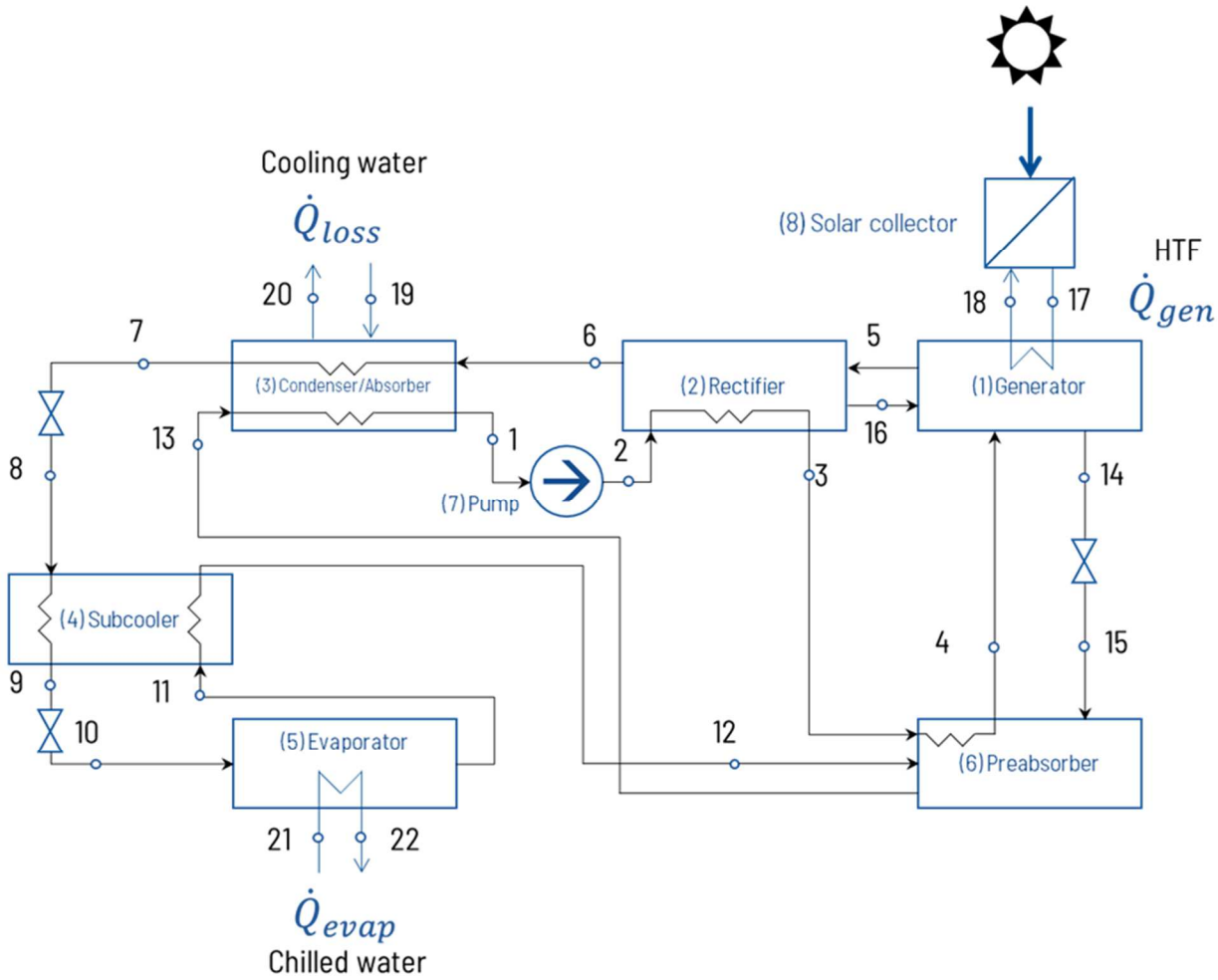

k	Component	Log-mean temperature difference
1	Generator	$\Delta T_{lg,1} = \frac{(T_{18} - T_4) - (T_{17} - T_{14})}{\ln \frac{(T_{18} - T_4)}{(T_{17} - T_{14})}}$
2	Rectifier	$\Delta T_{lg,2} = \frac{(T_6 - T_2) - (T_5 - T_3)}{\ln \frac{(T_6 - T_2)}{(T_5 - T_3)}}$
3	Condenser	$\Delta T_{lg,cond} = \frac{(T_6 - T_{20}) - (T_7 - T_{19})}{\ln \frac{(T_6 - T_{20})}{(T_7 - T_{19})}}$

3	Absorber	$\Delta T_{lg,abs} = \frac{(T_{13} - T_{20}) - (T_1 - T_{19})}{\ln \frac{(T_{13} - T_{20})}{(T_1 - T_{19})}}$
4	Subcooler	$\Delta T_{lg,4} = \frac{(T_8 - T_{12}) - (T_9 - T_{11})}{\ln \frac{(T_8 - T_{12})}{(T_9 - T_{11})}}$
5	Evaporator	$\Delta T_{lg,5} = \frac{(T_{21} - T_{11}) - (T_{22} - T_{10})}{\ln \frac{(T_{21} - T_{11})}{(T_{22} - T_{10})}}$
6	Preabsorber	$\Delta T_{lg,6} = \frac{(T_{15} - T_4) - (T_{13} - T_3)}{\ln \frac{(T_{15} - T_4)}{(T_{13} - T_3)}}$

APPENDIX B

METEOROLOGICAL CONDITIONS FOR REFERENCE DAYS OF THE MONTHS IN FLORENCE, ITALY

Table B.1 Representative days of the months in Florence – ambient temperature

hour	Ambient temperature, °C											
	Jan.	**Feb.**	**Mar.**	**Apr.**	**May**	**Jun.**	**Jul.**	**Aug.**	**Sep.**	**Oct.**	**Nov.**	**Dec.**
0	6.1	7.0	9.1	10.9	14.4	17.7	21.0	21.8	19.1	15.3	10.0	7.4
1	5.8	6.5	8.5	10.2	13.6	16.9	20.1	21.0	18.4	14.7	9.6	7.1
2	5.5	5.9	7.9	9.6	13.0	16.2	19.3	20.3	17.8	14.1	9.2	6.7
3	5.1	5.4	7.3	9.0	12.3	15.4	18.5	19.6	17.1	13.6	8.7	6.3
4	4.6	4.9	6.6	8.4	11.5	14.7	17.7	18.8	16.5	13.0	8.3	6.0
5	4.2	4.3	6.0	7.7	10.8	13.9	16.9	18.1	15.8	12.4	7.8	5.6
6	3.7	3.8	5.4	7.2	10.6	14.0	16.7	17.5	15.2	11.9	7.3	5.2
7	3.3	3.2	5.0	7.5	11.8	15.4	17.9	18.2	15.1	11.4	6.9	4.8
8	2.8	2.9	5.7	8.8	13.2	16.8	19.4	19.7	16.6	12.0	6.7	4.5
9	3.3	4.1	7.5	10.2	14.6	18.3	21.0	21.4	18.2	13.9	8.0	4.9
10	5.2	6.0	9.2	11.7	16.1	19.9	22.6	23.0	20.0	15.7	9.7	6.9
11	6.9	7.8	10.8	13.1	17.5	21.3	24.1	24.5	21.7	17.3	11.2	8.6
12	8.5	9.6	12.4	14.4	18.7	22.4	25.5	25.9	23.1	18.6	12.5	10.0
13	9.6	11.0	13.6	15.4	19.7	23.4	26.6	27.0	24.2	19.6	13.5	10.9
14	10.3	11.8	14.3	16.1	20.4	24.0	27.5	27.8	24.9	20.3	14.0	11.4
15	10.6	12.2	14.7	16.5	20.7	24.4	28.0	28.3	25.2	20.6	14.1	11.4
16	10.3	12.1	14.7	16.5	20.9	24.6	28.3	28.5	25.2	20.5	13.7	10.9
17	9.4	11.5	14.3	16.2	20.7	24.5	28.2	28.2	24.7	19.7	12.8	9.8
18	8.6	10.5	13.3	15.5	20.2	24.0	27.6	27.5	23.7	18.6	12.1	9.2
19	8.3	9.6	12.3	14.4	19.2	23.1	26.7	26.4	22.6	17.9	11.7	8.9
20	7.9	9.1	11.6	13.6	18.2	21.9	25.5	25.4	21.8	17.3	11.4	8.6
21	7.5	8.6	11.0	12.9	17.2	20.9	24.3	24.5	21.1	16.8	11.0	8.3
22	7.1	8.1	10.3	12.2	16.3	19.9	23.3	23.6	20.3	16.2	10.6	8.0
23	6.7	7.6	9.7	11.6	15.4	18.9	22.2	22.7	19.6	15.6	10.3	7.7

Table B.2 Representative days of the months in Florence – beam radiation on tracking surface

hour	Beam radiation, W/m^2											
	Jan.	**Feb.**	**Mar.**	**Apr.**	**May**	**Jun.**	**Jul.**	**Aug.**	**Sep.**	**Oct.**	**Nov.**	**Dec.**
0	0	0	0	0	0	0	0	0	0	0	0	0
1	0	0	0	0	0	0	0	0	0	0	0	0
2	0	0	0	0	0	0	0	0	0	0	0	0
3	0	0	0	0	0	0	0	0	0	0	0	0
4	0	0	0	0	0	0	0	0	0	0	0	0
5	0	0	0	0	0	0	0	0	0	0	0	0
6	0	0	0	0	66	113	98	6	0	0	0	0
7	0	0	10	103	198	247	263	208	103	0	0	0
8	0	13	123	198	304	353	421	355	257	132	30	0
9	79	136	177	257	344	429	493	456	358	240	130	66
10	115	175	223	313	373	469	539	485	405	249	145	148
11	130	165	213	314	375	460	551	469	389	228	153	133
12	131	179	248	327	346	456	580	467	384	219	141	100
13	110	160	199	306	372	433	559	446	341	218	125	87
14	127	172	195	319	358	416	560	476	336	243	159	110
15	149	192	226	307	379	487	597	508	394	287	161	118
16	152	193	245	314	408	472	602	488	359	258	160	85
17	79	182	193	298	365	440	557	429	300	169	46	0
18	0	29	108	165	309	359	469	311	165	12	0	0
19	0	0	0	44	149	181	294	149	1	0	0	0
20	0	0	0	0	0	60	47	0	0	0	0	0
21	0	0	0	0	0	0	0	0	0	0	0	0
22	0	0	0	0	0	0	0	0	0	0	0	0
23	0	0	0	0	0	0	0	0	0	0	0	0

Table B.3 Representative days of the months in Florence – total radiation on the sloped surface (45° facing South)

hour	Total radiation, W/m^2											
	Jan.	**Feb.**	**Mar.**	**Apr.**	**May**	**Jun.**	**Jul.**	**Aug.**	**Sep.**	**Oct.**	**Nov.**	**Dec.**
0	0	0	0	0	0	0	0	0	0	0	0	0
1	0	0	0	0	0	0	0	0	0	0	0	0
2	0	0	0	0	0	0	0	0	0	0	0	0
3	0	0	0	0	0	0	0	0	0	0	0	0
4	0	0	0	0	0	0	0	0	0	0	0	0
5	0	0	0	0	0	0	0	0	0	0	0	0
6	0	0	0	1	20	31	22	7	0	0	0	0
7	0	0	6	43	75	81	67	51	34	3	0	0
8	0	14	94	164	216	227	232	205	176	106	28	0
9	84	148	230	332	365	396	412	395	370	285	174	85
10	204	283	380	490	515	547	592	572	553	418	293	254
11	316	388	498	609	635	659	732	716	691	522	401	339
12	404	507	620	700	688	721	846	817	785	574	479	384
13	406	504	587	713	711	730	857	828	747	586	439	365
14	394	473	547	656	648	672	820	798	682	566	416	345
15	330	407	487	560	565	641	734	709	602	482	320	266
16	232	301	390	432	464	512	585	538	436	317	208	138
17	85	184	220	271	308	347	396	355	257	139	47	10
18	0	26	79	105	152	185	203	161	82	10	0	0
19	0	0	2	20	40	57	51	33	4	0	0	0
20	0	0	0	0	6	19	18	1	0	0	0	0
21	0	0	0	0	0	0	0	0	0	0	0	0
22	0	0	0	0	0	0	0	0	0	0	0	0
23	0	0	0	0	0	0	0	0	0	0	0	0

APPENDIX C

METEOROLOGICAL CONDITIONS FOR REFERENCE DAYS OF THE MONTHS IN WROCŁAW, POLAND

Table C.1 Representative days of the months in Wrocław – ambient temperature

hour	Ambient temperature, °C											
	Jan.	**Feb.**	**Mar.**	**Apr.**	**May**	**Jun.**	**Jul.**	**Aug.**	**Sep.**	**Oct.**	**Nov.**	**Dec.**
0	-2.4	-1.5	1.7	6.0	10.8	14.1	15.8	15.3	12.2	8.2	3.5	0.0
1	-2.5	-1.8	1.3	5.2	10.0	13.2	14.9	14.5	11.6	7.7	3.2	-0.2
2	-2.7	-2.2	0.8	4.5	9.3	12.5	14.2	13.7	11.0	7.2	2.8	-0.5
3	-3.0	-2.6	0.3	3.8	8.5	11.8	13.4	12.9	10.4	6.7	2.5	-0.8
4	-3.3	-3.0	-0.2	3.1	7.7	10.9	12.6	12.1	9.8	6.2	2.2	-1.1
5	-3.7	-3.4	-0.7	2.4	7.5	11.0	12.5	11.4	9.2	5.6	1.8	-1.4
6	-4.0	-3.8	-1.2	2.3	8.5	12.3	13.5	11.6	8.7	5.1	1.5	-1.7
7	-4.3	-4.2	-1.2	3.7	9.8	13.4	14.5	13.1	9.3	4.9	1.1	-2.0
8	-4.6	-4.2	-0.2	5.0	11.2	14.6	15.8	14.6	10.7	5.9	1.1	-2.4
9	-4.3	-3.3	1.2	6.5	12.7	15.9	17.3	16.2	12.1	7.6	1.9	-2.0
10	-3.1	-1.8	2.7	8.1	14.2	17.2	18.6	17.8	13.6	9.0	3.3	-0.7
11	-2.1	-0.4	4.0	9.5	15.5	18.3	19.8	19.2	14.8	10.4	4.6	0.4
12	-1.0	0.6	5.0	10.6	16.5	19.2	20.9	20.4	15.9	11.5	5.7	1.5
13	-0.1	1.3	5.8	11.5	17.5	20.0	21.8	21.3	16.7	12.4	6.4	2.0
14	0.4	1.9	6.3	12.0	18.2	20.7	22.4	22.1	17.2	12.9	6.7	2.2
15	0.4	1.9	6.4	12.2	18.4	21.0	22.7	22.4	17.3	12.9	6.4	2.1
16	-0.2	1.6	6.3	12.2	18.4	21.2	22.8	22.5	17.1	12.4	5.6	1.4
17	-0.7	0.8	5.7	11.8	18.2	21.0	22.6	22.2	16.5	11.5	5.1	0.9
18	-0.9	0.3	4.8	11.0	17.4	20.5	22.1	21.5	15.6	10.8	4.9	0.7
19	-1.1	0.0	4.1	9.9	16.4	19.6	21.3	20.4	14.8	10.3	4.6	0.6
20	-1.4	-0.3	3.7	9.0	15.3	18.6	20.2	19.3	14.2	9.9	4.4	0.5
21	-1.6	-0.6	3.2	8.2	14.2	17.5	19.2	18.3	13.6	9.4	4.1	0.3
22	-1.8	-0.9	2.8	7.5	13.2	16.4	18.1	17.3	13.1	8.9	3.9	0.2
23	-2.0	-1.2	2.3	6.7	12.1	15.3	17.0	16.3	12.5	8.4	3.7	0.0

Table C.2 Representative days of the months in Wrocław – beam radiation on tracking surface

hour	Beam radiation, W/m^2											
	Jan.	**Feb.**	**Mar.**	**Apr.**	**May**	**Jun.**	**Jul.**	**Aug.**	**Sep.**	**Oct.**	**Nov.**	**Dec.**
0	0	0	0	0	0	0	0	0	0	0	0	0
1	0	0	0	0	0	0	0	0	0	0	0	0
2	0	0	0	0	0	0	0	0	0	0	0	0
3	0	0	0	0	0	0	0	0	0	0	0	0
4	0	0	0	0	0	0	0	0	0	0	0	0
5	0	0	0	0	44	71	45	0	0	0	0	0
6	0	0	0	68	162	147	126	75	1	0	0	0
7	0	0	38	159	254	191	184	166	125	11	0	0
8	0	24	128	198	297	218	272	238	190	111	3	0
9	26	77	175	203	302	253	295	258	209	124	46	20
10	47	100	172	209	300	249	245	263	202	138	61	40
11	47	98	155	180	279	226	242	226	184	124	65	35
12	48	80	152	180	269	226	257	215	193	115	40	23
13	60	95	141	163	285	249	255	257	173	135	46	22
14	87	84	169	187	280	263	253	254	184	127	58	36
15	75	85	170	209	263	255	272	261	213	167	55	46
16	40	93	179	230	300	297	304	297	191	153	16	0
17	0	38	112	198	252	270	270	279	119	38	0	0
18	0	0	41	113	149	200	221	193	46	0	0	0
19	0	0	0	12	62	127	120	58	0	0	0	0
20	0	0	0	0	1	48	19	0	0	0	0	0
21	0	0	0	0	0	0	0	0	0	0	0	0
22	0	0	0	0	0	0	0	0	0	0	0	0
23	0	0	0	0	0	0	0	0	0	0	0	0

One can observe, that in the summer months, beam radiation reaching the tracking surface of collectors (with solar azimuth angle 21° from the South) is not of maximum value during noon hours. It can be explained with aid of the cosine effect phenomenon. It represents the difference between the amount of energy reaching a surface pointing at the sun, and a surface that is parallel to the surface of the earth [163]. The collectors are not tracking Sun on an evident

North/South axis and while at noon are pointed upwards, they cannot take the highest advantage of the incoming direct solar radiation.

Table C.3 Representative days of the months in Wrocław – total radiation on the sloped surface (45° facing South)

hour	Total radiation, W/m^2											
	Jan.	**Feb.**	**Mar.**	**Apr.**	**May**	**Jun.**	**Jul.**	**Aug.**	**Sep.**	**Oct.**	**Nov.**	**Dec.**
0	0	0	0	0	0	0	0	0	0	0	0	0
1	0	0	0	0	0	0	0	0	0	0	0	0
2	0	0	0	0	0	0	0	0	0	0	0	0
3	0	0	0	0	0	0	0	0	0	0	0	0
4	0	0	0	0	0	0	0	0	0	0	0	0
5	0	0	0	0	16	25	19	2	0	0	0	0
6	0	0	0	18	43	56	46	27	4	0	0	0
7	0	0	22	90	147	139	126	101	63	11	0	0
8	0	21	106	196	278	250	259	227	178	114	10	0
9	39	111	235	318	402	368	383	349	310	207	85	32
10	95	217	339	442	524	464	467	475	411	314	165	100
11	162	303	406	486	584	518	556	536	487	382	258	147
12	235	308	450	539	635	573	616	563	543	418	238	163
13	268	371	439	492	659	594	610	614	501	432	231	147
14	247	292	421	469	573	554	552	562	439	335	193	133
15	147	216	324	406	454	467	484	471	374	277	110	98
16	56	144	233	317	365	382	382	381	244	163	27	4
17	0	40	111	186	222	247	248	236	110	29	0	0
18	0	0	23	67	94	122	132	98	24	0	0	0
19	0	0	0	11	35	47	52	26	0	0	0	0
20	0	0	0	0	6	18	15	1	0	0	0	0
21	0	0	0	0	0	0	0	0	0	0	0	0
22	0	0	0	0	0	0	0	0	0	0	0	0
23	0	0	0	0	0	0	0	0	0	0	0	0